Oxidative insertion of amine into conjugated macrocycle: transformation of antiaromatic norcorrole into aromatic azacorrole

Sha Li, Yahan Sun, Xiaofang Li, Oskar Smaga, Sebastian Koniarz, Miłosz Pawlicki, and Piotr J. Chmielewski**

Table of Contents

General methods and instrumentation

All of the reagents from commercial suppliers were used without further purification. All of the solvents were freshly distilled from the appropriate drying agents before use. The analytical TLCs were performed with silica gel 60 F254 plates. Column chromatography was carried out by using silica gel 60 (200–300 mesh ASTM). The NMR spectra were recorded on a Bruker AV-II 500 MHz NMR spectrometer, operating at 500 MHz for ^{1}H, and 125 MHz for ^{13}C and Bruker Avance-II 600 MHz NMR spectrometer, operating at 600 MHz for ^{1}H, and 150 MHz for ^{13}C. TMS was used as an internal reference for ^{1}H and ^{13}C chemical shifts and $CDCl_3$ as a solvent. Standard pulse programs from the Bruker library were used for homo- and heteronuclear 2D experiments. MS was conducted by a Finnigan LCQ Advantage MAX and Shimadzu q-TOF mass spectrometers. Absorption UV/Vis/NIR spectra were recorded by using a Varian Cary 50 Bio and Jasco V-770 spectrophotometers. Electrochemical measurements were performed by means of Autolab (Metrohm) potentiostat/galvanostat system for dichloromethane solutions with a glassy carbon, a platinum wire, and Ag/Ag^+ as the working, auxiliary, and reference electrodes, respectively. Tetrabutylammonium hexafluorophosphate was used as a supporting electrolyte. The potentials were referenced with the ferrocene/ferrocenium couple used as an internal standard. Spectroelectrochemical measurements were conducted in dichloromethane solution with $[Bu_4N]PF_6$ supporting electrolyte by means of optically transparent thin-layer electrochemical (OTTLE) cell consisting of platinum gauze as working and auxiliary electrodes and a silver wire as a pseudoreference electrode sealed between transparent fluorite windows. EPR spectra (X-band) were recorded on a Bruker ELEXSYS E500 spectrometer. EPR spectra were simulated using WinEPR Simfonia v.1.25 (shareware version) by Bruker. X-ray diffraction data are summarized in Tables S6 and S7. The structures were solved by direct methods with SHELXS97[1] and refined by the full-matrix least-squares method on all F^2 data by using the SHELXL-2016/6 incorporated in the shelXle program[1,2]. All hydrogen atoms, including those located in the difference density map, were placed in calculated positions and refined as the riding model.

Computational methods

Density functional theory (DFT) calculations were performed by using the Gaussian 09 program[3]. DFT geometry optimizations were carried out in the unconstrained C_1 symmetry by using the X-ray structures, molecular mechanics, or semiempirical models as starting geometries. DFT geometries were refined to meet standard convergence criteria, and the existence of a local minimum was verified by a normal mode frequency calculation. DFT calculations were performed by using the hybrid B3LYP functional,[4-6] and the 6-31G(d,p) basis set with a LAN2DZ pseudopotential applied for nickel(II) center.. The electronic spectra were simulated by means of time-dependent density functional theory (TD-DFT) using the Tamm-Dancoff approximation for 50 states. For TD calculations, the polarizable continuum model of solvation was used (PCM, standard chloroform parametrization). The electronic transitions and UV/Vis/NIR spectra were analyzed by means of the GaussSum program.[7] The transitions were convoluted by Gaussian curves with 2000 cm^{-1} half line width. ^{1}H and ^{13}C NMR chemical shifts as well as nucleus-independent chemical shifts (NICS(–1,0,1)) were calculated by means of GIAO/B3LYP/6-31G(d,p)/LANL2DZ procedure included in the Gaussian program. The computational details are collected in Table S8.

Syntheses and characterizations

Synthesis of the precursors. Starting norcorrolatonickel(II) complex **1** was obtained as described previously.[8,9]

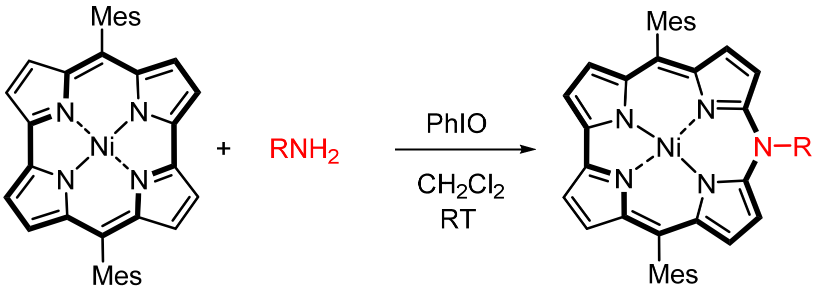

1 **2a-r** **3a-r**

General method of the 10-aryl-10-azacorroles synthesis. A solution of **1** (30 mg, 0.052 mmol) and amine **2** (0.234 mmol) in 5 ml anhydrous CH_2Cl_2 was stirred at room temperature in the presence of PhIO (40 mg, 0.18mmol). The reaction mixture was then passed through a short silica gel column with CH_2Cl_2 as eluent to collect all the moveable fractions, and after that the solvent was evaporated under vacuum. The residue was purified by silica preparative thin layer plate (1 mm, 20 x 20 cm) with petroleum ether/ CH_2Cl_2 (*v*/*v* = 4:1) as eluent to afford product **3.**

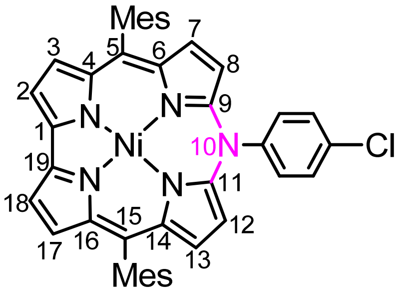

3a: yield, 22.3 mg (61%). ^{1}H NMR (600 MHz, $CDCl_3$, 300 K) δ: 8.27 (d, ^3J=4.2 Hz, 2H, 2,18-pyrr), 8.07 (d, ^3J=4.6 Hz, 2H, 7,13-pyrr), 7.89 (d, ^3J=4.2 Hz, 2H, 3,17-pyrr), 7.79 (m, 2H, 2,6-(4-ClPh)), 7.71 (m, 2H, 3,5-(4-ClPh)), 7.22 (d, ^3J=4.6 Hz, 2H, 8,12-pyrr), 7.13 (s, 4H, *m*-Mes), 2.51 (m, 6H, *p*-Me), 1.91 (s, 12H, *o*-Me). ^{13}C NMR (150 MHz, $CDCl_3$, 300 K) δ_C = 169.6, 144.6, 143.5, 140.8, 138.4, 137.5, 135.1, 133.1, 133.0, 131.7, 131.2, 129.2, 128.3, 127.7, 125.2, 117.1, 112.9, 21.3, 20.9. UV-vis (CH_2Cl_2) λ_{max}/nm (logε): 395 (4.80), 437 (4.22), 497 (3.65), 564 (3.74), 588 (3.63), 635 (3.69). ESI-HRMS calc. for $C_{42}H_{34}ClN_5Ni[M]^+$: 701.1856, Found: 701.1896.

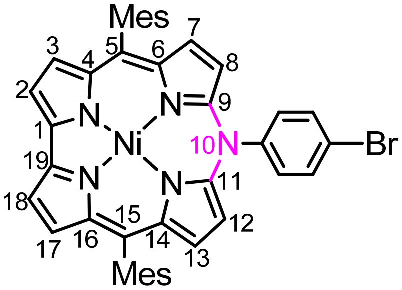

3b: yield, 21.0 mg (54%). ^{1}H NMR (600 MHz, CDCl$_3$, 300 K) δ: 8.28 (d, ^3J=4.2 Hz, 2H, 2,18-pyrr), 8.08 (d, ^3J=4.6 Hz, 2H, 7,13-pyrr), 7.90 (d, ^3J=4.2 Hz, 2H, 3,17-pyrr), 7.79 (m, 2H, 2,6-(4-BrPh)), 7.72 (m, 2H, 3,5-(4-BrPh)), 7.23 (d, ^3J=4.6 Hz, 2H, 8,12-pyrr), 7.13 (s, 4H, *m*-Mes), 2.52 (m, 6H, *p*-Me), 1.92 (s, 12H, *o*-Me). ^{13}C NMR (150 MHz, CDCl$_3$, 300 K) δ_C = 144.7, 143.4, 141.3, 138.4, 137.5, 135.1, 133.1, 133.0, 132.3, 131.7, 131.5, 128.4, 127.7, 125.2, 124.4, 117.1, 112.9, 21.4, 20.9. UV-vis (CH$_2$Cl$_2$) λ_{max}/nm (logε): 395 (4.94), 438 (4.36), 497 (3.80), 564 (3.89), 588 (3.78), 635 (3.84). ESI-HRMS calc. for C$_{42}$H$_{34}$BrN$_5$Ni[M]$^+$: 745.1351, Found: 745.1345.

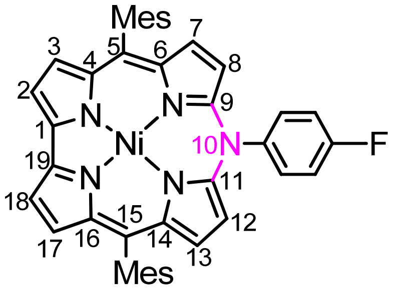

3c: yield, 23.2 mg (65%). ^{1}H NMR (600 MHz, CDCl$_3$, 300 K) δ: 8.28 (d, ^3J=4.2 Hz, 2H, 2,18-pyrr), 8.08 (d, ^3J=4.6 Hz, 2H, 7,13-pyrr), 7.90 (d, ^3J=4.2 Hz, 2H, 3,17-pyrr), 7.83 (m, 2H, 2,6-(4-FPh)), 7.41 (m, 2H, 3,5-(4-FPh)), 7.22 (d, ^3J=4.6 Hz, 2H, 8,12-pyrr), 7.13 (s, 4H, *m*-Mes), 2.51 (m, 6H, *p*-Me), 1.91 (s, 12H, *o*-Me). ^{13}C NMR (150 MHz, CDCl$_3$, 300 K) δ_C = 163.3 (d, $^1J_{FC}$ = 249.4 Hz), 144.6, 143.7, 138.44, 138.4 (d, $^4J_{FC}$ = 3.3 Hz), 137.5, 135.2, 133.2, 133.0, 131.7, 131.64, 131.59, 128.3, 127.7, 125.2, 117.1, 116.1, 115.9, 113.0, 21.3, 20.9. UV-vis (CH$_2$Cl$_2$) λ_{max}/nm (logε): 394 (5.07), 436 (4.50), 497 (3.93), 564 (4.03), 588 (3.93), 635 (3.98). ESI-HRMS calc. for C$_{42}$H$_{34}$FN$_5$Ni[M]$^+$: 685.2152, Found: 685.2164.

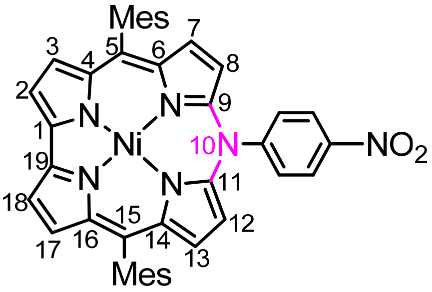

3d: yield, 26.3 mg (71%). ^{1}H NMR (600 MHz, CDCl$_3$, 300 K) δ: 8.61 (m, 2H, 3,5-(4-NO$_2$Ph)), 8.28 (d, ^3J=4.2 Hz, 2H, 2,18-pyrr), 8.09 (d, ^3J=4.6 Hz, 2H, 7,13-pyrr), 8.05 (m, 2H, 2,6-(4-NO$_2$Ph)), 7.90 (d, ^3J=4.2 Hz, 2H, 3,17-pyrr), 7.14 (d, ^3J=4.6 Hz, 2H, 8,12-pyrr), 7.13 (s, 4H, *m*-Mes), 2.51 (m, 6H, *p*-Me), 1.91 (s, 12H, *o*-Me). ^{13}C NMR (150 MHz, CDCl$_3$, 300 K) δ_C = 148.8, 147.4, 145.0, 142.8, 138.4, 137.6, 134.9, 133.2, 133.1, 131.9, 131.3, 129.0, 127.7, 125.7, 124.3, 117.5, 112.2, 21.3, 20.9. UV-vis (CH$_2$Cl$_2$) λ_{max}/nm (logε): 396 (5.02), 439 (4.46), 495 (3.93), 564 (3.98), 592 (3.81), 639 (3.92). ESI-HRMS calc. for C$_{42}$H$_{34}$N$_6$NiO2[M]$^+$: 712.2097, Found: 712.2144.

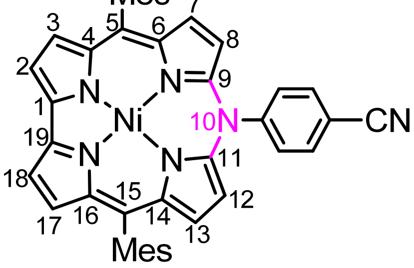

3e: yield, 29.2 mg (81%). ^{1}H NMR (600 MHz, $CDCl_3$, 300 K) δ: 8.28 (d, ^{3}J=4.2 Hz, 2H, 2,18-pyrr), 8.08 (d, ^{3}J=4.6 Hz, 2H, 7,13-pyrr), 8.05 (m, 2H, 2,6-(4-CNPh)), 7.99 (m, 2H, 3,5-(4-CNPh)), 7.90 (d, ^{3}J=4.2 Hz, 2H, 3,17-pyrr), 7.13 (s, 4H, *m*-Mes), 7.12 (d, ^{3}J=4.6 Hz, 2H, 8,12-pyrr), 2.51 (m, 6H, *p*-Me), 1.91 (s, 12H, *o*-Me). ^{13}C NMR (150 MHz, $CDCl_3$, 300 K) δ_C = 145.9, 145.0, 142.9, 138.4, 137.6, 135.0, 133.14, 133.06, 132.9, 131.9, 131.1, 128.9, 127.7, 125.6, 117.7, 117.4, 114.5, 112.3, 21.3, 20.9. UV-vis (CH_2Cl_2) λ_{max}/nm (logε): 396 (5.07), 439 (4.52), 495 (3.93), 563 (4.02), 587 (3.96), 630 (3.98). ESI-HRMS calc. for $C_{43}H_{34}N_6Ni[M]^+$: 692.2198, Found: 692.2157.

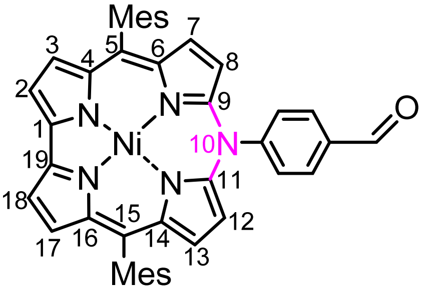

3f: yield, 30.4 mg (84%). ^{1}H NMR (600 MHz, $CDCl_3$, 300 K) δ: 10.30 (s, 1H, -CHO), 8.28 (d, ^{3}J=4.2 Hz, 2H, 2,18-pyrr), 8.26 (m, 2H, 2,6-(4-CHOPh)), 8.08 (d, ^{3}J=4.6 Hz, 2H, 7,13-pyrr), 8.04 (m, 2H, 3,5-(4-CHOPh)), 7.91 (d, ^{3}J=4.2 Hz, 2H, 3,17-pyrr), 7.17 (d, ^{3}J=4.6 Hz, 2H, 8,12-pyrr), 7.13 (s, 4H, *m*-Mes), 2.51 (m, 6H, *p*-Me), 1.92 (s, 12H, *o*-Me). ^{13}C NMR (150 MHz, $CDCl_3$, 300 K) δ_C = 191.0, 147.1, 144.8, 143.0, 138.4, 137.6, 137.3, 135.07, 133.09, 133.1, 131.8, 131.0, 130.2, 128.6, 127.7, 125.4, 117.3, 112.7, 21.4, 20.9. UV-vis (CH_2Cl_2) λ_{max}/nm (logε): 396 (5.03), 439 (4.48), 497 (3.92), 564 (4.00), 589 (3.86), 636 (3.94). ESI-HRMS calc. for $C_{43}H_{35}N_5NiO[M]^+$: 695.2195, Found: 695.2167.

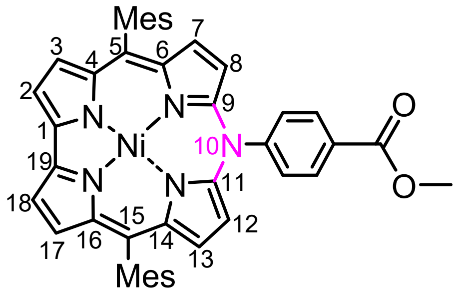

3g: yield, 27.2 mg (72%). ^{1}H NMR (600 MHz, $CDCl_3$, 300 K) δ: 8.42 (m, 2H, 2,6-(4-CO_2CH_3Ph)), 8.28 (d, ^{3}J=4.2 Hz, 2H, 2,18-pyrr), 8.07 (d, ^{3}J=4.6 Hz, 2H, 7,13-pyrr), 7.94 (m, 2H, 3,5-(4-CO_2CH_3Ph)), 7.90 (d, ^{3}J=4.2 Hz, 2H, 3,17-pyrr), 7.18 (d, ^{3}J=4.6 Hz, 2H, 8,12-pyrr), 7.13 (s, 4H, *m*-Mes), 4.06 (s, 3H, -CO_2CH_3), 2.51 (m, 6H, *p*-Me), 1.92 (s, 12H, *o*-Me). ^{13}C NMR (150 MHz, $CDCl_3$, 300 K) δ_C = 166.1, 146.0, 144.7, 143.2, 138.4, 137.5, 135.1, 133.1, 133.0, 131.9, 131.7, 130.3, 130.2, 128.4, 127.7, 125.3, 117.1, 112.9, 52.7, 21.3, 20.9. UV-vis (CH_2Cl_2) λ_{max}/nm (logε): 396 (5.08), 439 (4.50), 495 (3.93), 564 (4.02), 589 (3.90), 636 (3.97). ESI-HRMS calc. for $C_{44}H_{37}N_5NiO2[M]^+$: 725.2301, Found: 725.2280.

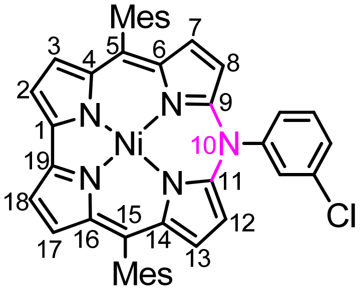

3h: yield, 29.2 mg (80%). ^1H NMR (600 MHz, $CDCl_3$, 300 K) δ: 8.29 (d, ^3J=4.2 Hz, 2H, 2,18-pyrr), 8.10 (d, ^3J=4.6 Hz, 2H, 7,13-pyrr), 7.90 (d, ^3J=4.2 Hz, 2H, 3,17-pyrr), 7.88 (m, 1H, 2-(3-ClPh)), 7.78 (m, 2H, 4,6-(3-ClPh)), 7.66 (m, 1H, 5-(3-ClPh)), 7.24 (d, ^3J=4.6 Hz, 2H, 8,12-pyrr), 7.14 (s, 4H, *m*-Mes), 2.52 (m, 6H, *p*-Me), 1.94 (s, 6H, *o*-Me), 1.93 (s, 6H, *o*-Me). ^{13}C NMR (150 MHz, $CDCl_3$, 300 K) δ_C = 144.7, 143.4, 143.3, 138.5, 138.4, 137.5, 135.1, 134.8, 133.2, 133.0, 131.8, 130.6, 130.4, 129.9, 128.5, 128.3, 127.70, 127.67, 125.3, 117.1, 112.9, 21.4, 20.9. UV-vis (CH_2Cl_2) λ_{max}/nm (logε): 395 (4.82), 437 (4.24), 497 (3.66), 564 (3.76), 588 (3.64), 635 (3.72). ESI-HRMS calc. for $C_{42}H_{34}ClN_5Ni[M]^+$: 701.1856, Found: 701.1799.

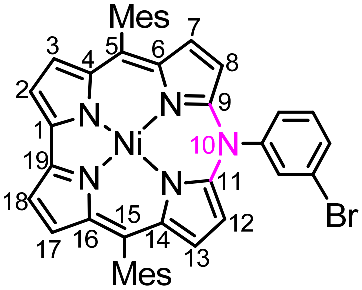

3i: yield, 31.9 mg (82%). ^1H NMR (600 MHz, $CDCl_3$, 300 K) δ: 8.28 (d, ^3J=4.2 Hz, 2H, 2,18-pyrr), 8.08 (d, ^3J=4.6 Hz, 2H, 7,13-pyrr), 8.03 (t, ^4J=1.9 Hz, 1H, 2-(3-BrPh)), 7.94 (m, 1H, 4-(3-BrPh)), 7.90 (d, ^3J=4.2 Hz, 2H, 3,17-pyrr), 7.81 (m, 1H, 6-(3-BrPh)), 7.60 (t, ^3J=8.1 Hz, 1H, 5-(3-BrPh)), 7.24 (d, ^3J=4.6 Hz, 2H, 8,12-pyrr), 7.14 (s, 4H, *m*-Mes), 2.52 (m, 6H, *p*-Me), 1.93 (s, 6H, *o*-Me), 1.91 (s, 6H, *o*-Me). ^{13}C NMR (150 MHz, $CDCl_3$, 300 K) δ_C = 144.7, 143.42, 143.37, 138.5, 138.4, 137.5, 135.1, 133.5, 133.2, 133.1, 133.0, 131.8, 130.1, 128.8, 128.5, 127.71, 127.67, 125.3, 122.5, 117.1, 113.0, 21.4, 20.9. UV-vis (CH_2Cl_2) λ_{max}/nm (logε): 395 (5.08), 437 (4.49), 497 (3.91), 564 (4.02), 588 (3.89), 635 (3.97). ESI-HRMS calc. for $C_{42}H_{34}BrN_5Ni[M]^+$: 745.1351, Found: 745.1395.

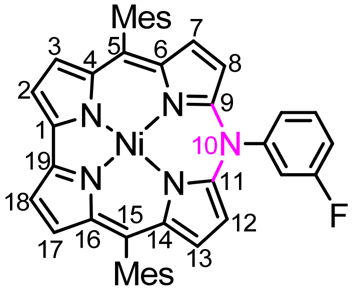

3j: yield, 29.3 mg (82%). ^1H NMR (600 MHz, $CDCl_3$, 300 K) δ: 8.27 (d, ^3J=4.2 Hz, 2H, 2,18-pyrr), 8.08 (d, ^3J=4.6 Hz, 2H, 7,13-pyrr), 7.89 (d, ^3J=4.2 Hz, 2H, 3,17-pyrr), 7.70 (m, 2H, 2-(3-FPh), 4-(3-FPh)), 7.62 (m, 1H, 6-(3-FPh)), 7.52 (m, 1H, 5-(3-FPh)), 7.23 (d, ^3J=4.6 Hz, 2H, 8,12-pyrr), 7.13 (s, 4H, *m*-Mes), 2.51 (m, 6H, *p*-Me), 1.92 (s, 12H, *o*-Me). ^{13}C NMR (150 MHz, $CDCl_3$, 300 K) δ_C = 162.4 (d, $^1J_{FC}$ = 252.5 Hz), 161.6, 144.7, 143.5 (d, ${}^4J_{FC}$ = 9.5 Hz), 143.47, 143.4, 138.5, 138.4, 137.5, 135.1, 133.1, 133.0, 131.7, 130.1 (d, ${}^4J_{FC}$ = 8.8 Hz), 128.4, 127.7, 127.6, 126.08, 126.06, 125.2, 117.9 (d, ${}^3J_{FC}$ = 22.7 Hz), 117.5 (d, ${}^3J_{FC}$ = 20.8 Hz), 117.1, 112.9, 21.4, 20.9. UV-vis (CH_2Cl_2) λ_{max}/nm (logε): 394 (5.02), 436 (4.43), 497 (3.85), 564 (3.96), 588 (3.85), 635 (3.94). ESI-HRMS calc. for $C_{42}H_{34}FN_5Ni[M]^+$: 685.2152, Found: 685.2164.

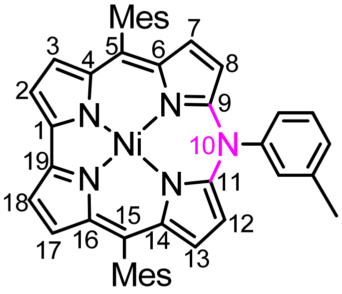

3k: yield, 27.7 mg (78%). ^{1}H NMR (600 MHz, $CDCl_3$, 300 K) δ: 8.28 (d, ${}^3J$=4.2 Hz, 2H, 2,18-pyrr), 8.06 (d, ${}^3J$=4.6 Hz, 2H, 7,13-pyrr), 7.89 (d, ${}^3J$=4.2 Hz, 2H, 3,17-pyrr), 7.66 (m, 2H, 2,4-(3-CH_3Ph)), 7.59 (m, 2H, 5,6-(3-CH_3Ph)), 7.25 (d, ${}^3J$=4.6 Hz, 2H, 8,12-pyrr), 7.13 (s, 4H, *m*-Mes), 2.55 (s, 3H, -CH_3), 2.51 (m, 6H, *p*-Me), 1.92 (s, 6H, *o*-Me), 1.91 (s, 6H, *o*-Me). ^{13}C NMR (150 MHz, $CDCl_3$, 300 K) δ_C = 144.4, 143.8, 142.3, 139.1, 138.50, 138.49, 137.4, 135.3, 133.2, 132.9, 131.5, 130.8, 130.5, 128.7, 127.9, 127.6, 127.0, 124.9, 116.8, 113.5, 21.4, 20.9. UV-vis (CH_2Cl_2) λ_{max}/nm (logε): 395 (4.90), 442 (4.30), 497 (3.72), 562 (3.84), 587 (3.78), 630 (3.78). ESI-HRMS calc. for $C_{43}H_{37}N_5Ni[M]^+$: 681.2402, Found: 681.2375.

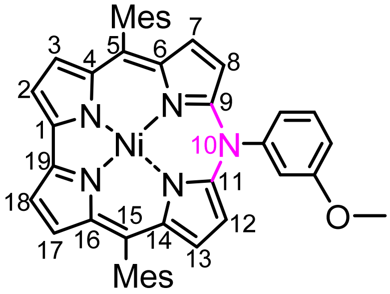

3l: yield, 26.9 mg (74%). ^{1}H NMR (600 MHz, $CDCl_3$, 300 K) δ: 8.29 (d, ${}^3J$=4.2 Hz, 2H, 2,18-pyrr), 8.08 (d, ${}^3J$=4.6 Hz, 2H, 7,13-pyrr), 7.90 (d, ${}^3J$=4.2 Hz, 2H, 3,17-pyrr), 7.61 (t, ${}^3J$=8.1 Hz, 1H, 5-(3-OCH_3Ph)), 7.48 (m, 1H, 4/6-(3-OCH_3Ph)), 7.42 (t, ${}^4J$=2.2 Hz, 1H, 2-(3-OCH_3Ph)), 7.32 (m, 1H, 4/6-(3-OCH_3Ph)), 7.30 (d, ${}^3J$=4.6 Hz, 2H, 8,12-pyrr), 7.14 (s, 4H, *m*-Mes), 3.90 (s, 3H, -O-CH_3), 2.52 (m, 6H, *p*-Me), 1.94 (s, 6H, *o*-Me), 1.93 (s, 6H, *o*-Me). ^{13}C NMR (150 MHz, $CDCl_3$, 300 K) δ_C = 159.9, 144.5, 143.7, 143.3, 138.50, 138.48, 137.4, 135.3, 133.2, 132.9, 131.6, 129.5, 128.0, 127.7, 124.9, 122.4, 116.9, 116.1, 115.7, 113.5, 55.7, 21.4, 20.9. UV-vis (CH_2Cl_2) λ_{max}/nm (logε): 395 (5.01), 437 (4.43), 494 (3.80), 564 (3.94), 586 (3.86), 631 (3.89). ESI-HRMS calc. for $C_{43}H_{37}N_5NiO[M]^+$: 697.2352, Found: 697.2371.

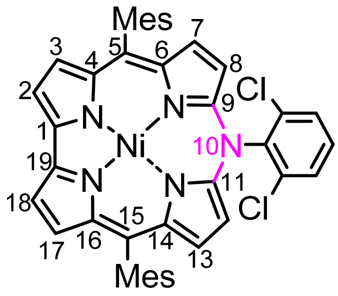

3m: yield, 10.0 mg (26%). ^{1}H NMR (600 MHz, CDCl$_3$, 300 K) δ: 8.20 (d, ^3J=4.2 Hz, 2H, 2,18-pyrr), 8.04 (d, ^3J=4.6 Hz, 2H, 7,13-pyrr), 7.84 (d, ^3J=4.2 Hz, 2H, 3,17-pyrr), 7.70 (m, 3H, 3,4,5-(2,6-Cl$_2$Ph)), 7.12 (s, 4H, *m*-Mes), 7.11 (d, ^3J=4.6 Hz, 2H, 8,12-pyrr), 2.51 (m, 6H, *p*-Me), 1.94 (s, 12H, *o*-Me). ^{13}C NMR (150 MHz, CDCl$_3$, 300 K) δ_C = 145.1, 142.4, 138.5, 137.5, 136.5, 135.0, 133.3, 132.9, 132.4, 131.8, 129.0, 128.9, 127.6, 125.3, 116.9, 111.1, 21.3, 21.0. UV-vis (CH$_2$Cl$_2$) λ_{max}/nm (logε): 395 (5.13), 435 (4.56), 499 (4.00), 564 (4.09), 594 (3.90), 642 (4.06). ESI-HRMS calc. for $C_{42}H_{33}Cl_2N_5Ni[M]^+$: 735.1466, Found: 735.1426.

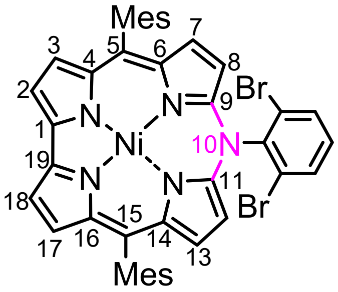

3n: yield, 10.3 mg (24%). ^{1}H NMR (600 MHz, CDCl$_3$, 300 K) δ: 8.20 (d, ^3J=4.2 Hz, 2H, 2,18-pyrr), 8.04 (d, ^3J=4.6 Hz, 2H, 7,13-pyrr), 7.92 (d, ^3J=8.2 Hz, 2H, 3,5-(2,6-Br$_2$Ph)), 7.84 (d, ^3J=4.2 Hz, 2H, 3,17-pyrr), 7.51 (t, ^3J=8.2 Hz, 1H, 4-(2,6-Br$_2$Ph)), 7.12 (s, 4H, *m*-Mes), 7.10 (d, ^3J=4.6 Hz, 2H, 8,12-pyrr), 2.50 (m, 6H, *p*-Me), 1.94 (s, 12H, *o*-Me). ^{13}C NMR (150 MHz, CDCl$_3$, 300 K) δ_C = 145.0, 142.2, 140.1, 138.5, 137.5, 135.0, 133.3, 132.9, 132.7, 132.4, 129.0, 127.6, 125.8, 125.3, 116.8, 111.4, 21.3, 21.0. UV-vis (CH$_2$Cl$_2$) λ_{max}/nm (logε): 395 (4.96), 435 (4.39), 499 (3.82), 564 (3.93), 594 (3.73), 642 (3.88). ESI-HRMS calc. for $C_{42}H_{33}Br_2N_5Ni[M]^+$: 823.0456, Found: 823.0455.

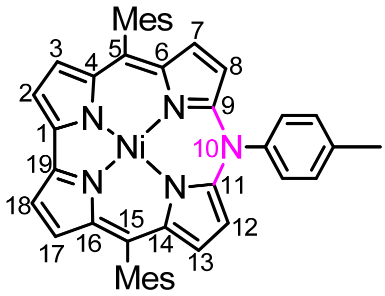

3o: yield, 18.4 mg (52%). ^{1}H NMR (600 MHz, CDCl$_3$, 300 K) δ: 8.28 (d, ^3J=4.2 Hz, 2H, 2,18-pyrr), 8.06 (d, ^3J=4.6 Hz, 2H, 7,13-pyrr), 7.89 (d, ^3J=4.2 Hz, 2H, 3,17-pyrr), 7.72 (m, 2H, 2,6-(4-CH$_3$Ph)), 7.51 (m, 2H, 3,5-(4-CH$_3$Ph)), 7.26 (d, ^3J=4.6 Hz, 2H, 8,12-pyrr), 7.13 (s, 4H, *m*-Mes), 2.63 (s, 3H, -CH$_3$), 2.51 (m, 6H, *p*-Me), 1.92 (s, 12H, *o*-Me). ^{13}C NMR (150 MHz, CDCl$_3$, 300 K) δ_C = 144.4, 143.9, 140.2, 139.9, 138.5, 137.4, 135.3, 133.2, 132.8, 131.5, 129.6, 129.5, 127.8, 127.6, 124.8, 116.8, 113.5, 21.4, 20.9. UV-vis (CH$_2$Cl$_2$) λ_{max}/nm (logε): 394 (4.92), 439 (4.39), 497 (3.82), 562 (3.88), 587 (3.83), 630 (3.83). ESI-HRMS calc. for $C_{43}H_{37}N_5Ni$ $[M]^+$: 681.2402, Found: 681.2375.

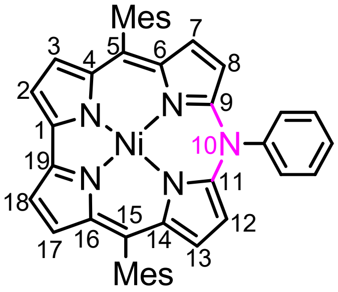

3p: yield, 19.1 mg (55%). ^{1}H NMR (600 MHz, CDCl$_3$, 300 K) δ: 8.29 (d, ^{3}J=4.2 Hz, 2H, 2,18-pyrr), 8.07 (d, ^{3}J=4.6 Hz, 2H, 7,13-pyrr), 7.90 (d, ^{3}J=4.2 Hz, 2H, 3,17-pyrr), 7.85 (m, 2H, 2,6-Ph), 7.79 (m, 1H, 4-Ph), 7.73 (m, 2H, 3,5-Ph), 7.23 (d, ^{3}J=4.6 Hz, 2H, 8,12-pyrr), 7.13 (s, 4H, *m*-Mes), 2.51 (m, 6H, *p*-Me), 1.92 (s, 12H, *o*-Me). ^{13}C NMR (150 MHz, CDCl$_3$, 300 K) δ_C = 144.5, 143.8, 142.4, 138.5, 137.4, 135.3, 133.2, 132.9, 131.6, 130.1, 129.9, 129.0, 128.0, 127.6, 125.0, 116.9, 113.4, 21.4, 20.9. UV-vis (CH$_2$Cl$_2$) λ_{max}/nm (logε): 395 (4.92), 435 (4.36), 490 (3.80), 564 (3.87), 587 (3.80), 632 (3.83). ESI-HRMS calc. for $C_{42}H_{35}N_5Ni[M]^+$: 667.2246, Found: 667.2299.

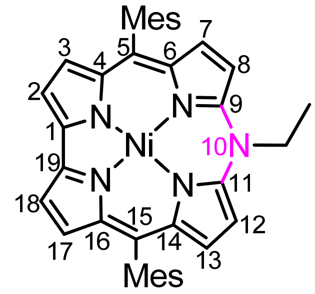

3q: yield, 8.4 mg (26%) ^{1}H NMR (600 MHz, CDCl$_3$, 300 K) δ: 8.24 (d, ^{3}J=4.2 Hz, 2H, 2,18-pyrr), 8.20 (d, ^{3}J=4.6 Hz, 2H, 7,13-pyrr), 8.05 (d, ^{3}J=4.2 Hz, 2H, 3,17-pyrr), 7.85 (d, ^{3}J=4.6 Hz, 2H, 8,12-pyrr), 7.14 (s, 4H, *m*-Mes), 5.83 (q, ^{3}J=7.4 Hz, 2H, -CH$_2$-), 2.52 (m, 6H, *p*-Me), 2.11 (t, ^{3}J=7.4 Hz, 3H, -CH$_3$), 1.91 (s, 12H, *o*-Me). ^{13}C NMR (150 MHz, CDCl$_3$, 300 K) δ_C = 144.4, 142.5, 138.5, 137.4, 135.3, 133.1, 132.8, 132.3, 127.6, 127.5, 124.8, 116.8, 110.8, 49.3, 21.4, 20.9, 17.1. UV-vis (CH$_2$Cl$_2$) λ_{max}/nm (logε): 395 (4.89), 437 (4.37), 495 (3.76), 563 (3.84), 587 (3.77), 632 (3.86). ESI-HRMS calc. for $C_{38}H_{35}N_5Ni[M]^+$: 619.2246, Found: 619.2239.

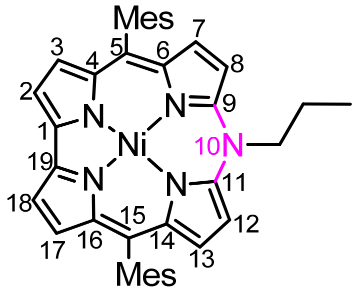

3r: yield, 12.9 mg (39%) ^{1}H NMR (600 MHz, CDCl$_3$, 300 K) δ: 8.24 (d, ^{3}J=4.2 Hz, 2H, 2,18-pyrr), 8.19 (d, ^{3}J=4.6 Hz, 2H, 7,13-pyrr), 8.03 (d, ^{3}J=4.2 Hz, 2H, 3,17-pyrr), 7.86 (d, ^{3}J=4.6 Hz, 2H, 8,12-pyrr), 7.15 (s, 4H, *m*-Mes), 5.69 (t, ^{3}J=8.1 Hz, 2H, -CH$_2$-), 5.83 (m, ^{3}J=8.1 Hz, 2H, -CH$_2$-), 2.52 (m, 6H, *p*-Me), 1.9 (s, 12H, *o*-Me), 1.24 (t, ^{3}J=8.1 Hz, 3H, -CH$_3$). ^{13}C NMR (150 MHz, CDCl$_3$, 300 K) δ_C = 144.4, 142.9, 138.5, 137.4, 135.3, 133.0, 132.8, 132.2, 127.6, 127.5, 124.8, 116.8, 111.1, 55.6, 25.4, 21.4, 20.9. UV-vis (CH$_2$Cl$_2$) λ_{max}/nm (logε): 395 (4.90), 440 (4.35), 493 (3.75), 563 (3.82), 587 (3.75), 632 (3.83). ESI-HRMS calc. for $C_{39}H_{37}N_5Ni[M]^+$: 633.2402, Found: 633.2370.

A solution of **1** (30 mg, 0.052 mmol) and *p*-anisidine **2s** (29 mg, 0.234 mmol) in 5 ml anhydrous CH$_2$Cl$_2$ was stirred at room temperature in the presence of isoamyl nitrite (21 mg, 0.18 mmol) for 30 min. The reaction mixture was the passed through a short silica gel column with CH$_2$Cl$_2$ as eluent to collect all the moveable fraction, then the solvent was evaporated under vacuum. The residue was purified by silica preparative thin layer plate (1 mm, 20 x 20 cm) with petroleum ether/ CH$_2$Cl$_2$ (*v*/*v* = 4:1) as eluent to afford product **3s.**

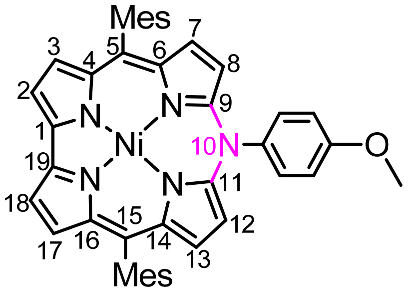

3s: yield, 10.9 mg (30%) ^{1}H NMR (600 MHz, $CDCl_3$, 300 K) δ: 8.28 (d, ^3J=4.2 Hz, 2H, 2,18-pyrr), 8.07 (d, ^3J=4.6 Hz, 2H, 7,13-pyrr), 7.89 (d, ^3J=4.2 Hz, 2H, 3,17-pyrr), 7.74 (m, 2H, 2,6-(4-OCH_3Ph)), 7.28 (d, ^3J=4.6 Hz, 2H, 8,12-pyrr), 7.19 (m, 2H, 3,5-(4-OCH_3Ph)), 7.13 (s, 4H, *m*-Mes), 4.01 (s, 3H, -O-CH_3) 2.51 (m, 6H, *p*-Me), 1.92 (s, 12H, *o*-Me). ^{13}C NMR (150 MHz, $CDCl_3$, 300 K) δ_C = 160.6, 144.4, 144.2, 138.5, 137.4, 135.3, 135.2, 133.2, 132.8, 131.5, 130.8, 127.9, 127.6, 124.9, 116.8, 114.0, 113.5, 55.8, 21.4, 20.9. UV-vis (CH_2Cl_2) λ_{max}/nm (logε): 395 (4.94), 437 (4.36), 497 (3.78), 564 (3.87), 585 (3.86), 629 (3.80). ESI-HRMS calc. for $C_{43}H_{37}N_5NiO[M]^+$: 697.2352, Found: 697.2371.

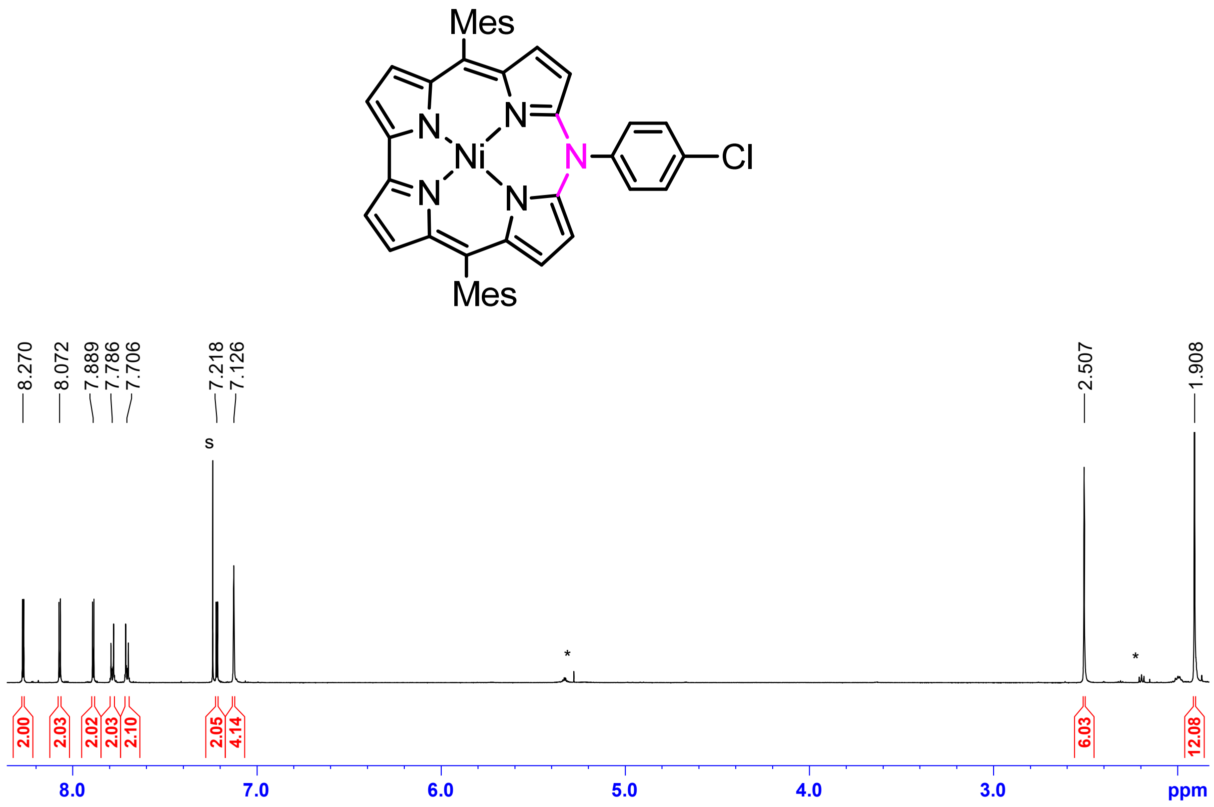

Figure S1. ^{1}H NMR spectrum (600 MHz, $CDCl_3$, 300 K) of **3a**.

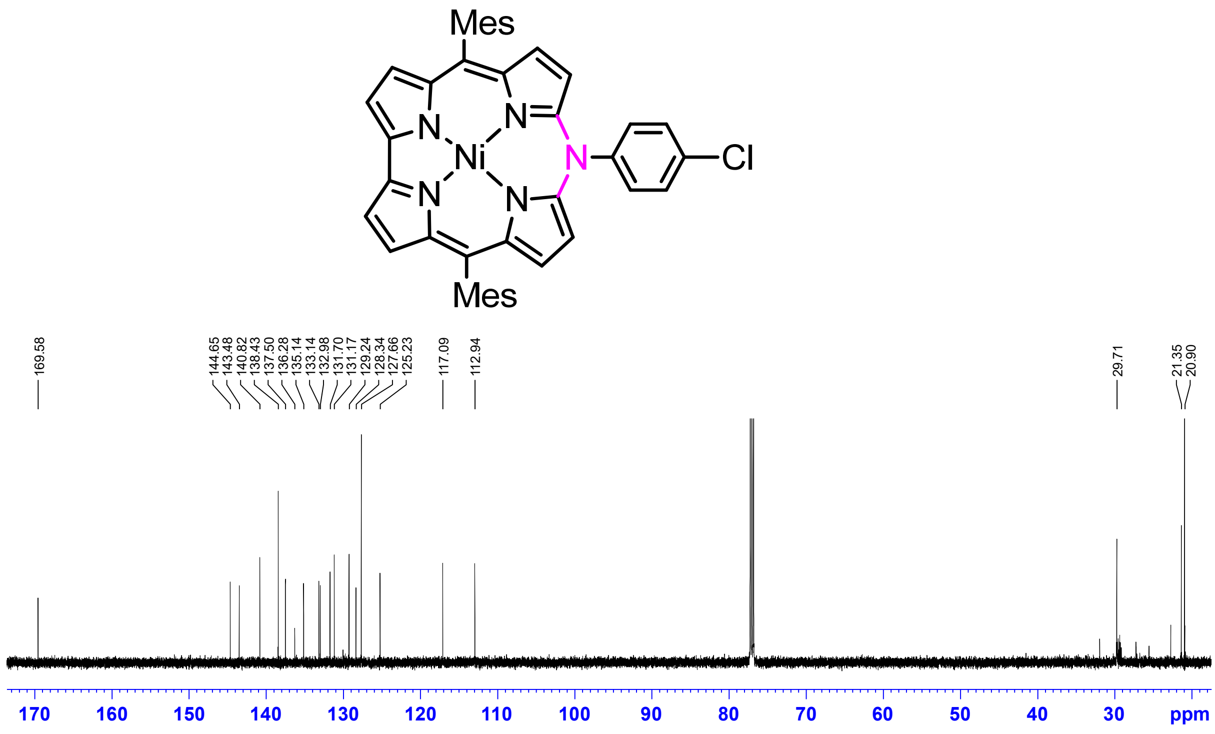

Figure S2. ^{13}C NMR spectrum (150 MHz, $CDCl_3$, 300 K) of **3a**.

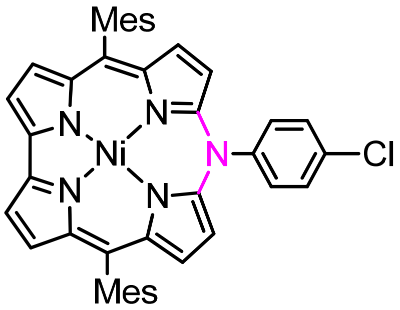

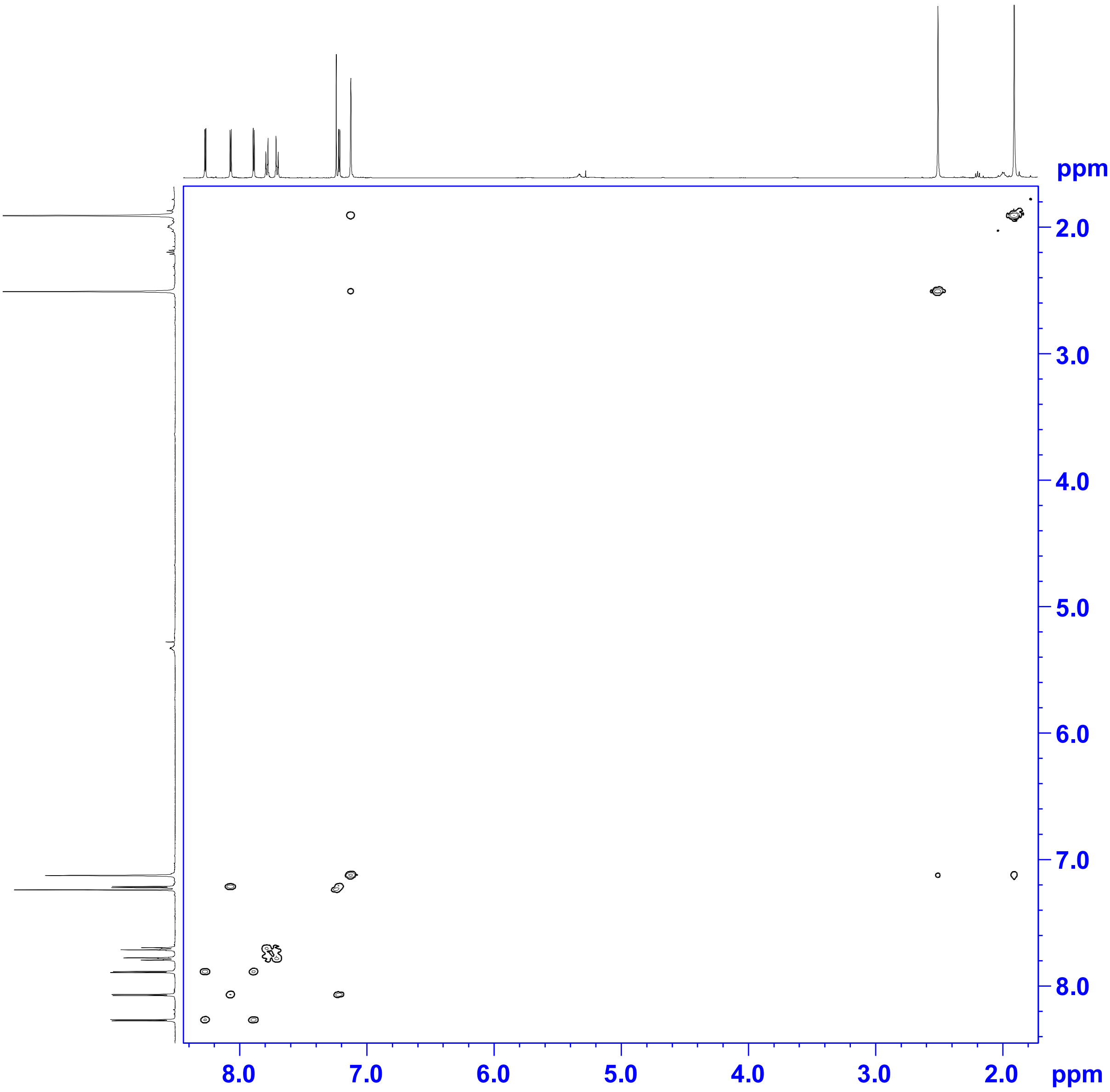

Figure S3. ^{1}H,^{1}H COSY spectrum (500 MHz, $CDCl_3$, 300 K) of **3a**.

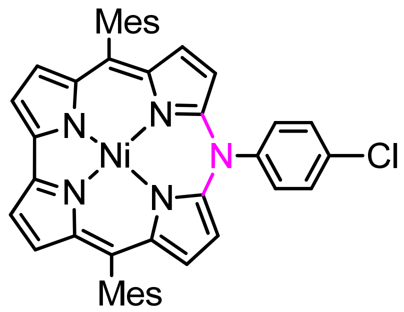

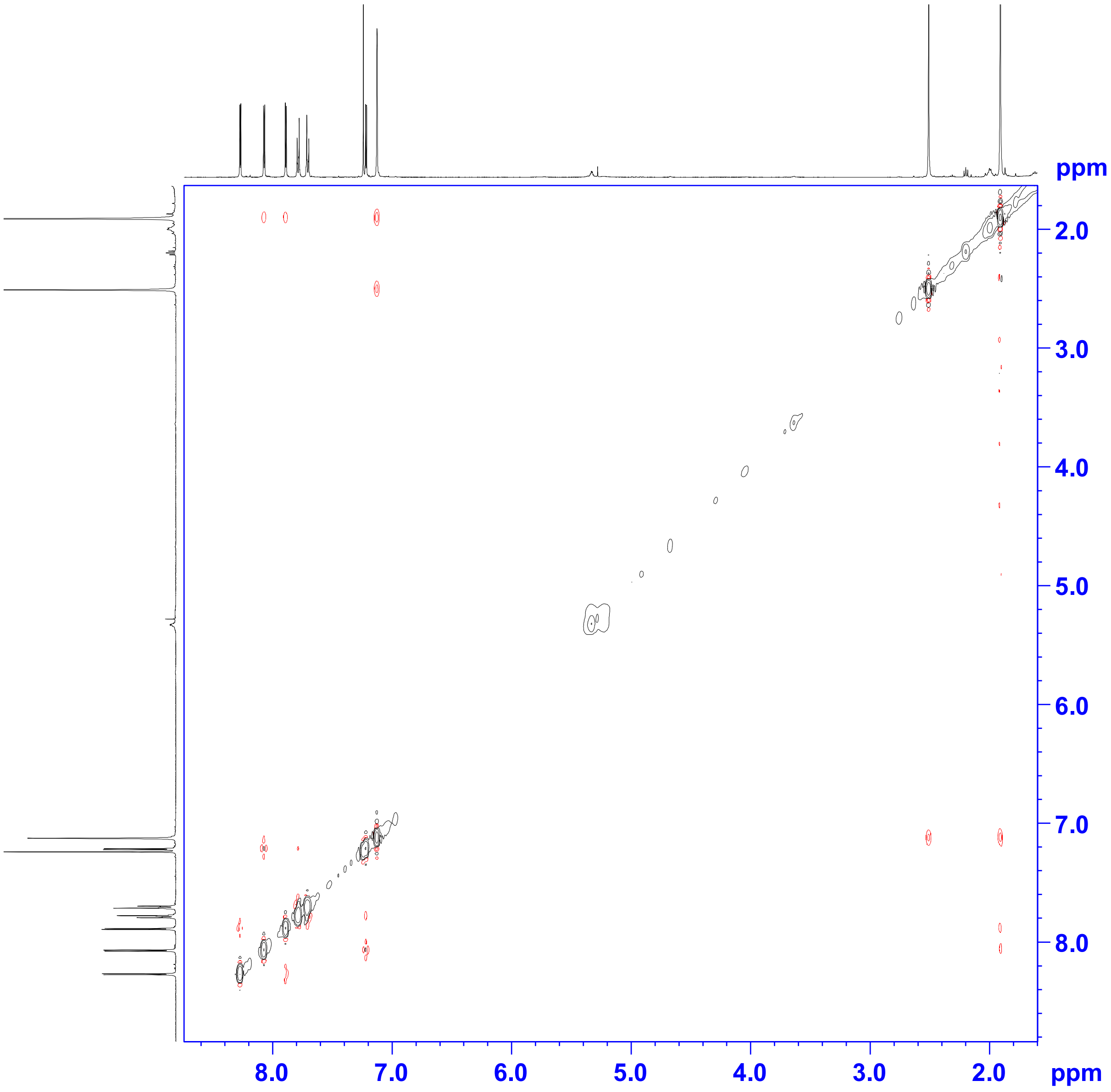

Figure S4. ^{1}H,^{1}H NOESY spectrum (600 MHz, CDCl$_3$, 300 K) of **3a**.

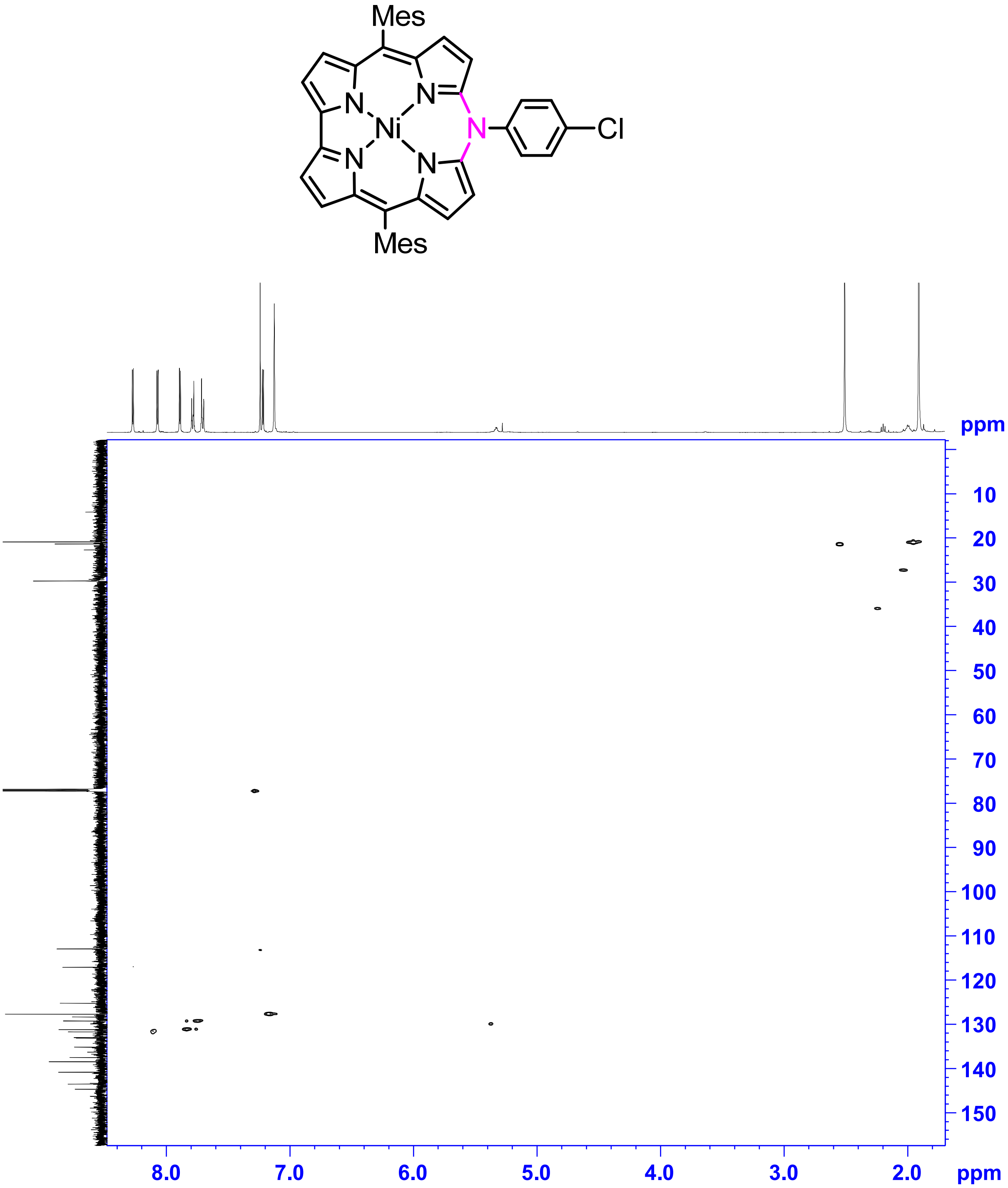

Figure S5. ^{1}H,^{13}C HSQC spectrum (500/125 MHz, CDCl$_3$, 300 K) of **3a**.

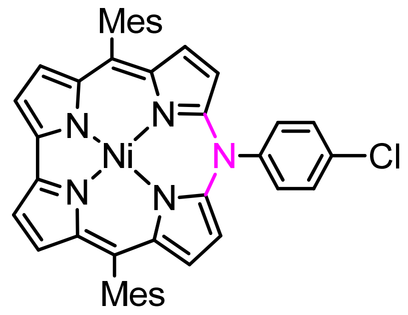

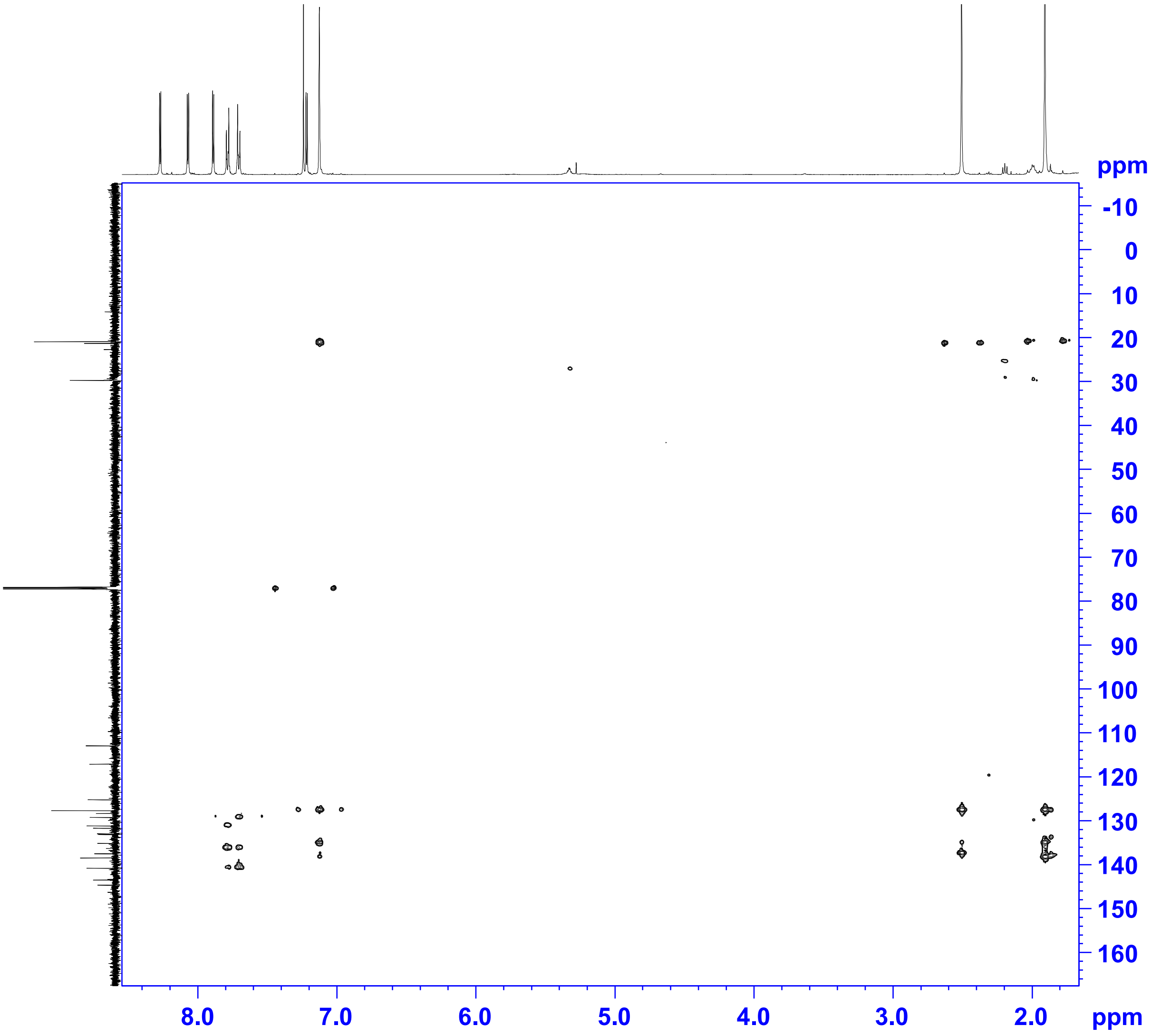

Figure S6. $^1H,^{13}C$ HMBC spectrum (500/125 MHz, $CDCl_3$, 300 K) of **3a**.

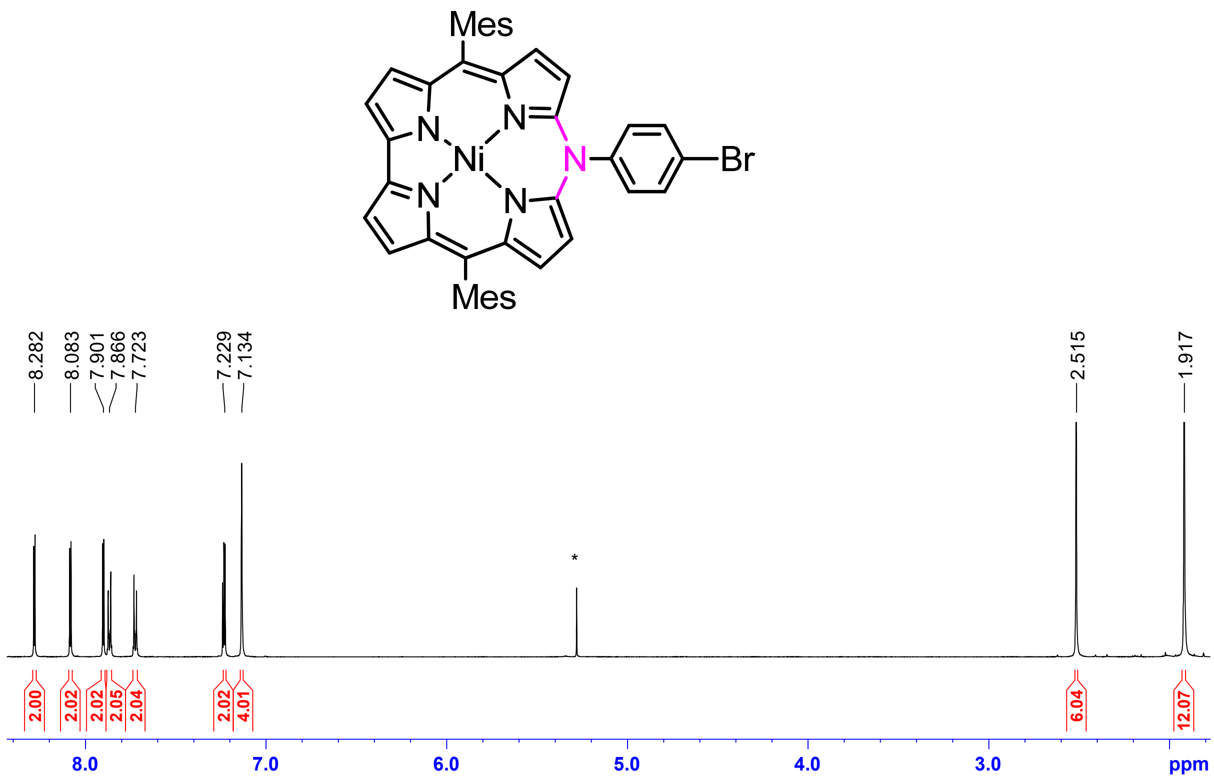

Figure S7. ^{1}H NMR spectrum (600 MHz, CDCl$_3$, 300 K) of **3b**.

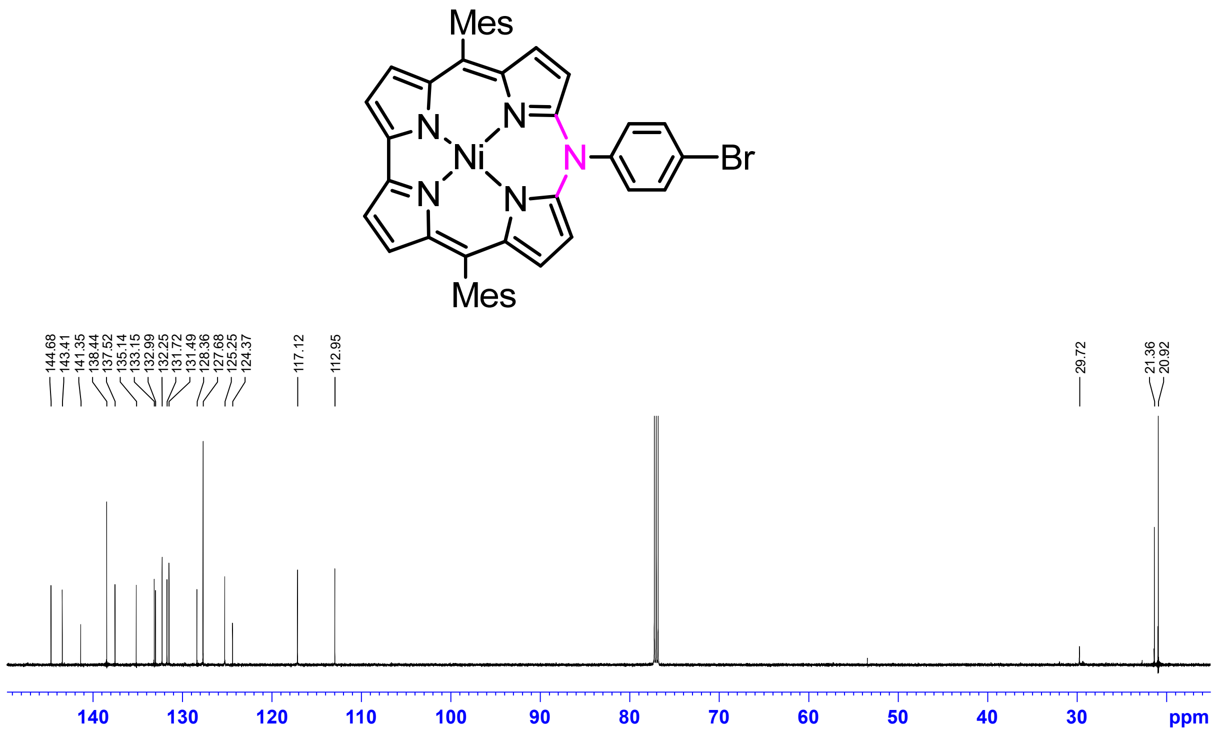

Figure S8. ^{13}C NMR spectrum (150 MHz, CDCl$_3$, 300 K) of **3b**.

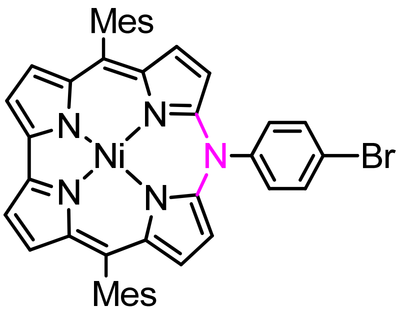

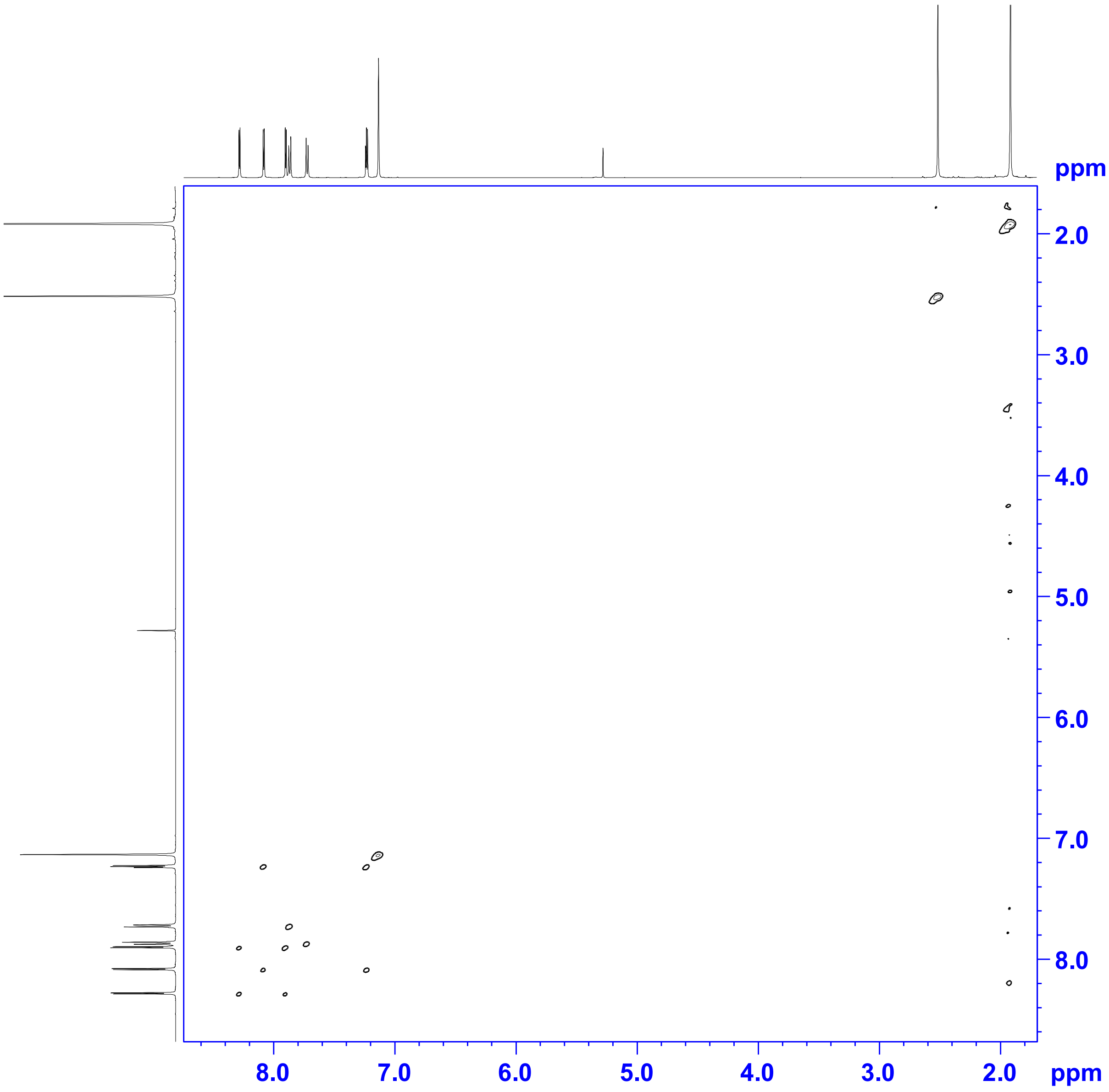

Figure S9. ^{1}H,^{1}H COSY spectrum (500 MHz, CDCl$_3$, 300 K) of **3b**.

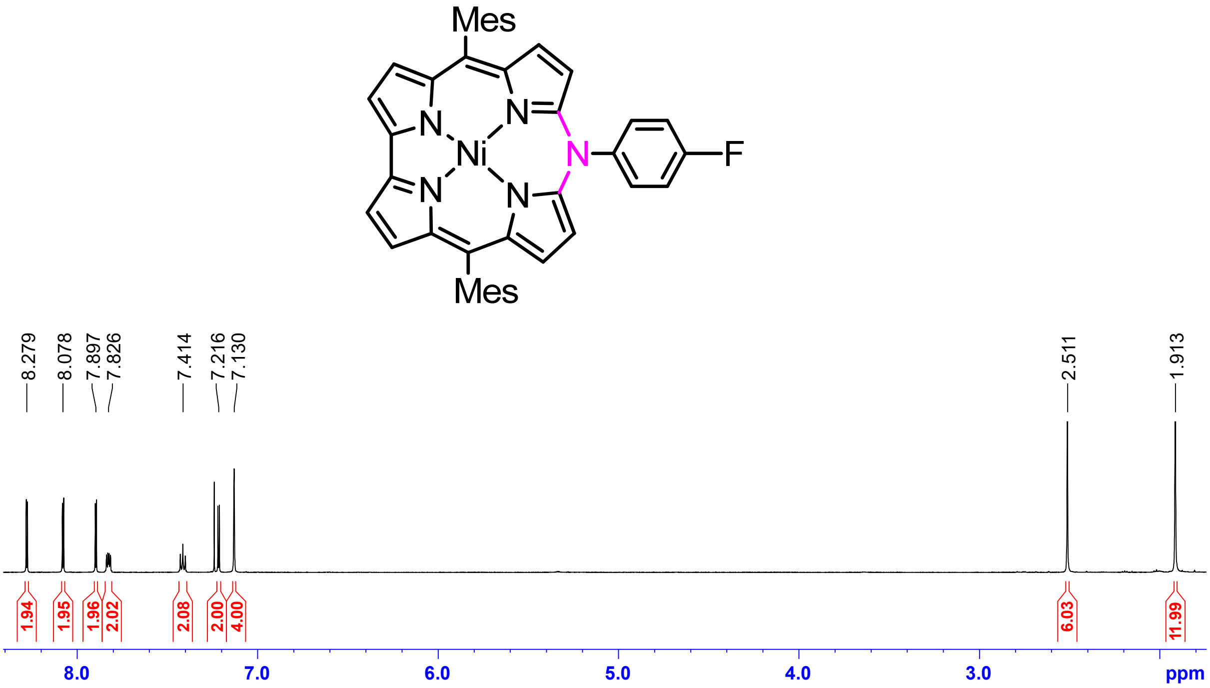

Figure S10. ^{1}H NMR spectrum (600 MHz, $CDCl_3$, 300 K) of **3c**.

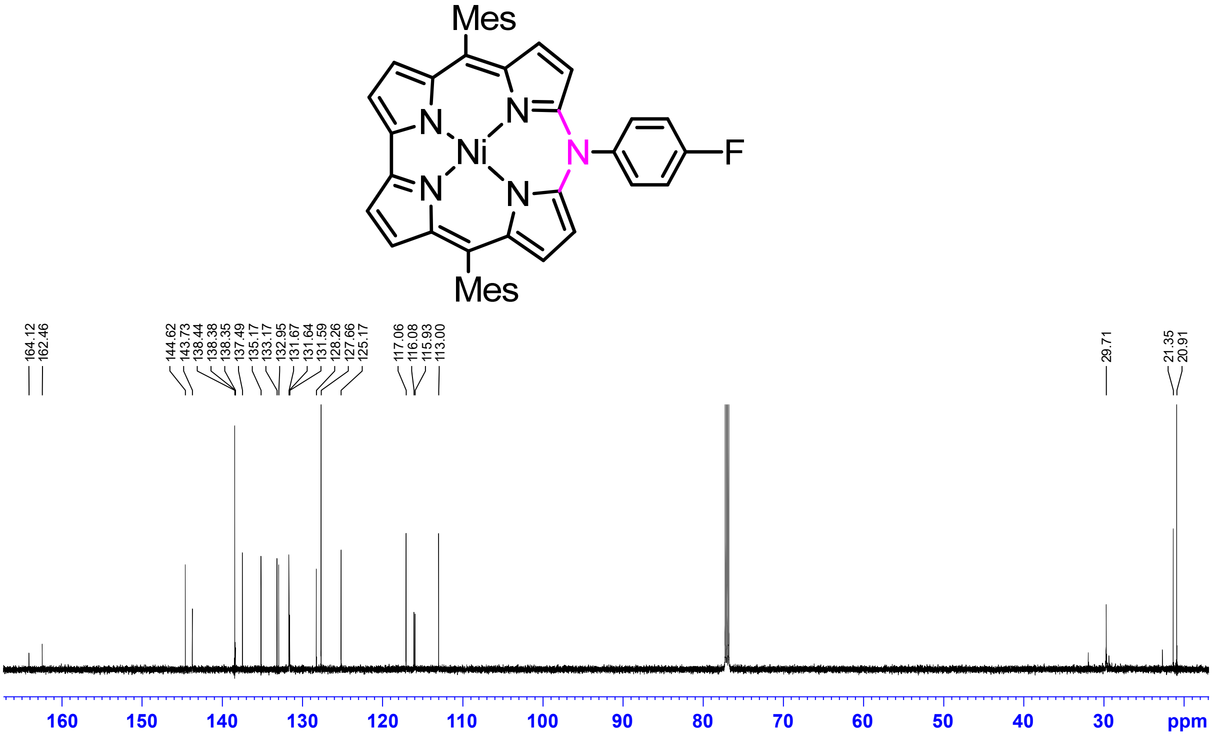

Figure S11. ^{13}C NMR spectrum (150 MHz, $CDCl_3$, 300 K) of **3c**.

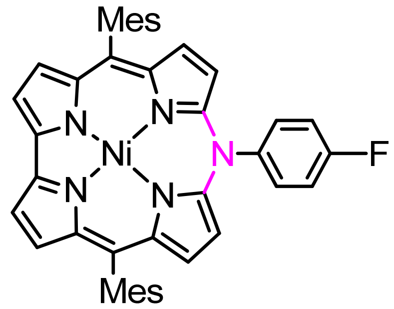

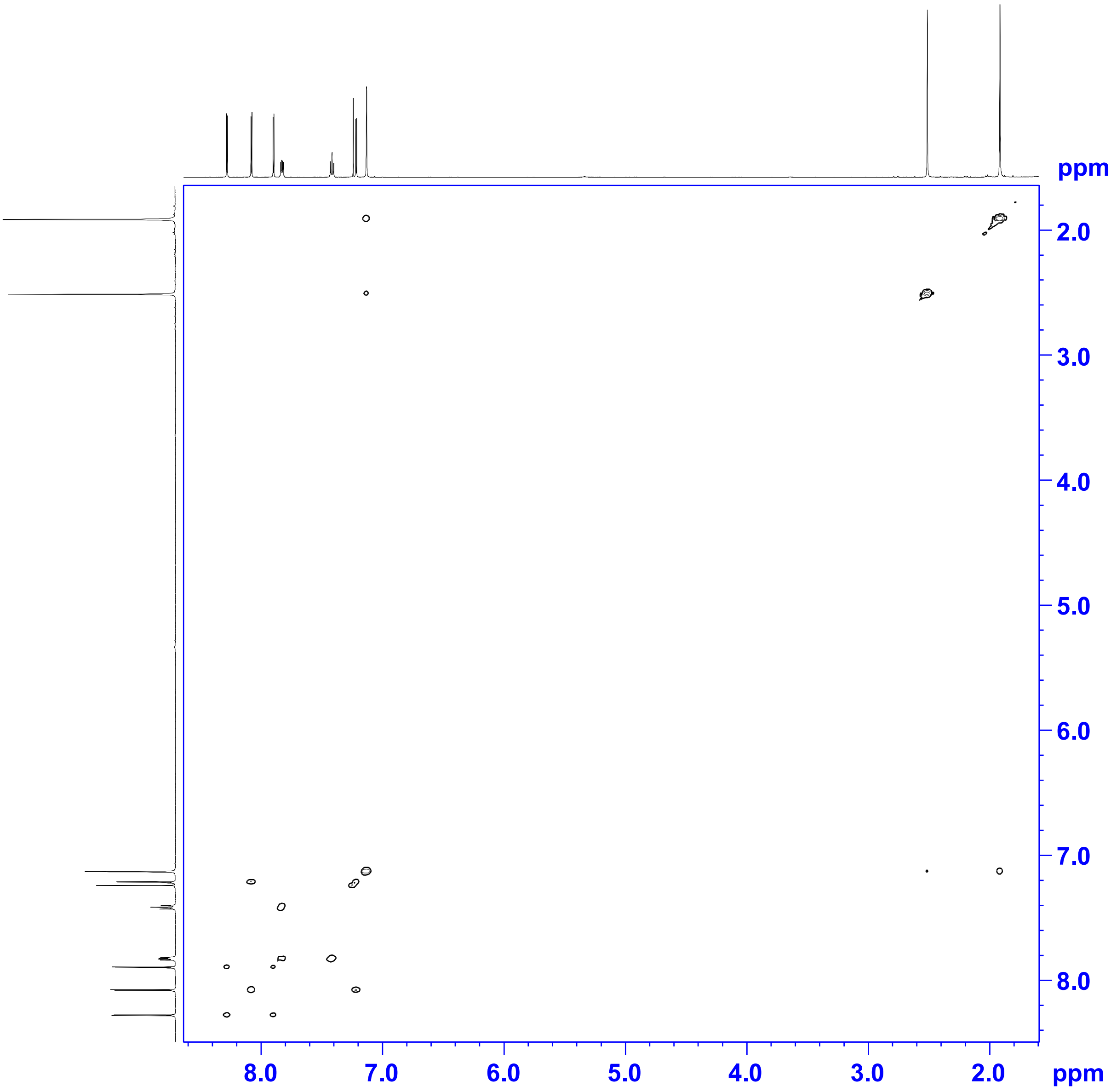

Figure S12. $^{1}H,^{1}H$ COSY spectrum (500 MHz, $CDCl_3$, 300 K) of **3c**.

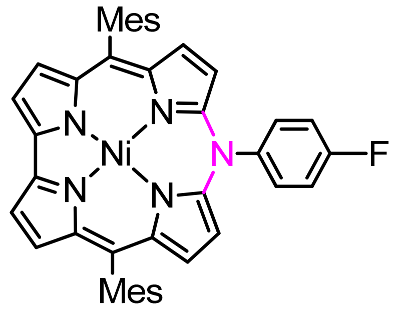

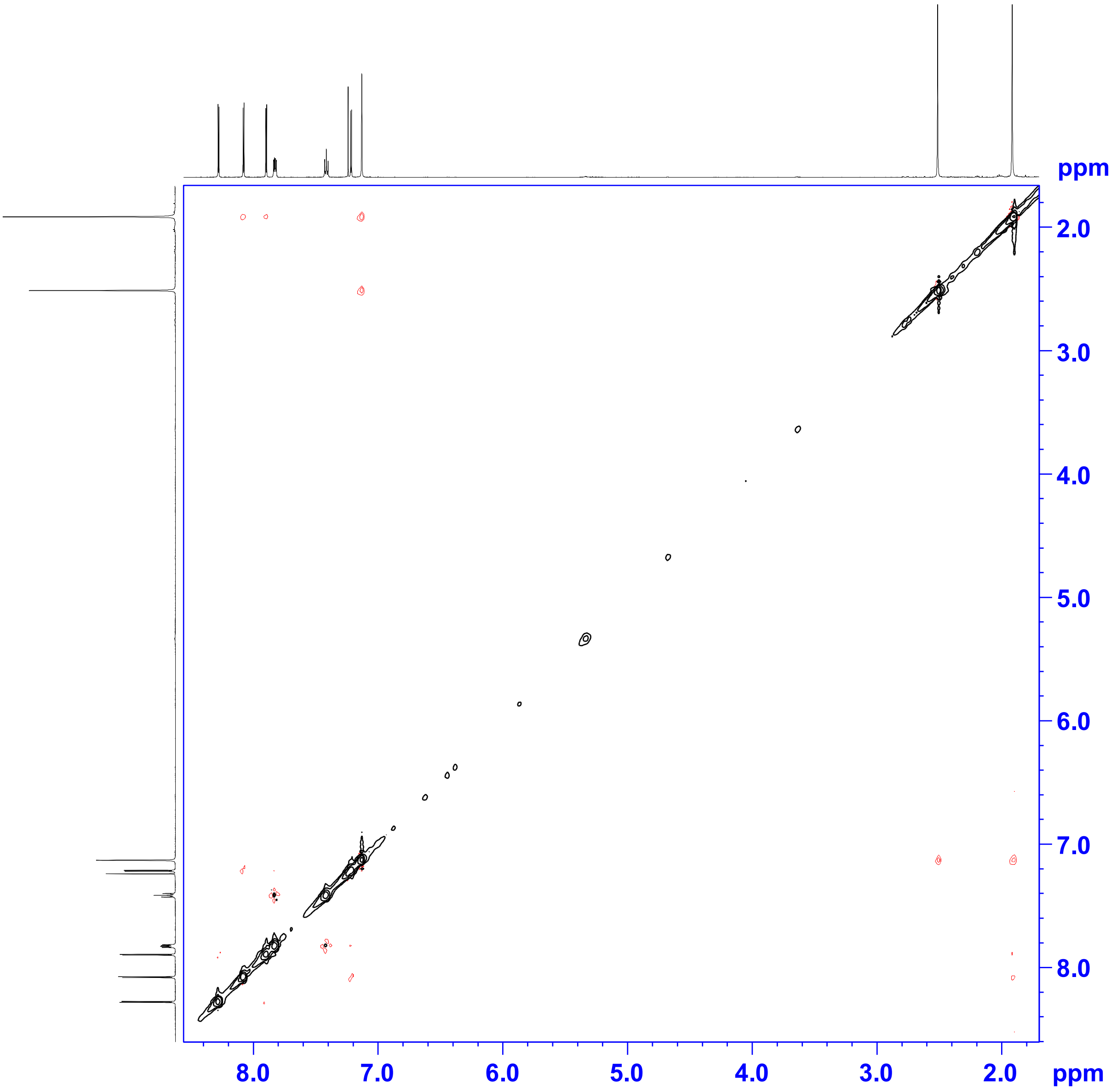

Figure S13. ^{1}H,^{1}H NOESY spectrum (600 MHz, CDCl$_3$, 300 K) of **3c**.

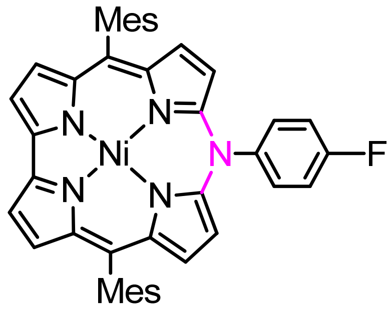

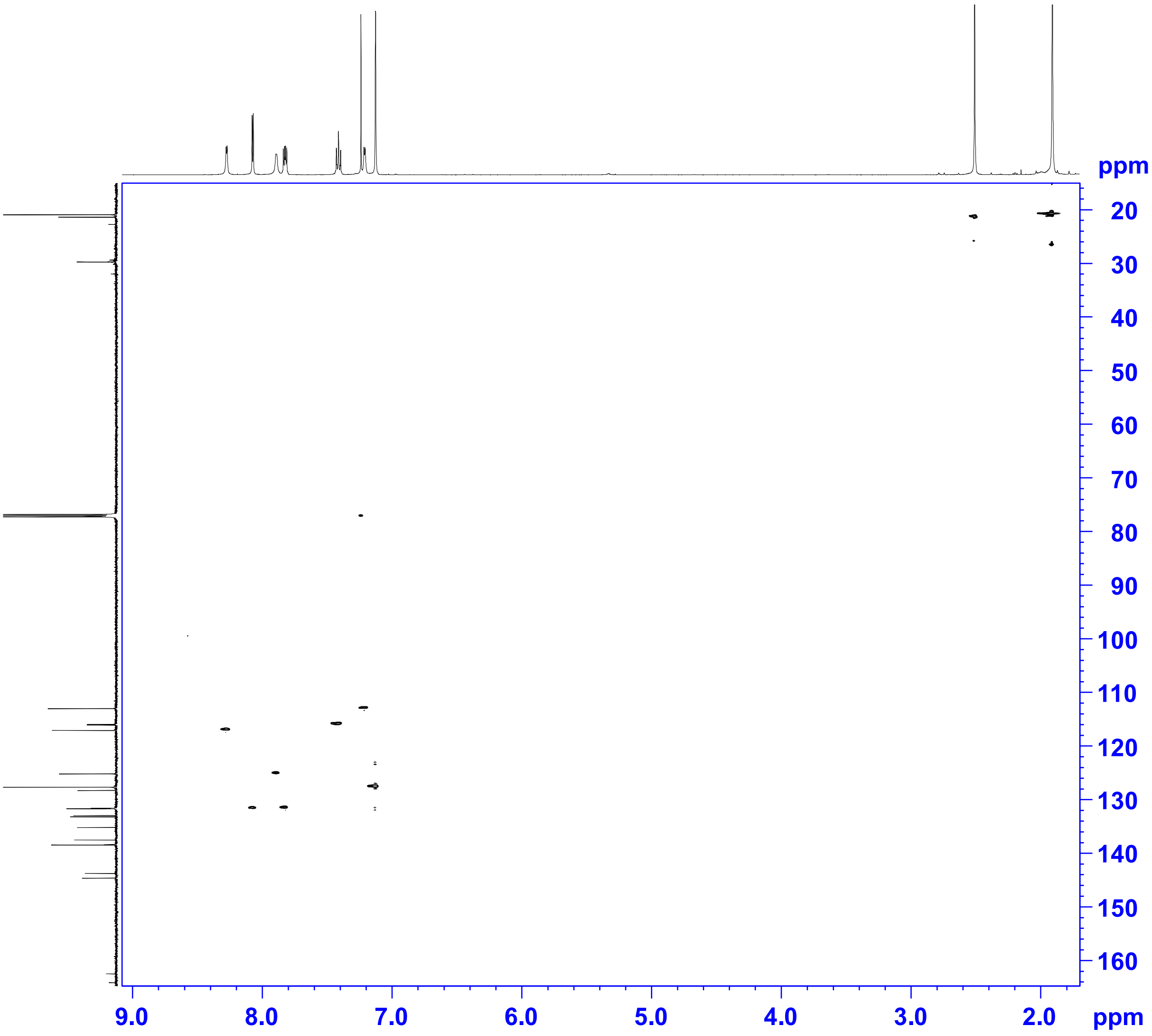

Figure S14. ^{1}H,^{13}C HSQC spectrum (600/150 MHz, CDCl$_3$, 300 K) of **3c**.

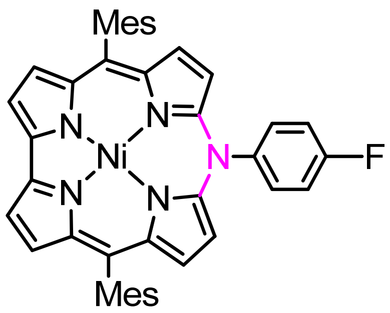

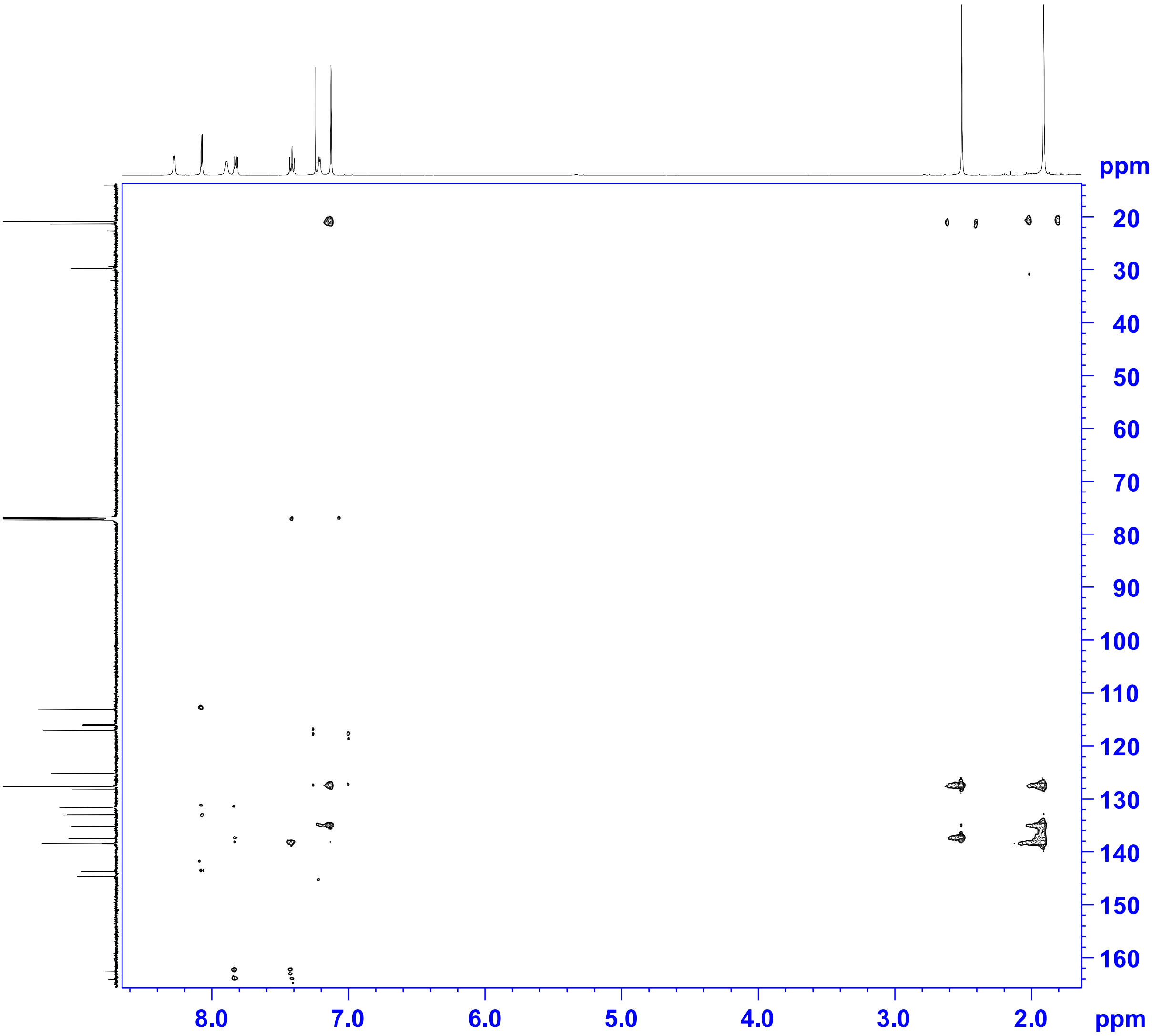

Figure S15. $^1H,^{13}C$ HMBC spectrum (600/150 MHz, $CDCl_3$, 300 K) of **3c**.

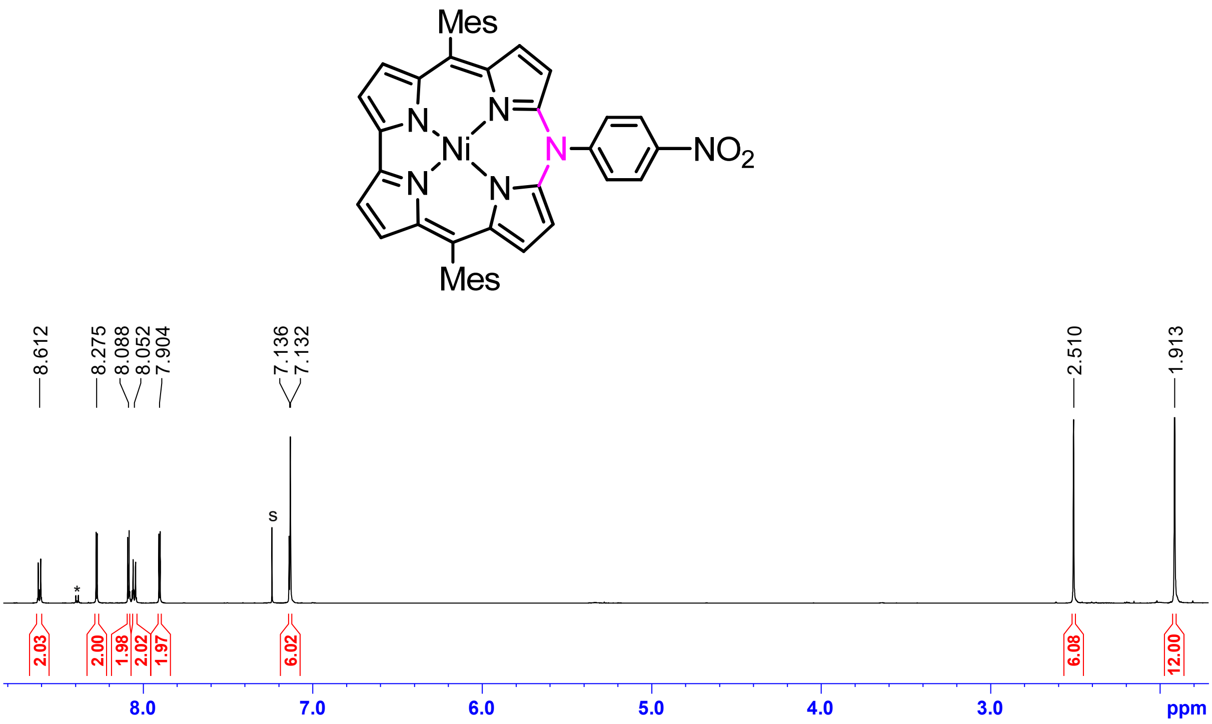

Figure S16. ^{1}H NMR spectrum (600 MHz, $CDCl_3$, 300 K) of **3d**.

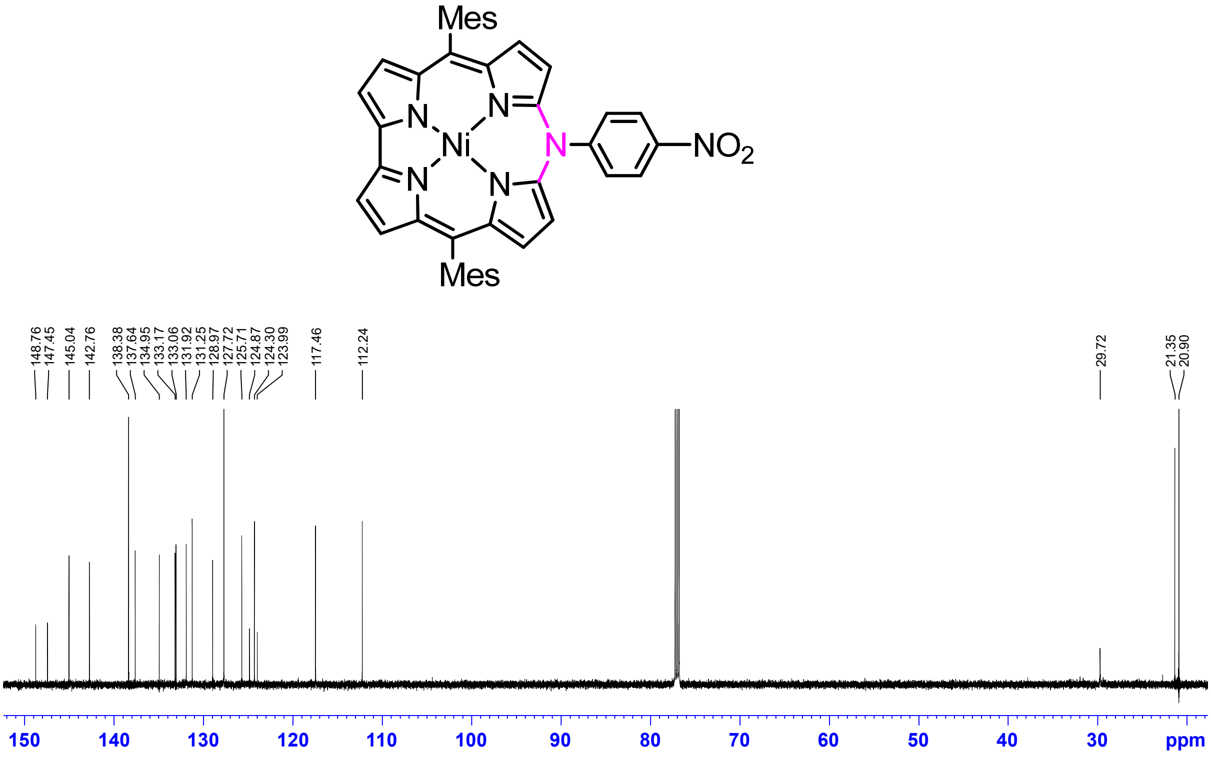

Figure S17. ^{13}C NMR spectrum (150 MHz, $CDCl_3$, 300 K) of **3d**.

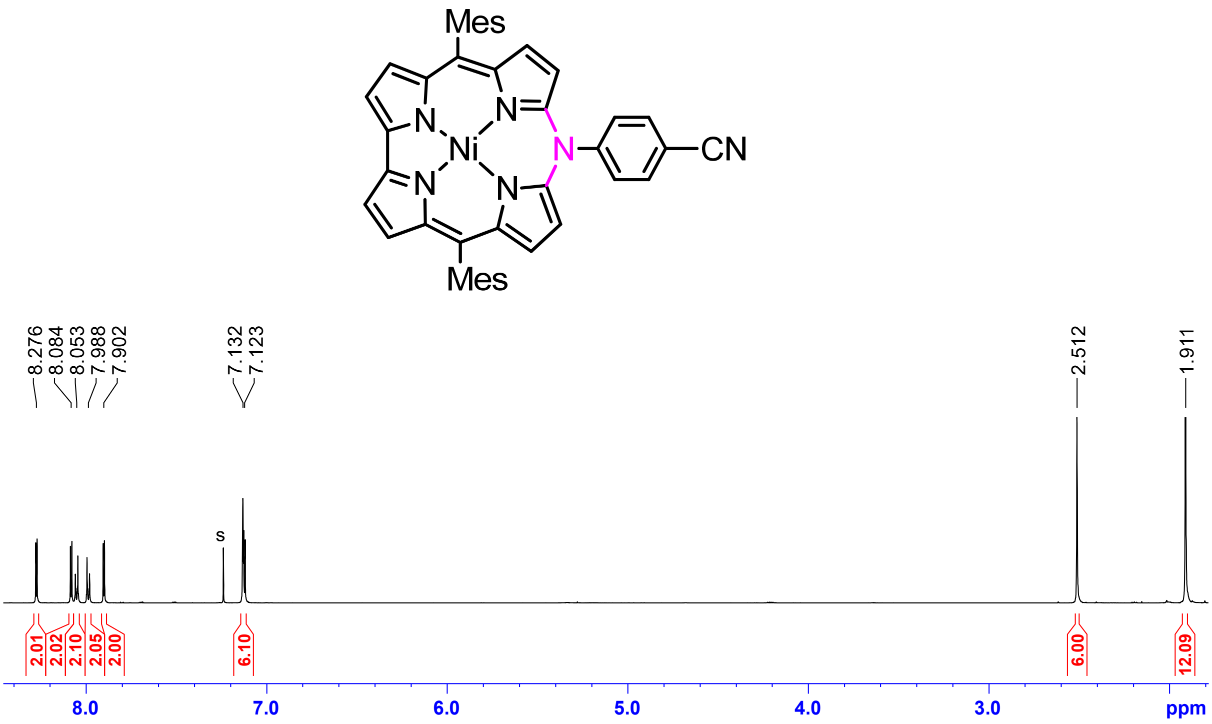

Figure S18. ^{1}H NMR spectrum (600 MHz, CDCl$_3$, 300 K) of **3e**.

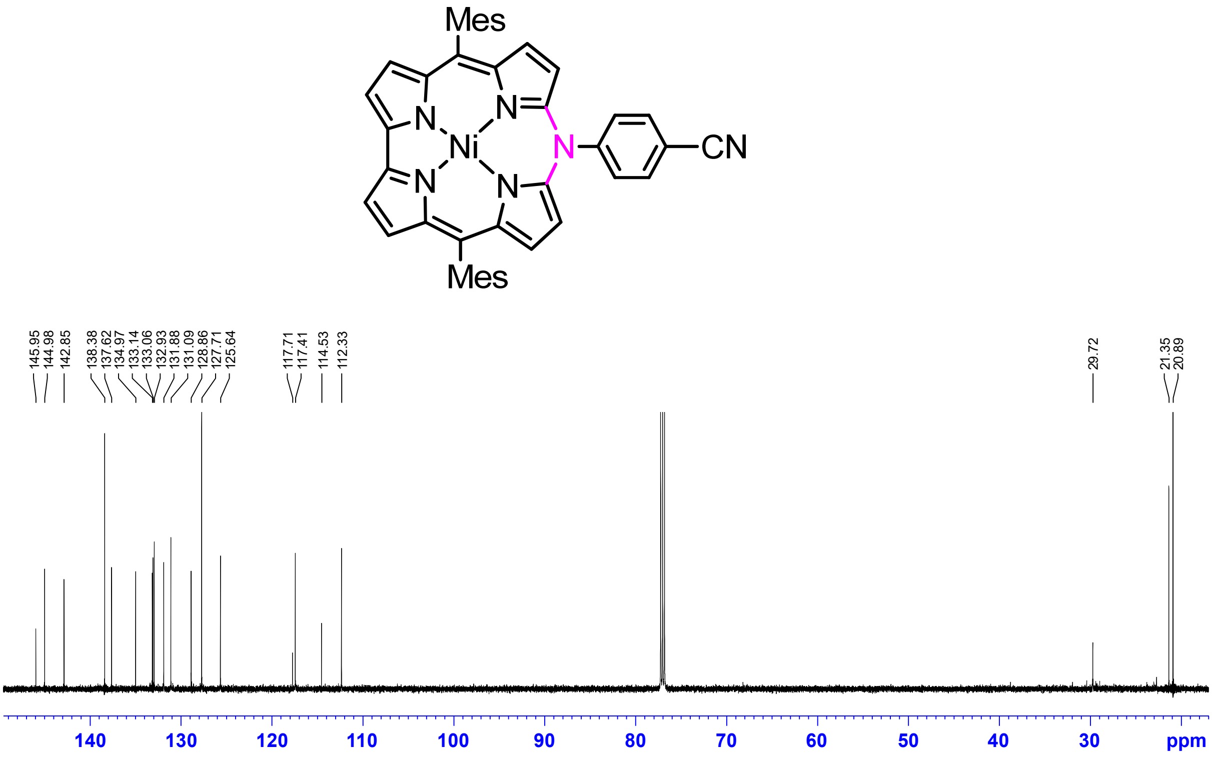

Figure S19. ^{13}C NMR spectrum (150 MHz, CDCl$_3$, 300 K) of **3e**.

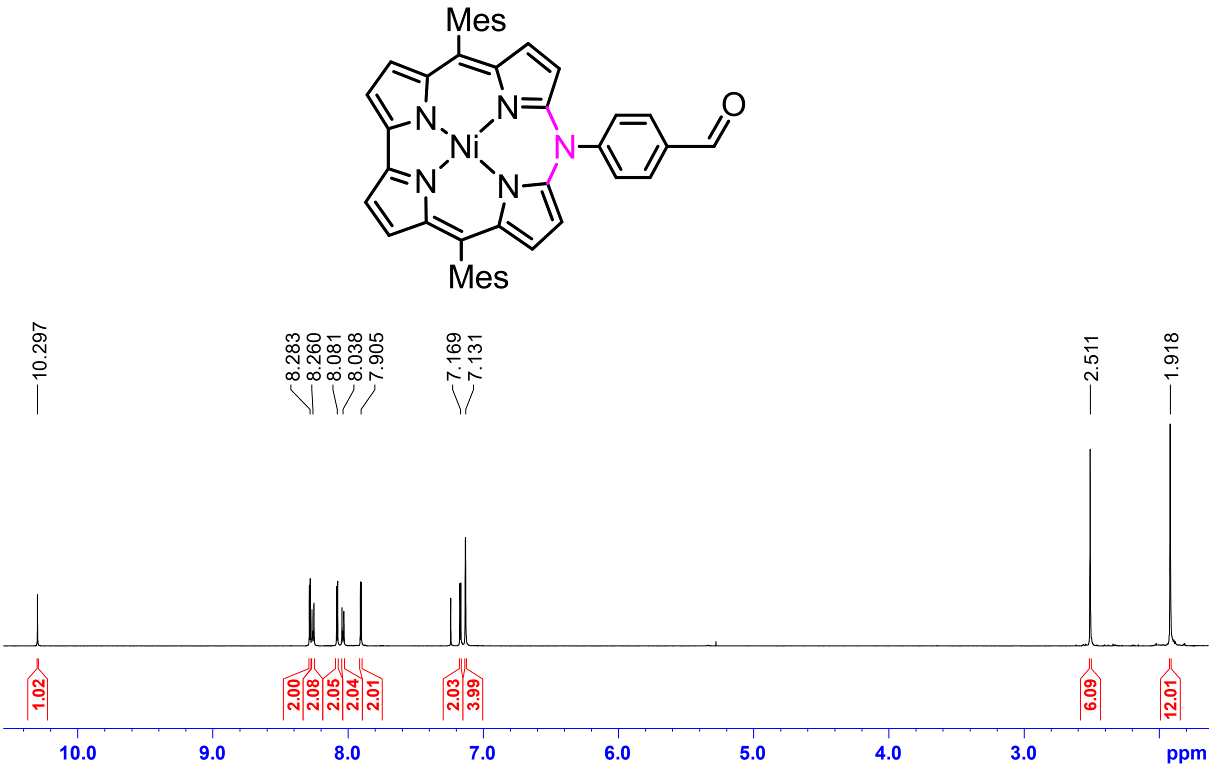

Figure S20. ^{1}H NMR spectrum (600 MHz, $CDCl_3$, 300 K) of **3f**.

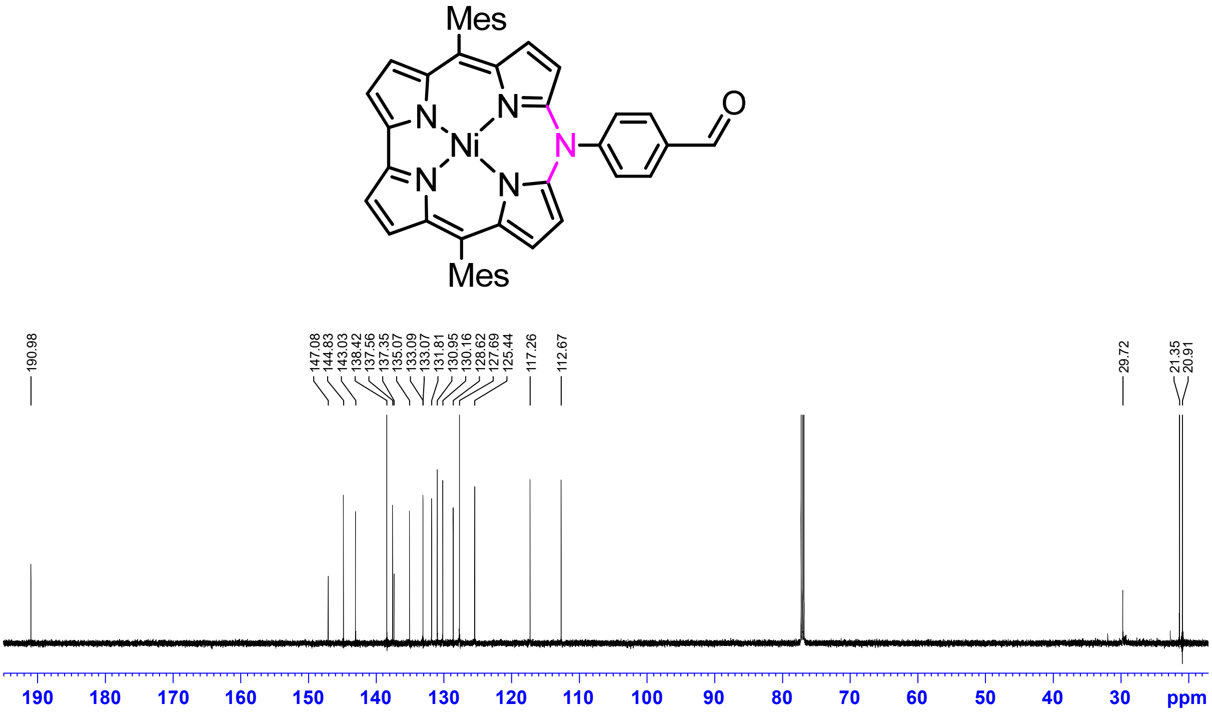

Figure S21. ^{13}C NMR spectrum (150 MHz, $CDCl_3$, 300 K) of **3f**.

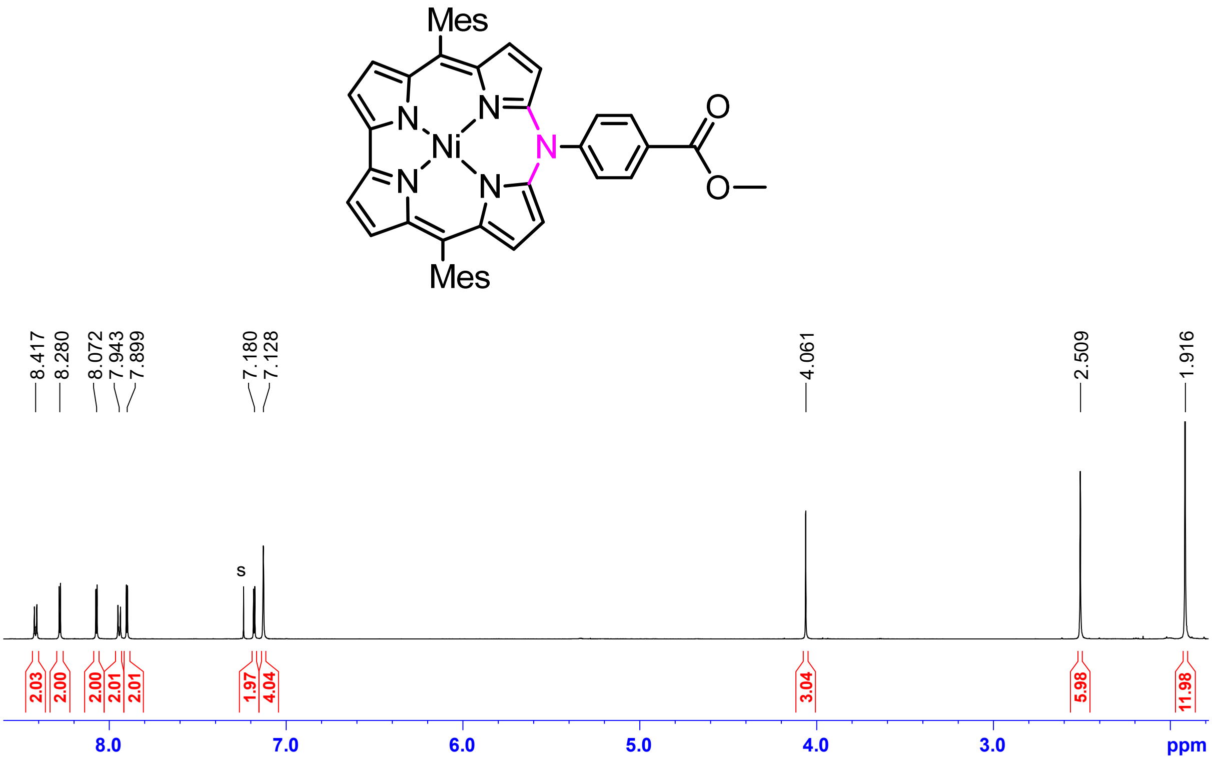

Figure S22. ^{1}H NMR spectrum (600 MHz, $CDCl_3$, 300 K) of **3g**.

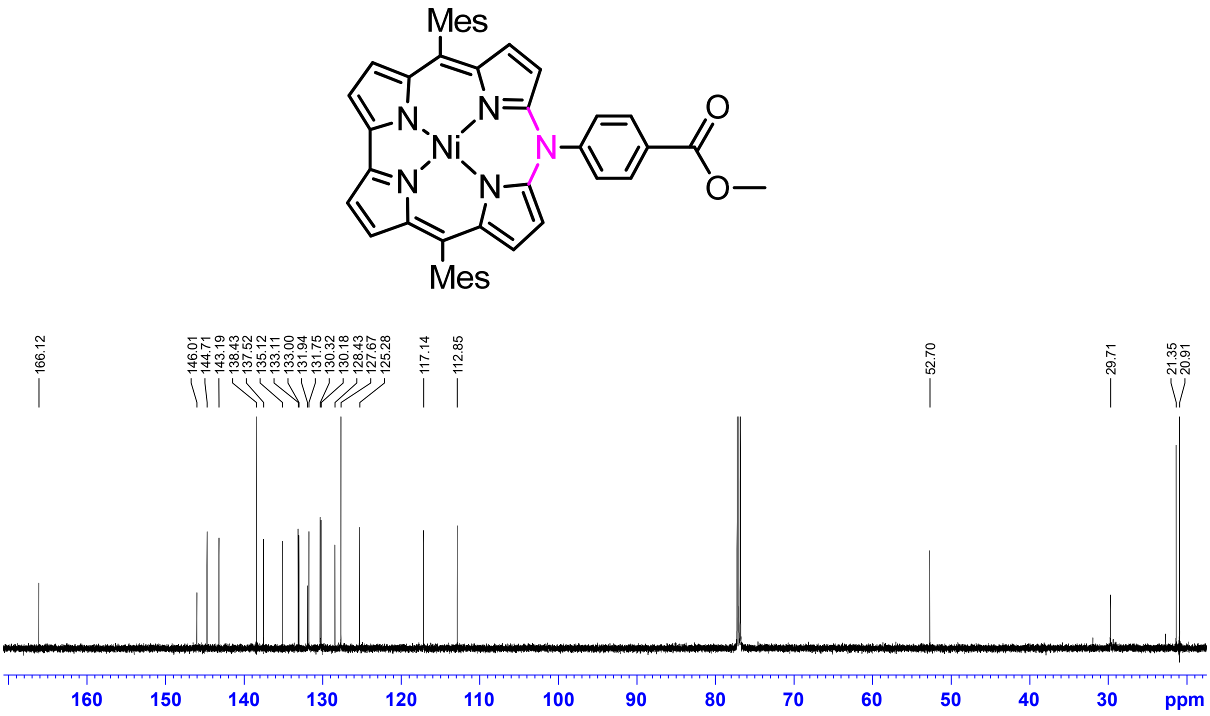

Figure S23. ^{13}C NMR spectrum (150 MHz, $CDCl_3$, 300 K) of **3g**.

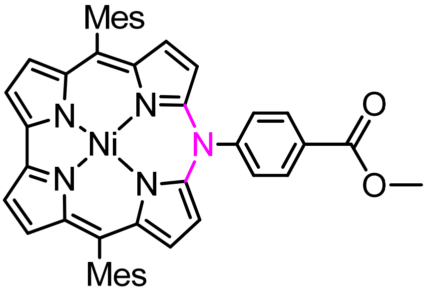

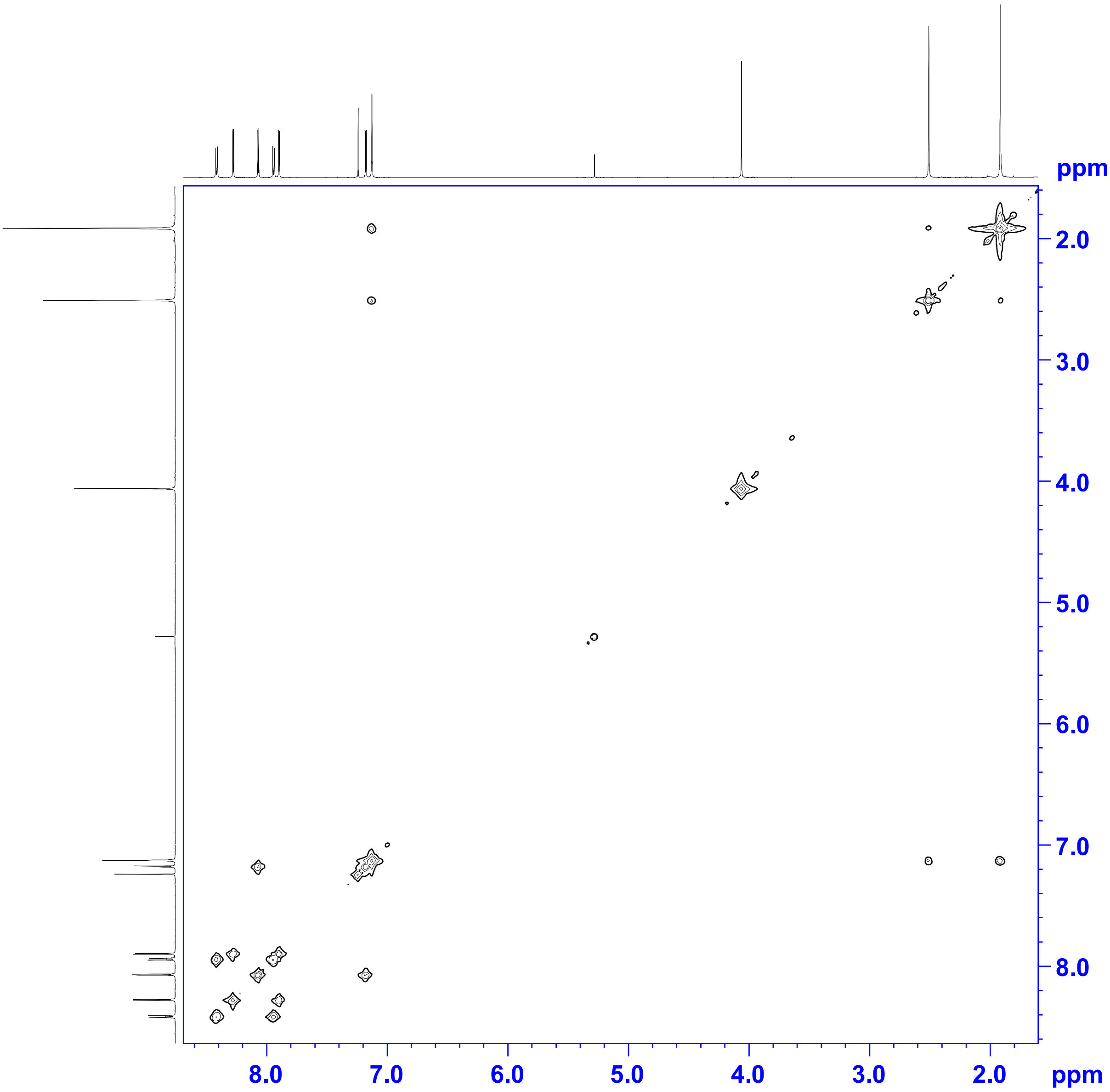

Figure S24. $^1H,^1H$ COSY spectrum (600 MHz, $CDCl_3$, 300 K) of **3g**.

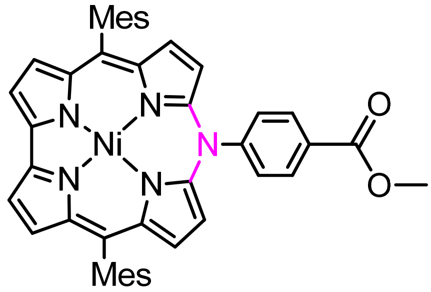

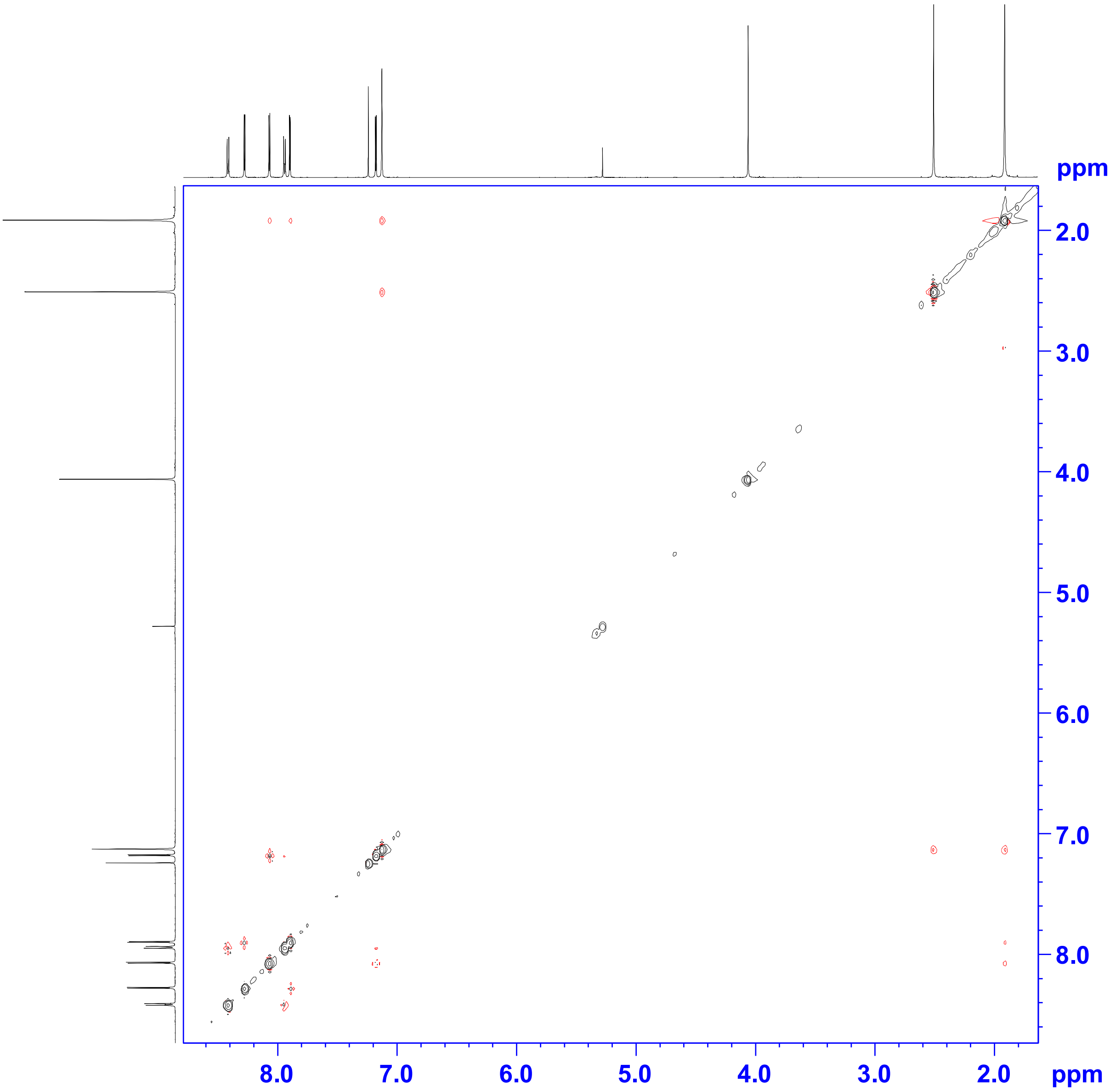

Figure S25. $^{1}H,^{1}H$ NOESY spectrum (600 MHz, $CDCl_3$, 300 K) of **3g**.

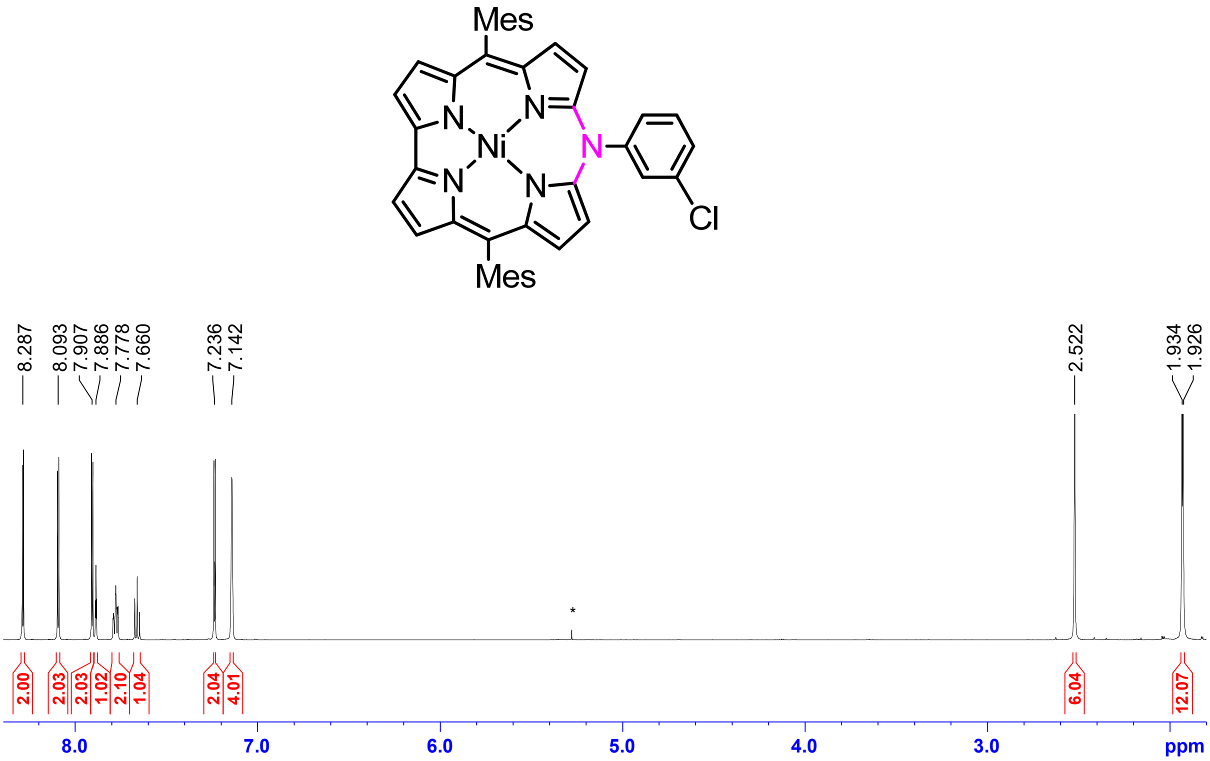

Figure S26. ^{1}H NMR spectrum (600 MHz, $CDCl_3$, 300 K) of **3h**.

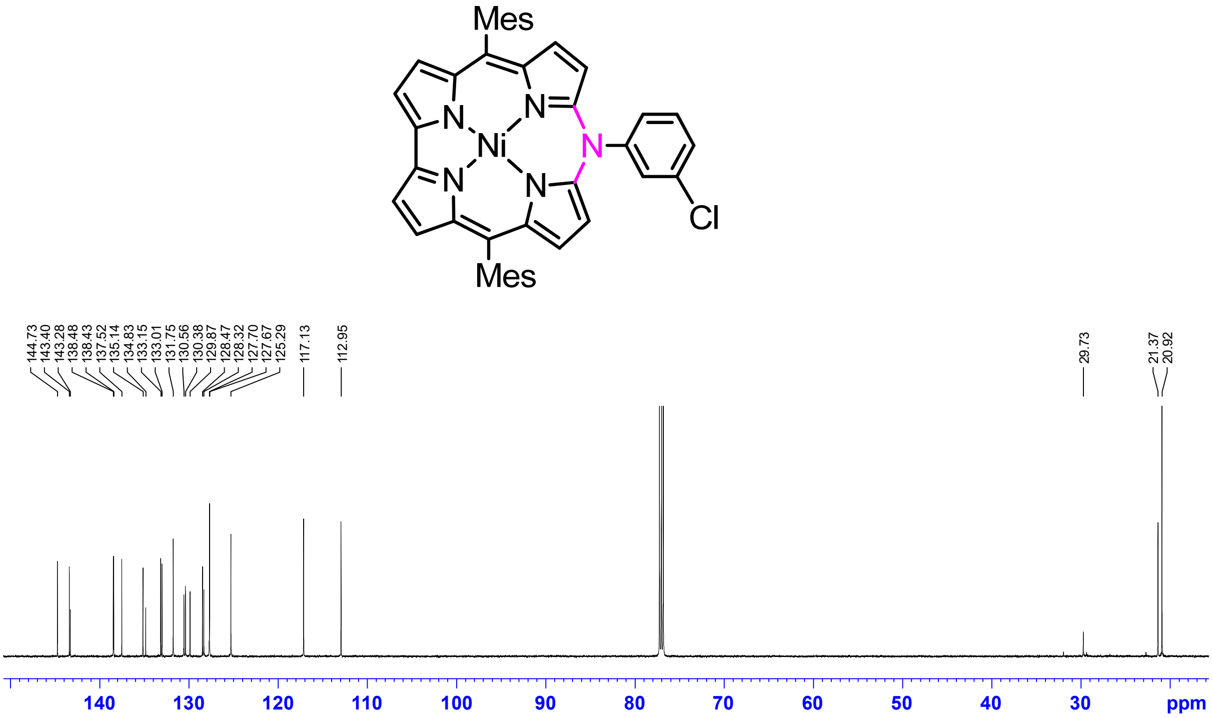

Figure S27. ^{13}C NMR spectrum (150 MHz, $CDCl_3$, 300 K) of **3h**.

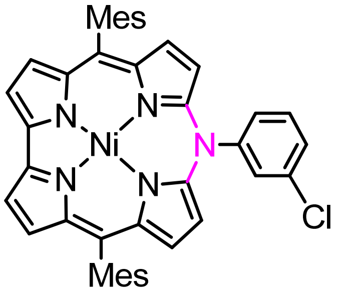

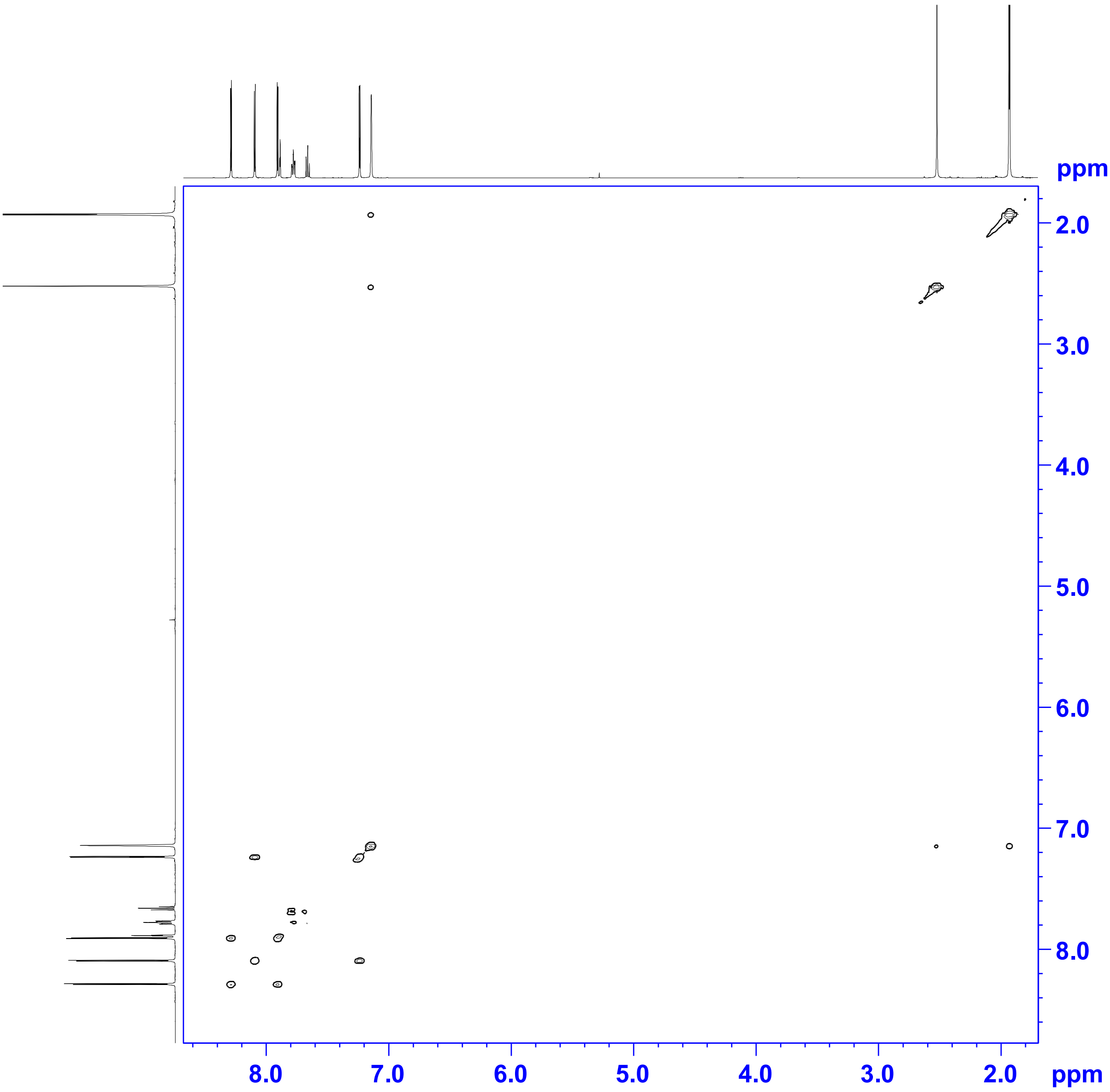

Figure S28. $^1H,^1H$ COSY spectrum (500 MHz, $CDCl_3$, 300 K) of **3h**.

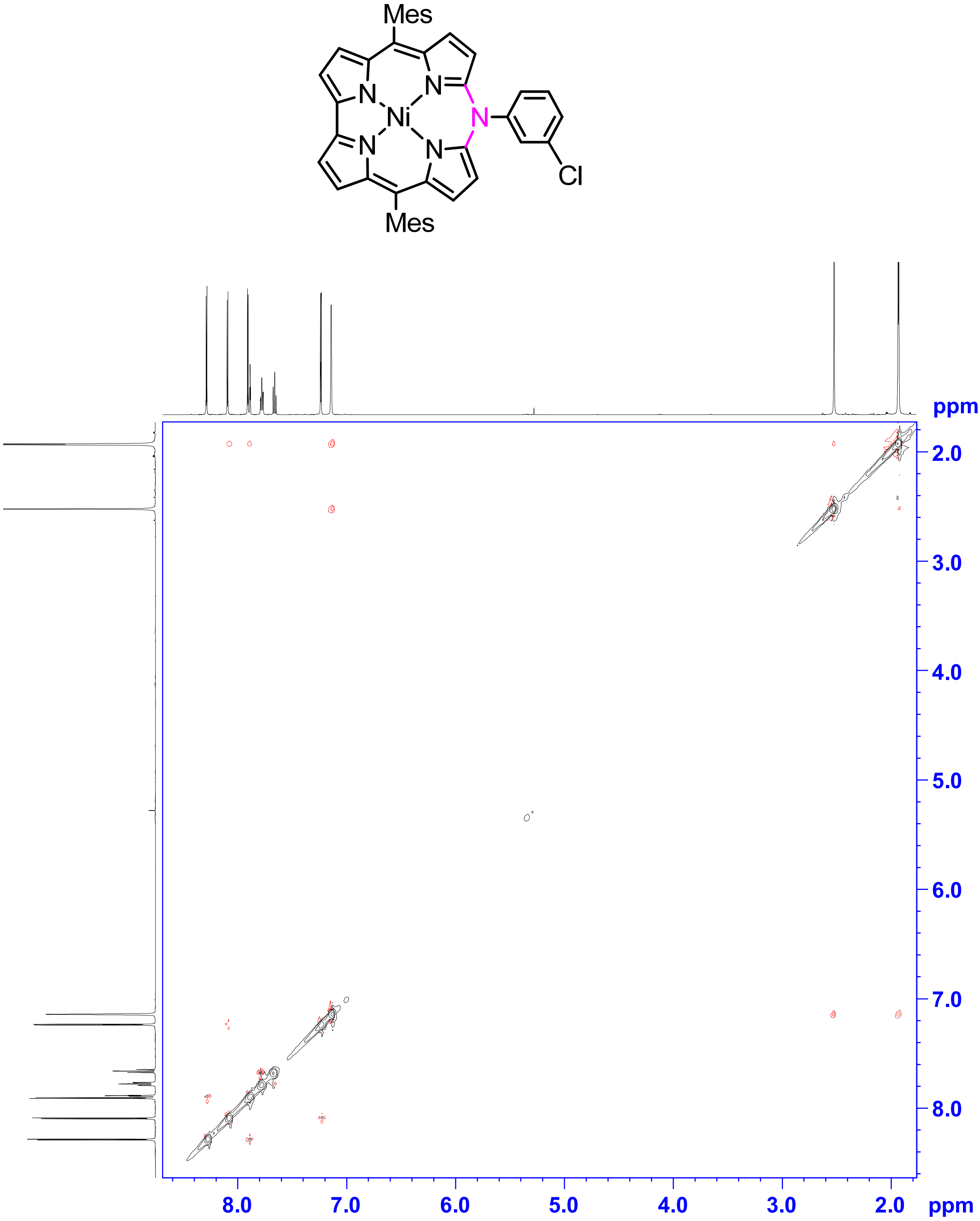

Figure S29. $^{1}H,^{1}H$ NOESY spectrum (600 MHz, $CDCl_3$, 300 K) of **3h**.

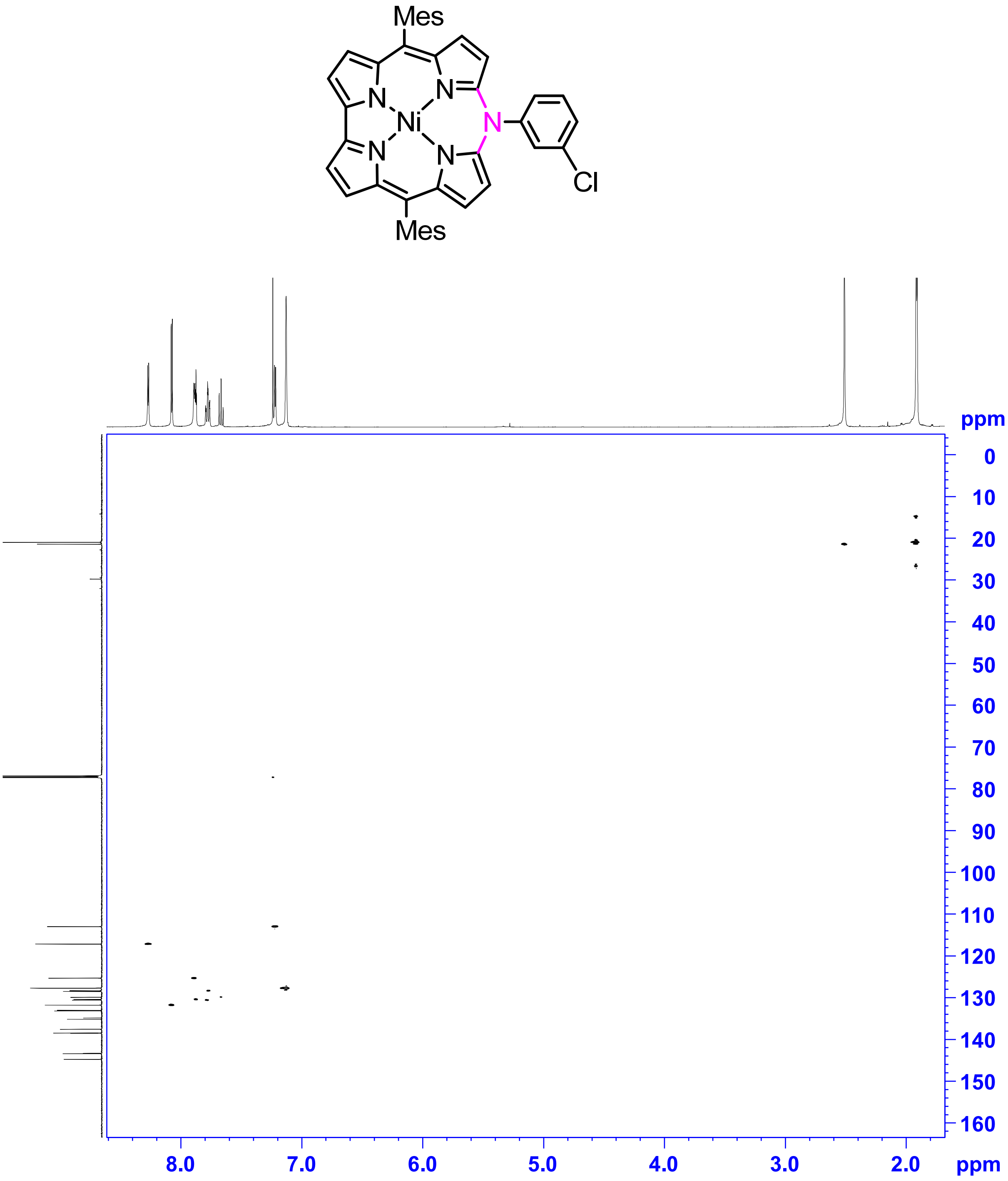

Figure S30. ^{1}H,^{13}C HSQC spectrum (600/150 MHz, $CDCl_3$, 300 K) of **3h**.

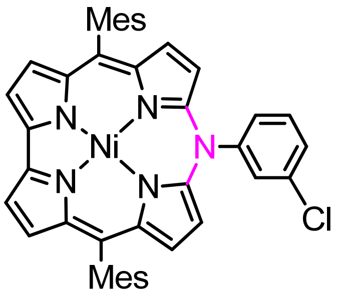

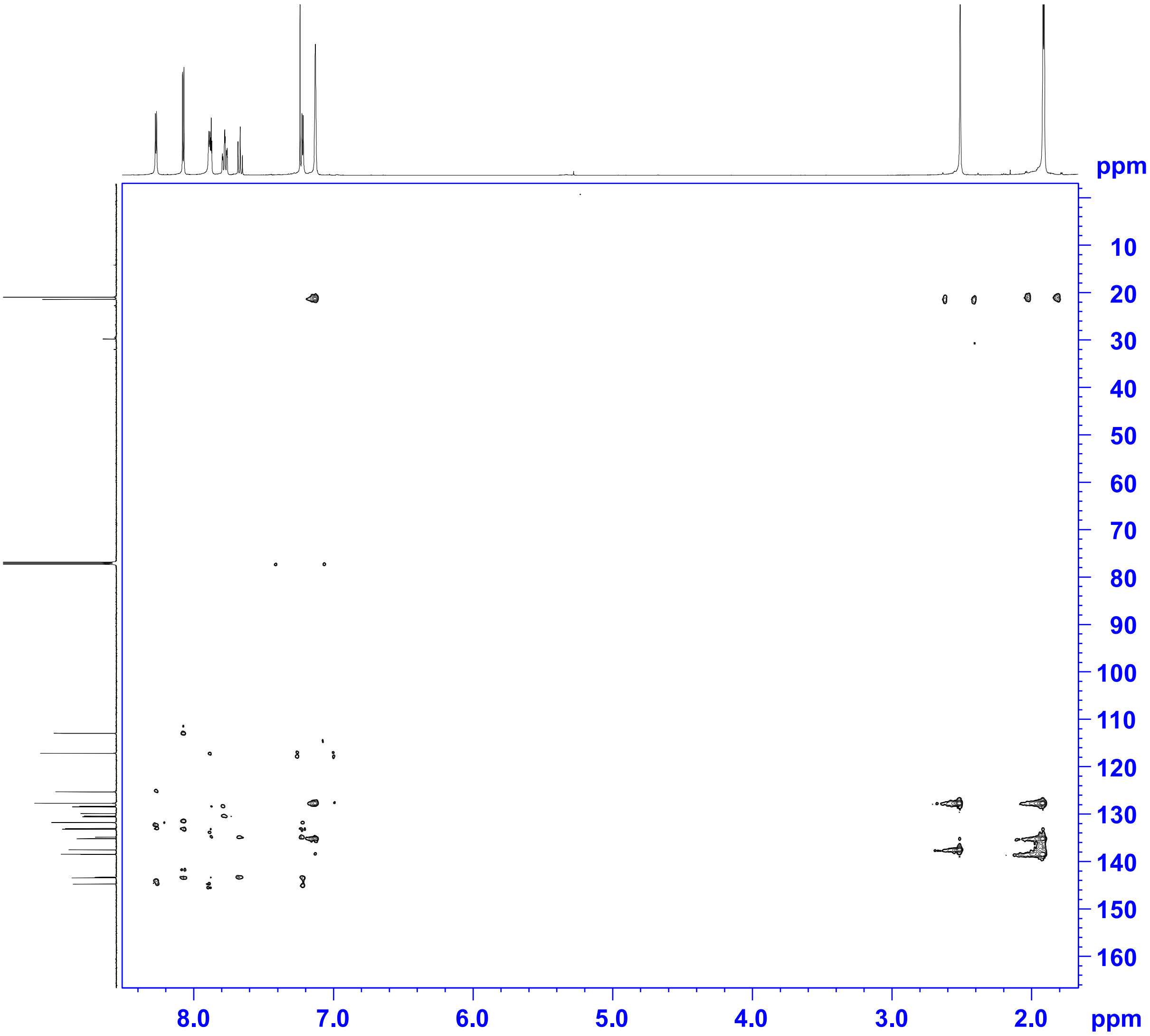

Figure S31. ^{1}H,^{13}C HMBC spectrum (600/150 MHz, $CDCl_3$, 300 K) of **3h**.

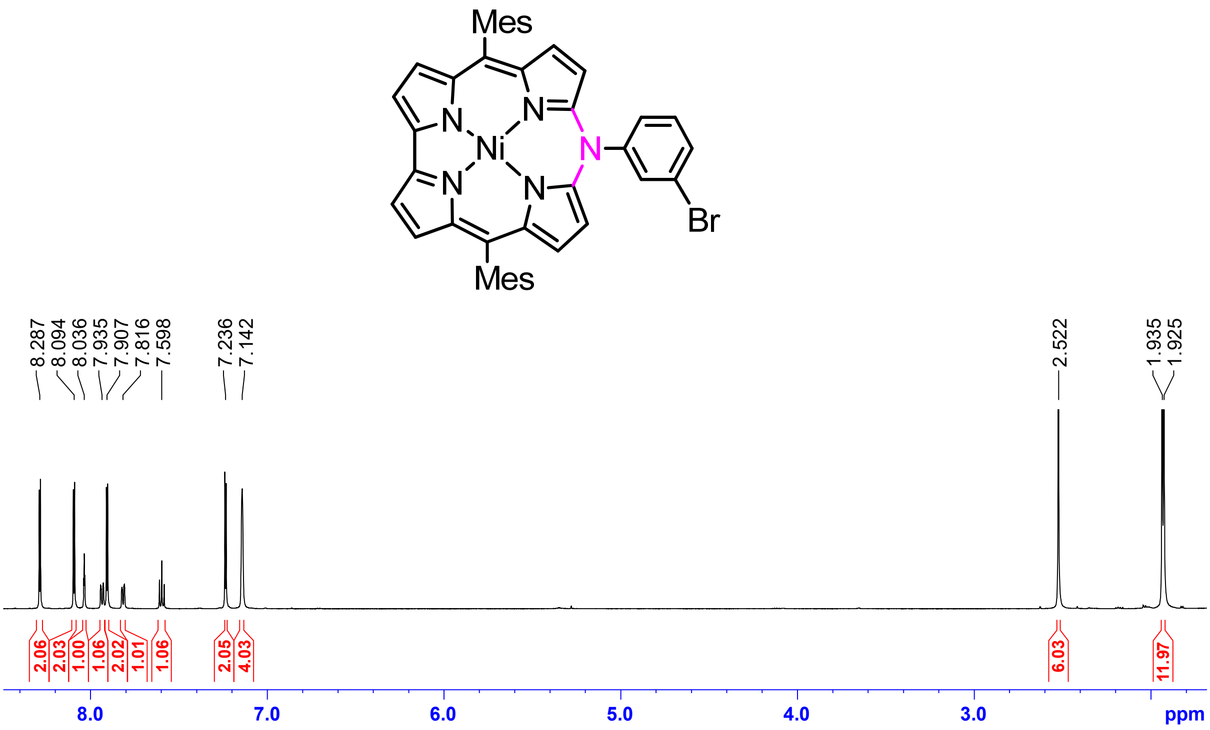

Figure S32. ^{1}H NMR spectrum (600 MHz, CDCl$_3$, 300 K) of **3i**.

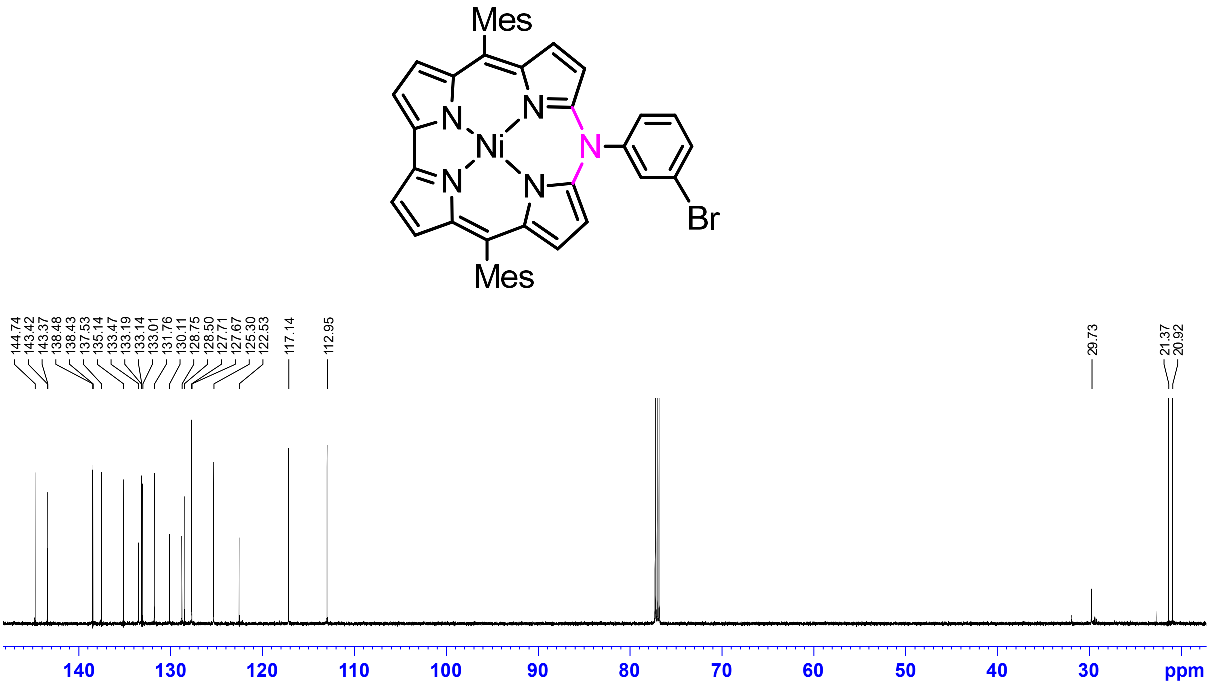

Figure S33. ^{13}C NMR spectrum (150 MHz, CDCl$_3$, 300 K) of **3i**.

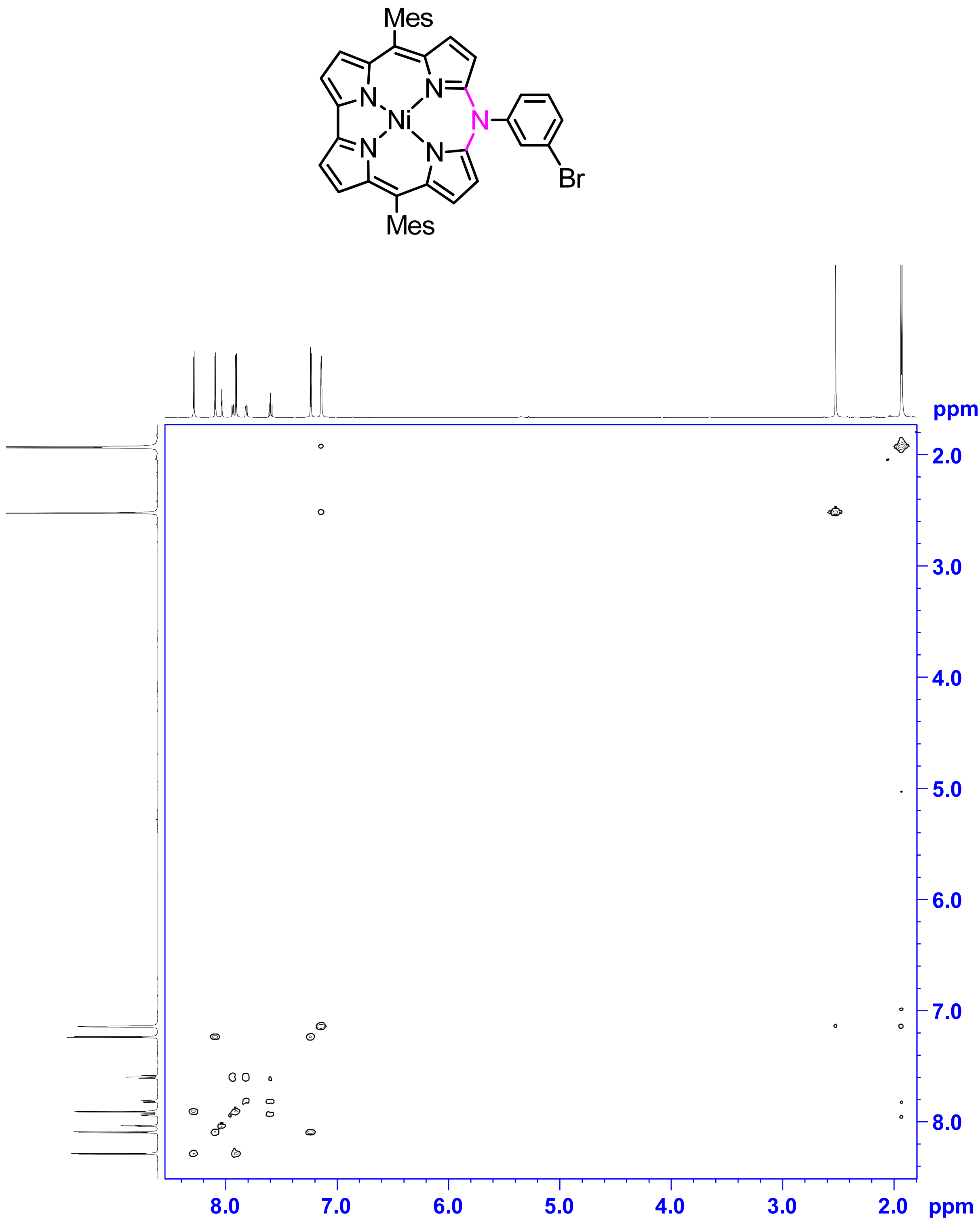

Figure S34. $^1H,^1H$ COSY spectrum (500 MHz, $CDCl_3$, 300 K) of **3i**.

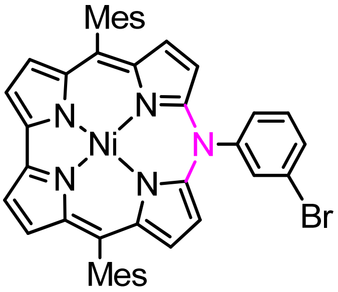

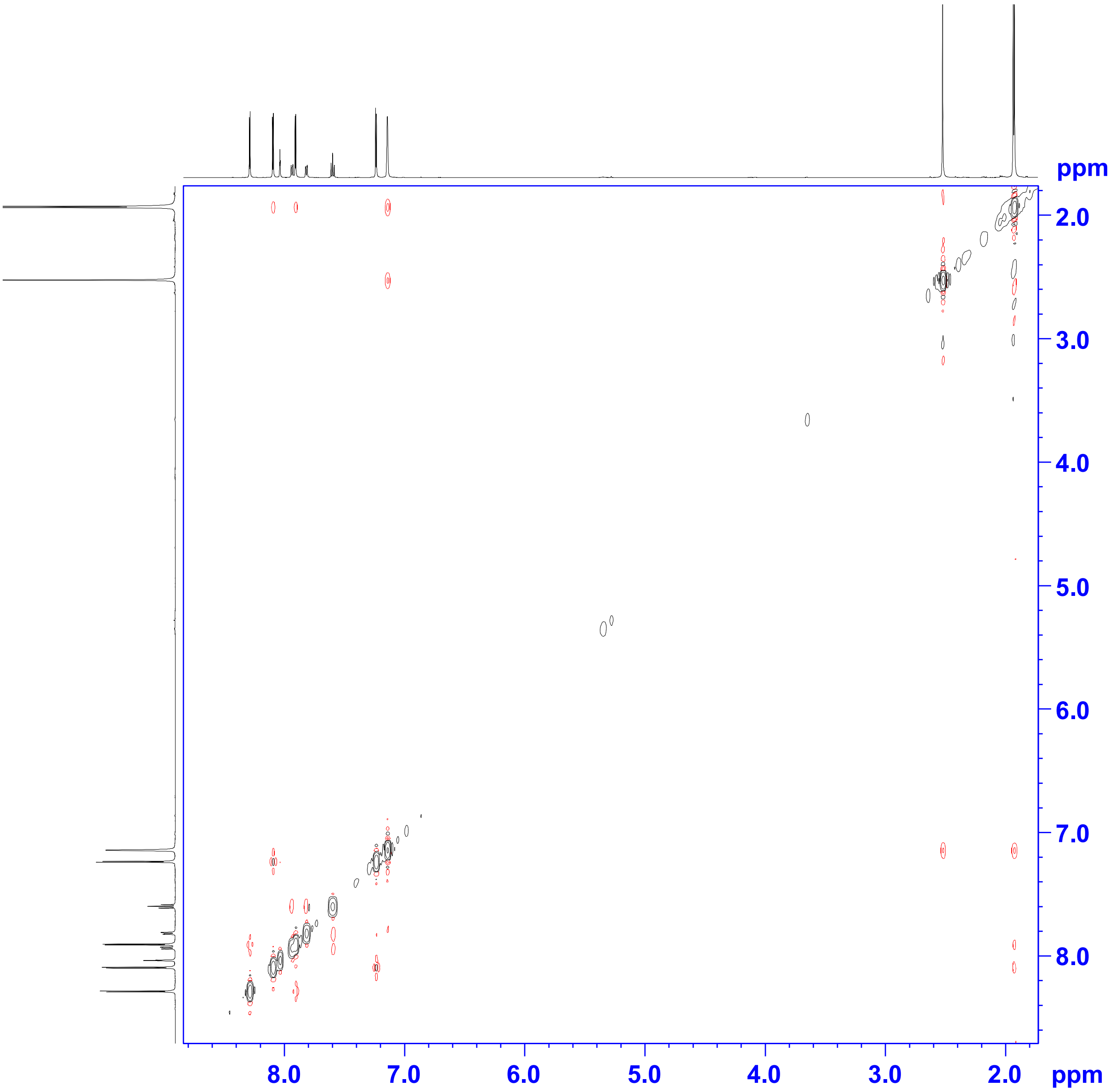

Figure S35. $^1H,^1H$ NOESY spectrum (500 MHz, $CDCl_3$, 300 K) of **3i**.

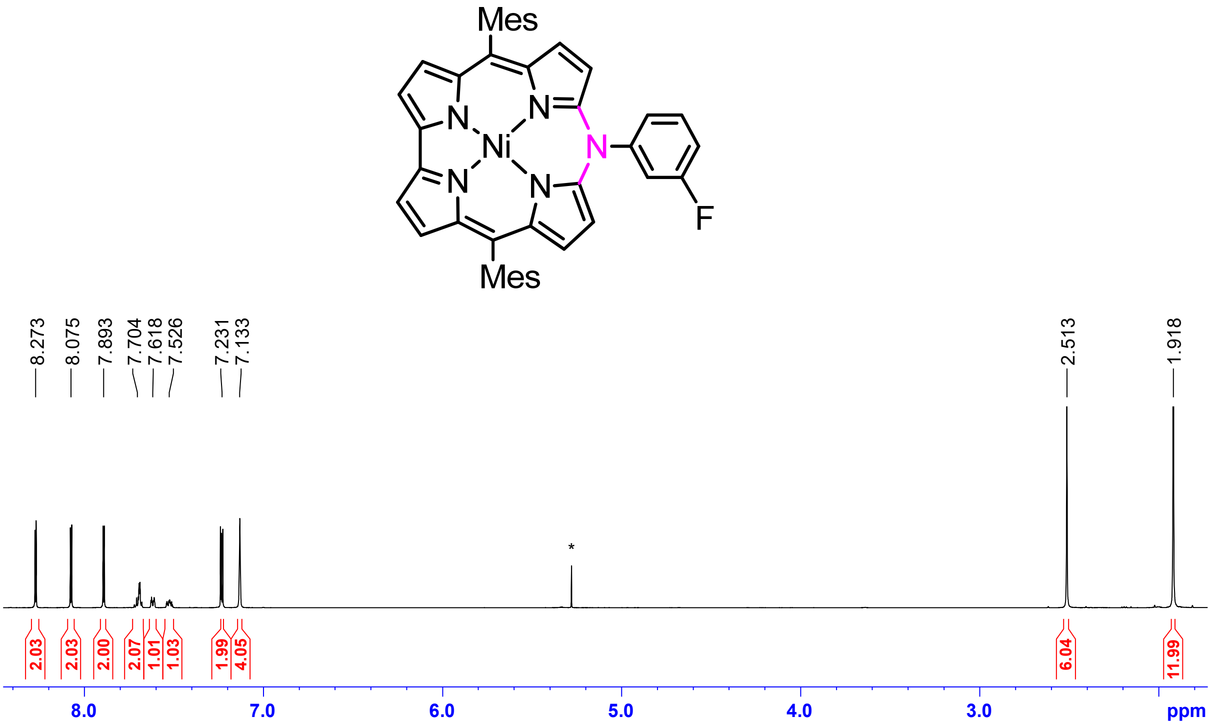

Figure S36. ^{1}H NMR spectrum (600 MHz, $CDCl_3$, 300 K) of **3j**.

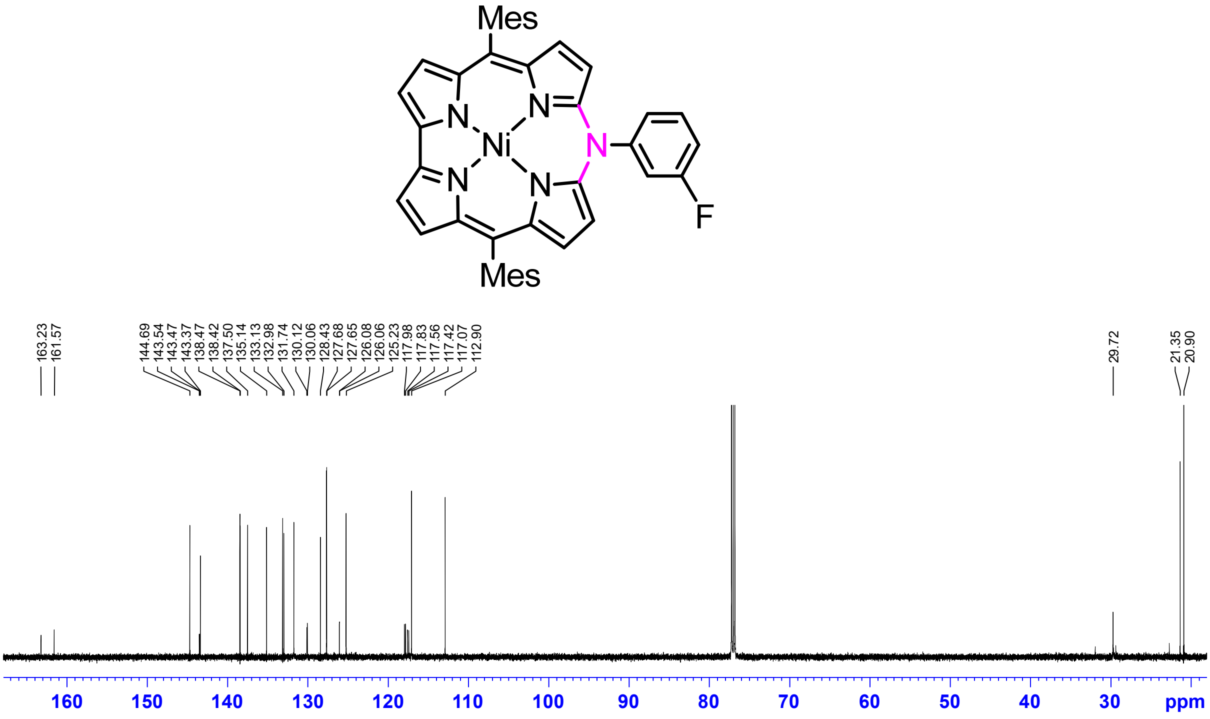

Figure S37. ^{13}C NMR spectrum (150 MHz, $CDCl_3$, 300 K) of **3j**.

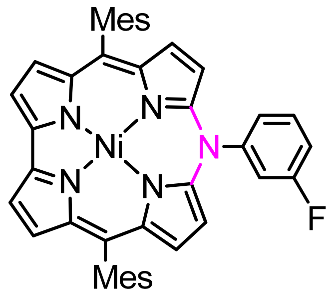

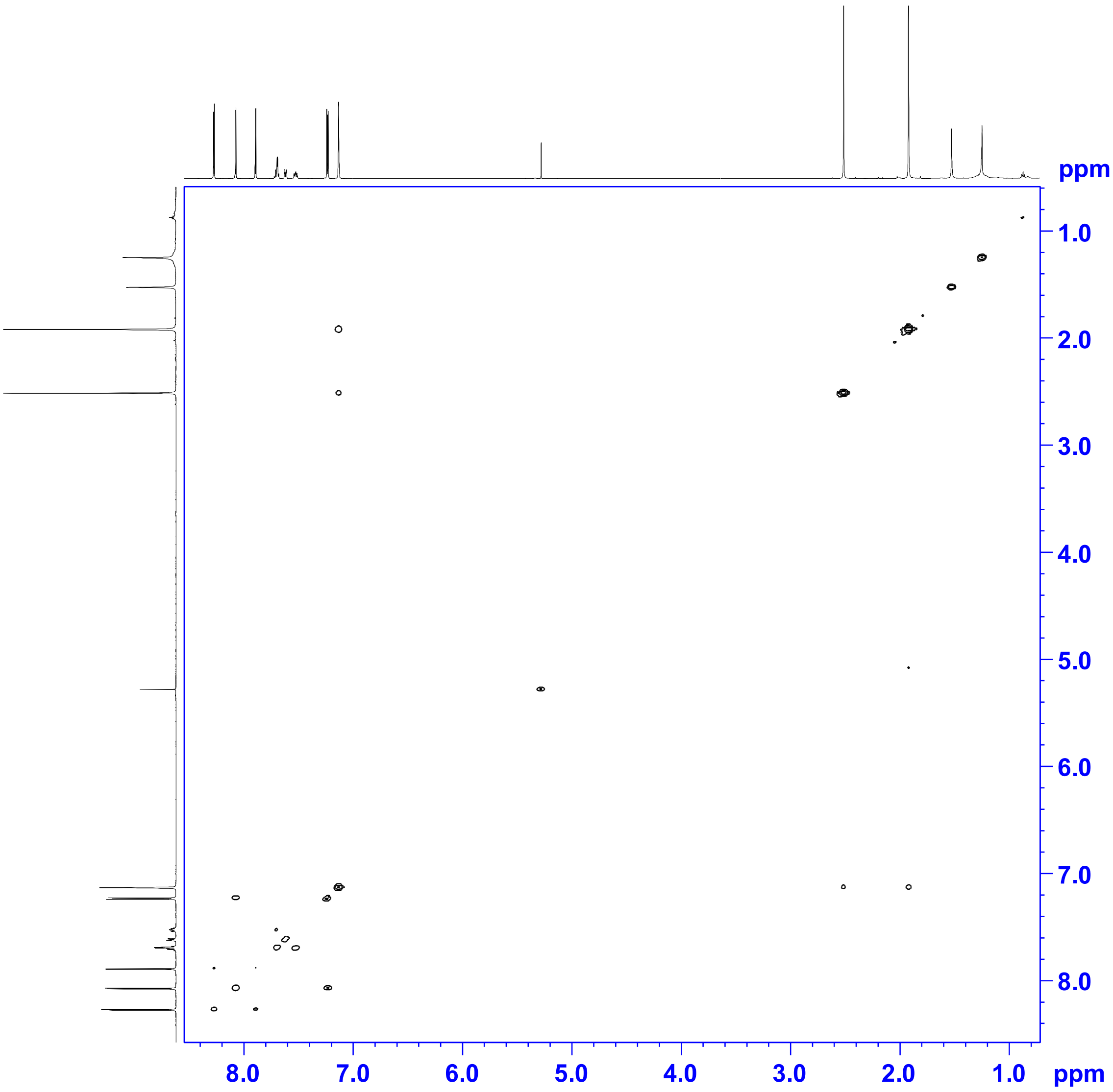

Figure S38. ^{1}H,^{1}H COSY spectrum (500 MHz, CDCl$_3$, 300 K) of **3j**.

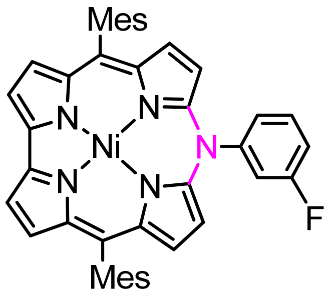

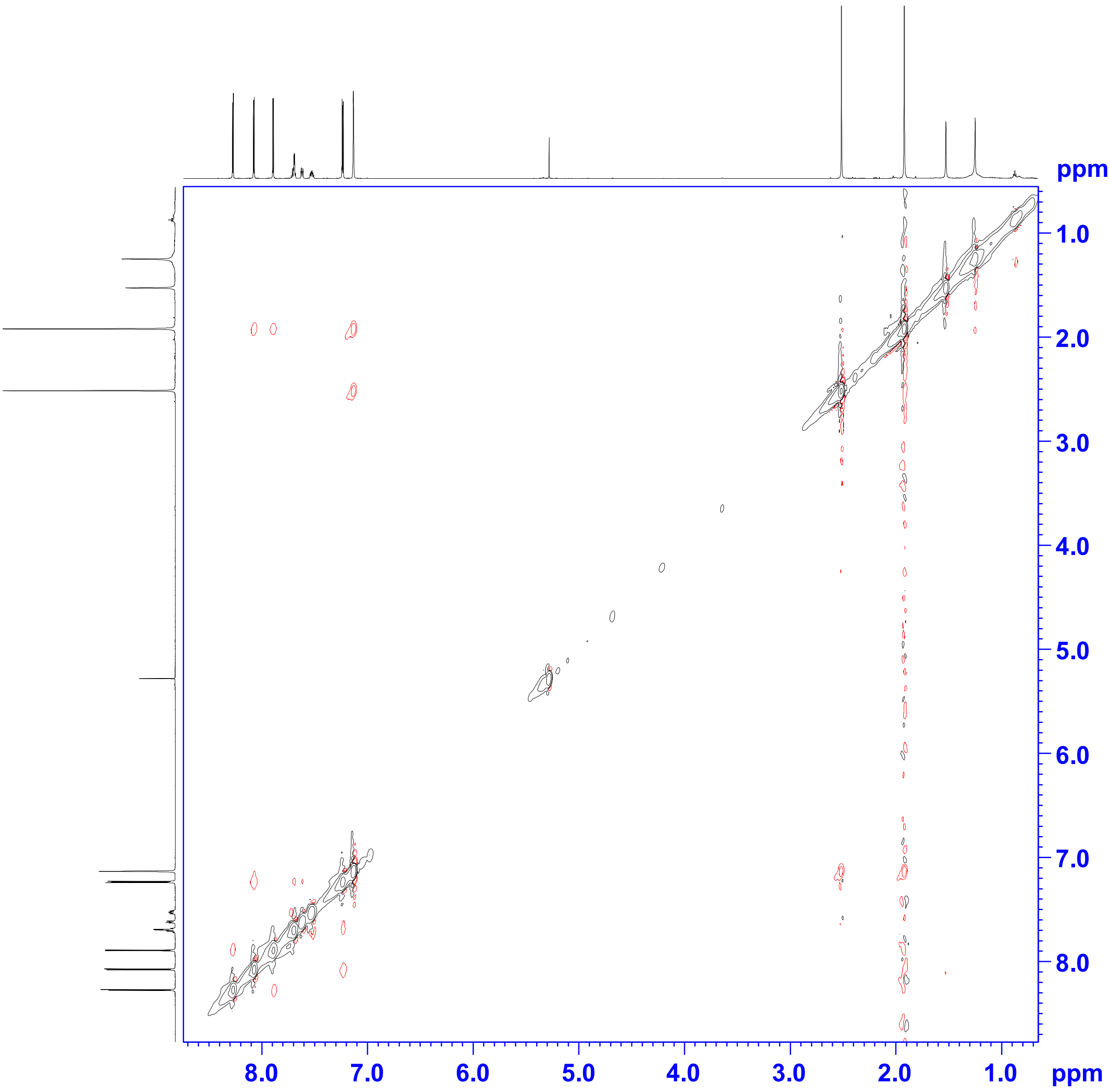

Figure S39. ^{1}H,^{1}H NOESY spectrum (500 MHz, CDCl$_3$, 300 K) of **3j**.

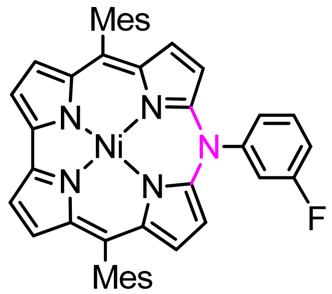

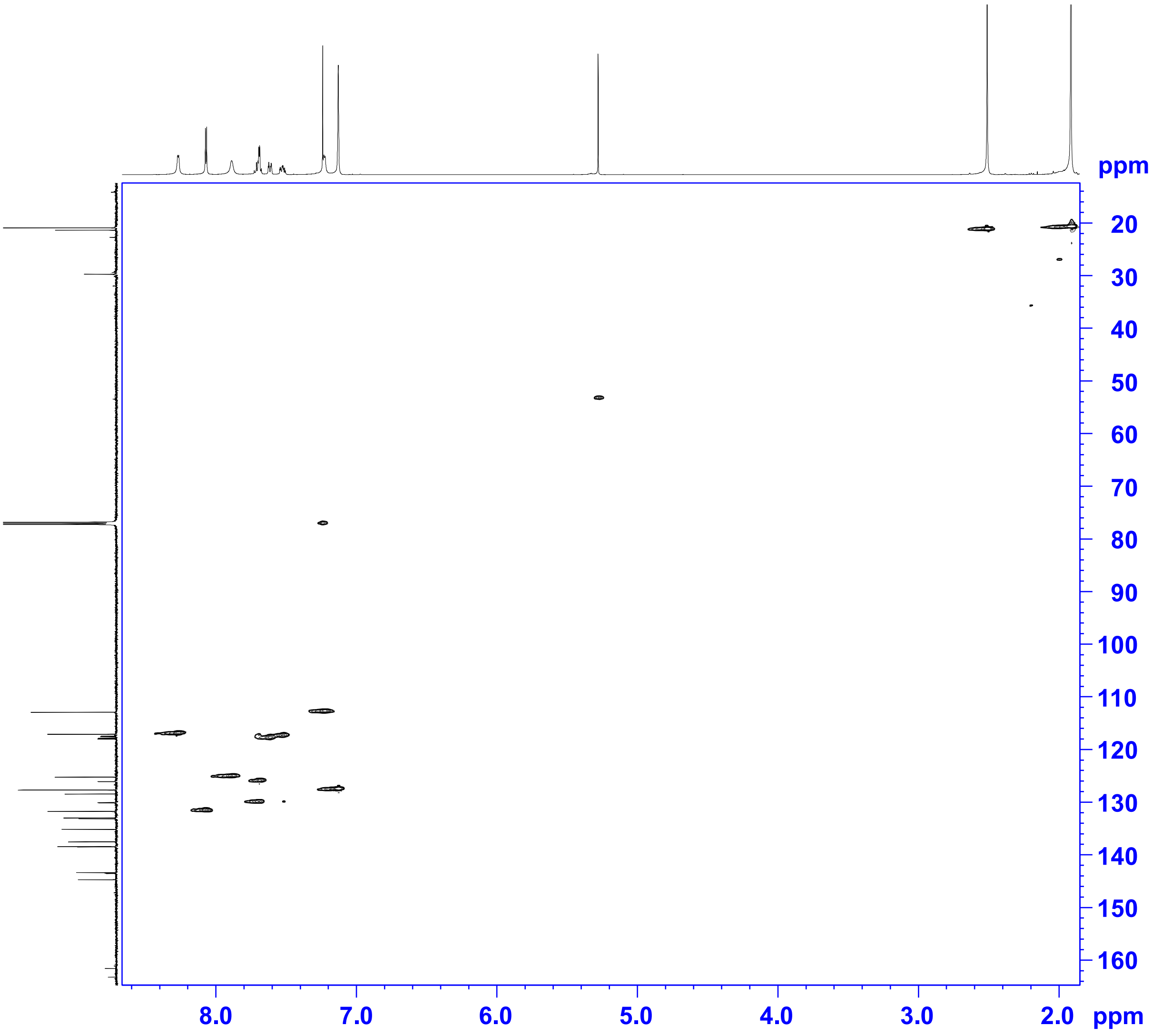

Figure S40. ^{1}H,^{13}C HSQC spectrum (500/125 MHz, CDCl$_3$, 300 K) of **3j**.

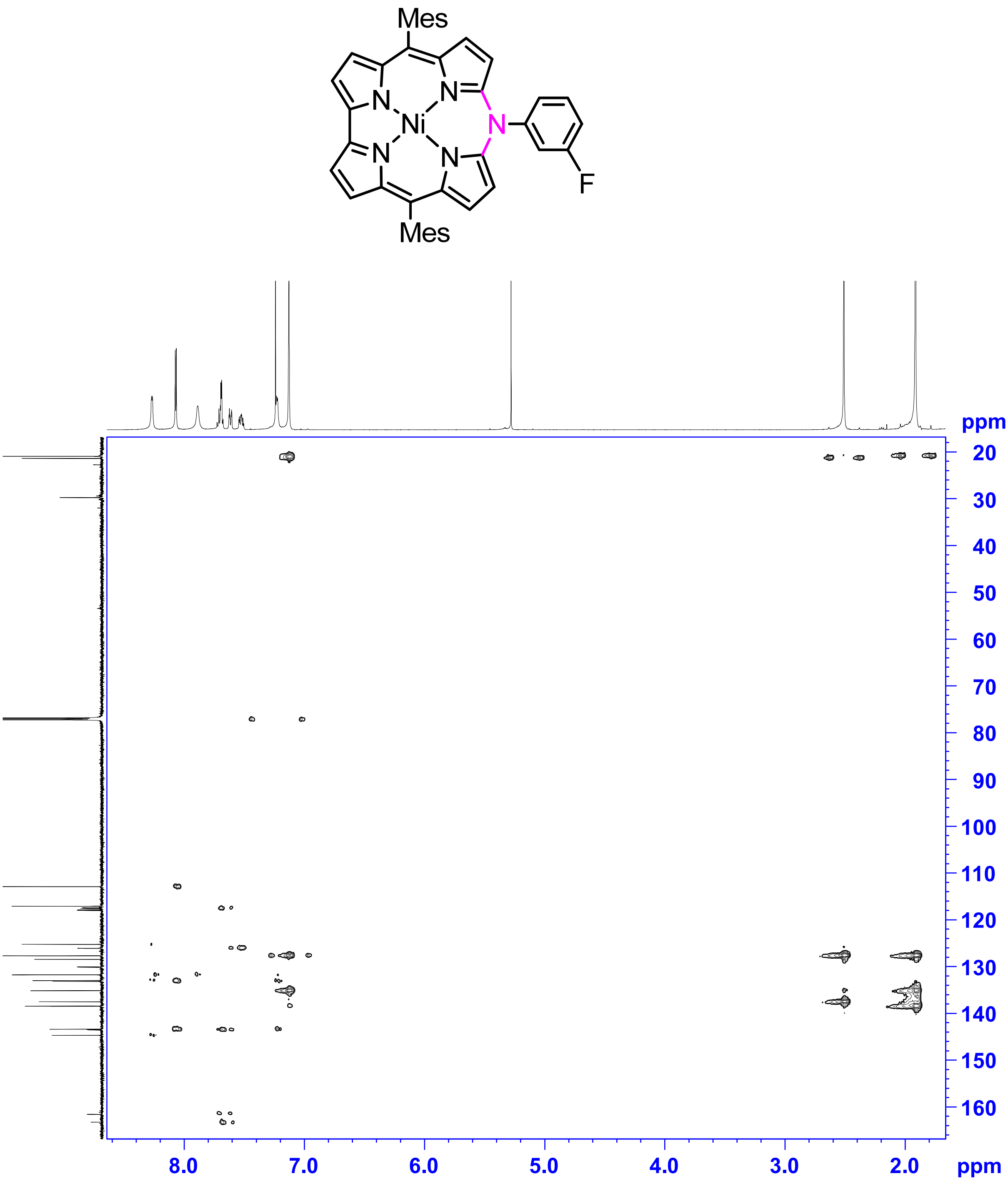

Figure S41. $^{1}H,^{13}C$ HMBC spectrum (500/125 MHz, $CDCl_3$, 300 K) of **3j**.

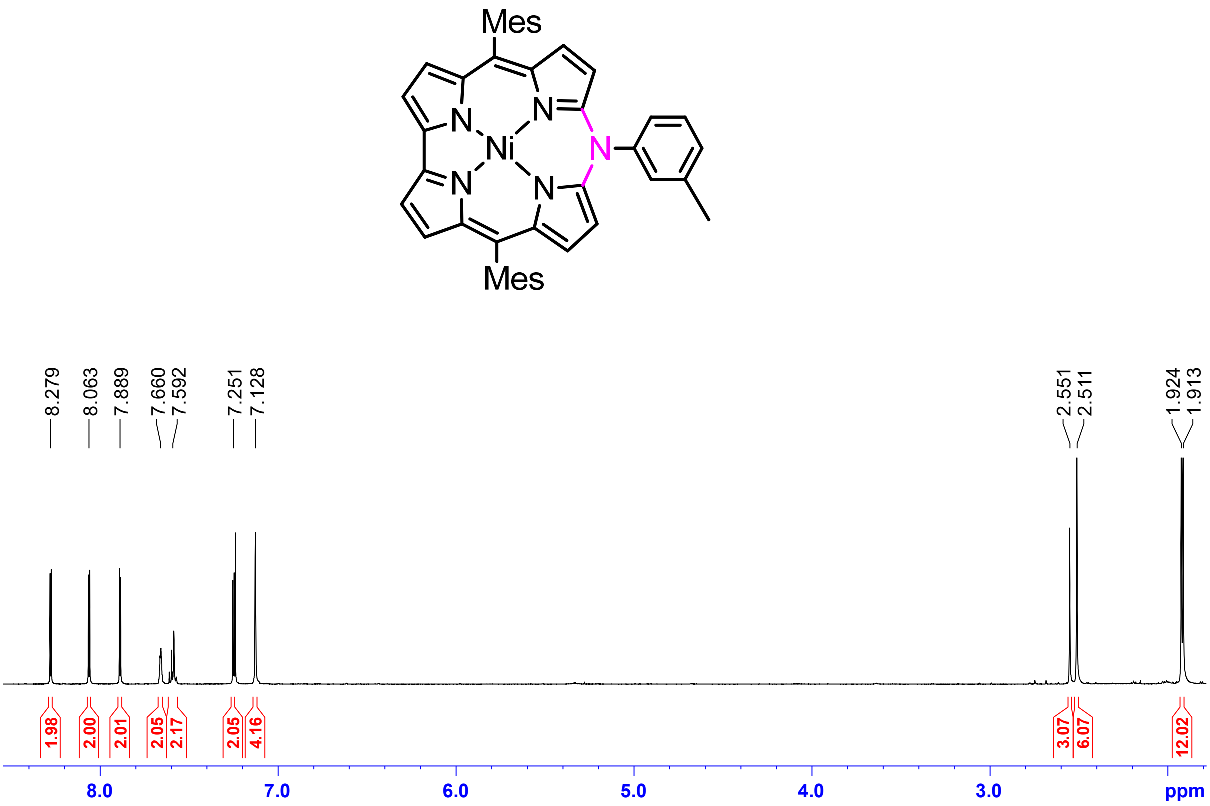

Figure S42. ^{1}H NMR spectrum (600 MHz, CDCl$_3$, 300 K) of **3k**.

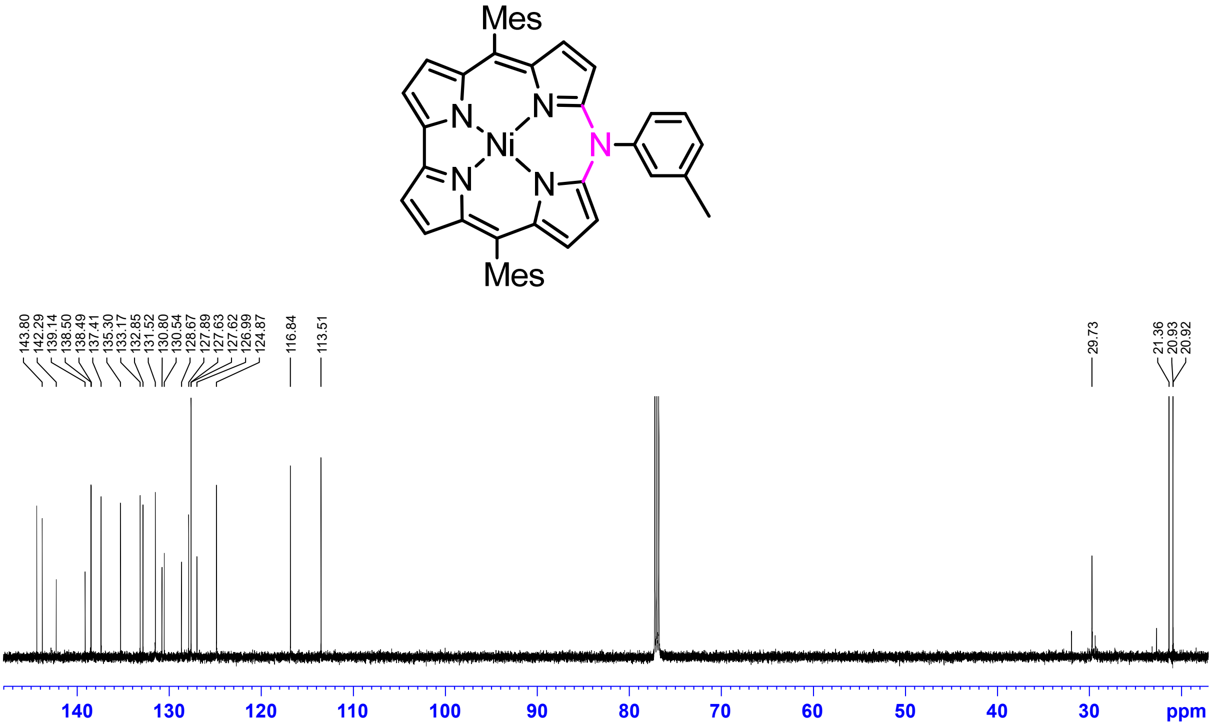

Figure S43. ^{13}C NMR spectrum (150 MHz, CDCl$_3$, 300 K) of **3k**.

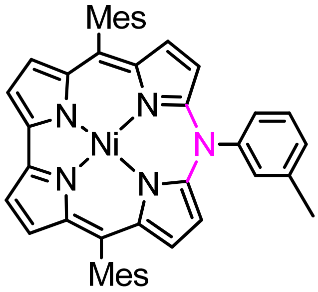

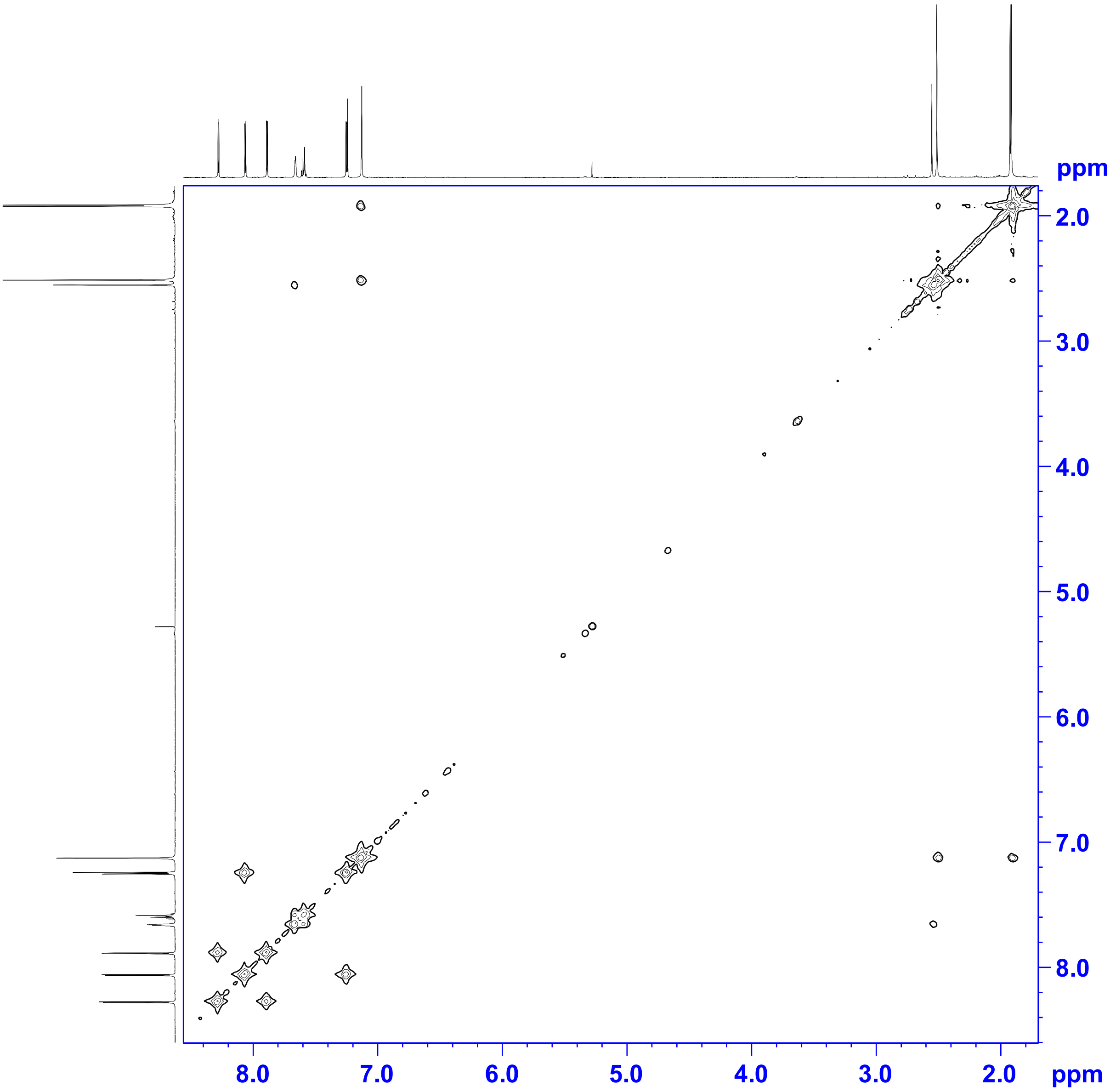

Figure S44. ^{1}H,^{1}H COSY spectrum (600 MHz, $CDCl_3$, 300 K) of **3k**.

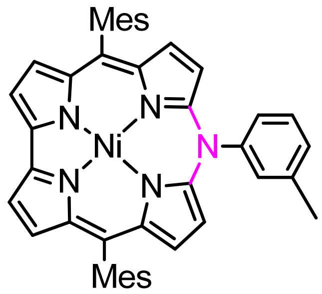

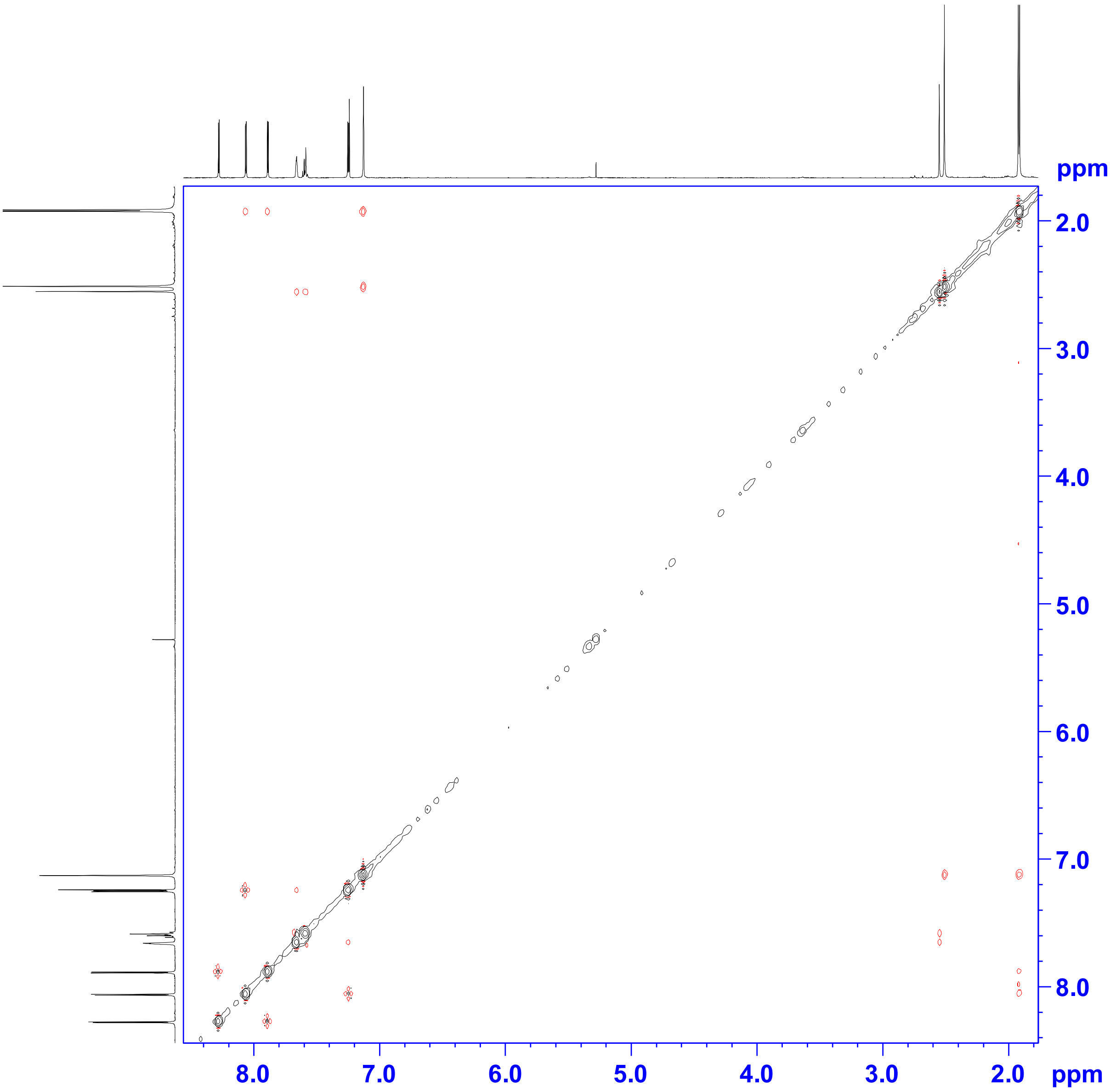

Figure S45. ^{1}H,^{1}H NOESY spectrum (600 MHz, CDCl$_3$, 300 K) of **3k**.

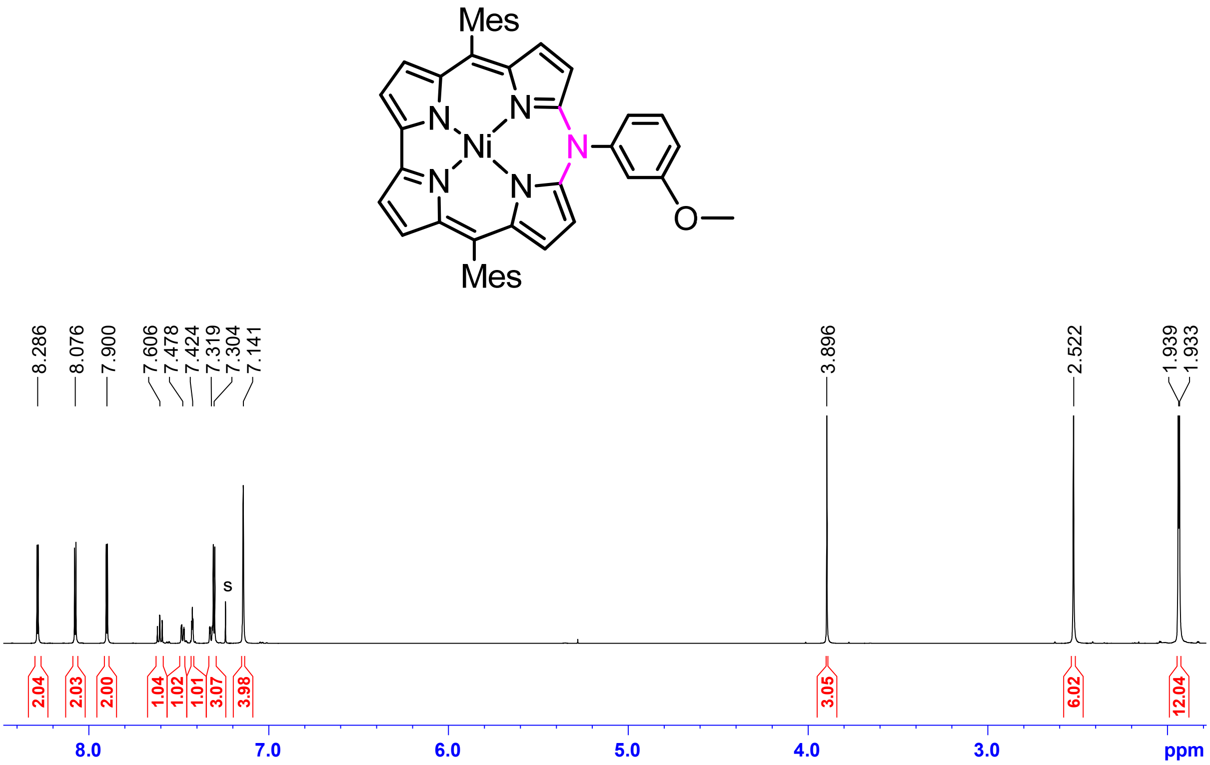

Figure S46. ^{1}H NMR spectrum (600 MHz, CDCl$_3$, 300 K) of **3l**.

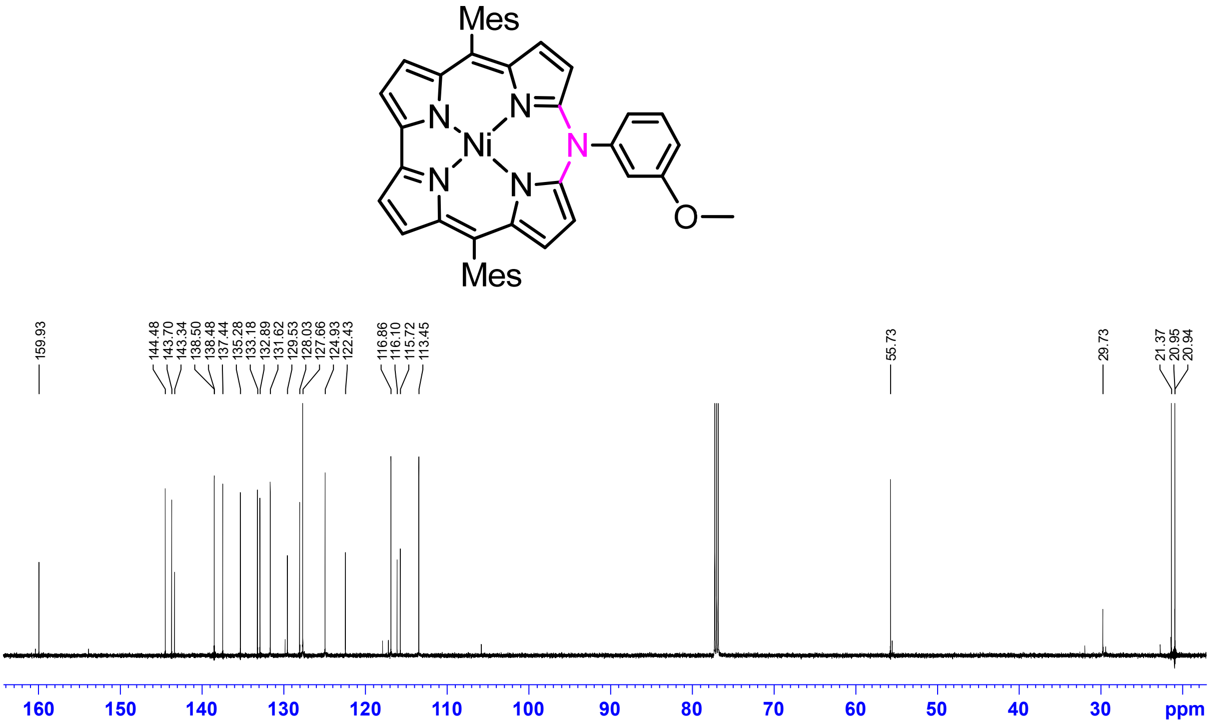

Figure S47. ^{13}C NMR spectrum (150 MHz, CDCl$_3$, 300 K) of **3l**.

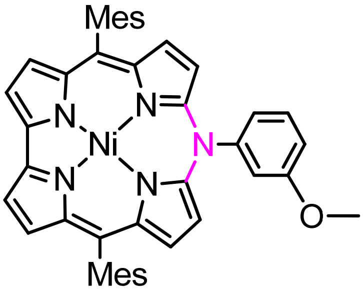

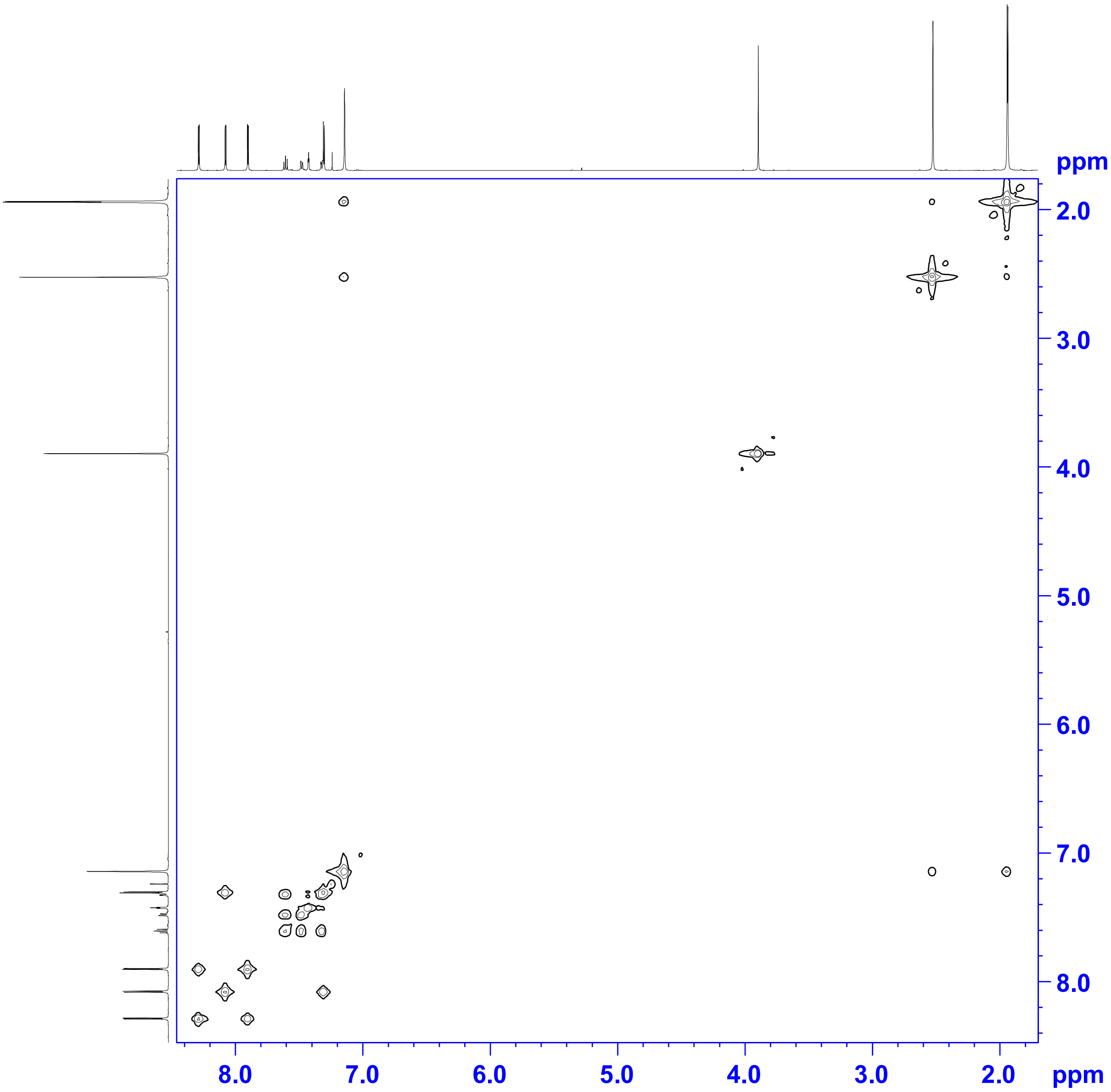

Figure S48. ^{1}H,^{1}H COSY spectrum (600 MHz, CDCl$_3$, 300 K) of **3l**.

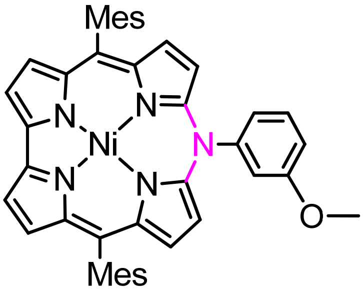

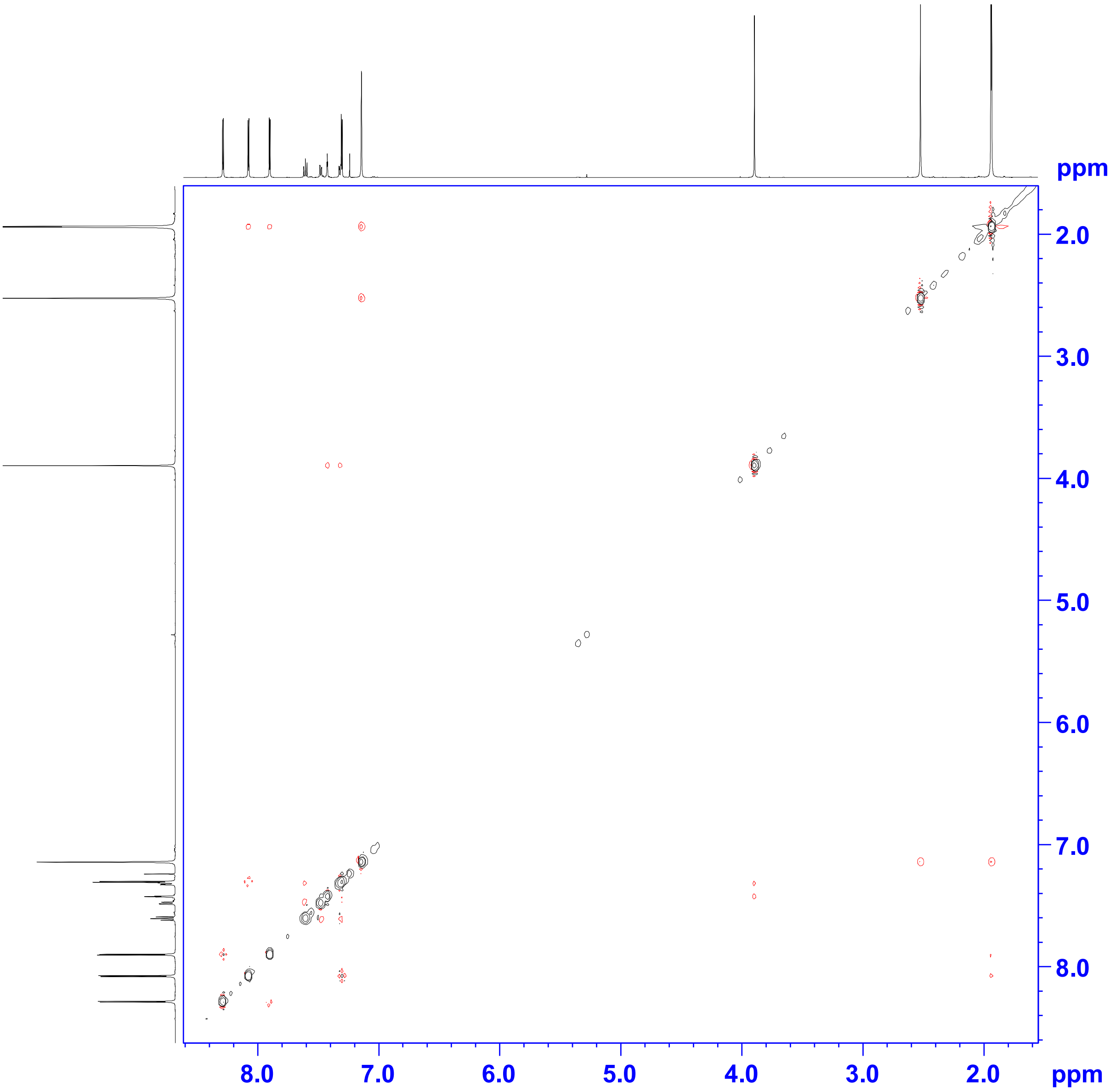

Figure S49. $^1H,^1H$ NOESY spectrum (600 MHz, $CDCl_3$, 300 K) of **3l**.

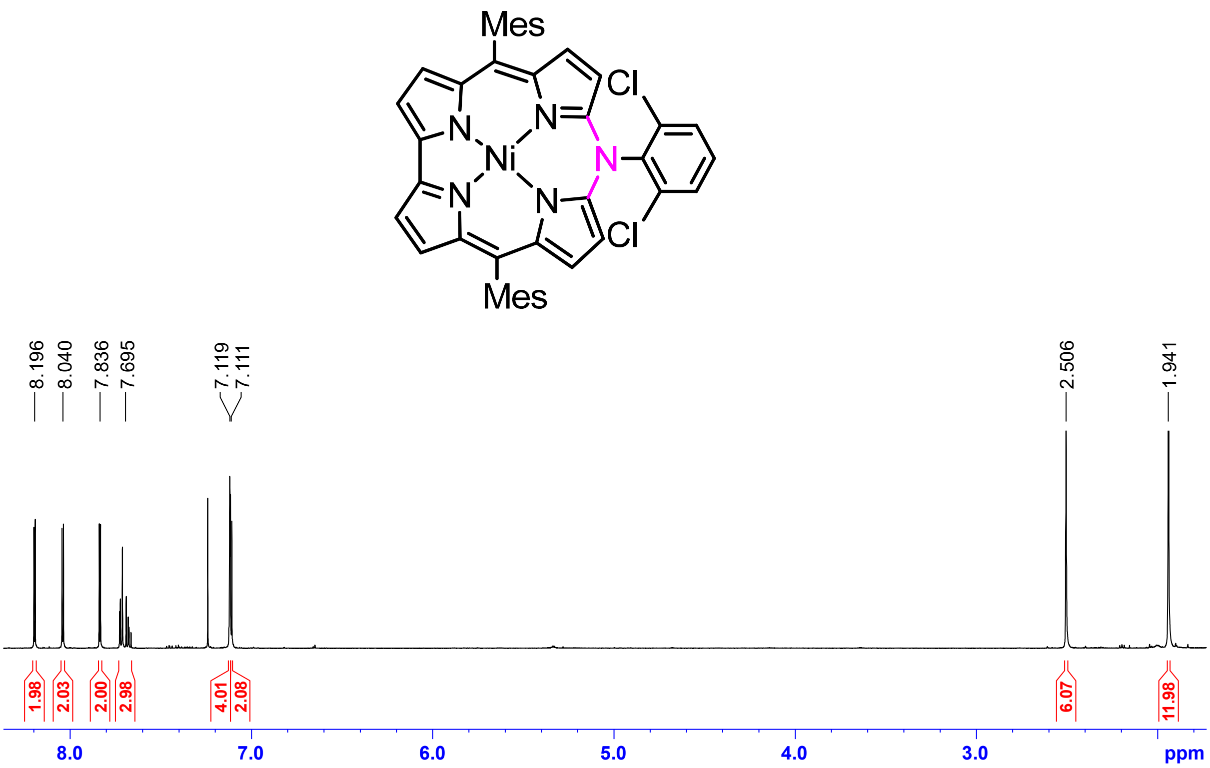

Figure S50. ^{1}H NMR spectrum (600 MHz, $CDCl_3$, 300 K) of **3m**.

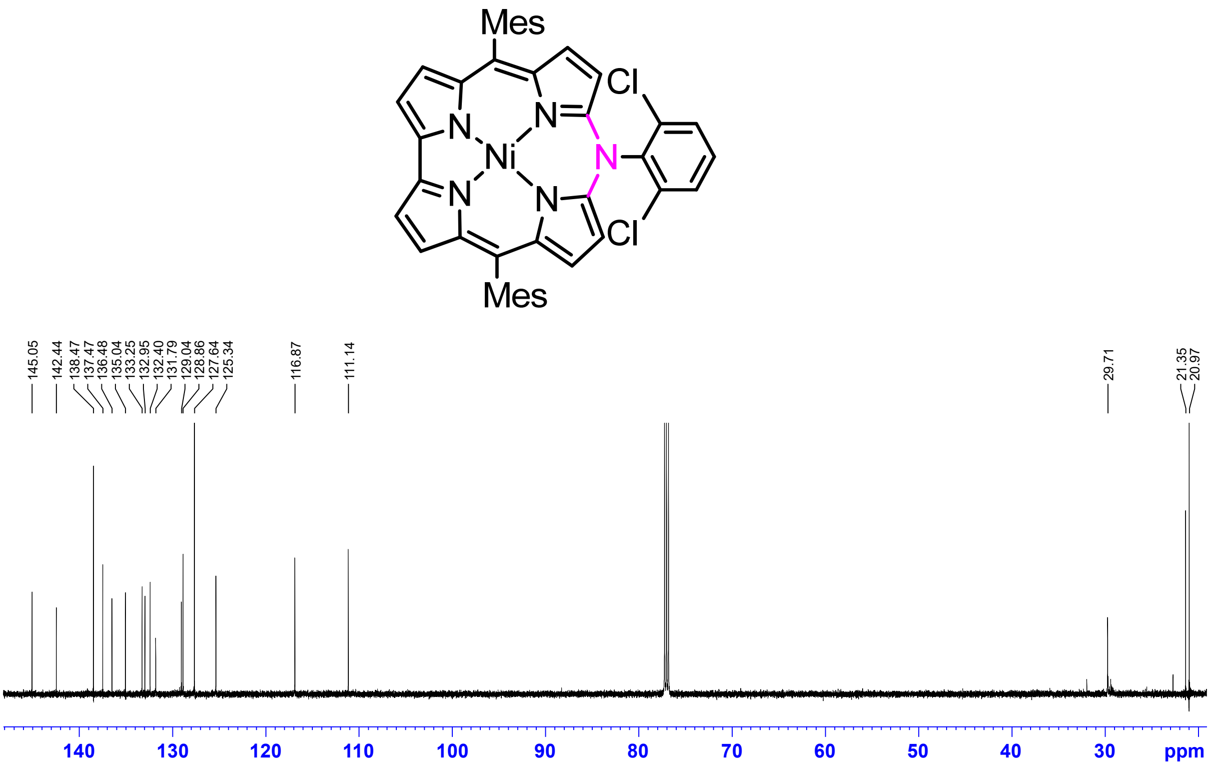

Figure S51. ^{13}C NMR spectrum (150 MHz, $CDCl_3$, 300 K) of **3m**.

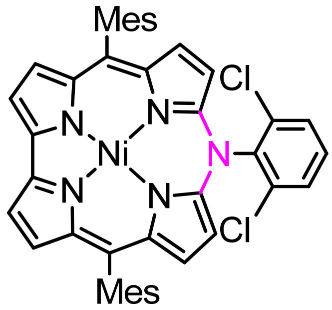

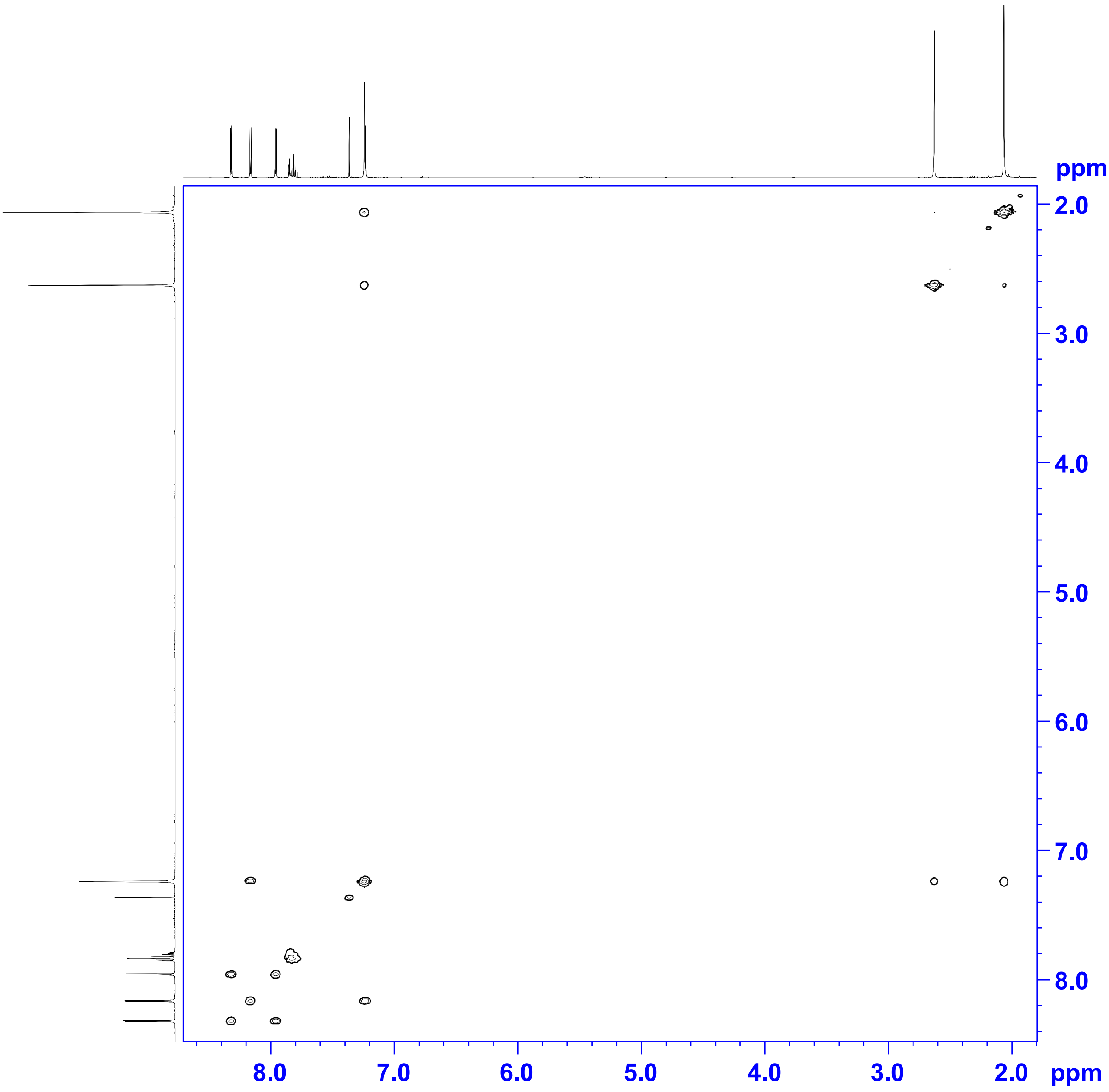

Figure S52. ^{1}H,^{1}H COSY spectrum (500 MHz, CDCl$_3$, 300 K) of **3m**.

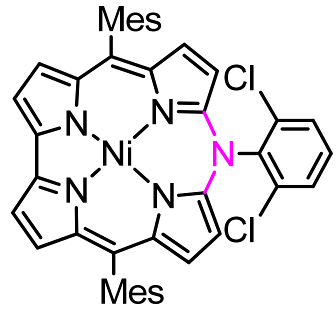

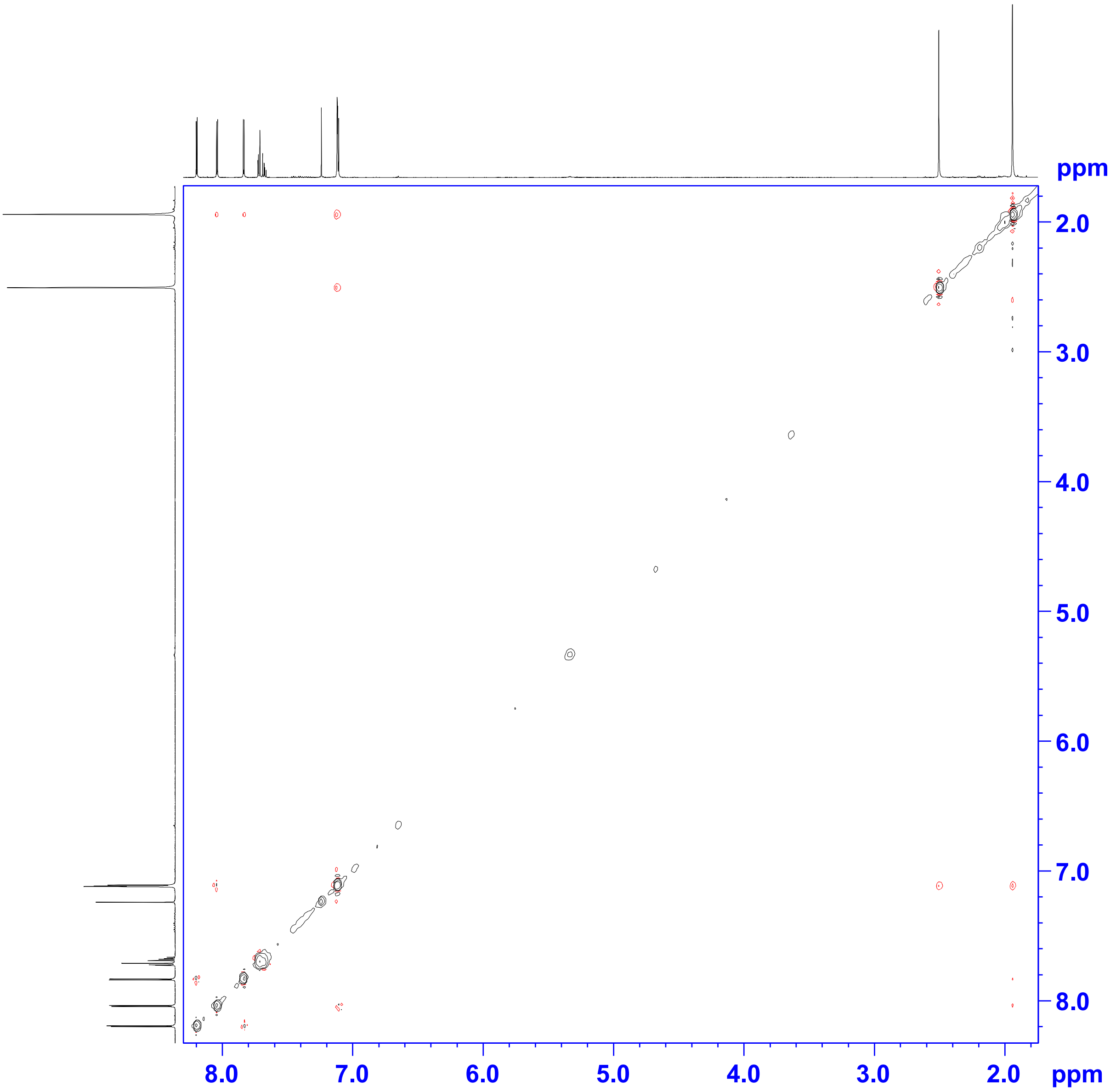

Figure S53. ^{1}H,^{1}H NOESY spectrum (500 MHz, CDCl$_3$, 300 K) of **3m**.

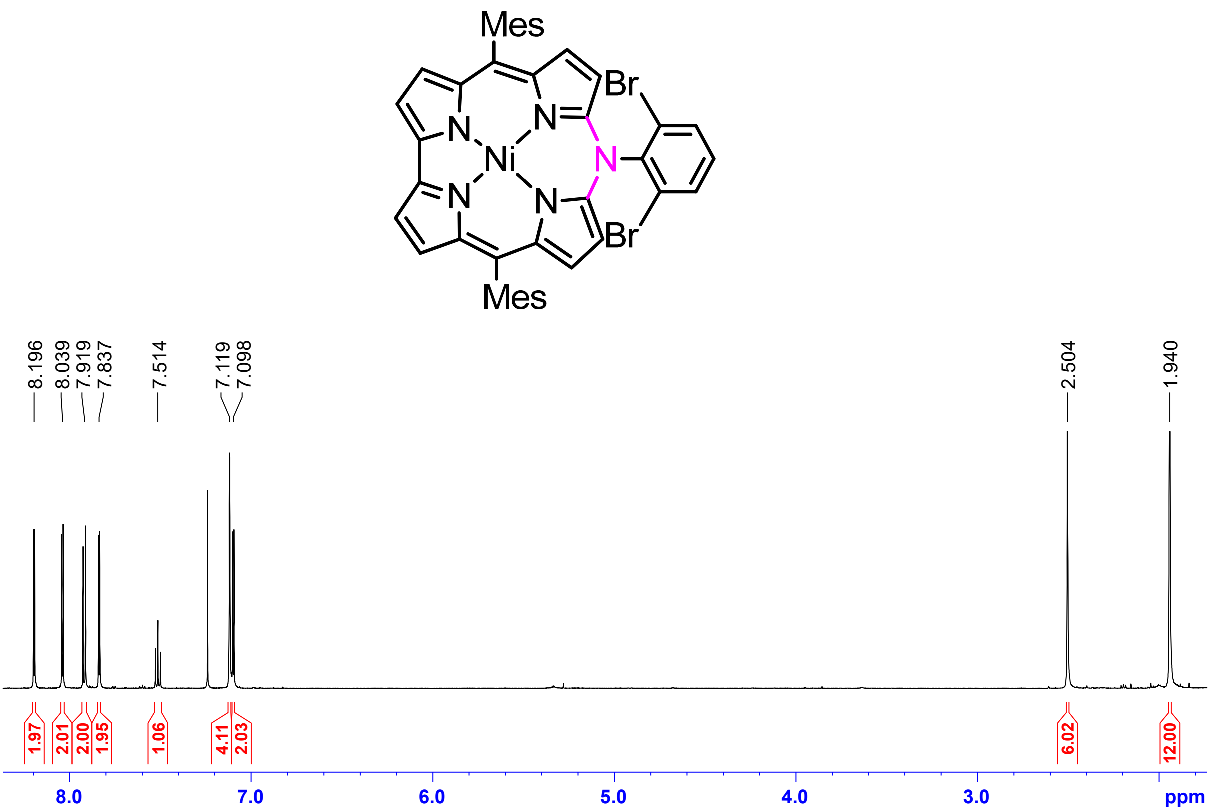

Figure S54. ^{1}H NMR spectrum (600 MHz, $CDCl_3$, 300 K) of **3n**.

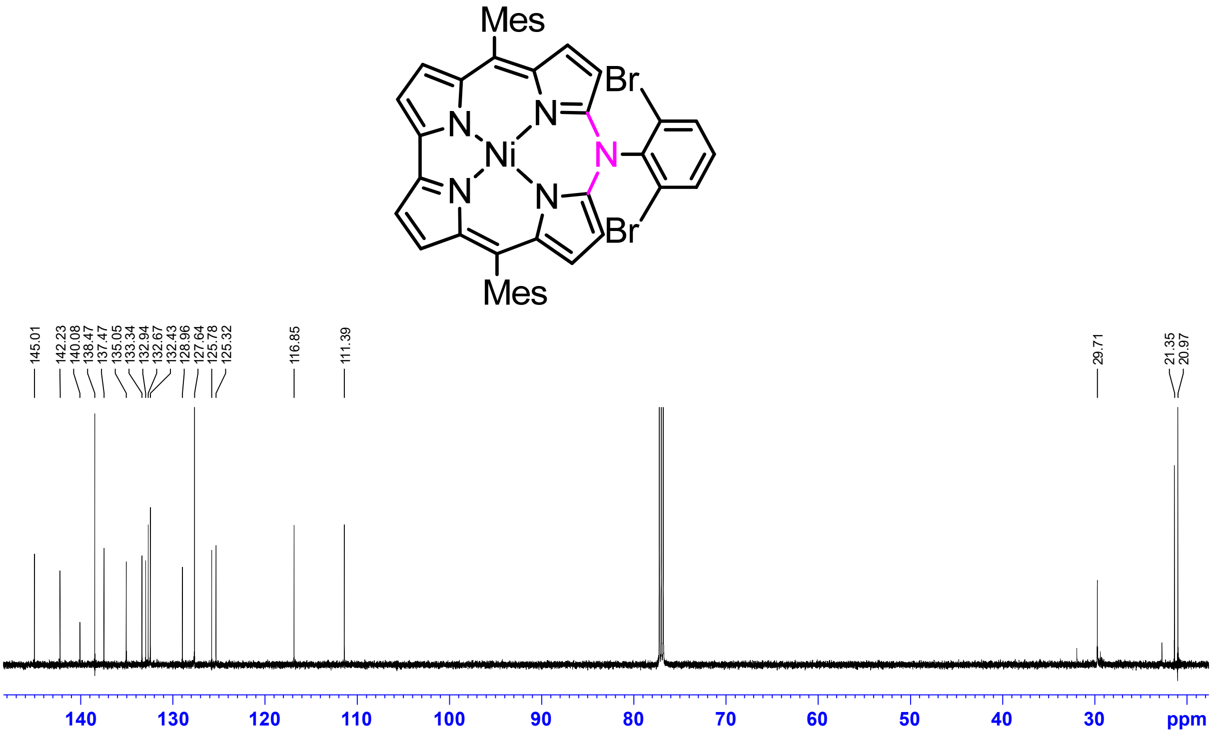

Figure S55. ^{13}C NMR spectrum (150 MHz, $CDCl_3$, 300 K) of **3n**.

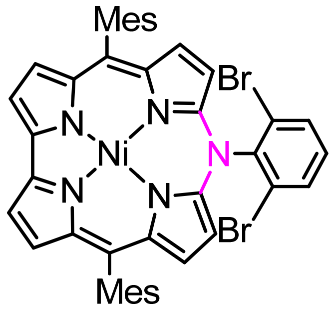

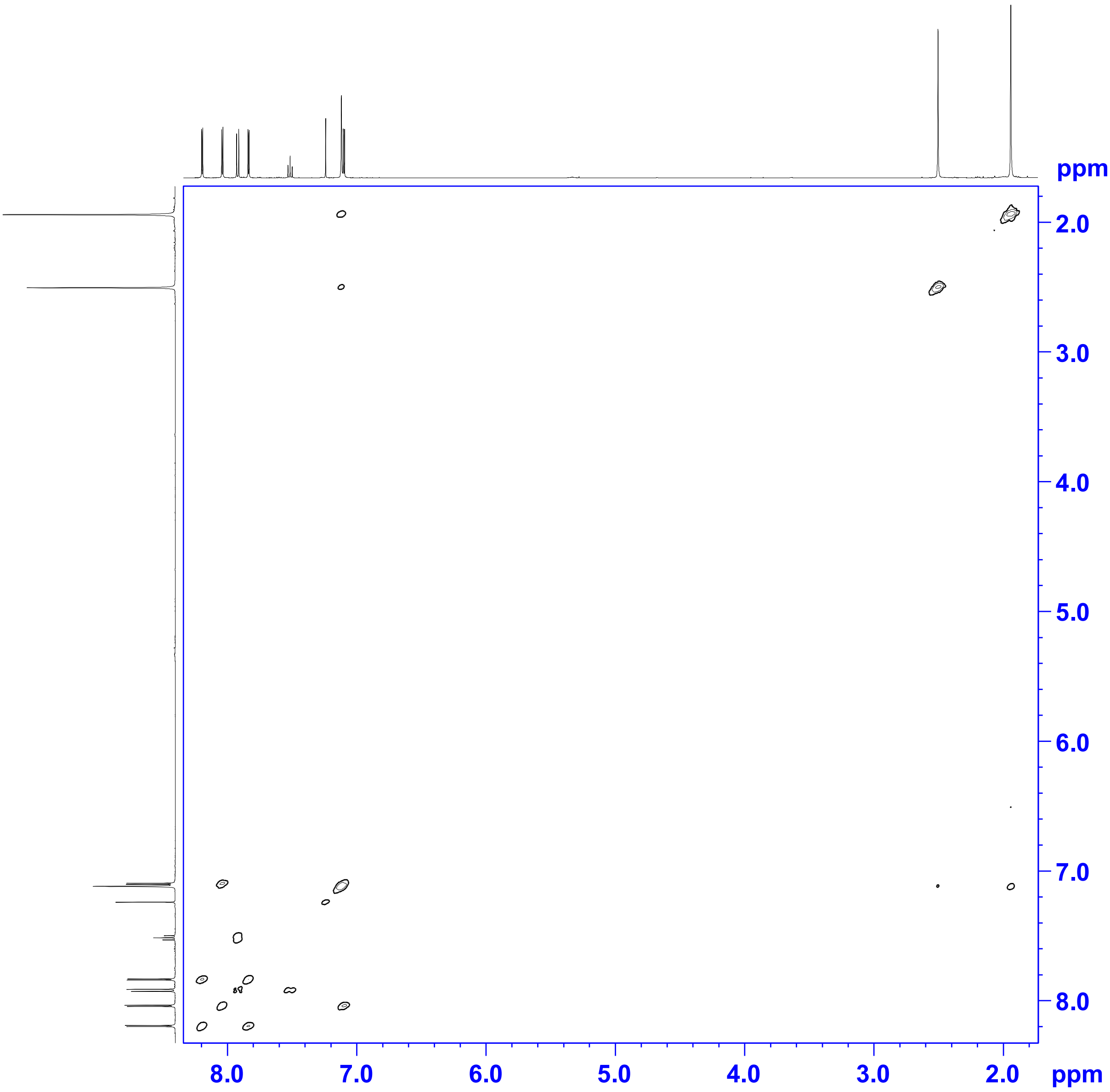

Figure S56. $^{1}H,^{1}H$ COSY spectrum (500 MHz, $CDCl_3$, 300 K) of **3n**.

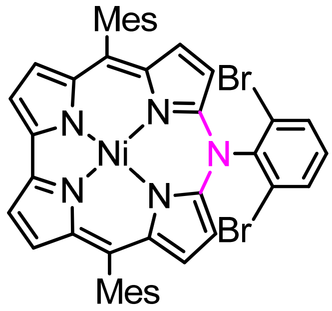

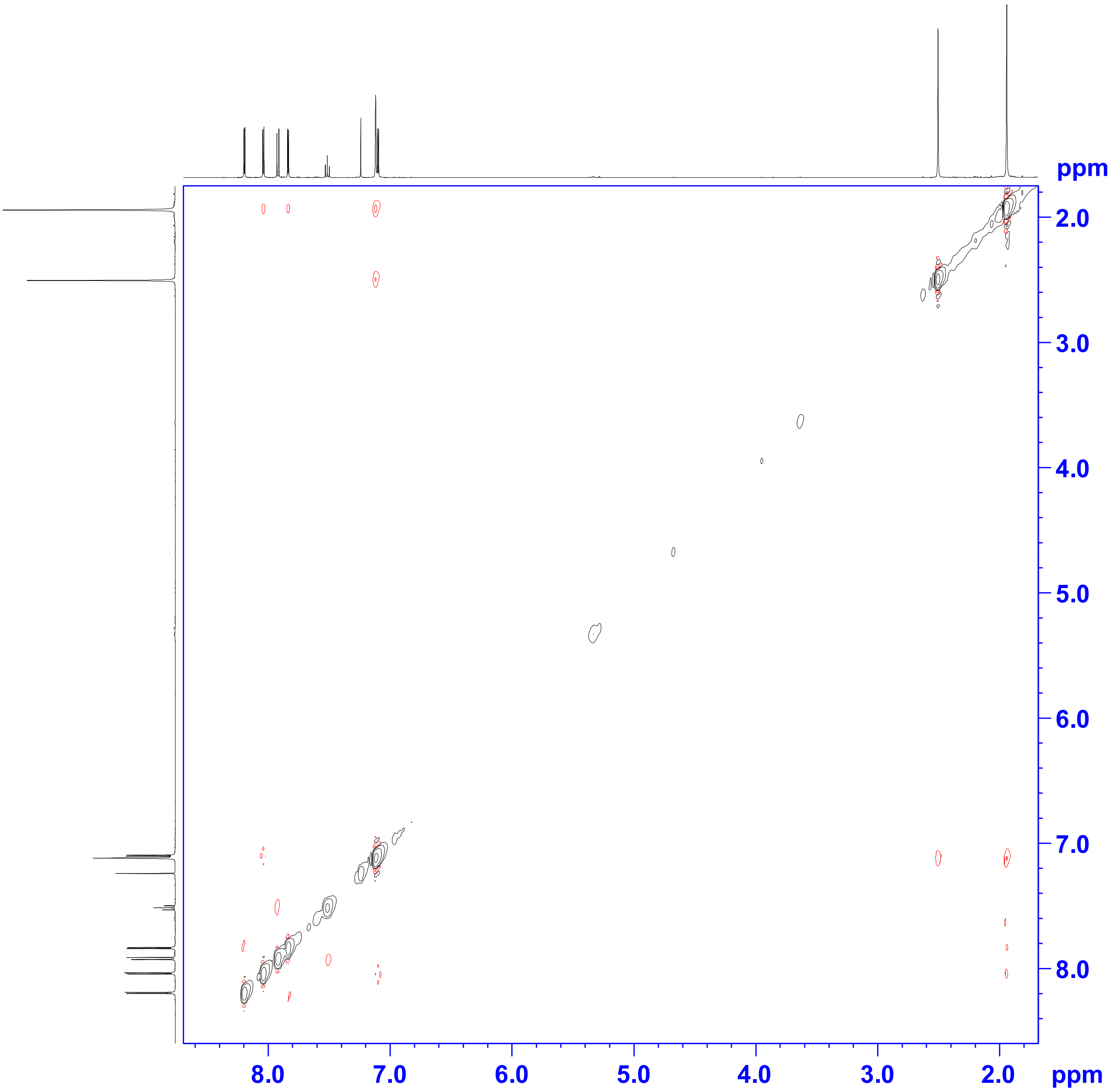

Figure S57. ^{1}H,^{1}H NOESY spectrum (500 MHz, CDCl$_3$, 300 K) of **3n**.

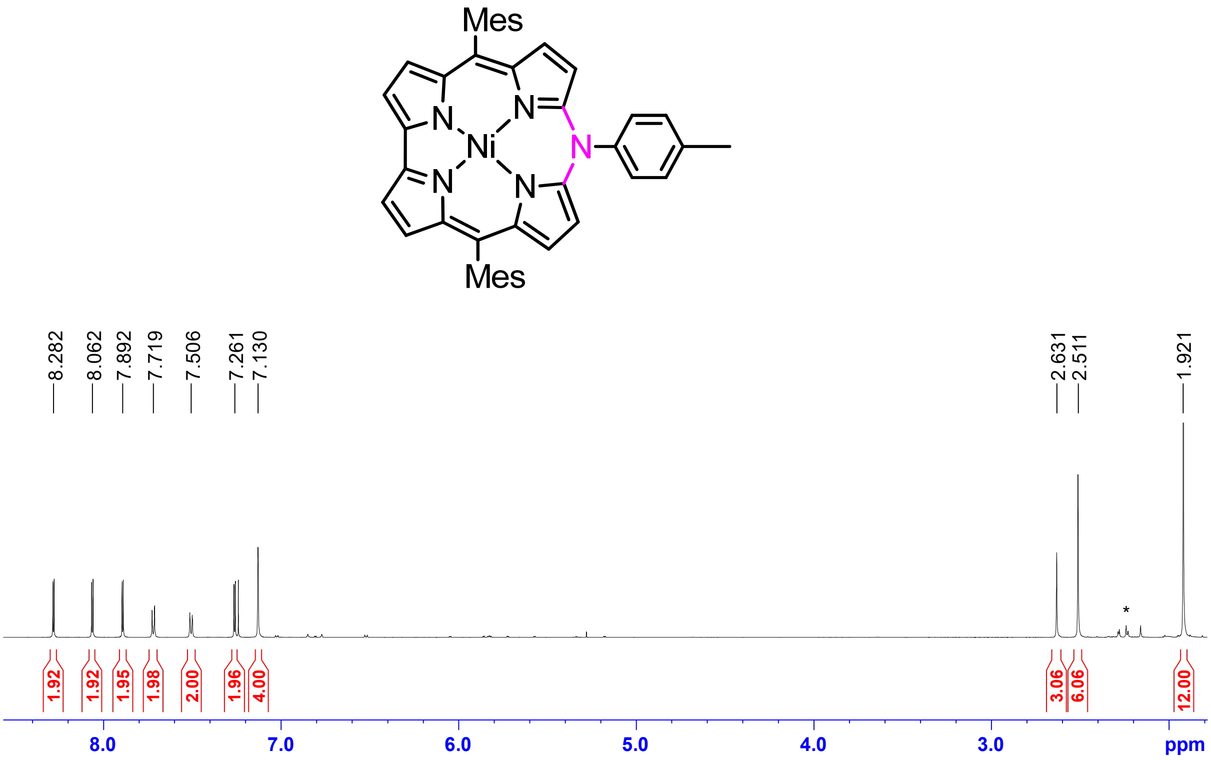

Figure S58. ^{1}H NMR spectrum (600 MHz, CDCl$_3$, 300 K) of **3o**.

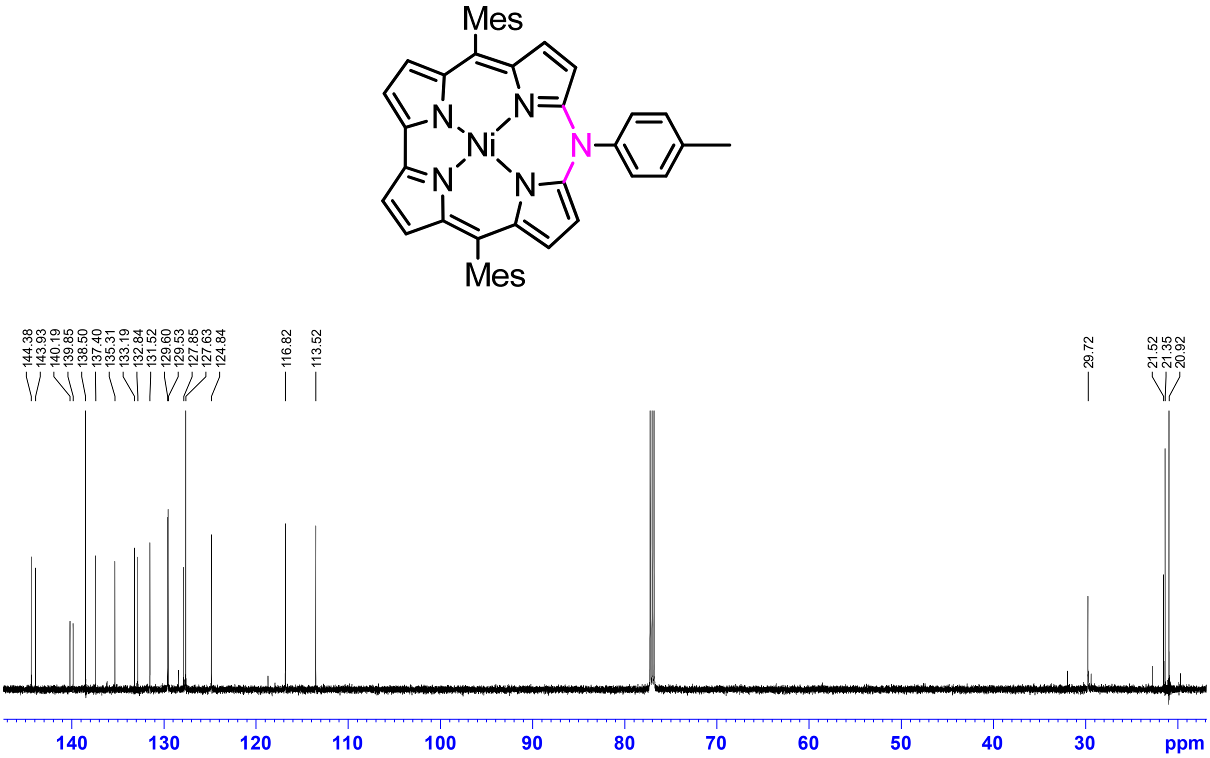

Figure S59. ^{13}C NMR spectrum (150 MHz, CDCl$_3$, 300 K) of **3o**.

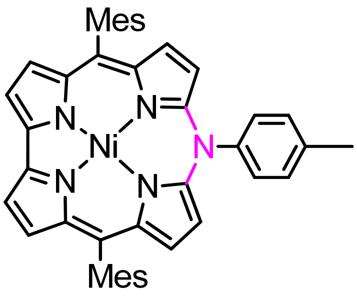

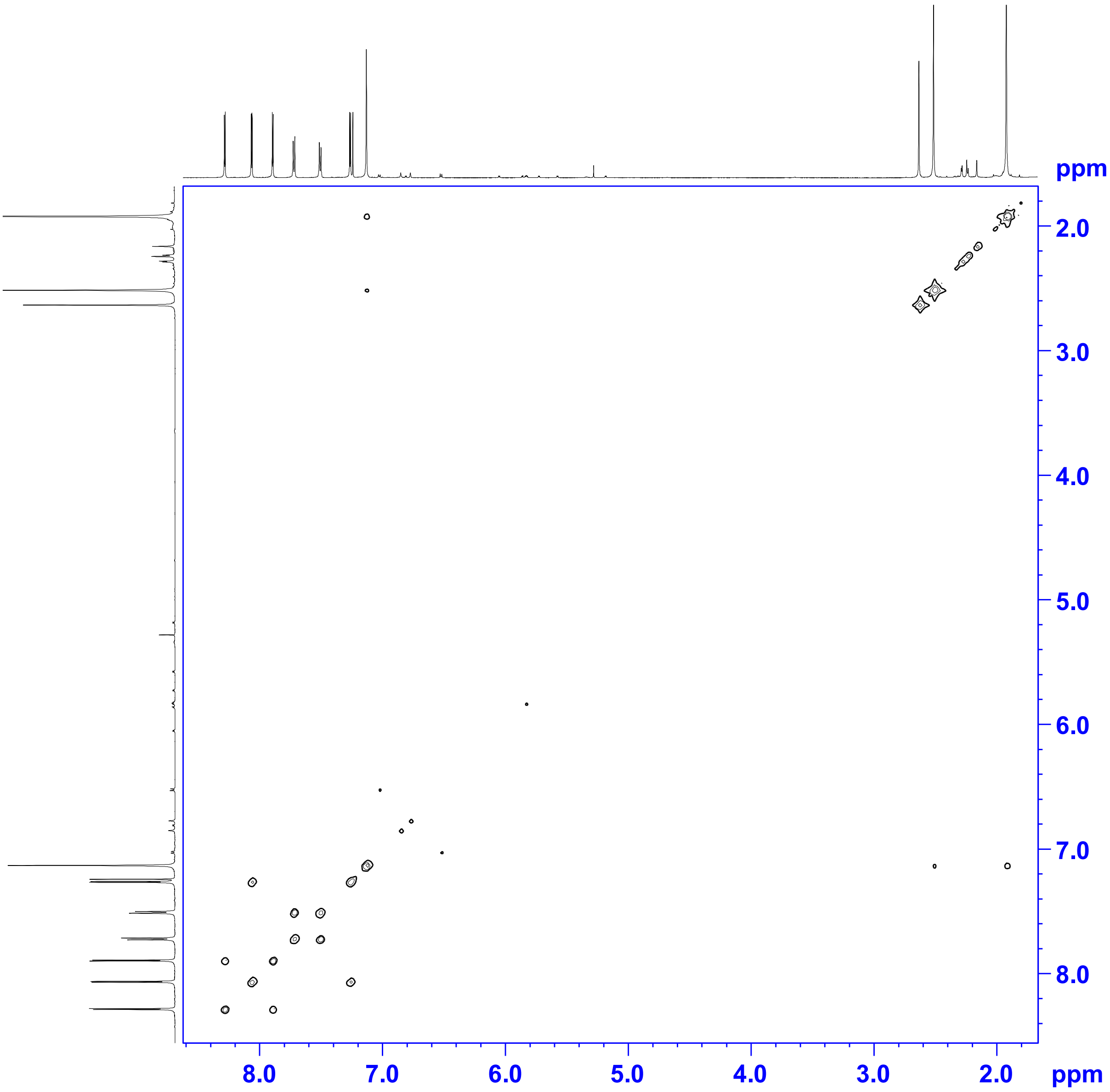

Figure S60. $^1H,^1H$ COSY spectrum (600 MHz, $CDCl_3$, 300 K) of **3o**.

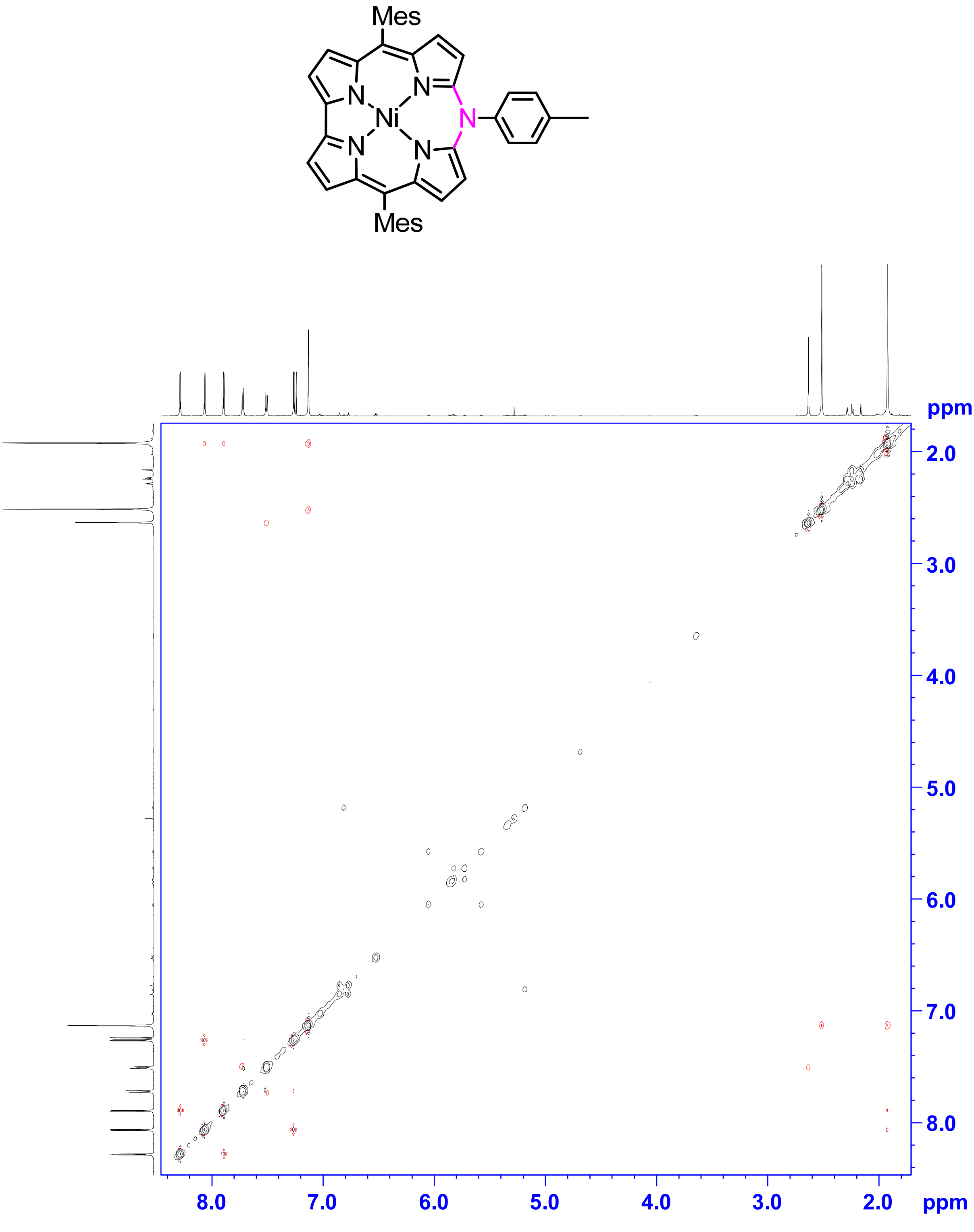

Figure S61. ^{1}H,^{1}H NOESY spectrum (600 MHz, CDCl$_3$, 300 K) of **3o**.

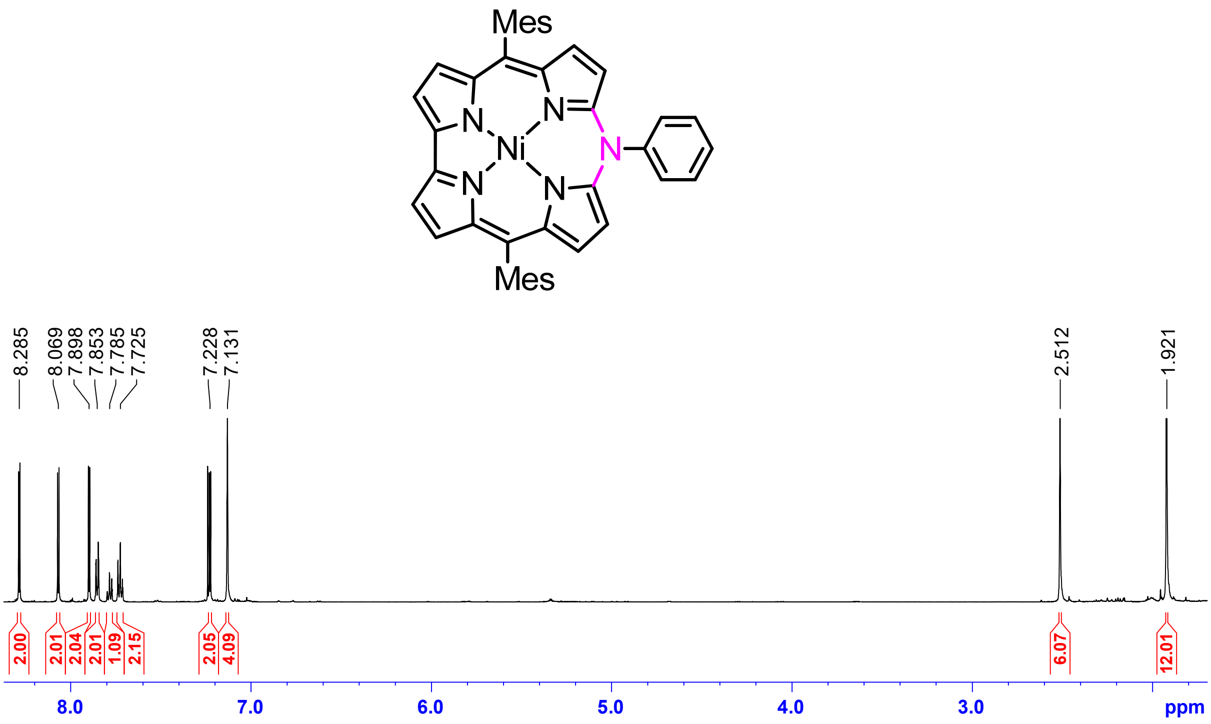

Figure S62. ^{1}H NMR spectrum (600 MHz, CDCl$_3$, 300 K) of **3p**.

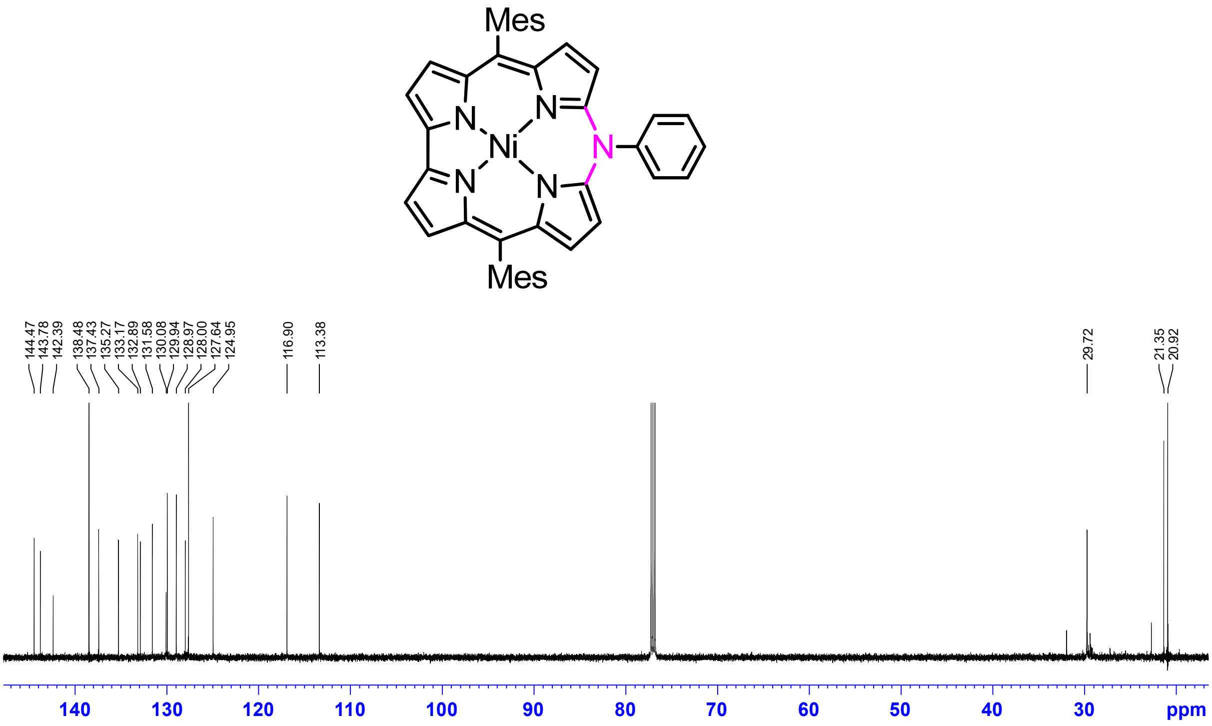

Figure S63. ^{13}C NMR spectrum (150 MHz, CDCl$_3$, 300 K) of **3p**.

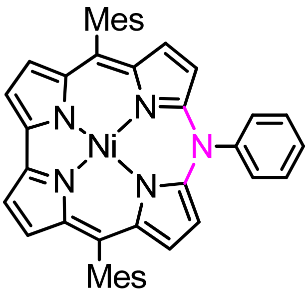

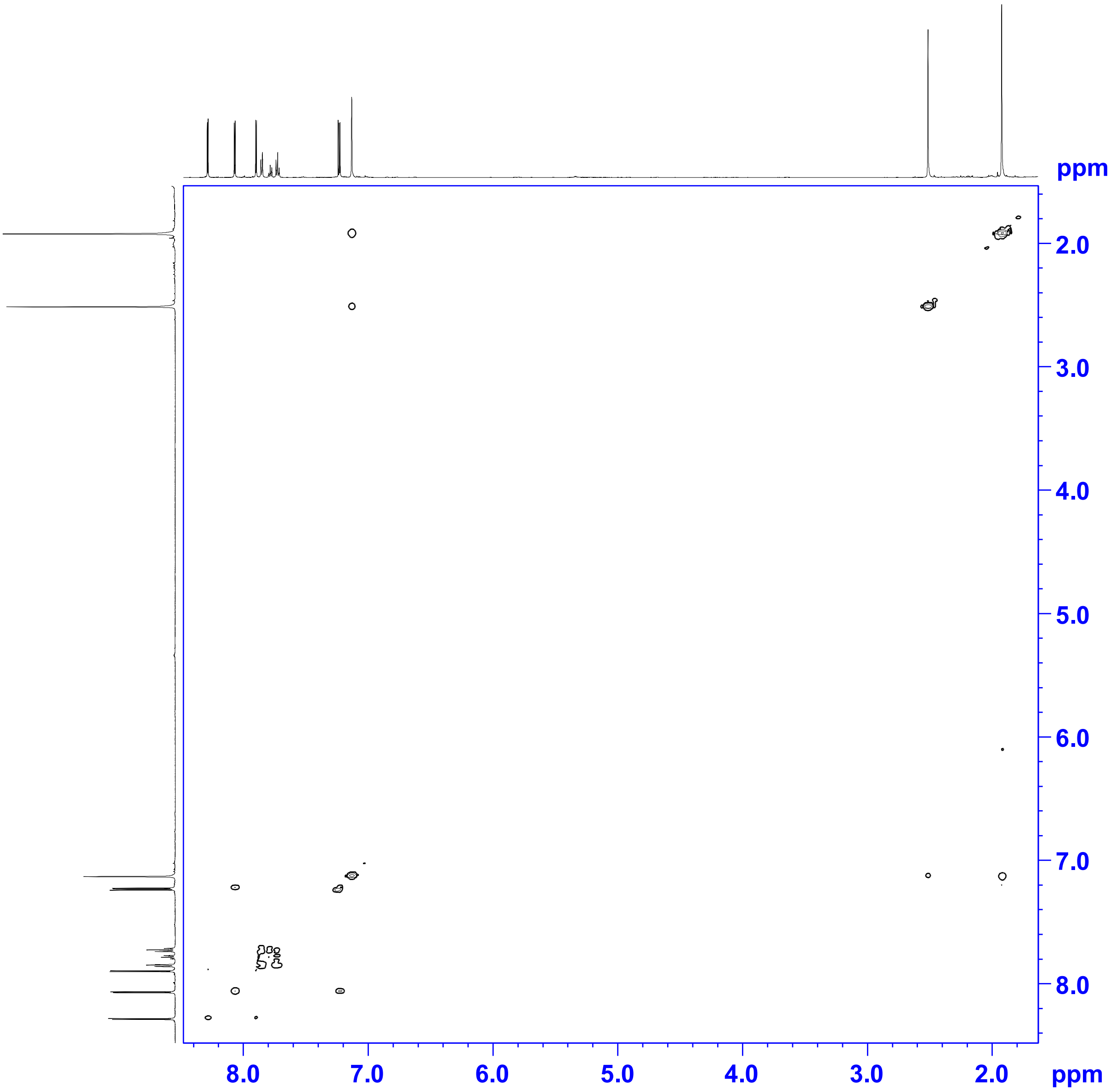

Figure S64. ^{1}H,^{1}H COSY spectrum (500 MHz, $CDCl_3$, 300 K) of **3p**.

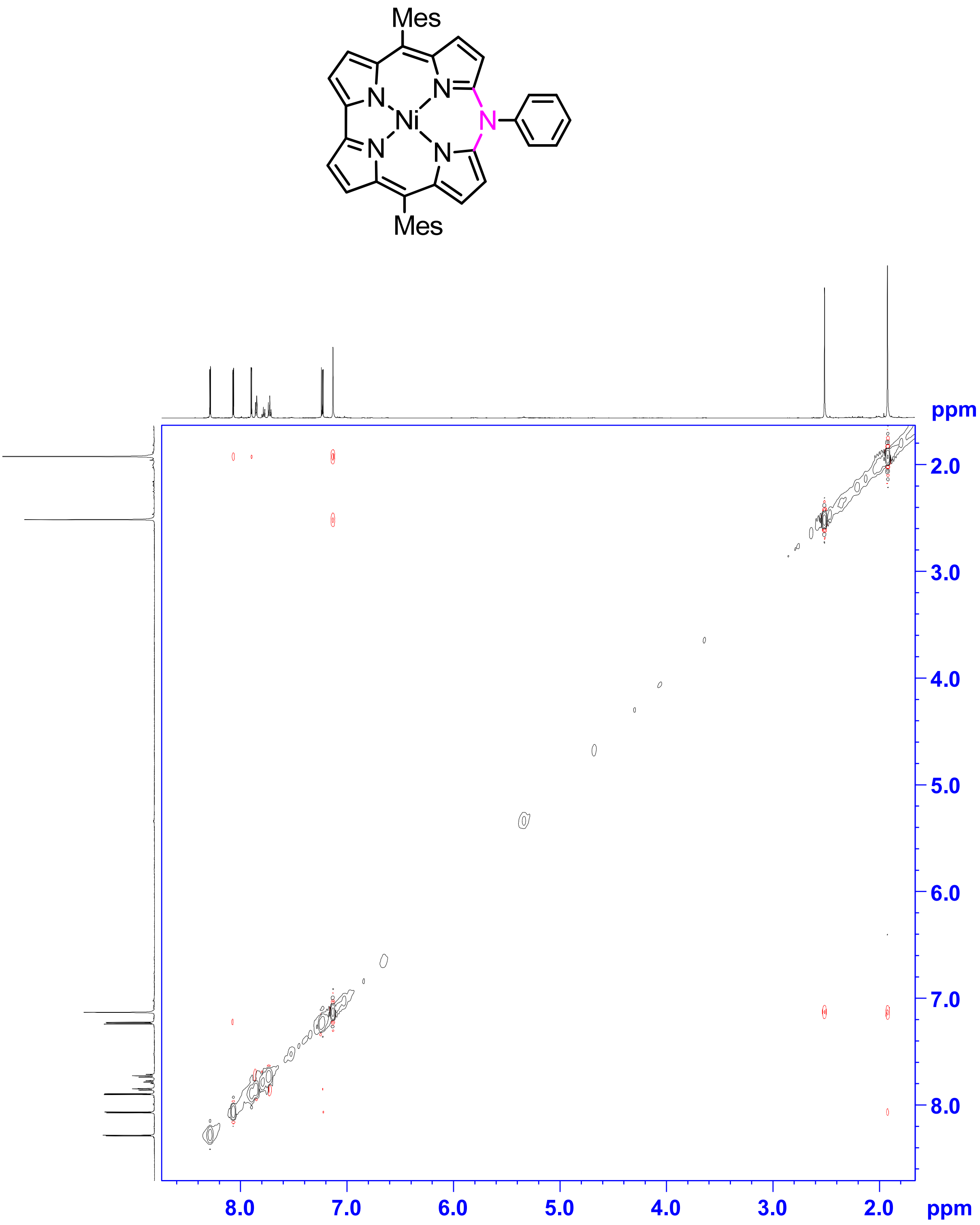

Figure S65. ^{1}H,^{1}H NOESY spectrum (500 MHz, CDCl$_3$, 300 K) of **3p**.

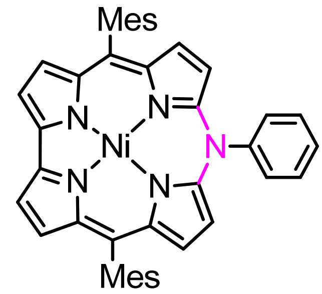

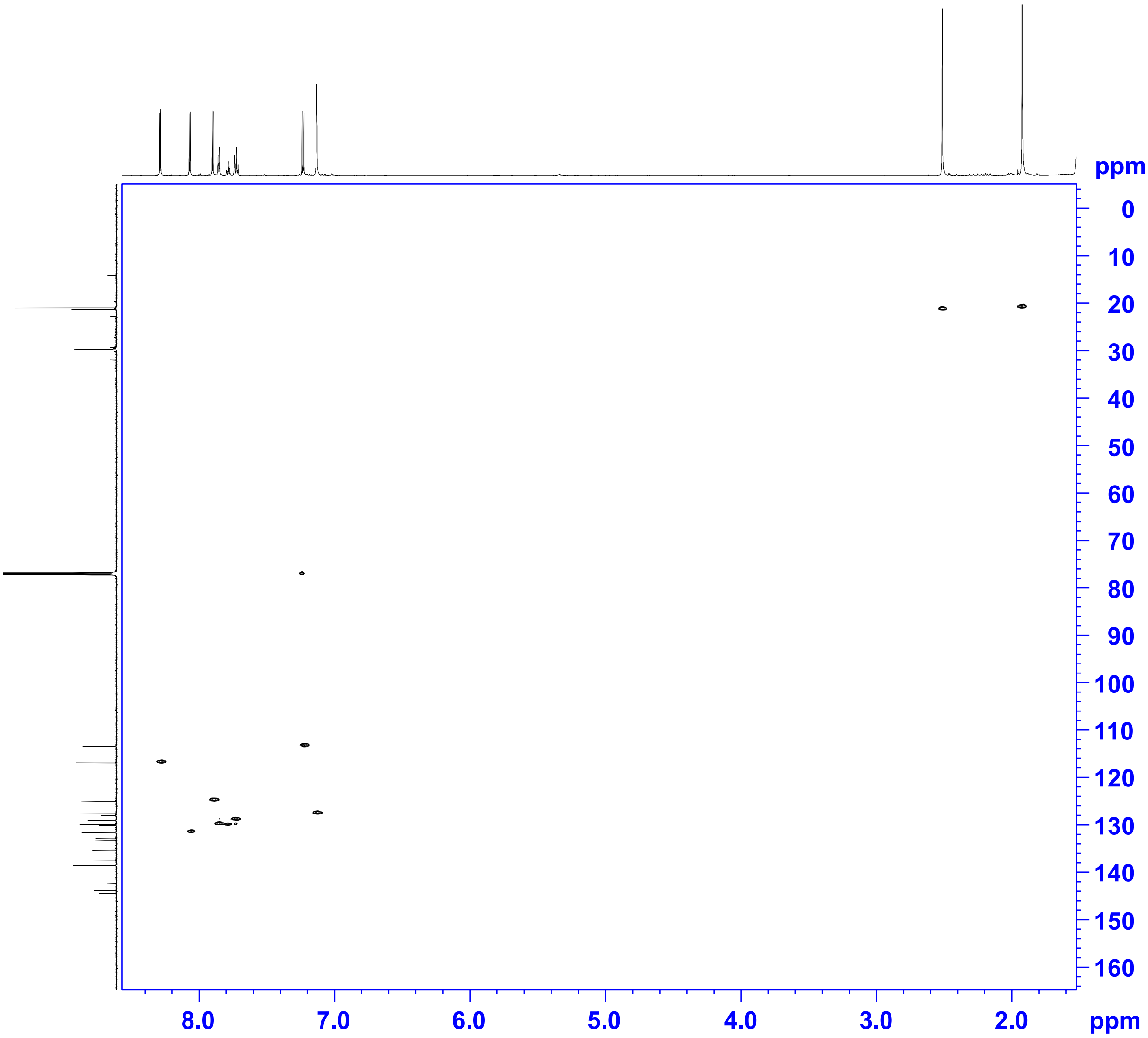

Figure S66. $^1H,^{13}C$ HSQC spectrum (500/125 MHz, $CDCl_3$, 300 K) of **3p**.

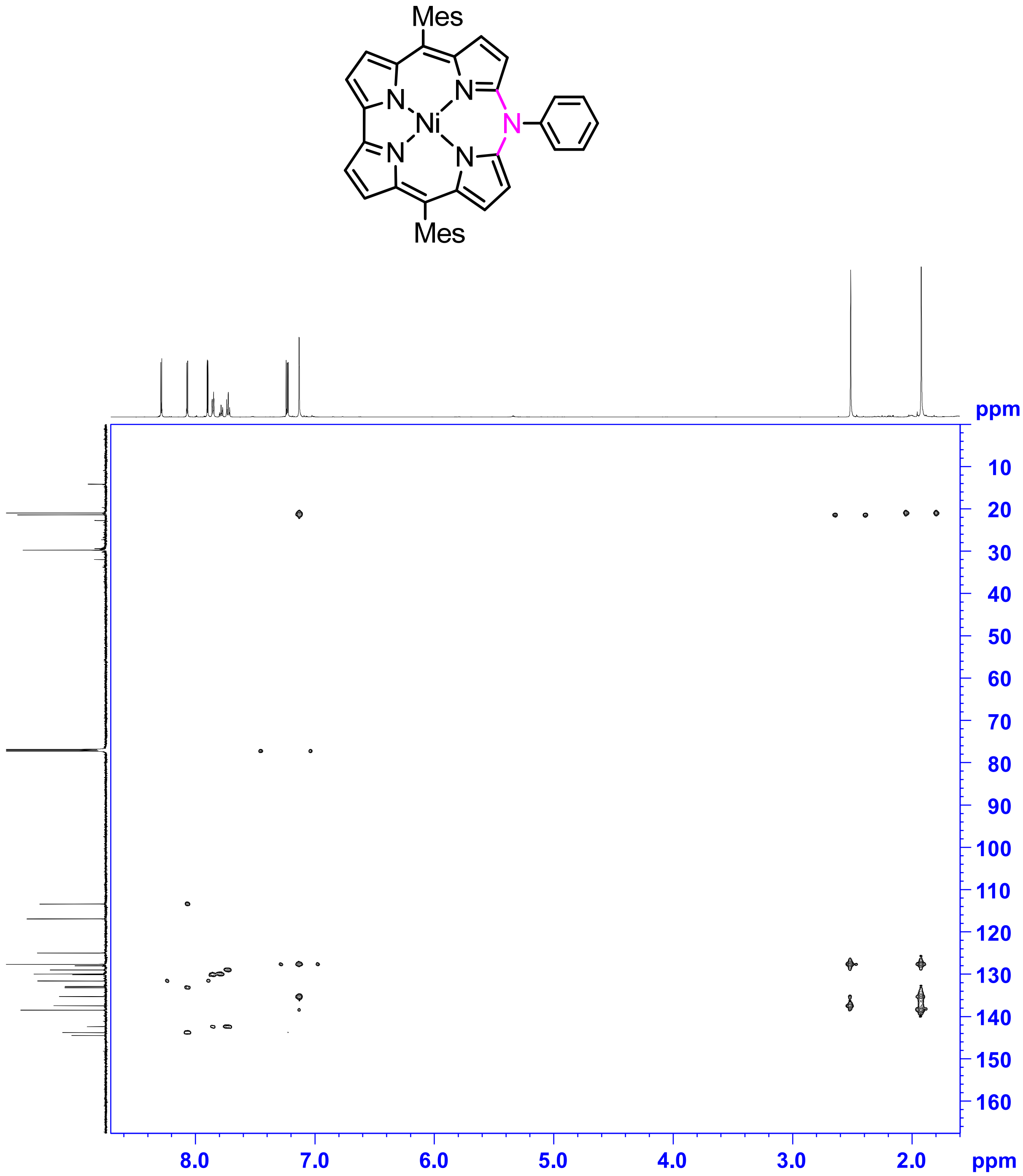

Figure S67. ^{1}H,^{13}C HMBC spectrum (500/125 MHz, CDCl$_3$, 300 K) of **3p**.

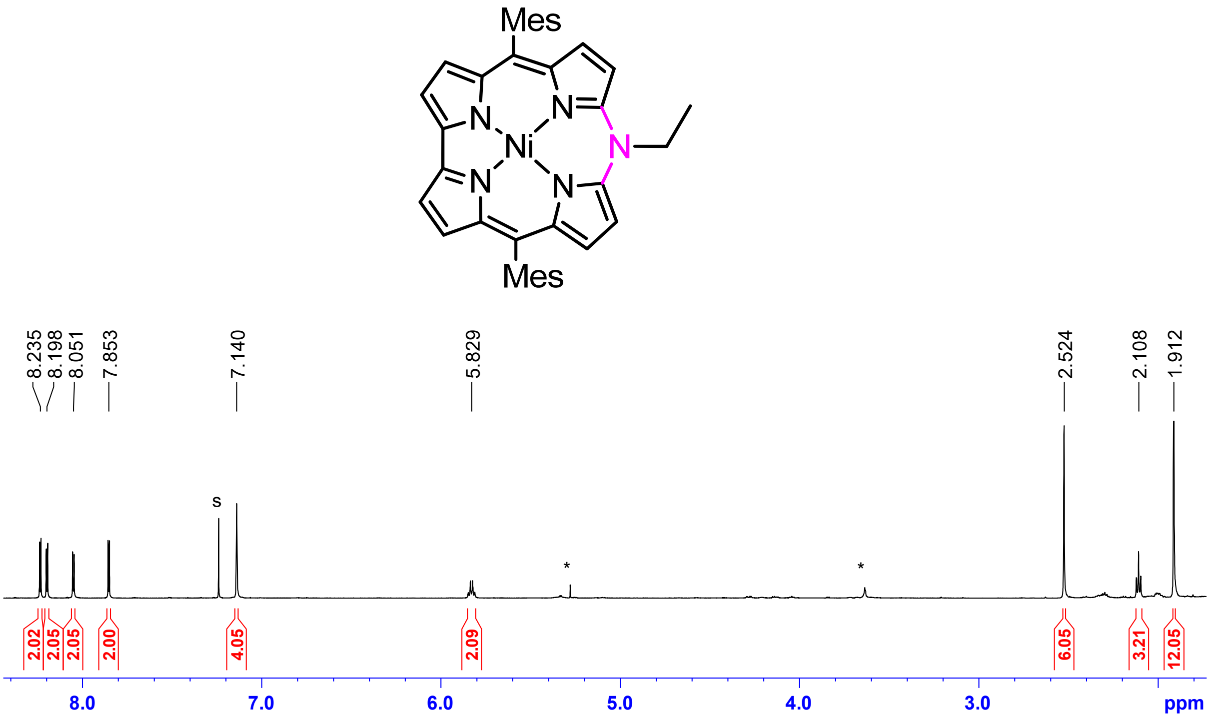

Figure S68. ^{1}H NMR spectrum (600 MHz, CDCl$_3$, 300 K) of **3q**.

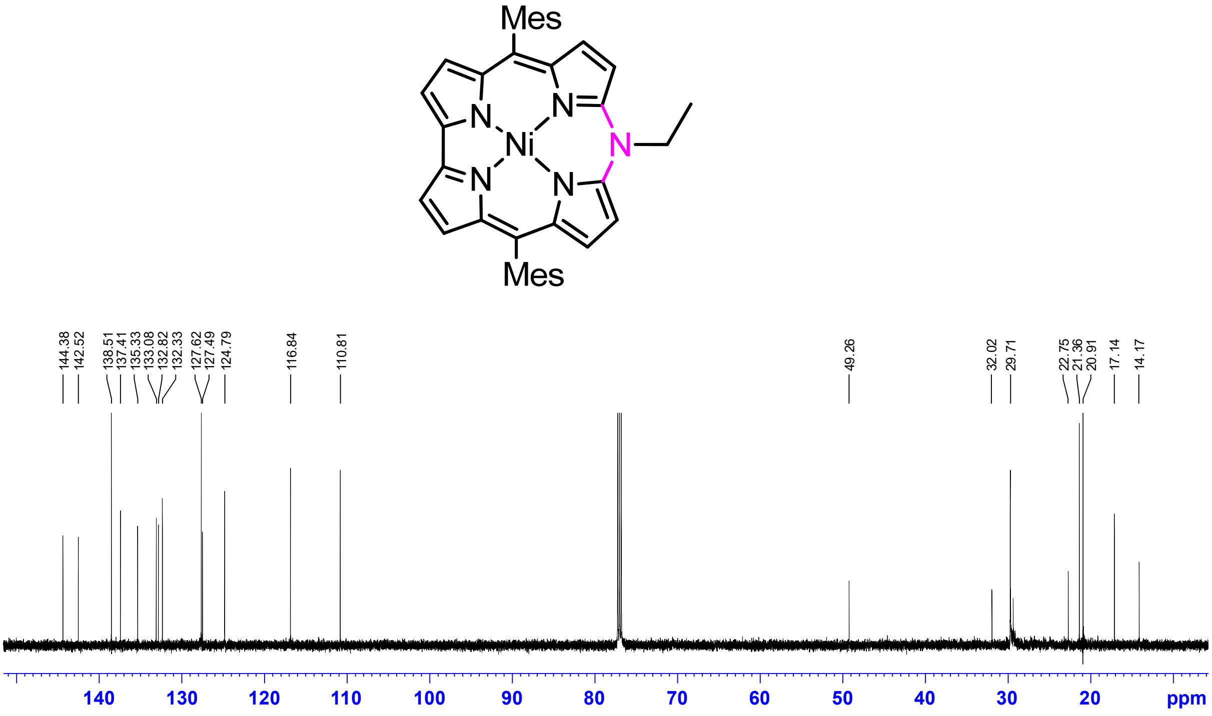

Figure S69. ^{13}C NMR spectrum (150 MHz, CDCl$_3$, 300 K) of **3q**.

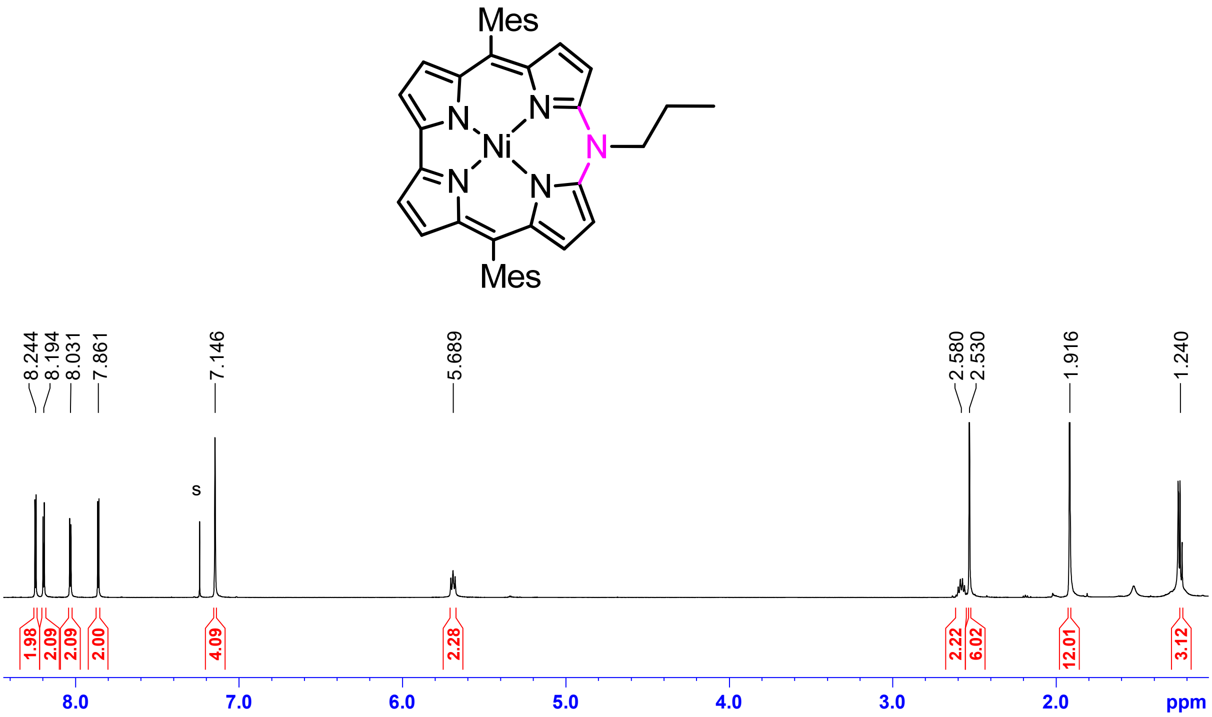

Figure S70. ^{1}H NMR spectrum (600 MHz, CDCl$_3$, 300 K) of **3r**.

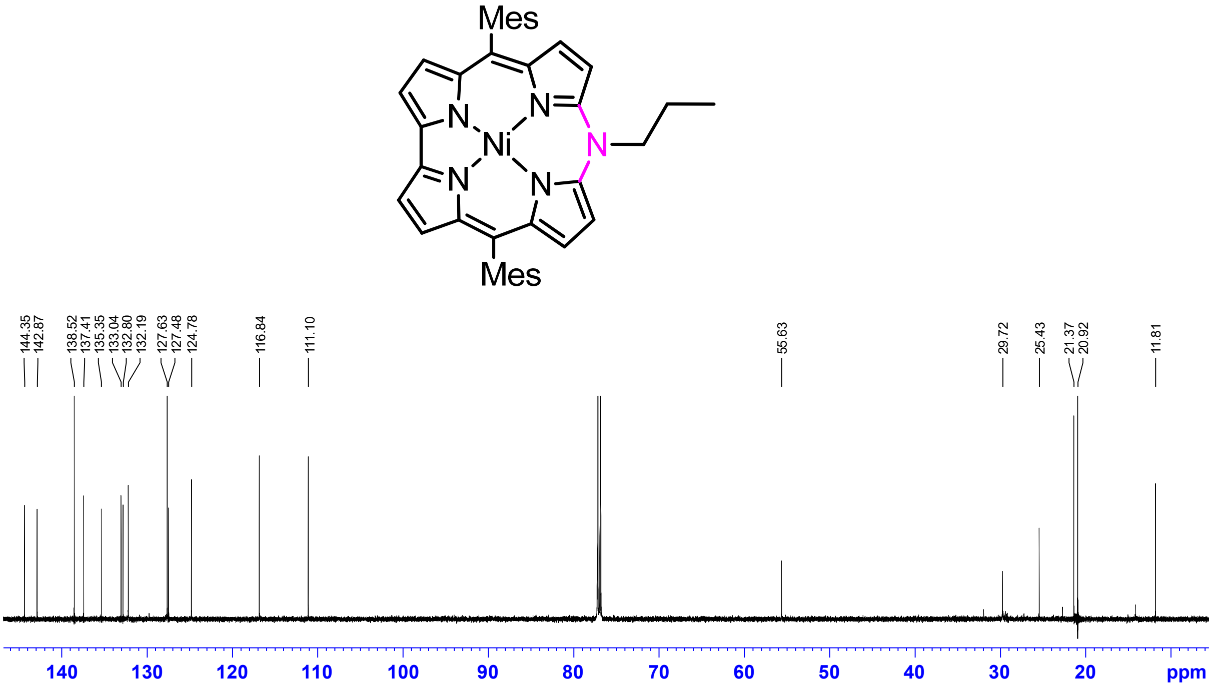

Figure S71. ^{13}C NMR spectrum (150 MHz, CDCl$_3$, 300 K) of **3r**.

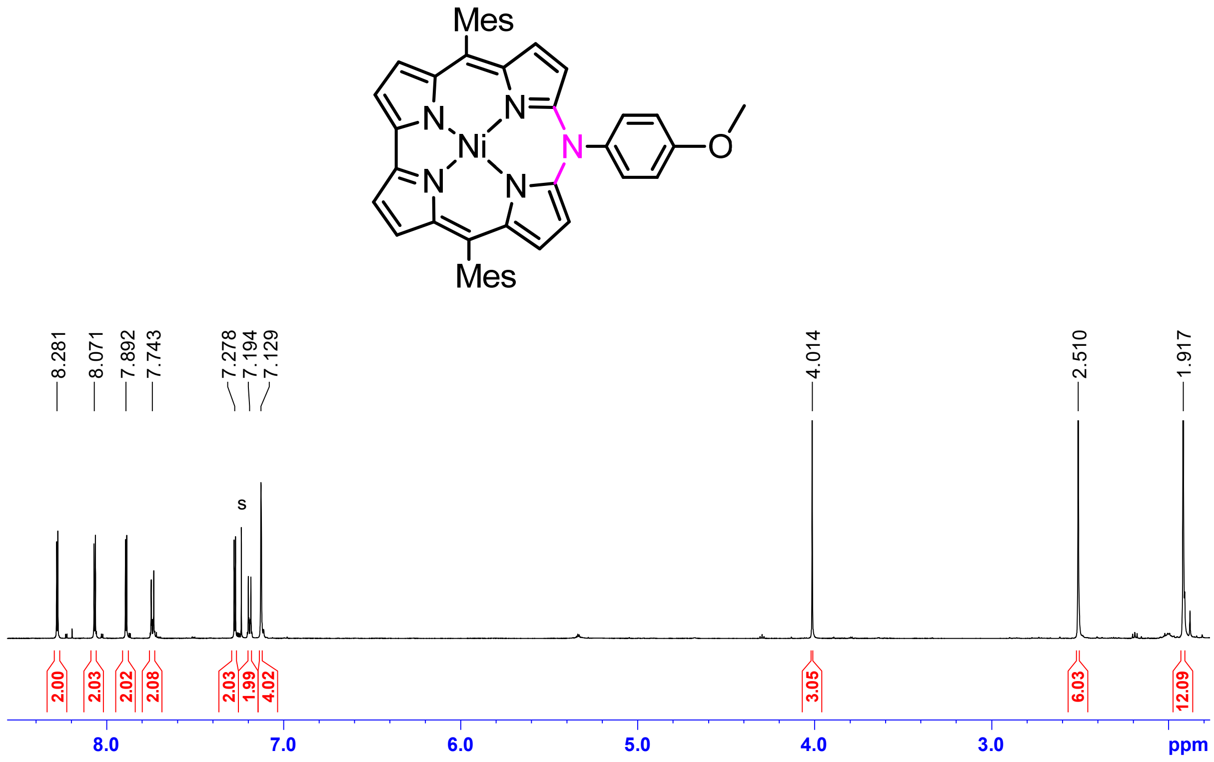

Figure S72. ^{1}H NMR spectrum (600 MHz, $CDCl_3$, 300 K) of **3s**.

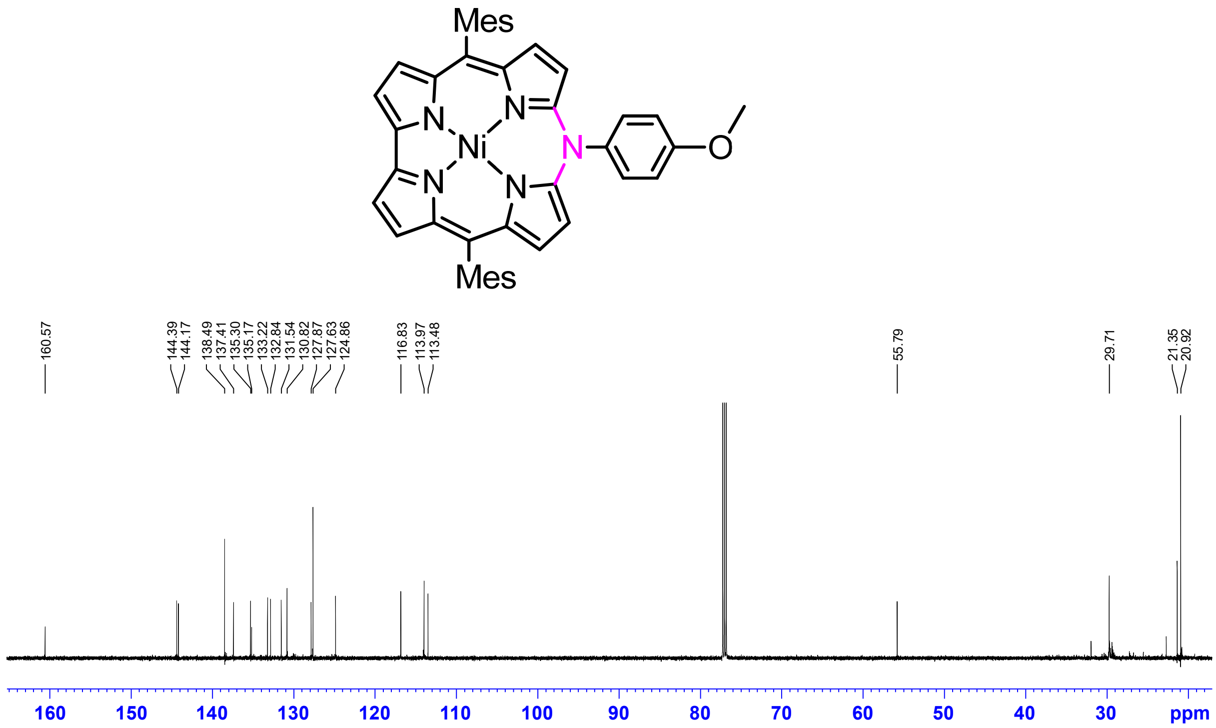

Figure S73. ^{13}C NMR spectrum (150 MHz, $CDCl_3$, 300 K) of **3s**.

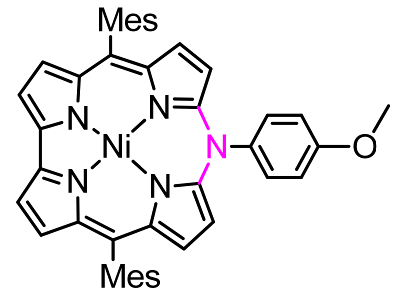

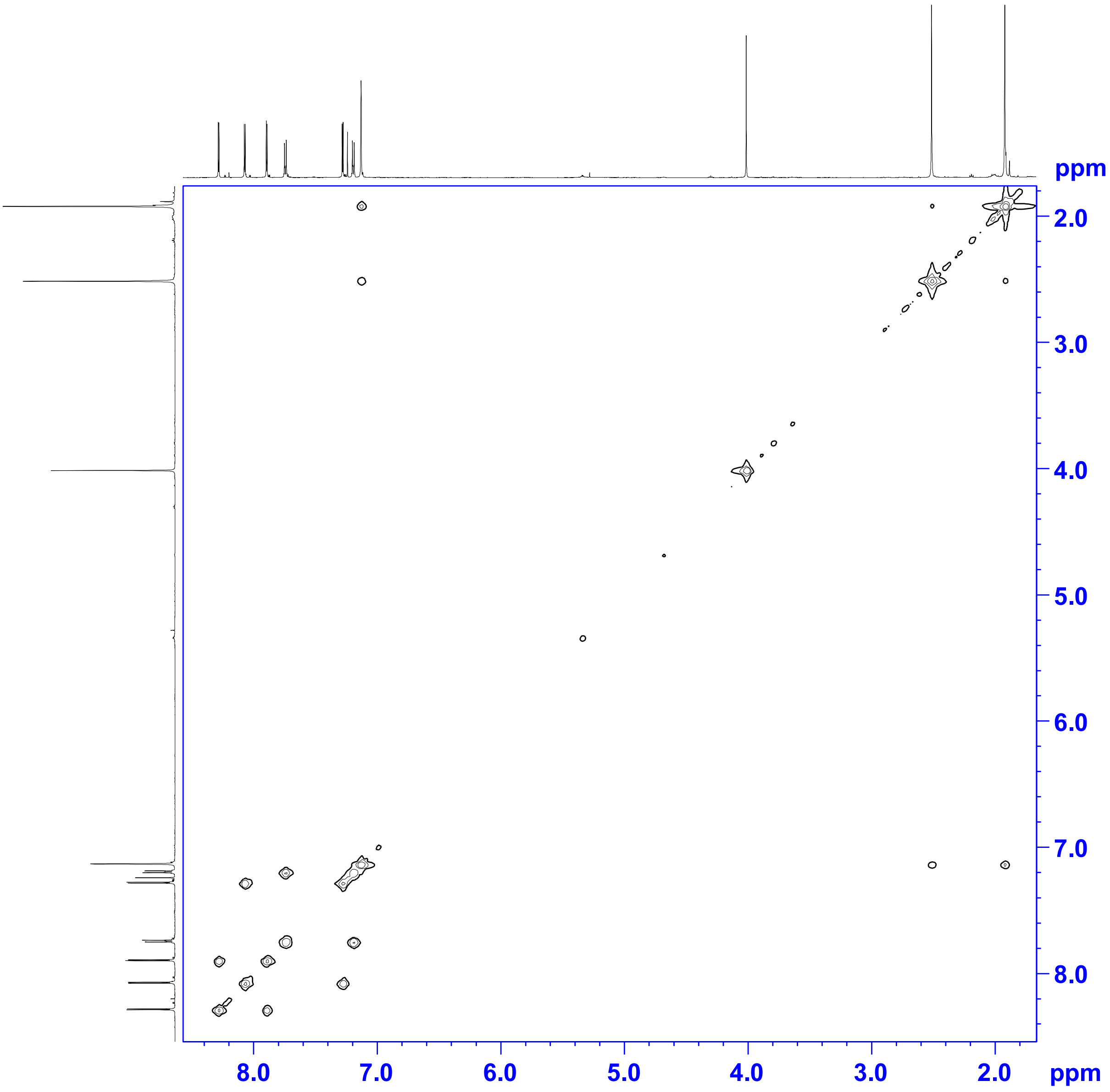

Figure S74. ^{1}H,^{1}H COSY spectrum (600 MHz, CDCl$_3$, 300 K) of **3s**.

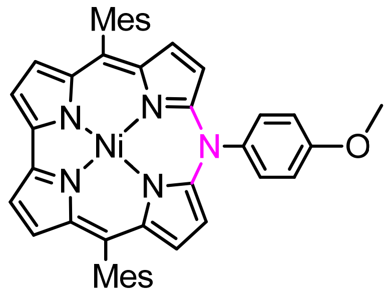

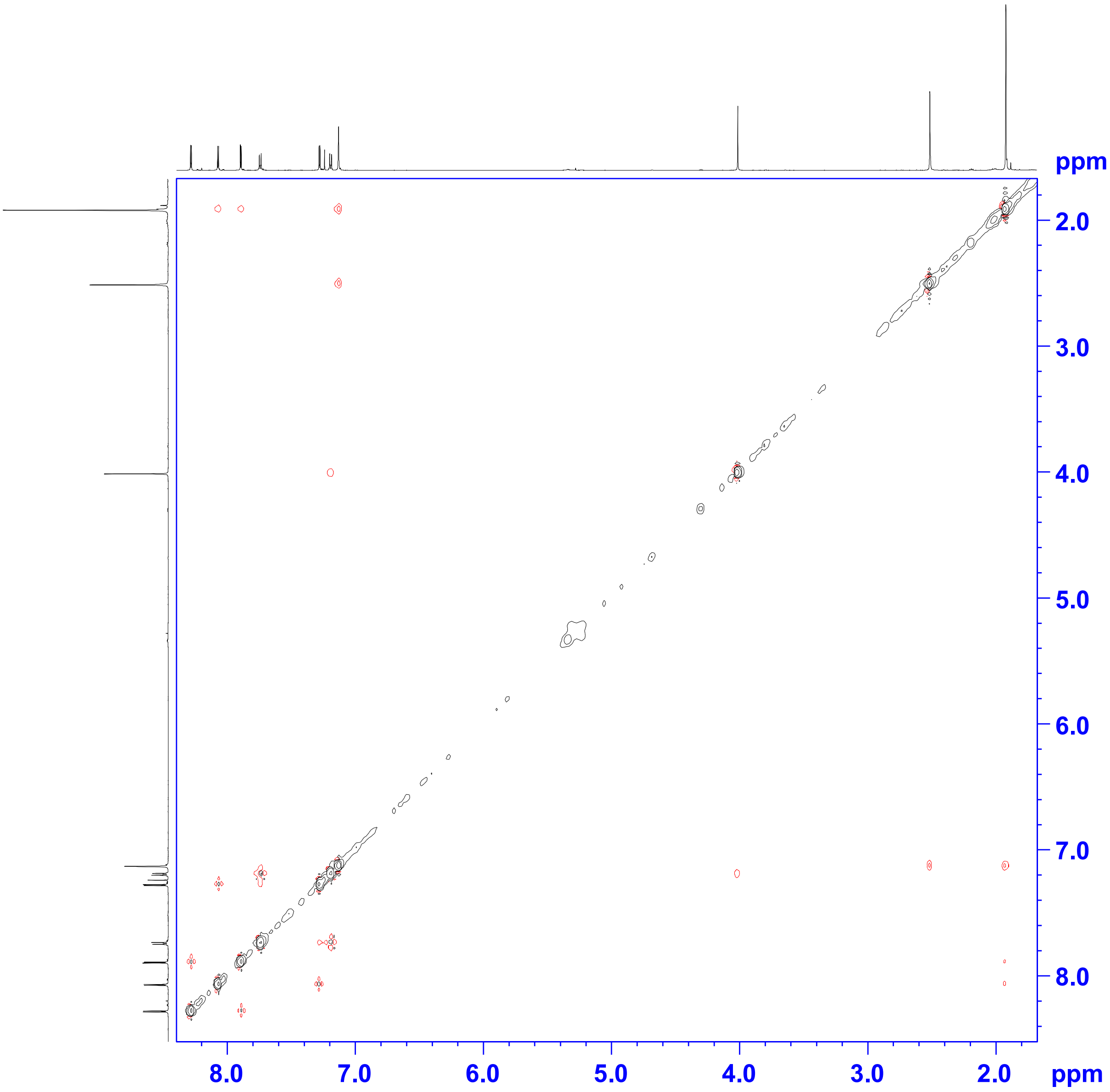

Figure S75. $^1H,^1H$ NOESY spectrum (600 MHz, $CDCl_3$, 300 K) of **3s**.

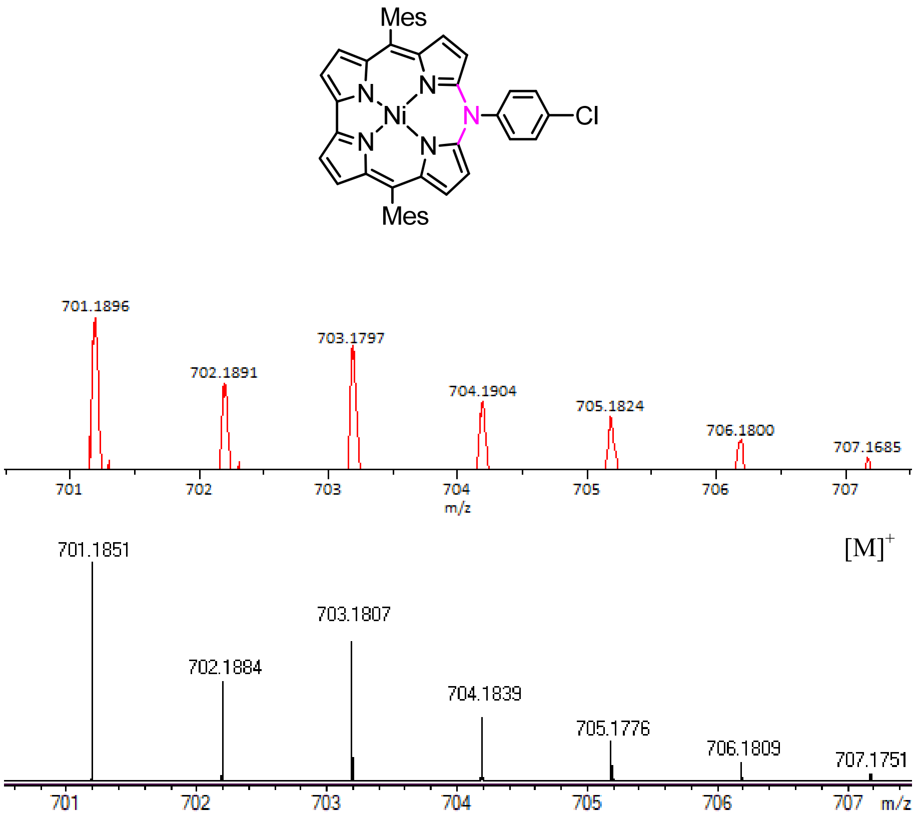

Figure S76. ESI(+) HRMS spectrum of **3a** (experimental: red, upper trace; simulated: black, bottom trace).

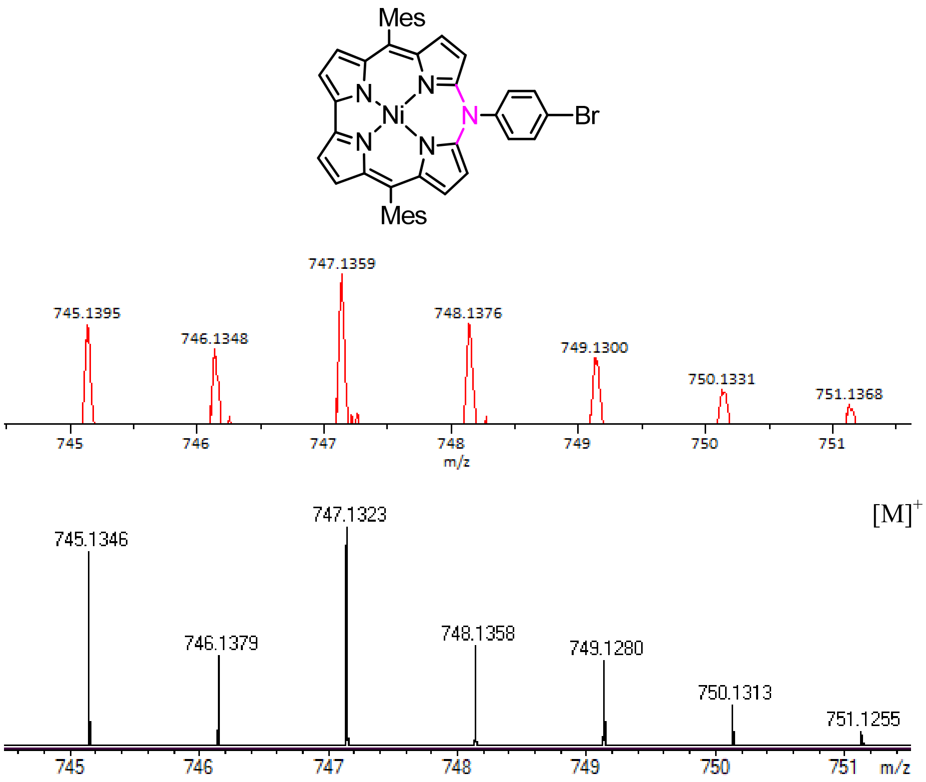

Figure S77. ESI(+) HRMS spectrum of **3b** (experimental: red, upper trace; simulated: black, bottom trace).

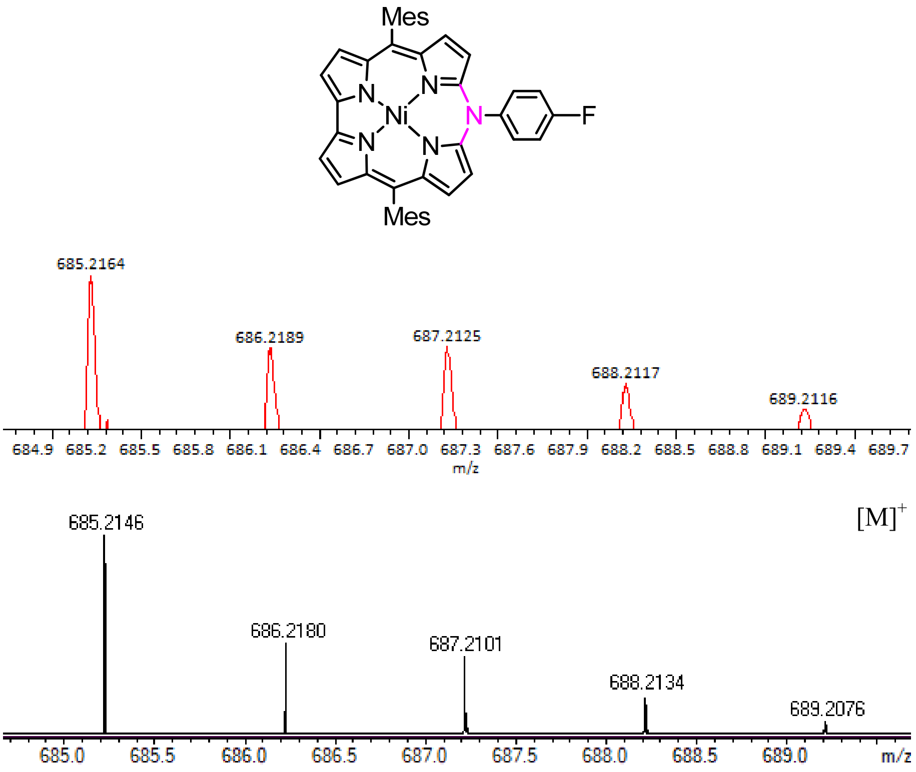

Figure S78. ESI(+) HRMS spectrum of **3c** (experimental: red, upper trace; simulated: black, bottom trace).

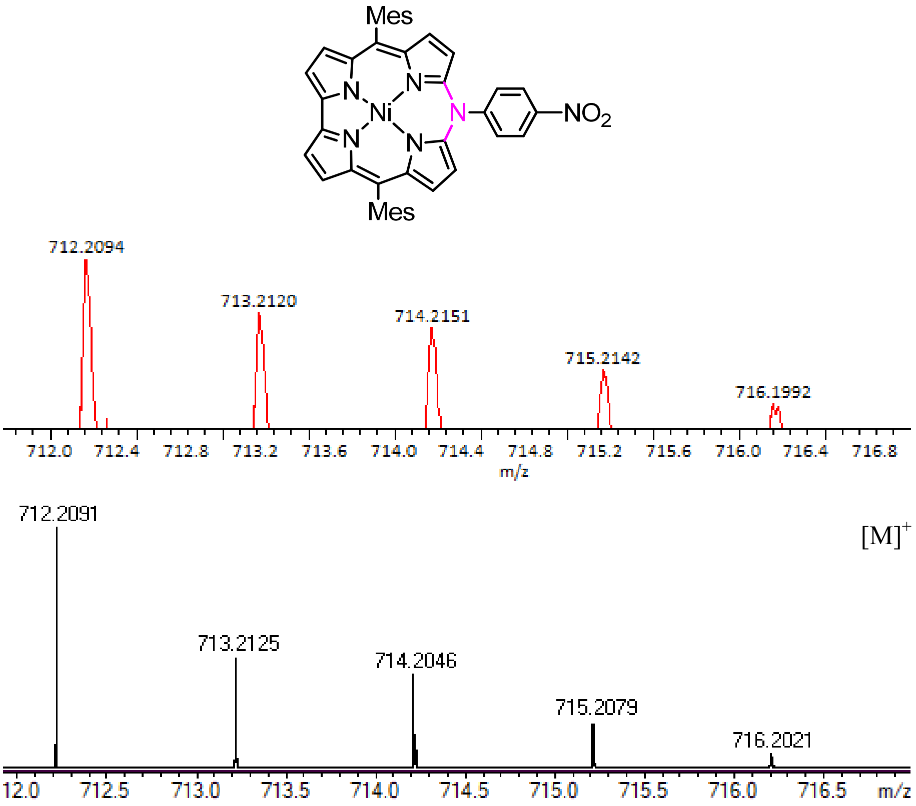

Figure S79. ESI(+) HRMS spectrum of **3d** (experimental: red, upper trace; simulated: black, bottom trace).

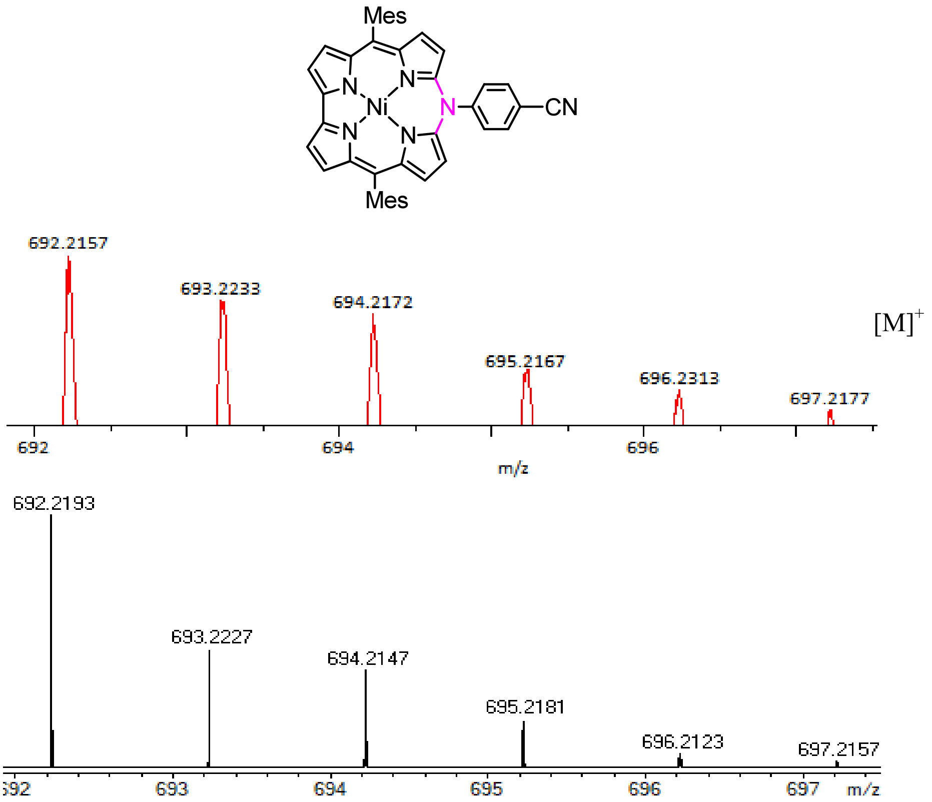

Figure S80. ESI(+) HRMS spectrum of **3e** (experimental: red, upper trace; simulated: black, bottom trace).

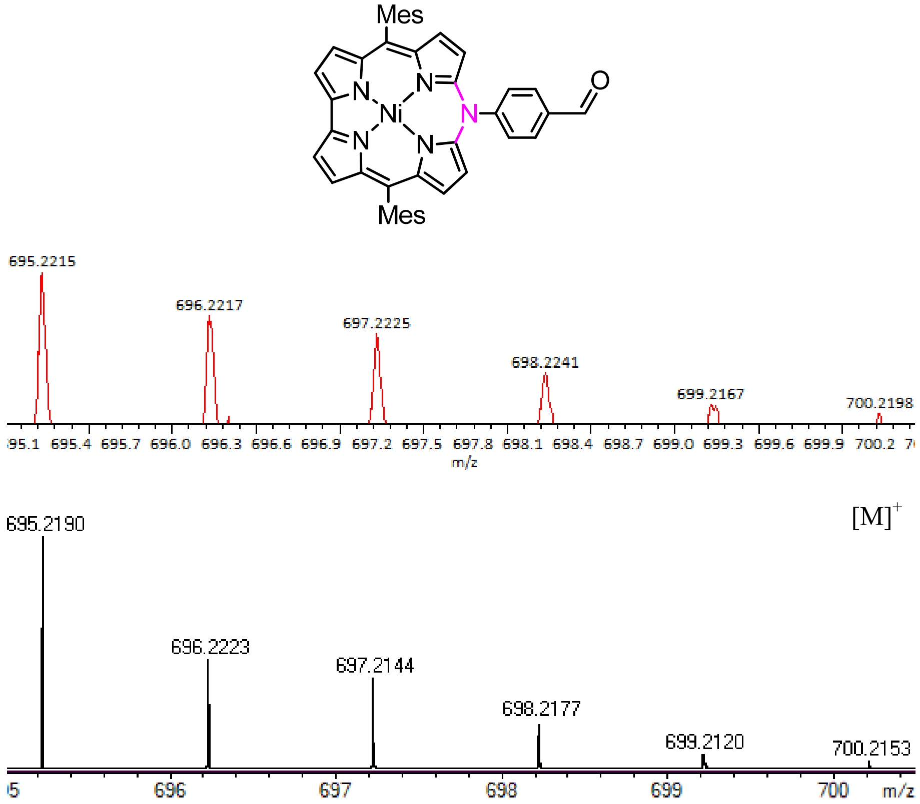

Figure S81. ESI(+) HRMS spectrum of **3f** (experimental: red, upper trace; simulated: black, bottom trace).

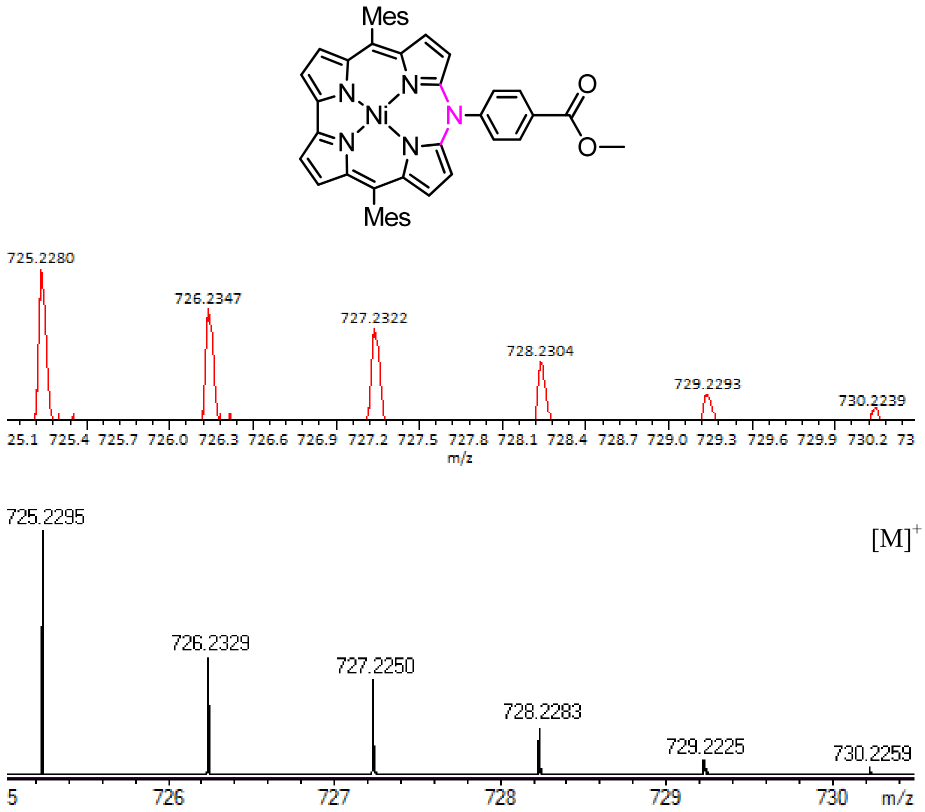

Figure S82. ESI(+) HRMS spectrum of **3g** (experimental: red, upper trace; simulated: black, bottom trace).

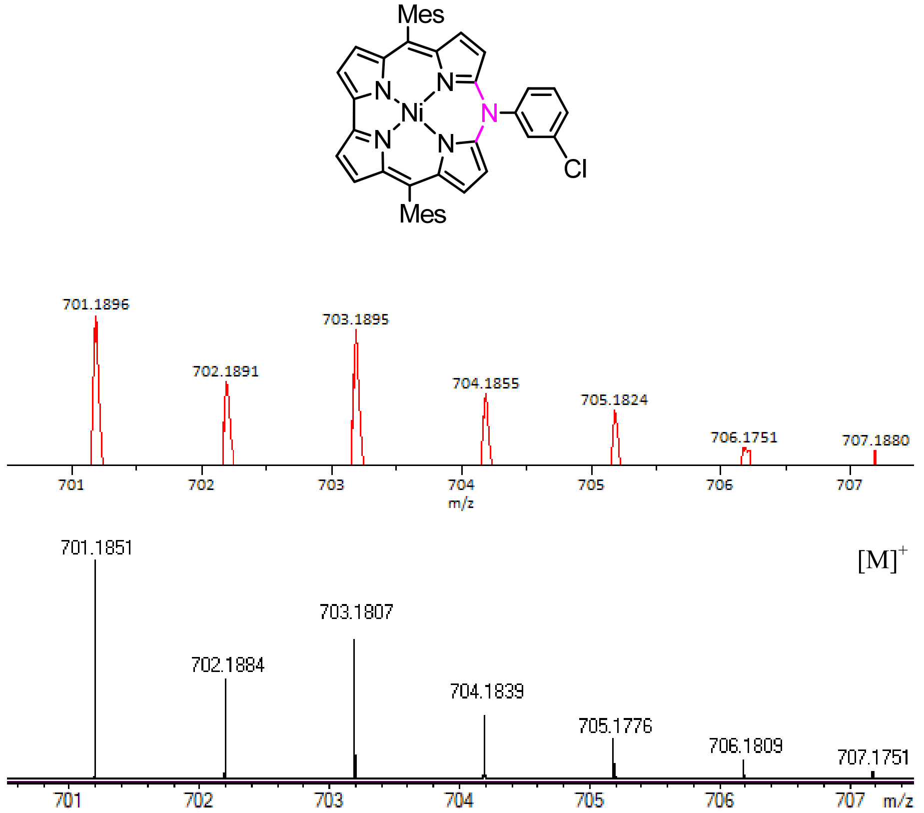

Figure S83. ESI(+) HRMS spectrum of **3h** (experimental: red, upper trace; simulated: black, bottom trace).

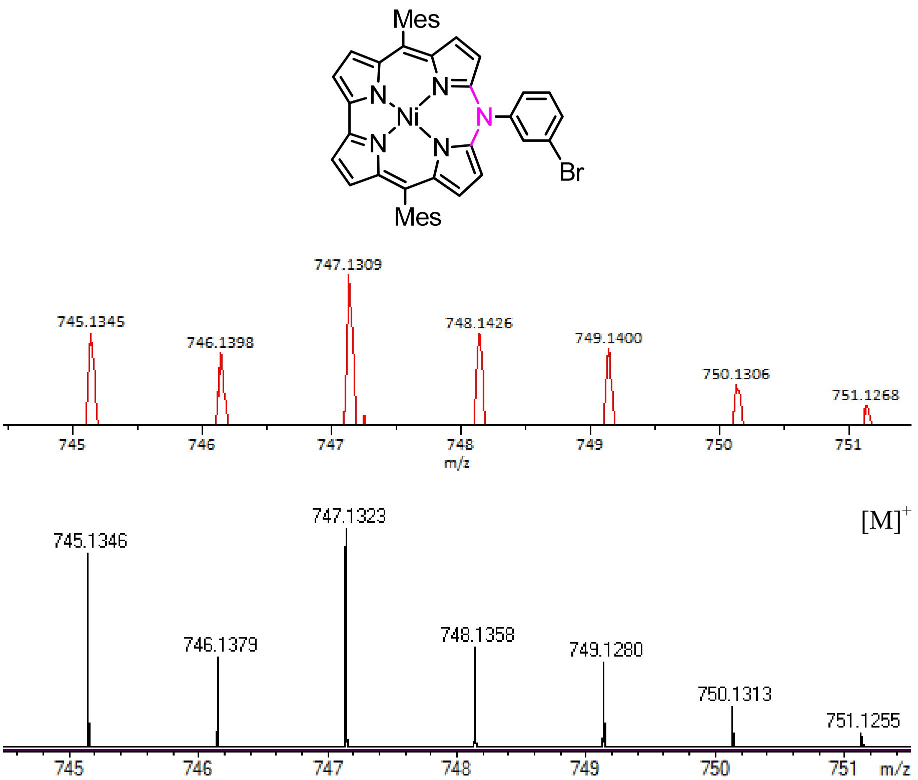

Figure S84. ESI(+) HRMS spectrum of **3i** (experimental: red, upper trace; simulated: black, bottom trace).

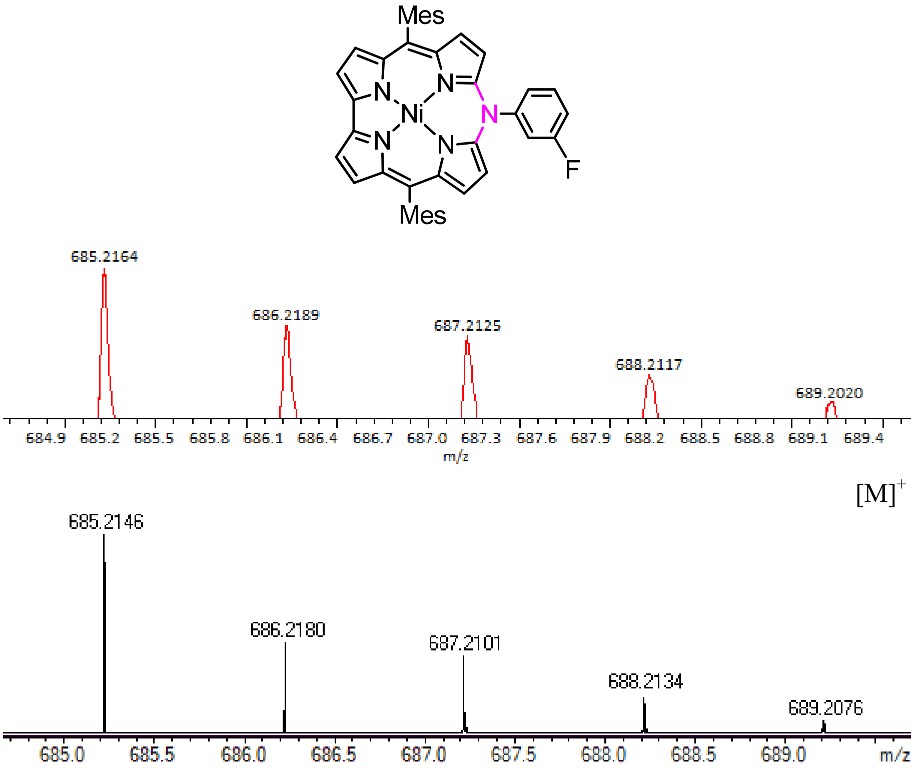

Figure S85. ESI(+) HRMS spectrum of **3j** (experimental: red, upper trace; simulated: black, bottom trace).

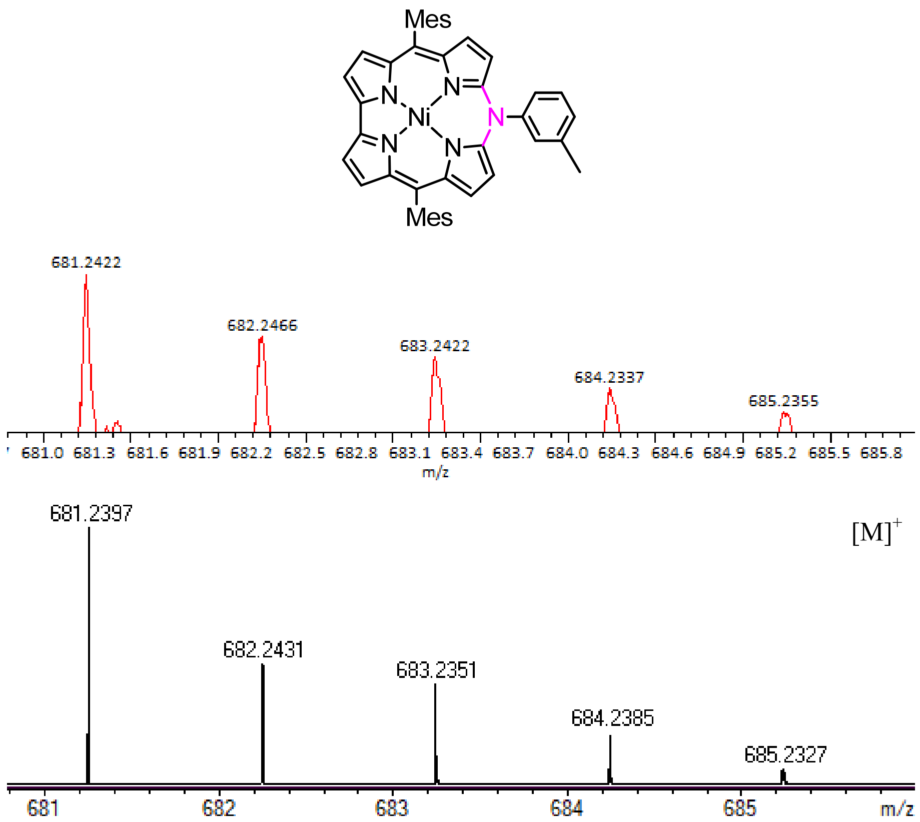

Figure S86. ESI(+) HRMS spectrum of **3k** (experimental: red, upper trace; simulated: black, bottom trace).

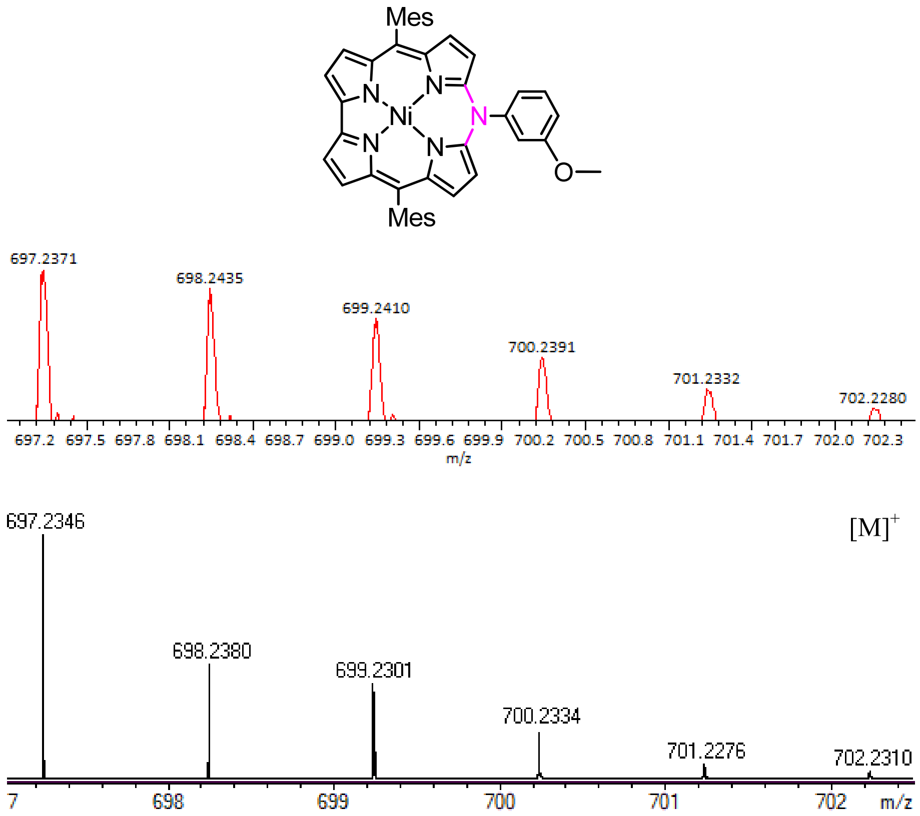

Figure S87. ESI(+) HRMS spectrum of **3l** (experimental: red, upper trace; simulated: black, bottom trace).

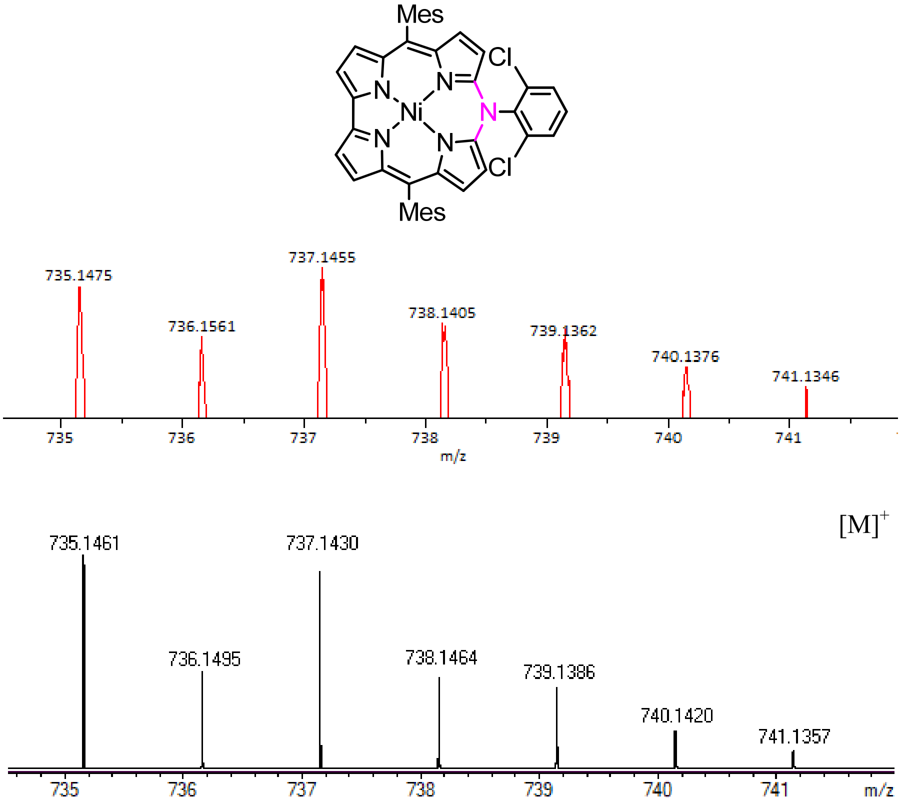

Figure S88. ESI(+) HRMS spectrum of **3m** (experimental: red, upper trace; simulated: black, bottom trace).

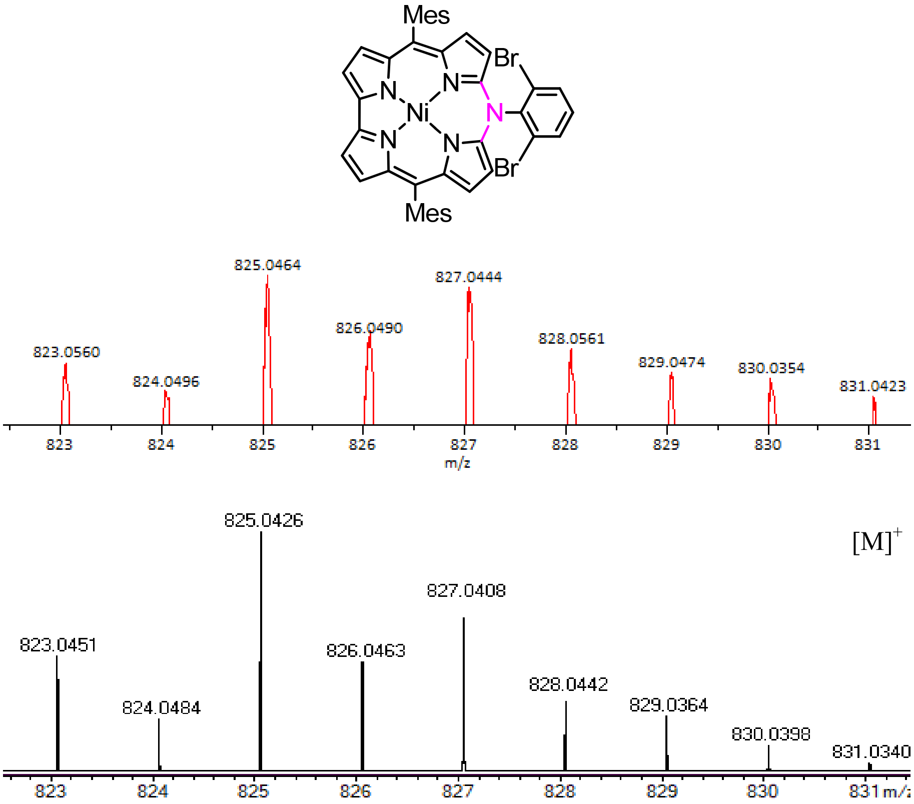

Figure S89. ESI(+) HRMS spectrum of **3n** (experimental: red, upper trace; simulated: black, bottom trace).

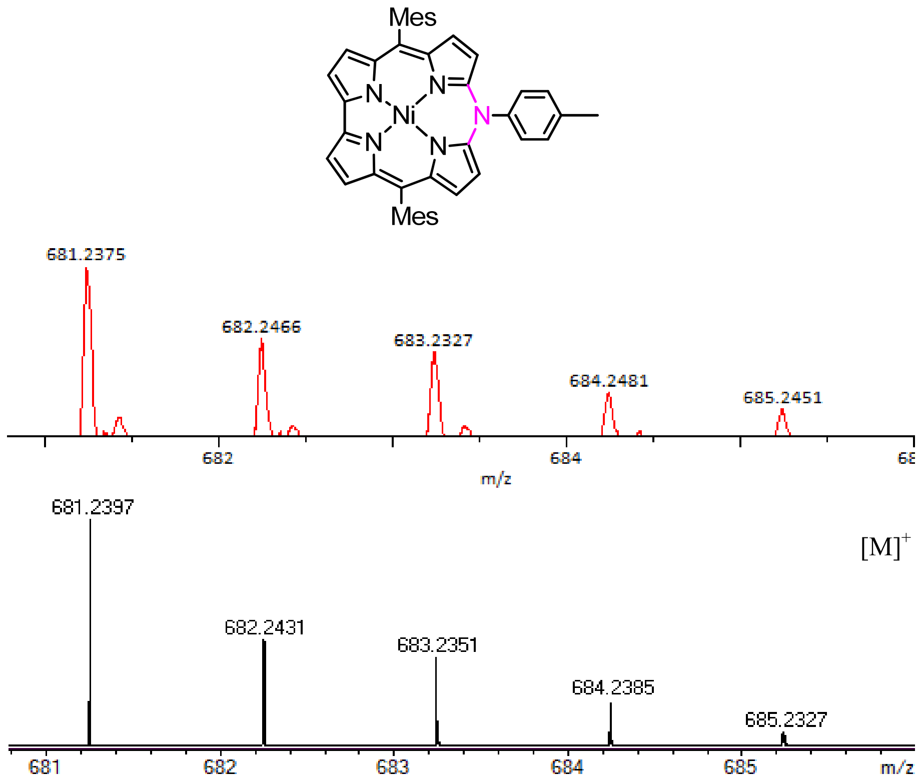

Figure S90. ESI(+) HRMS spectrum of **3o** (experimental: red, upper trace; simulated: black, bottom trace).

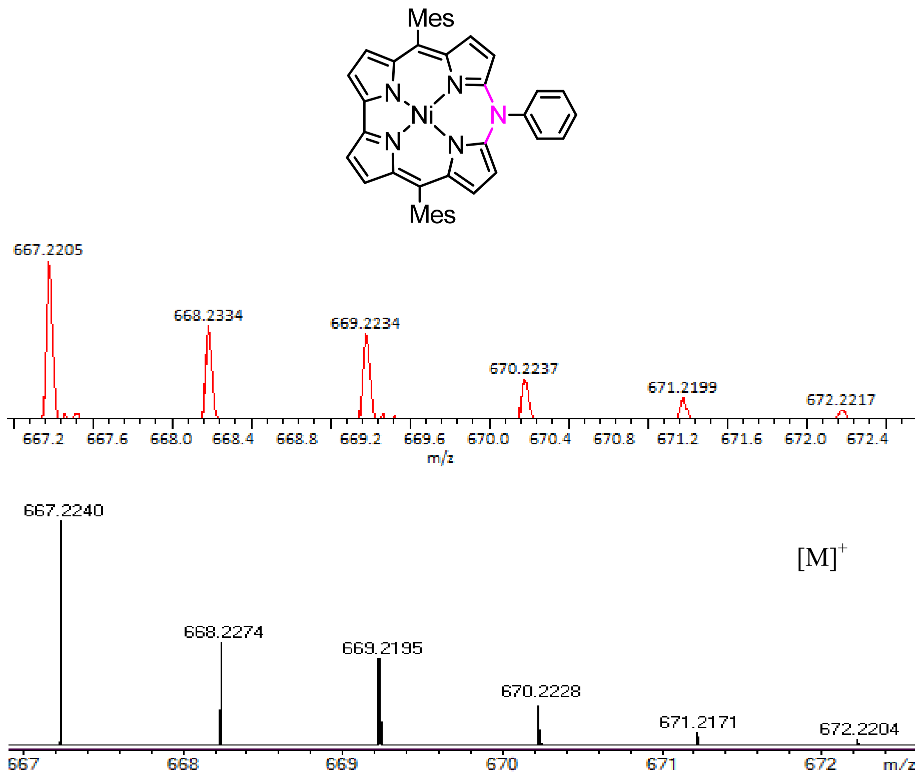

Figure S91. ESI(+) HRMS spectrum of **3p** (experimental: red, upper trace; simulated: black, bottom trace).

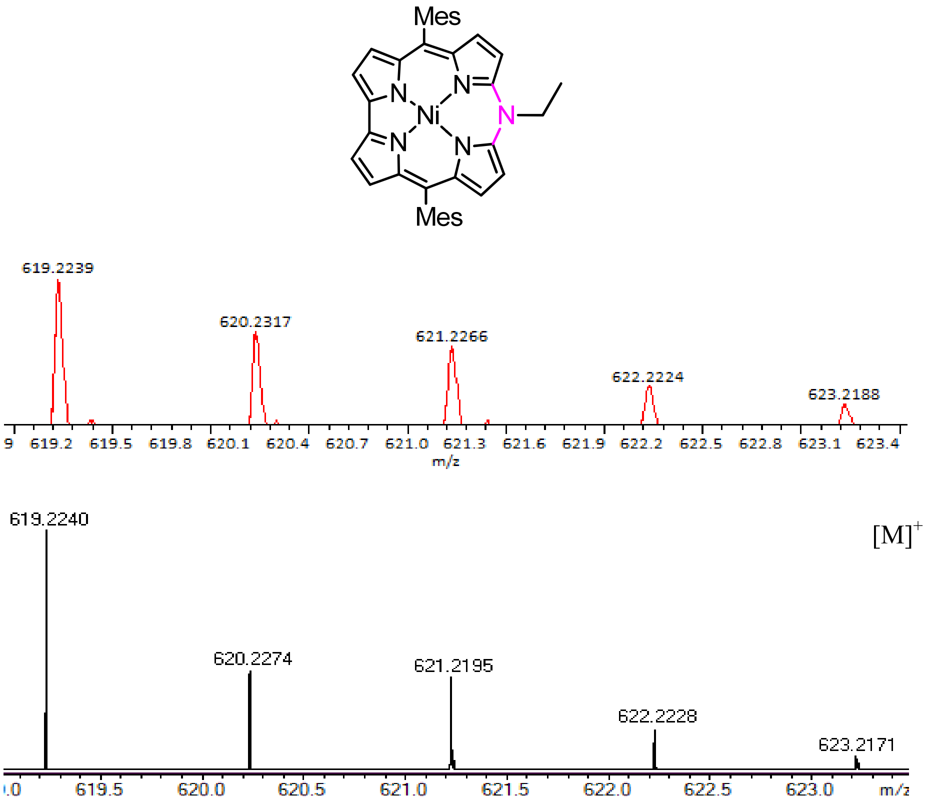

Figure S92. ESI(+) HRMS spectrum of **3q** (experimental: red, upper trace; simulated: black, bottom trace).

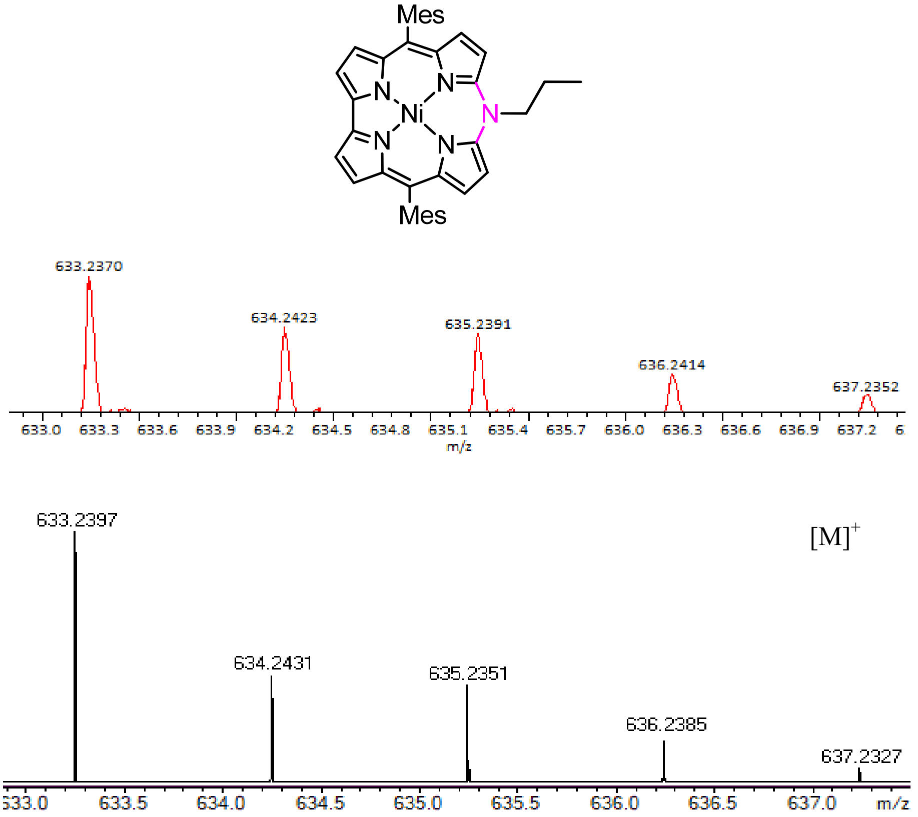

Figure S93. ESI(+) HRMS spectrum of **3r** (experimental: red, upper trace; simulated: black, bottom trace).

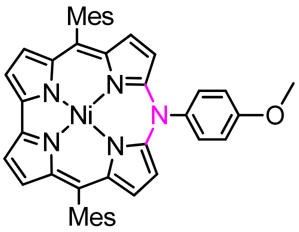

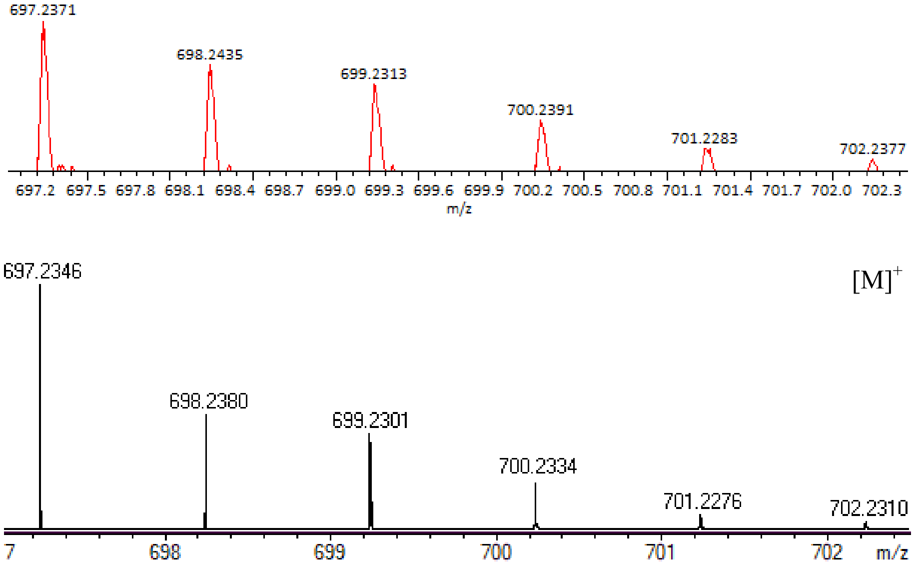

Figure S94. ESI(+) HRMS spectrum of **3s** (experimental: red, upper trace; simulated: black, bottom trace).

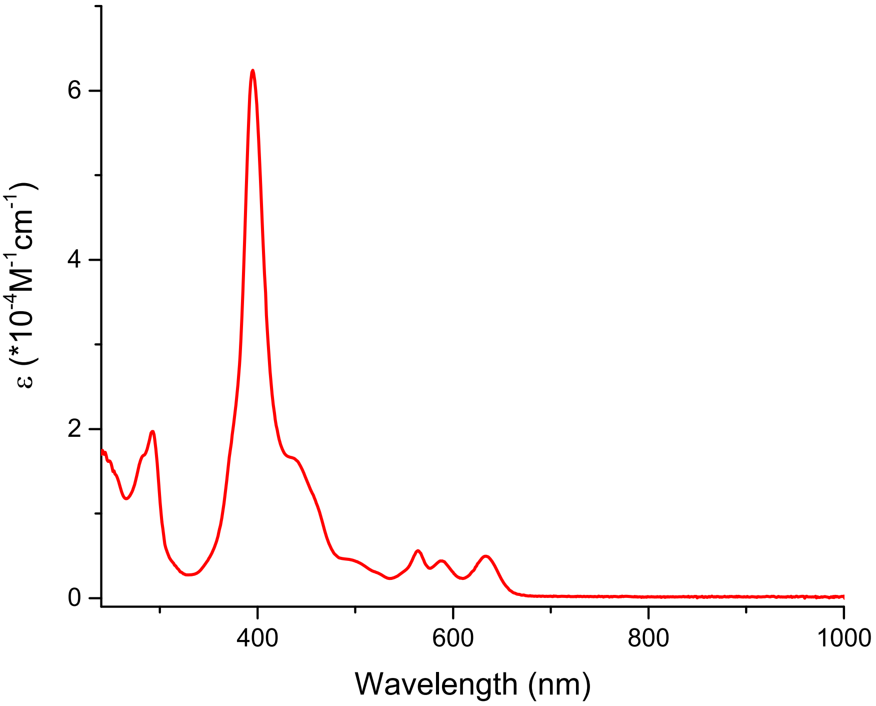

Figure S95. UV-vis spectrum of **3a** in dichloromethane.

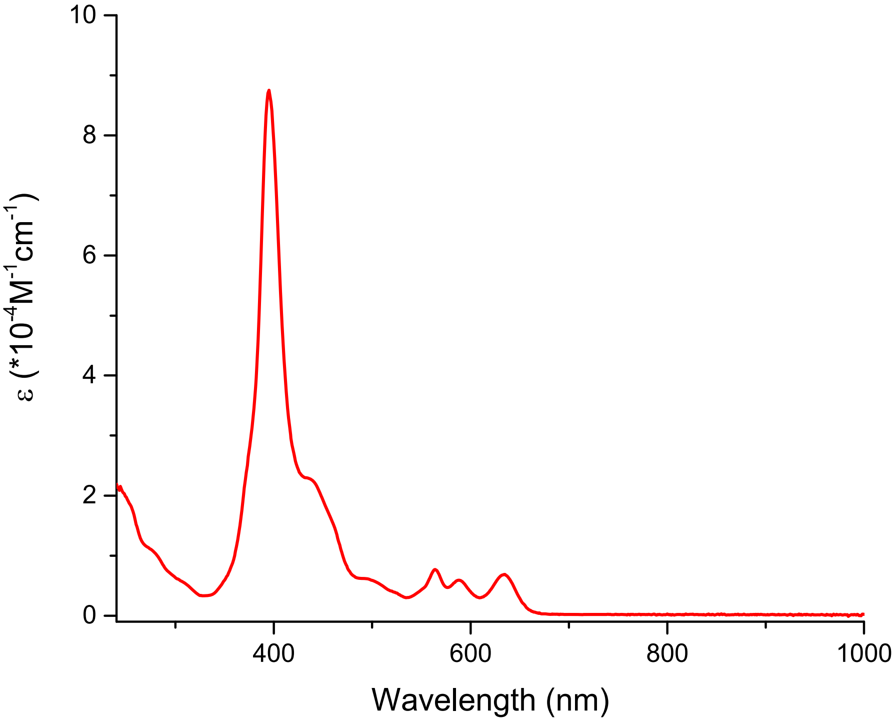

Figure S96. UV-vis spectrum of **3b** in dichloromethane.

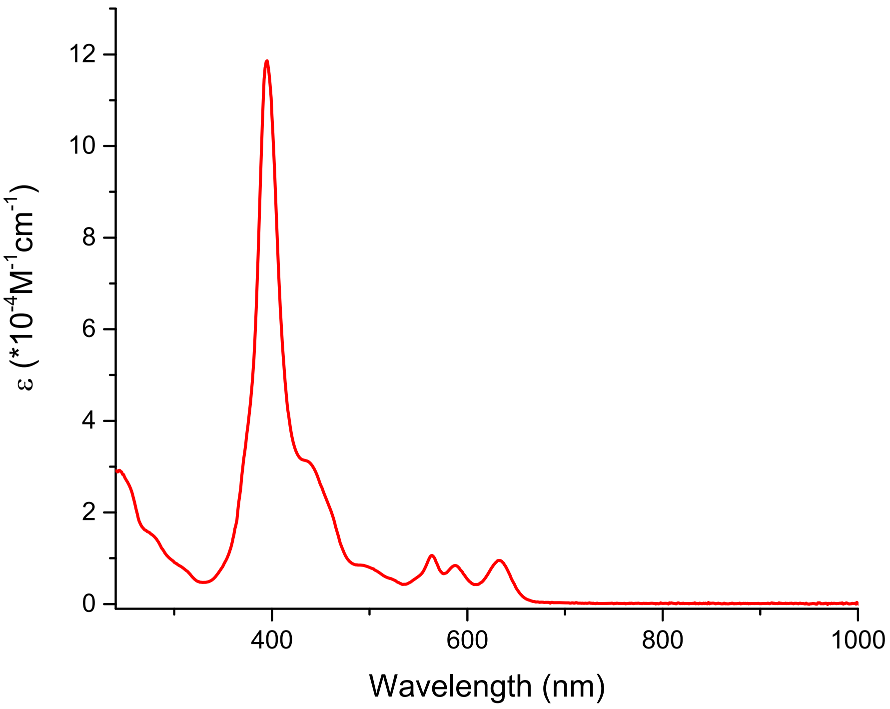

Figure S97. UV-vis spectrum of **3c** in dichloromethane.

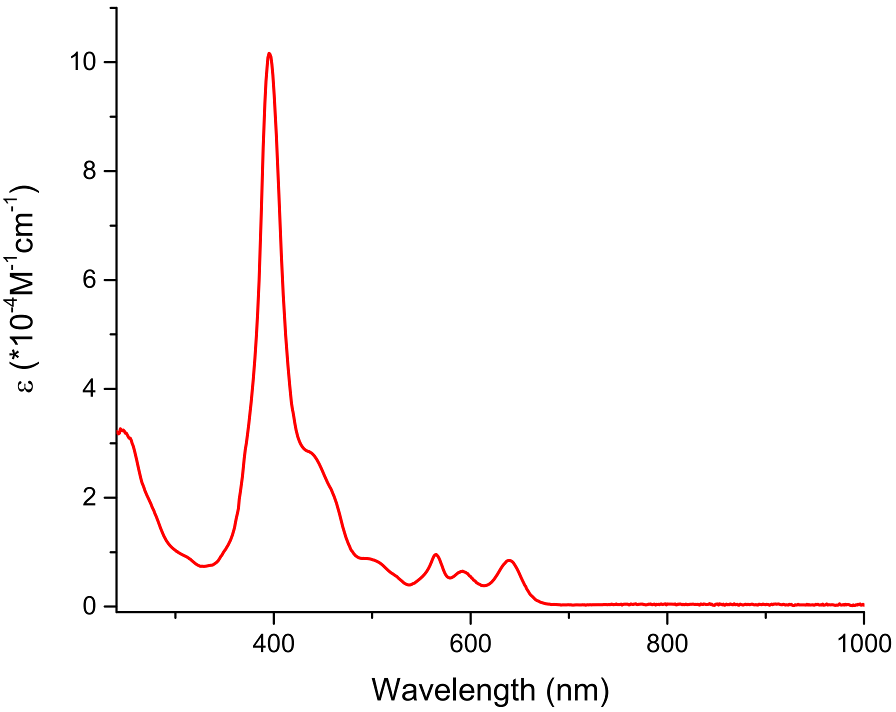

Figure S98. UV-vis spectrum of **3d** in dichloromethane.

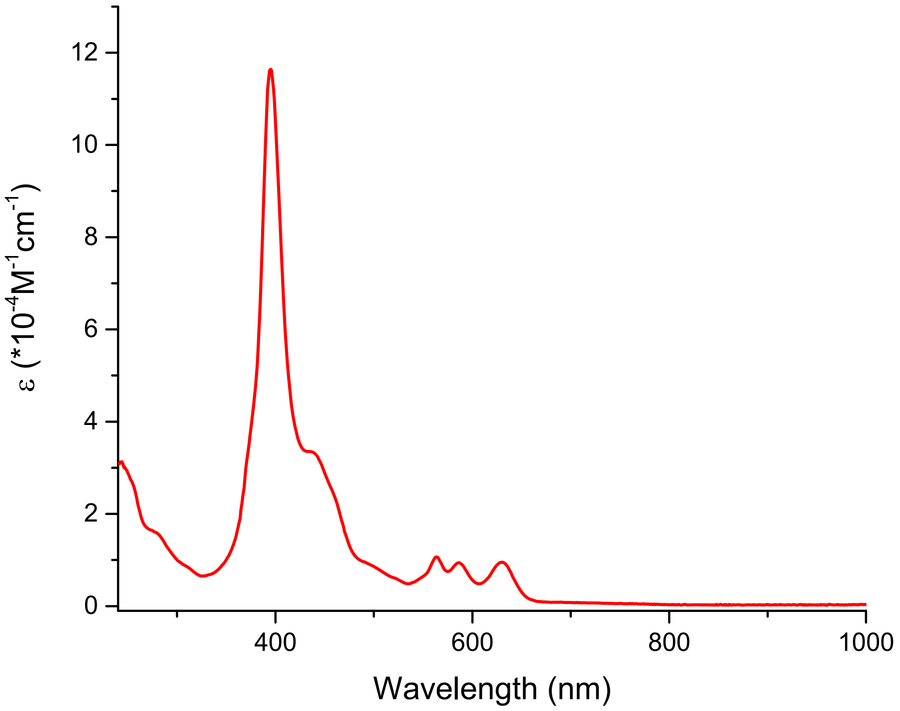

Figure S99. UV-vis spectrum of **3e** in dichloromethane.

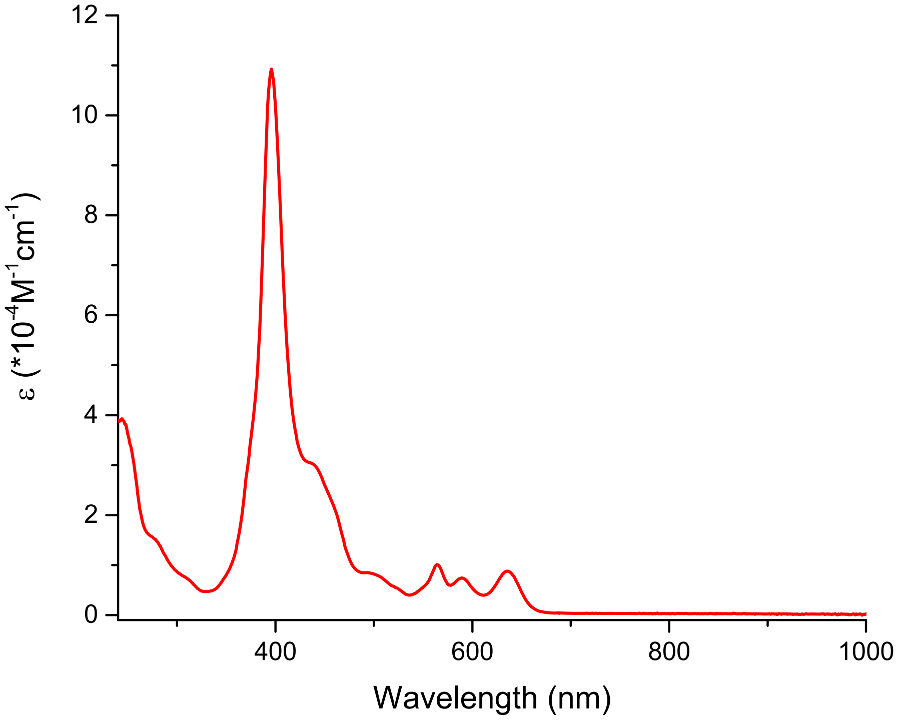

Figure S100. UV-vis spectrum of **3f** in dichloromethane.

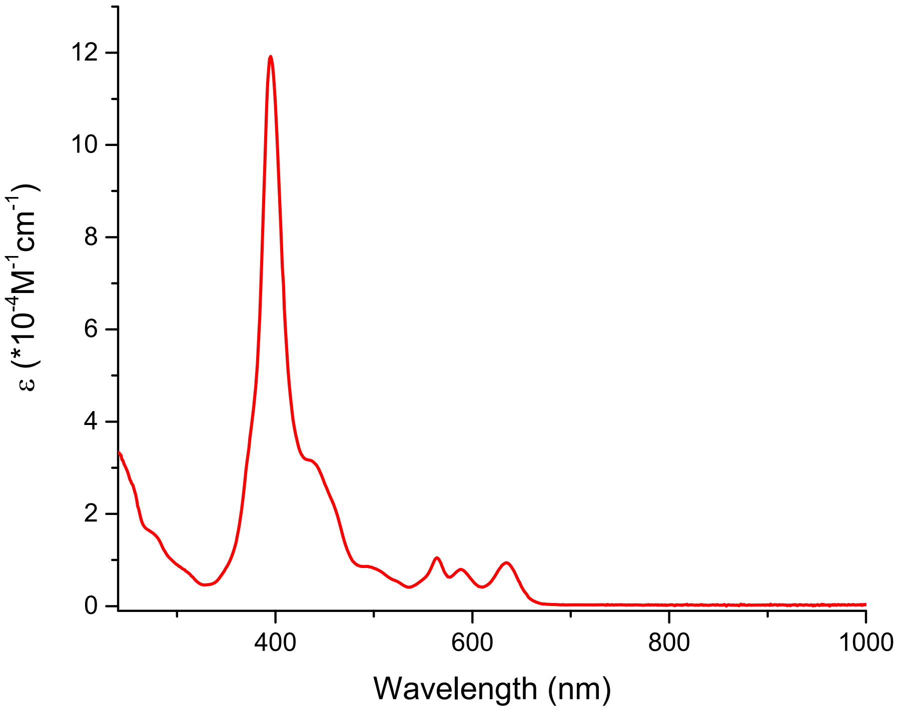

Figure S101. UV-vis spectrum of **3g** in dichloromethane.

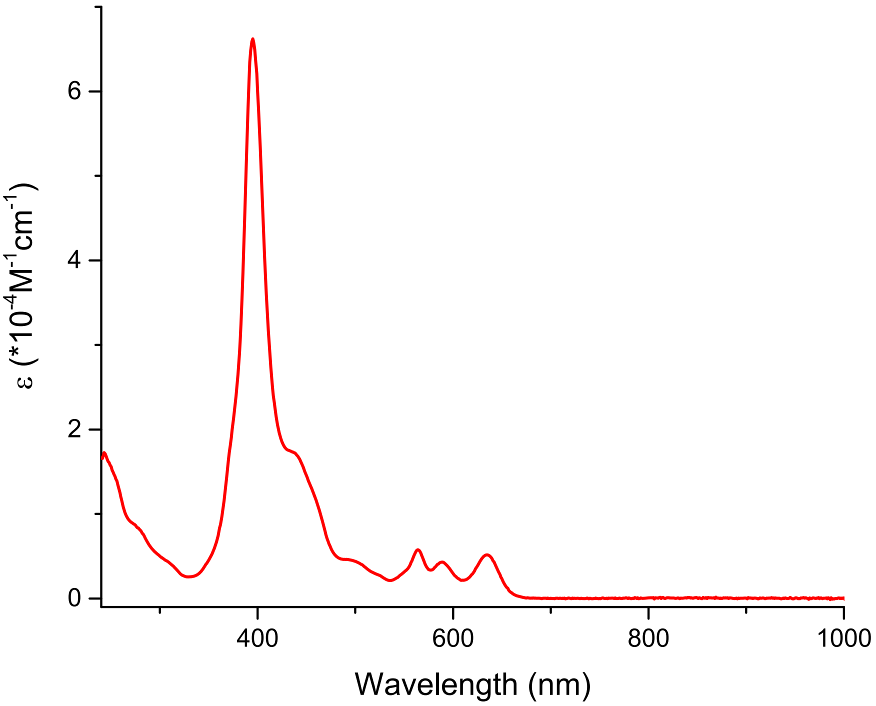

Figure S102. UV-vis spectrum of **3h** in dichloromethane.

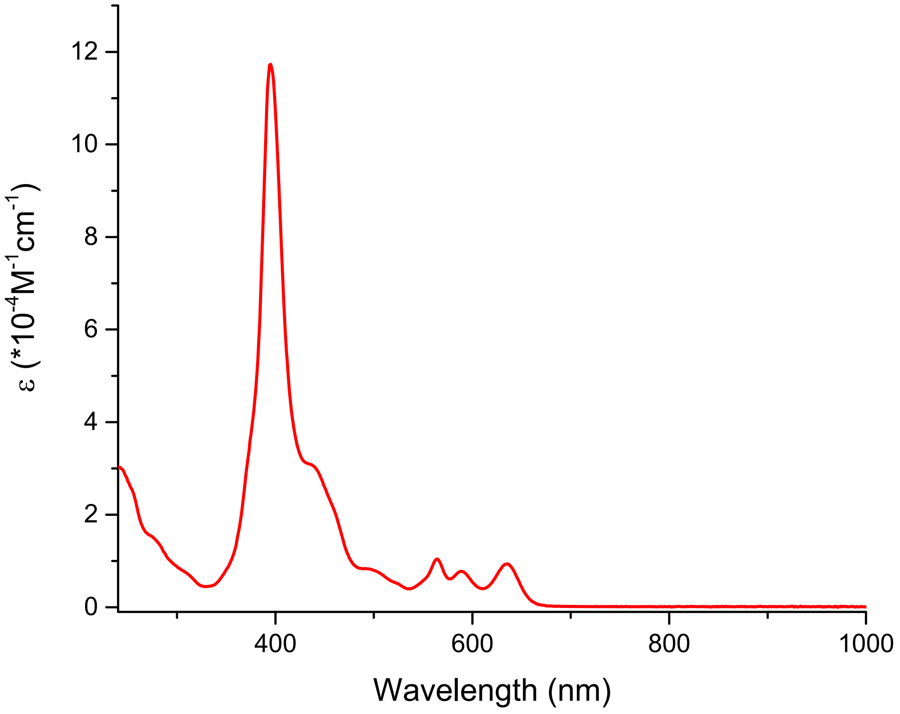

Figure S103. UV-vis spectrum of **3i** in dichloromethane.

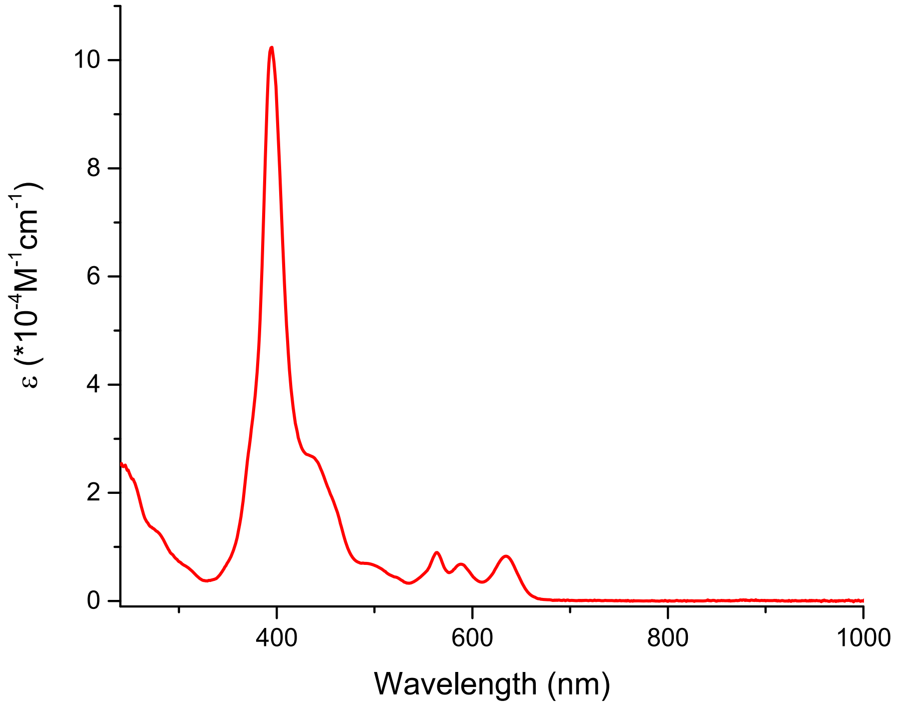

Figure S104. UV-vis spectrum of **3j** in dichloromethane.

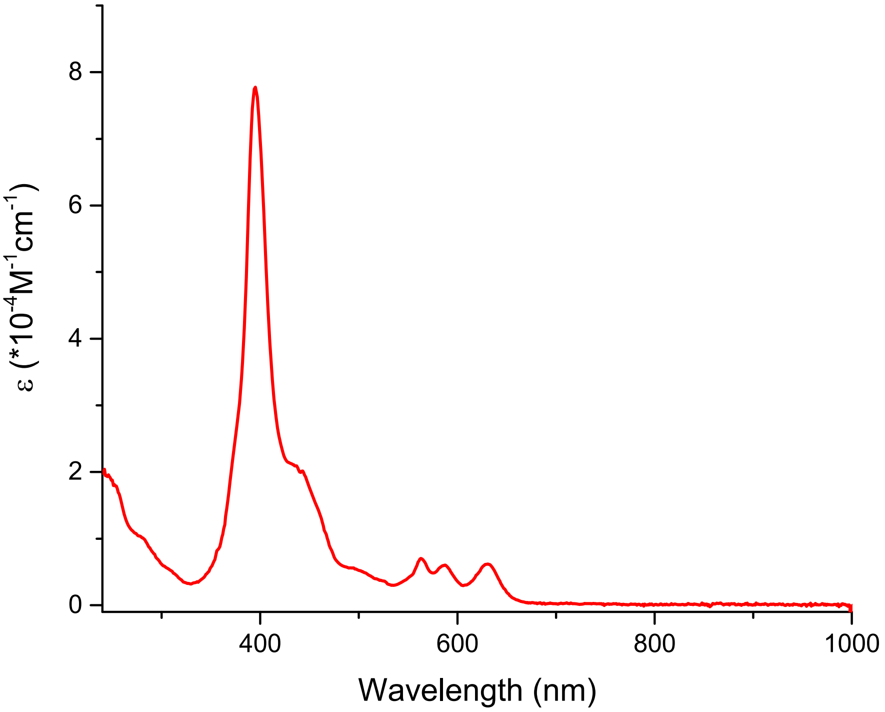

Figure S105. UV-vis spectrum of **3k** in dichloromethane.

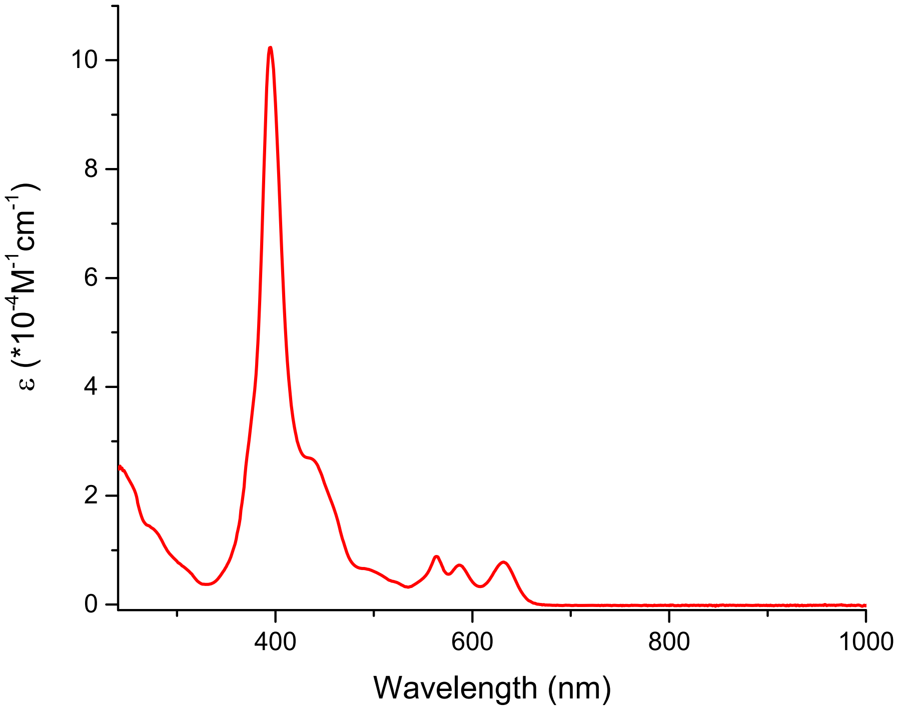

Figure S106. UV-vis spectrum of **3l** in dichloromethane.

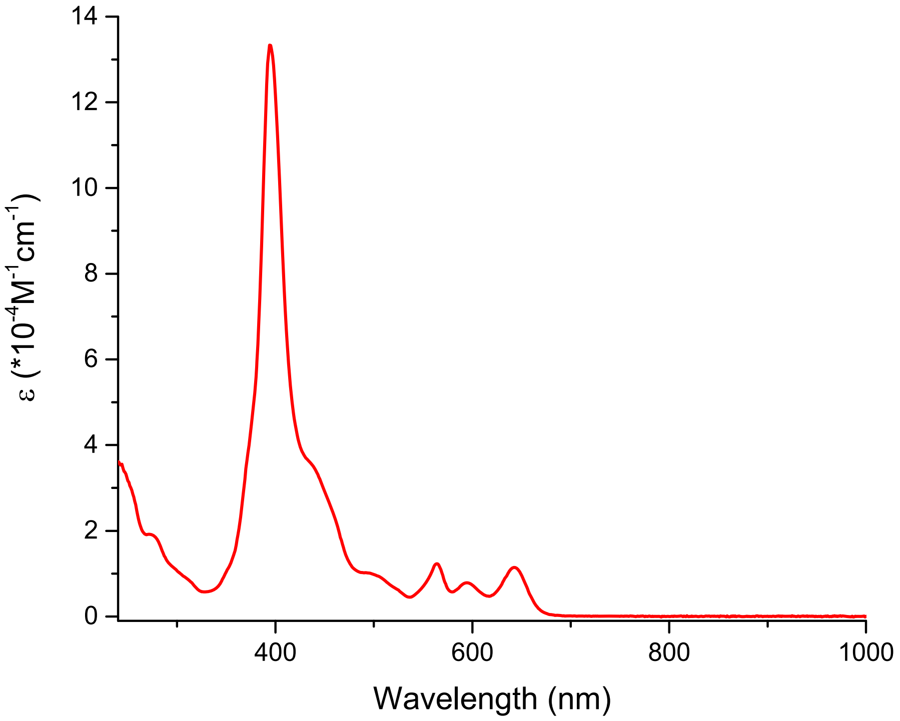

Figure S107. UV-vis spectrum of **3m** in dichloromethane.

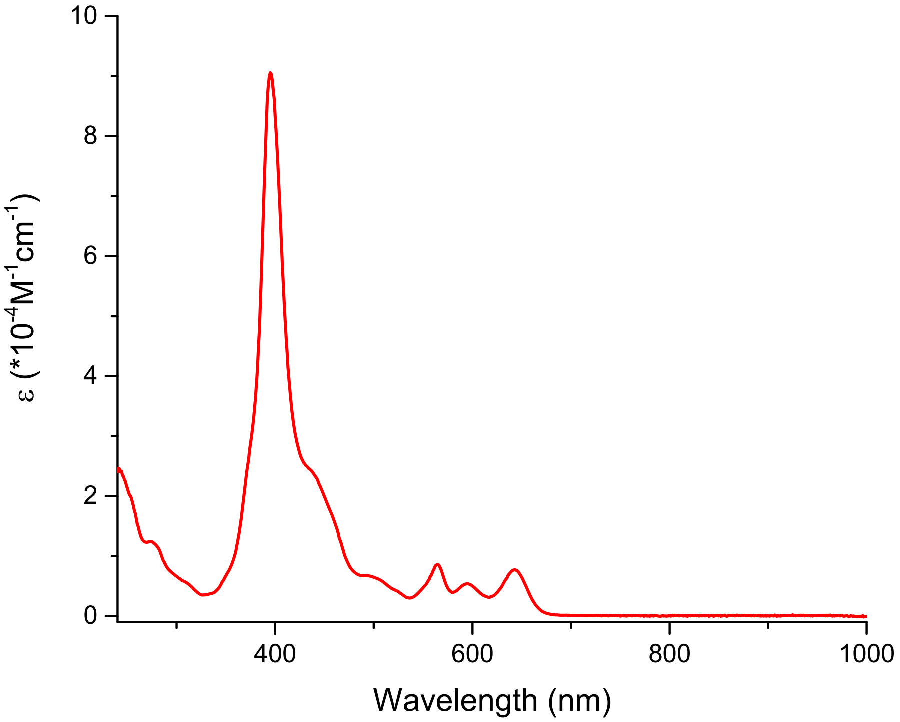

Figure S108. UV-vis spectrum of **3n** in dichloromethane.

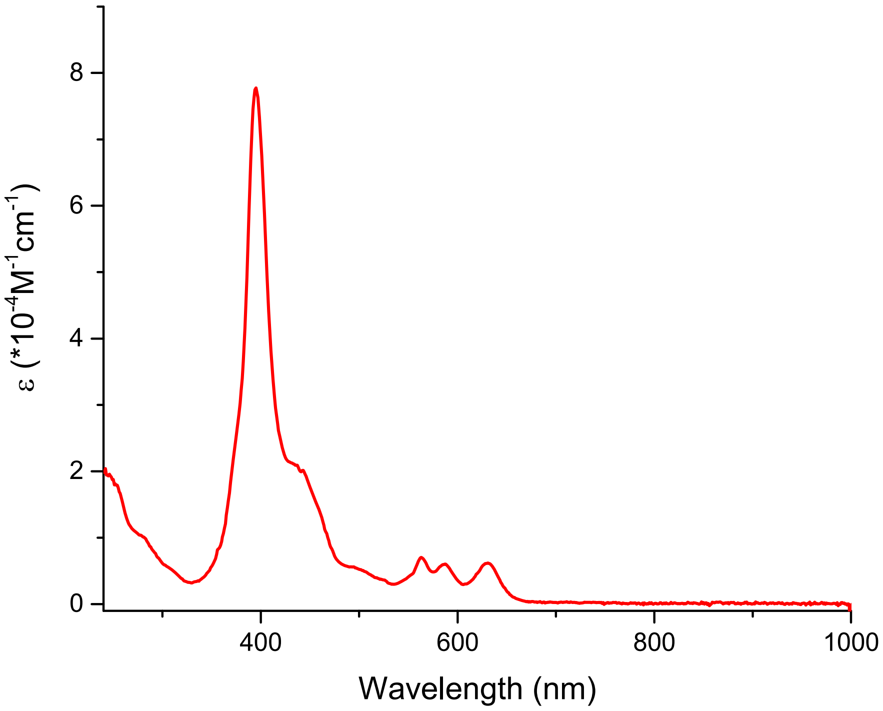

Figure S109. UV-vis spectrum of **3o** in dichloromethane.

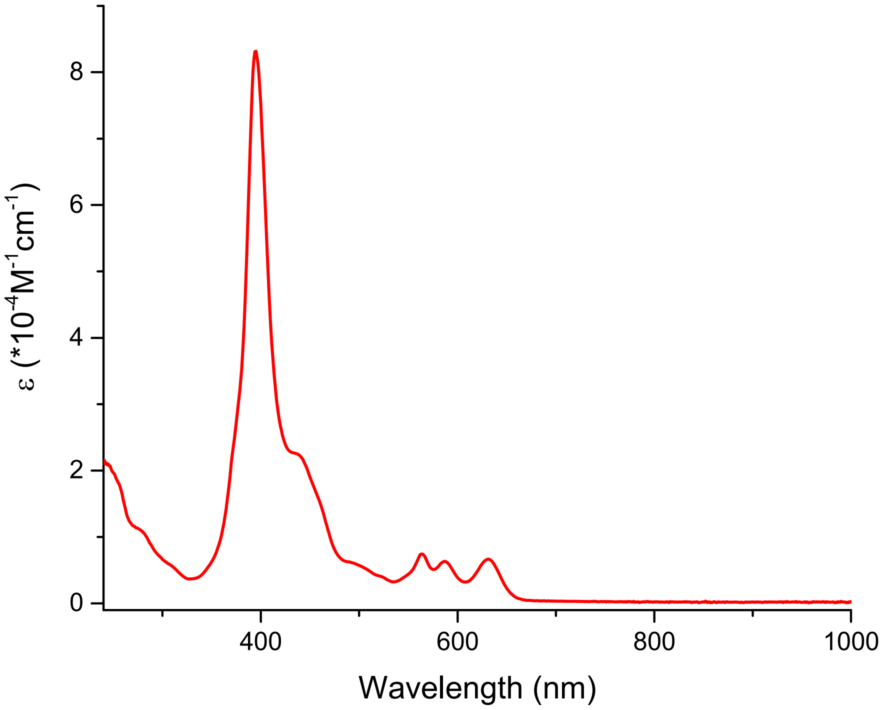

Figure S110. UV-vis spectrum of **3p** in dichloromethane.

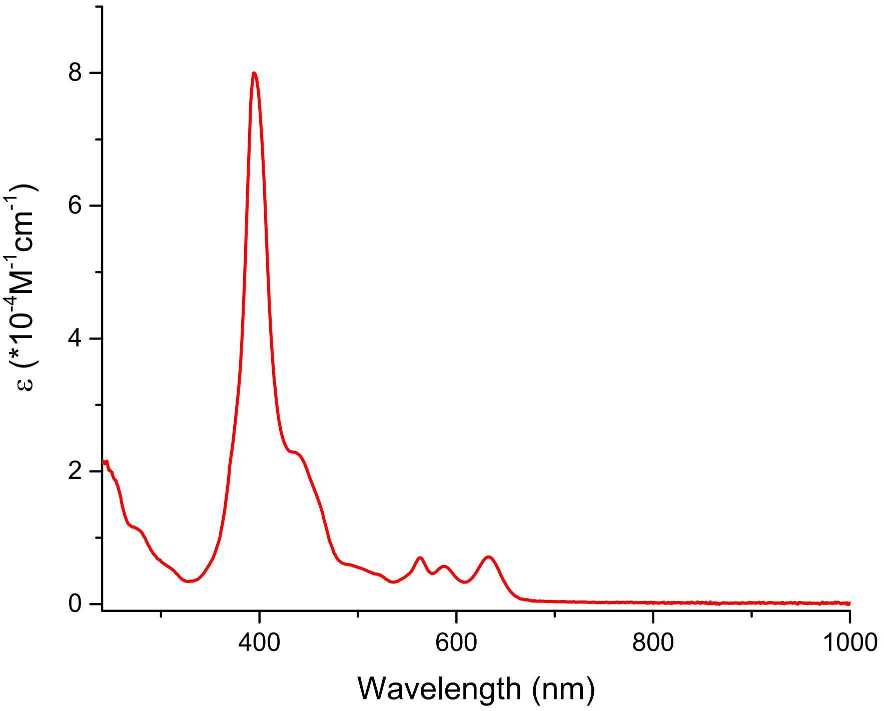

Figure S111. UV-vis spectrum of **3q** in dichloromethane.

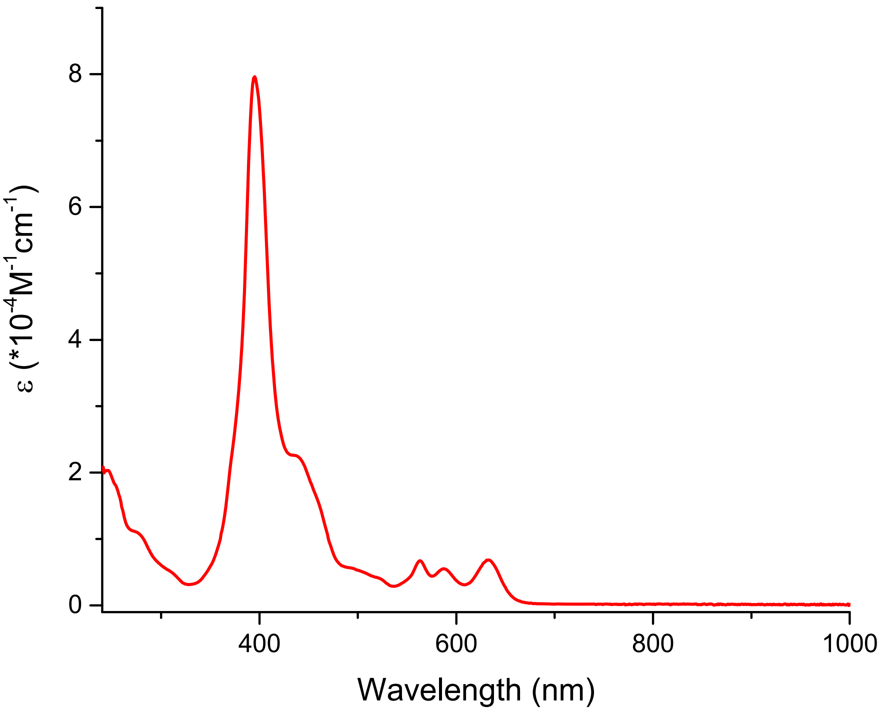

Figure S112. UV-vis spectrum of **3r** in dichloromethane.

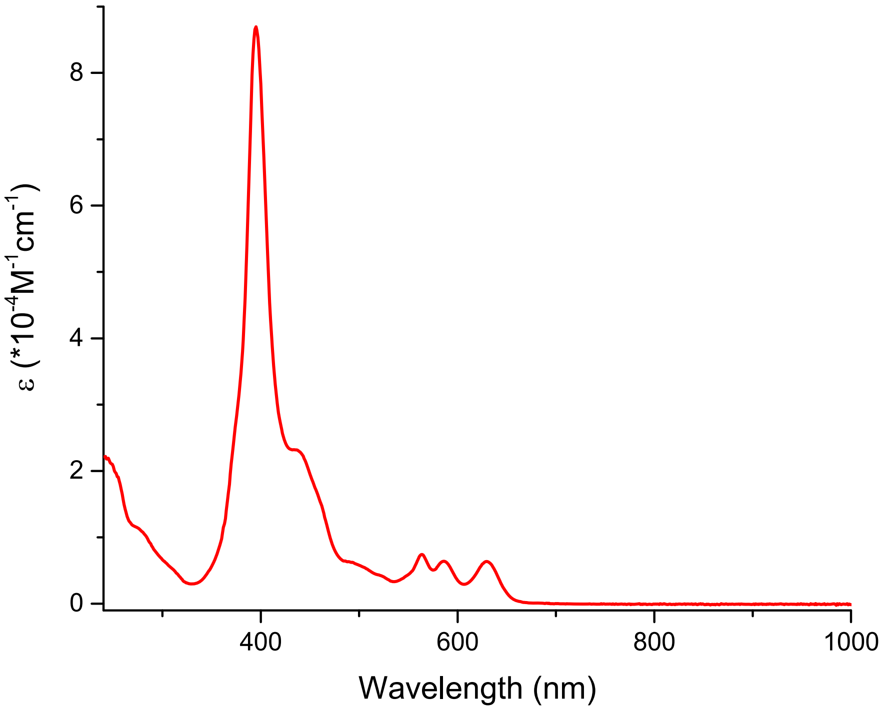

Figure S113. UV-vis spectrum of **3s** in dichloromethane.

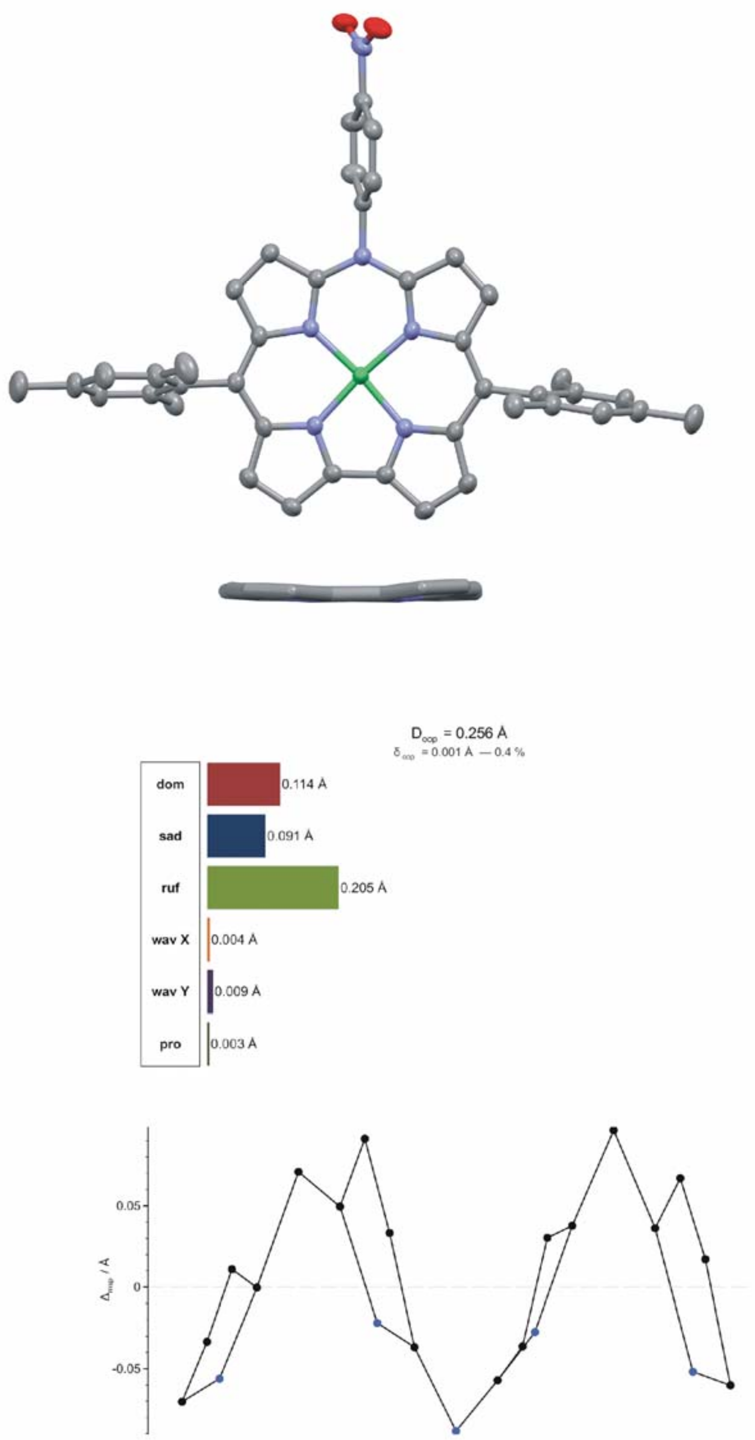

Figure S114. Out-of-plane displacement for macrocyclic ring of **3d** calculated on the basis of XRD structure. Color code: brown, doming (*dom*); dark blue, saddling (*sad*); green, ruffling (*ruf*); orange, waving *x* (wav X); purple, waving *y* (wav Y); olive, propellering (*pro*). D_{oop}, the total out-of-plane distortion; δ_{oop}, difference between D_{oop} calculated by *PorphyStruct*[11] and estimated by of the normal-coordinate structure decomposition (NSD) simulation.[12,13]

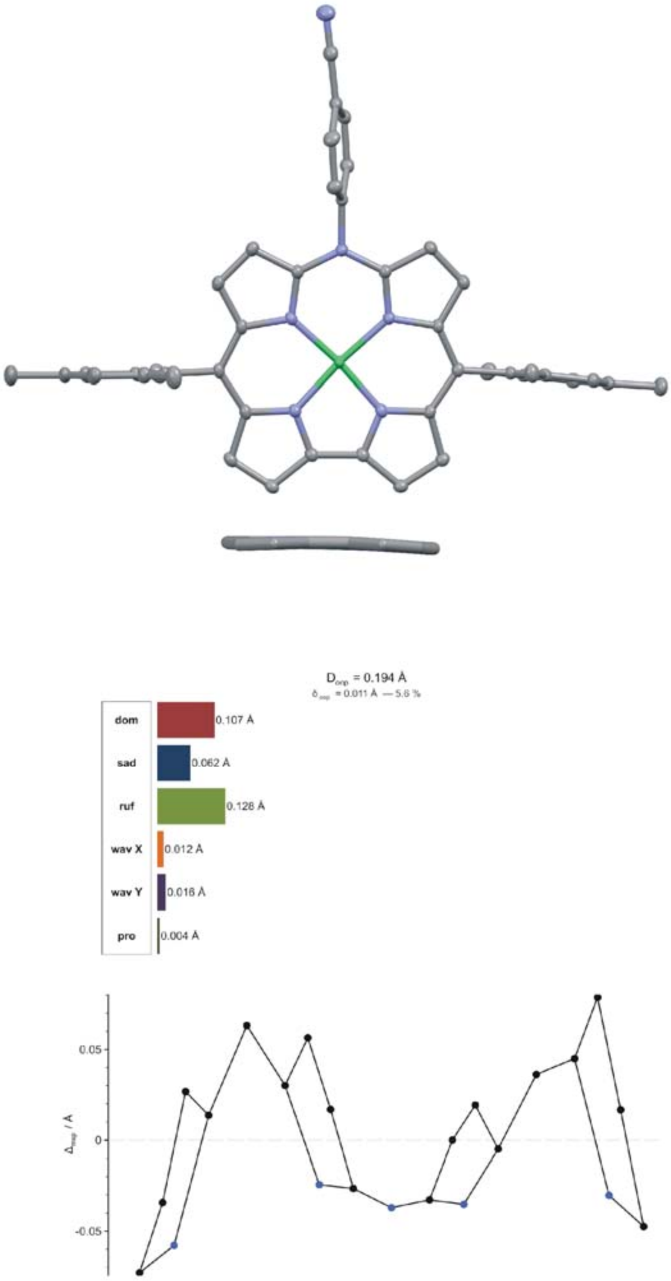

Figure S115. Out-of-plane displacement for macrocyclic ring of **3e** calculated on the basis of XRD structure. Color code: brown, doming (*dom*); dark blue, saddling (*sad*); green, ruffling (*ruf*); orange, waving *x* (wav X); purple, waving *y* (wav Y); olive, propellering (*pro*). D_{oop}, the total out-of-plane distortion; δ_{oop}, difference between D_{oop} calculated by *PorphyStruct*[11] and estimated by of the normal-coordinate structure decomposition (NSD) simulation.[12,13]

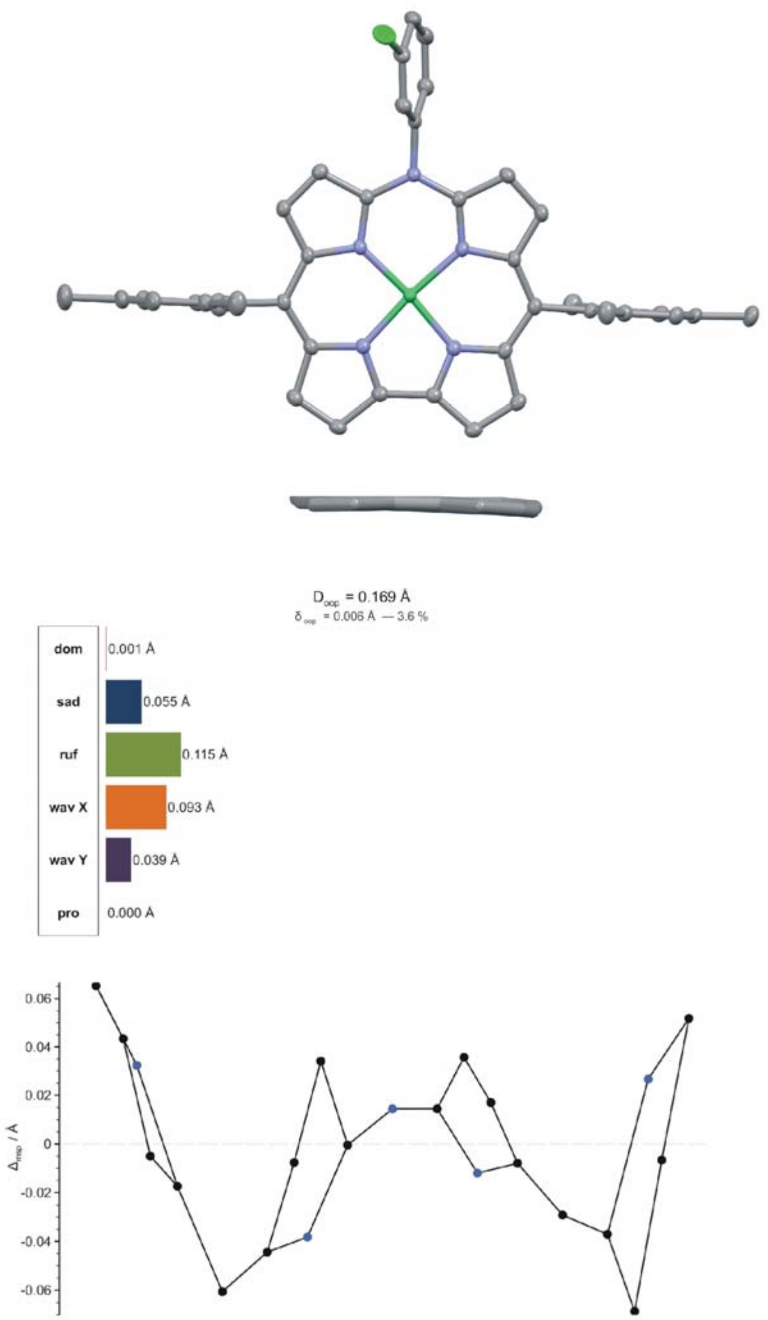

Figure S116. Out-of-plane displacement for macrocyclic ring of **3h** calculated on the basis of XRD structure. Color code: brown, doming (*dom*); dark blue, saddling (*sad*); green, ruffling (*ruf*); orange, waving *x* (wav X); purple, waving *y* (wav Y); olive, propellering (*pro*). D_{oop}, the total out-of-plane distortion; δ_{oop}, difference between D_{oop} calculated by *PorphyStruct*[11] and estimated by of the normal-coordinate structure decomposition (NSD) simulation.[12,13]

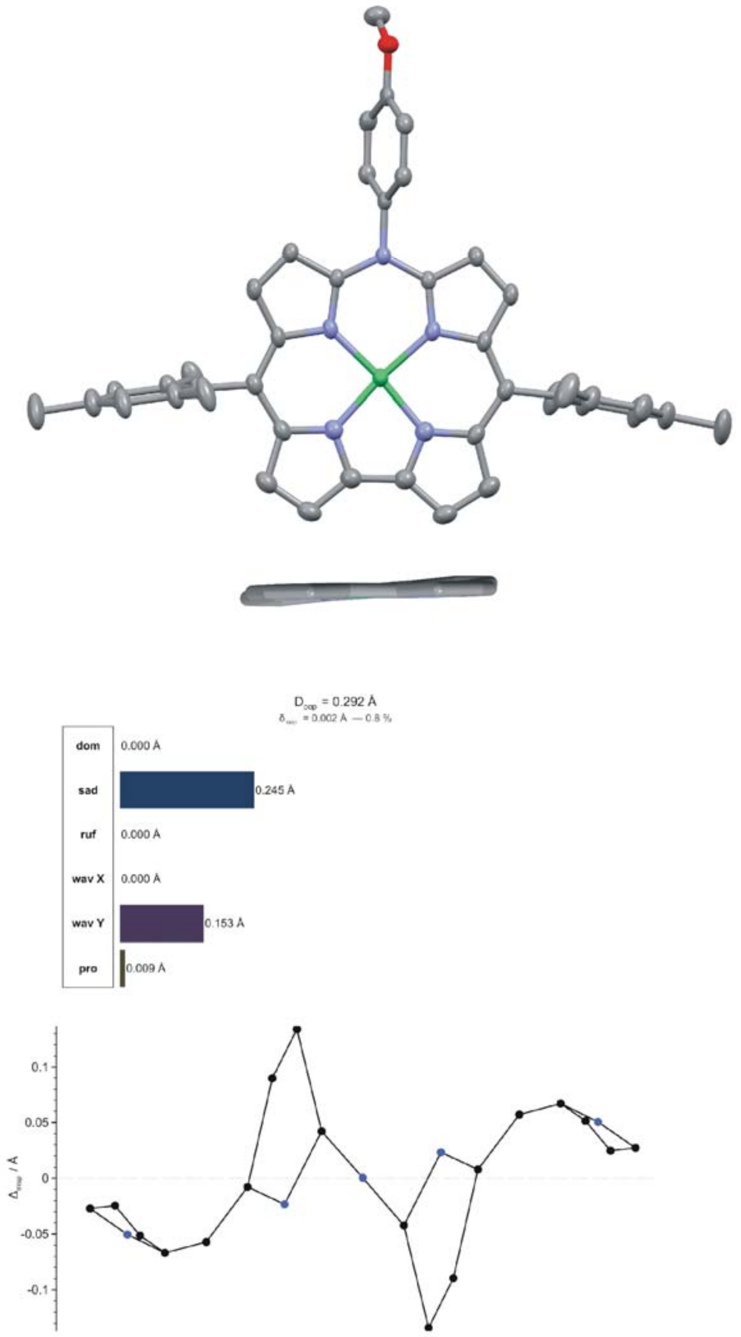

Figure S117. Out-of-plane displacement for macrocyclic ring of **3s** calculated on the basis of XRD structure. Color code: brown, doming (*dom*); dark blue, saddling (*sad*); green, ruffling (*ruf*); orange, waving *x* (wav X); purple, waving *y* (wav Y); olive, propellering (*pro*). D_{oop}, the total out-of-plane distortion; δ_{oop}, difference between D_{oop} calculated by *PorphyStruct*[11] and estimated by of the normal-coordinate structure decomposition (NSD) simulation.[12,13]

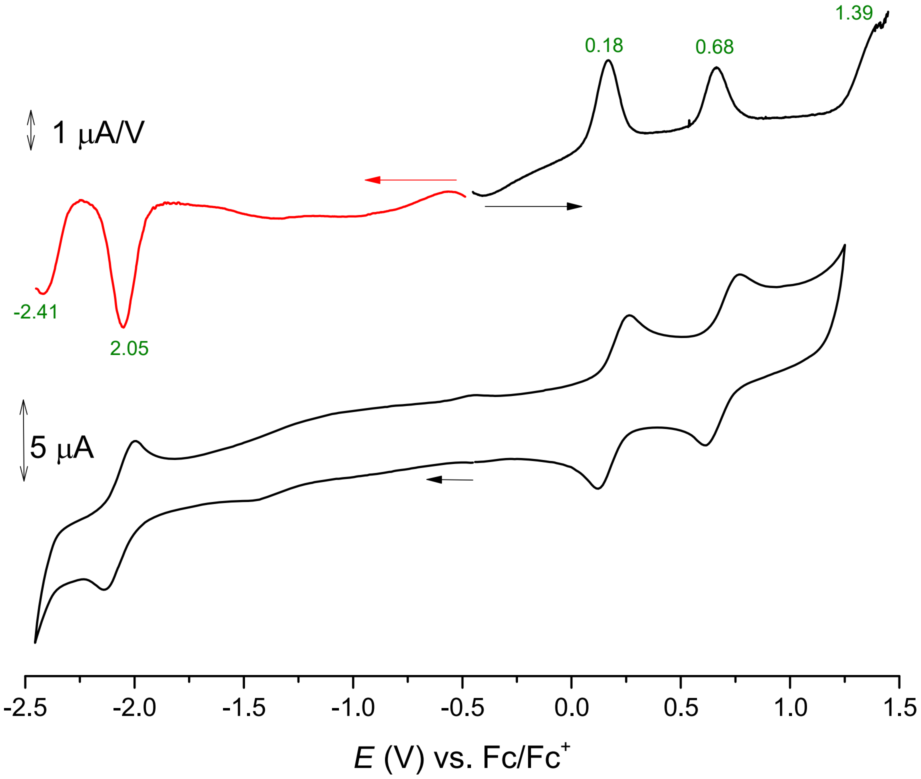

Figure S118. Differential pulse (DP) and cyclic (CV) voltammograms recorded for **3a** in DCM with $[Bu_4N]PF_6$ as supporting electrolyte.

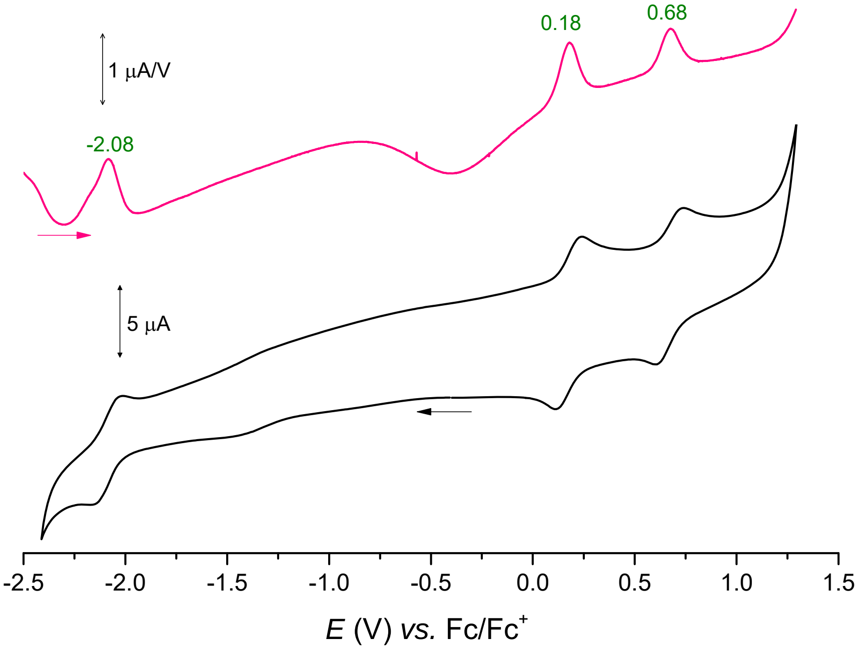

Figure S119. Differential pulse (DP) and cyclic (CV) voltammograms recorded for **3b** in DCM with $[Bu_4N]PF_6$ as supporting electrolyte.

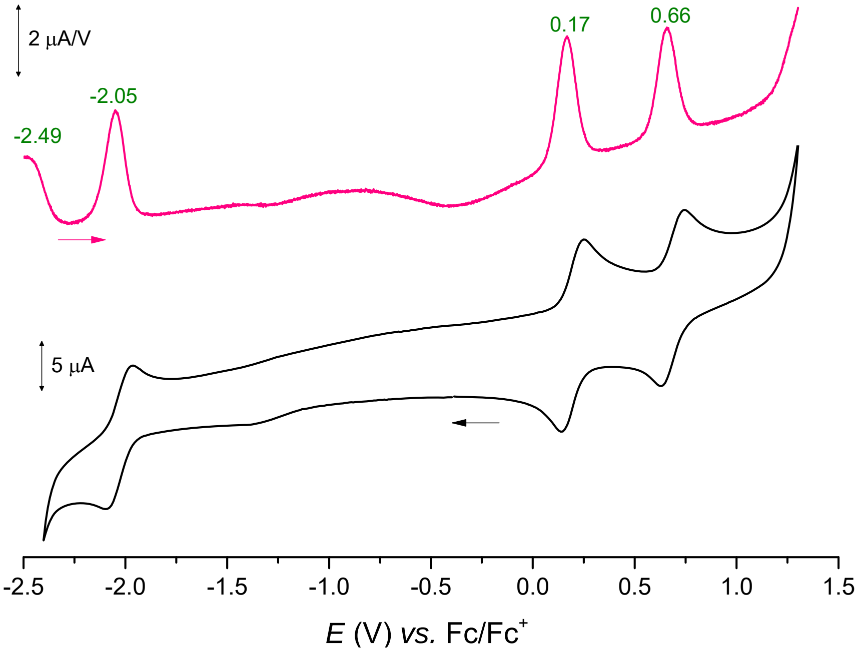

Figure S120. Differential pulse (DP) and cyclic (CV) voltammograms recorded for **3c** in DCM with $[Bu_4N]PF_6$ as supporting electrolyte.

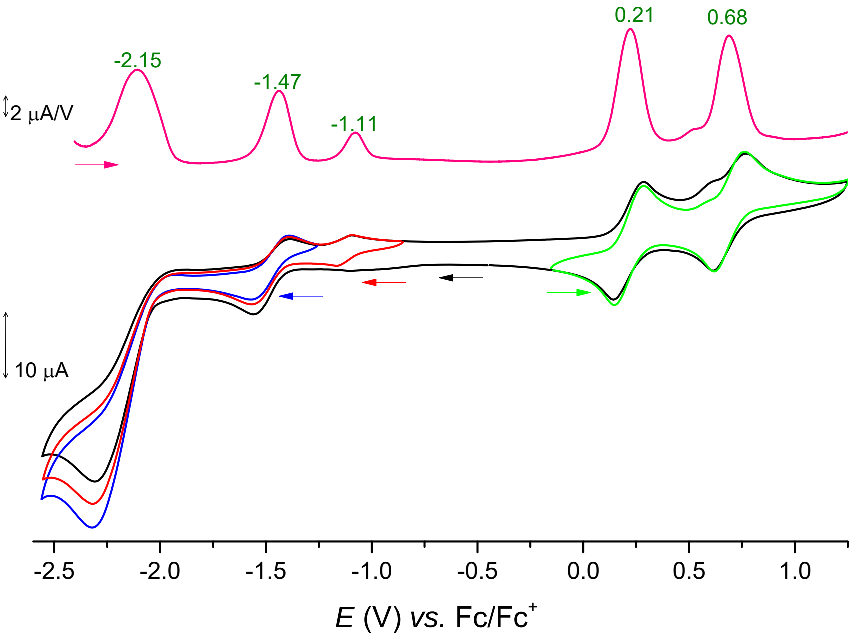

Figure S121. Differential pulse (DP) and cyclic (CV) voltammograms recorded for **3d** in DCM with $[Bu_4N]PF_6$ as supporting electrolyte. Rhe waves at –1.47 and –1.11 V are due to the reduction of NO_2 group.

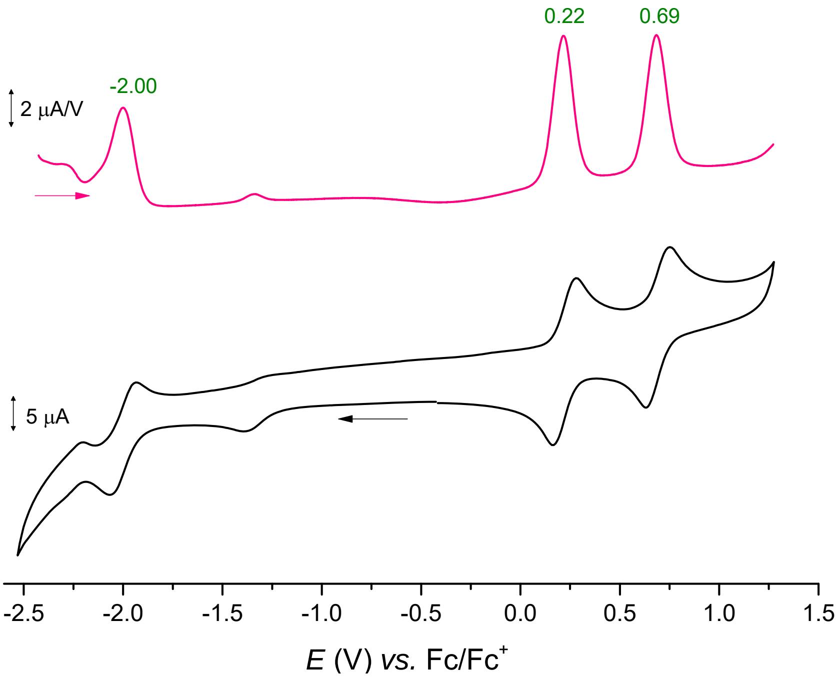

Figure S122. Differential pulse (DP) and cyclic (CV) voltammograms recorded for **3e** in DCM with $[Bu_4N]PF_6$ as supporting electrolyte.

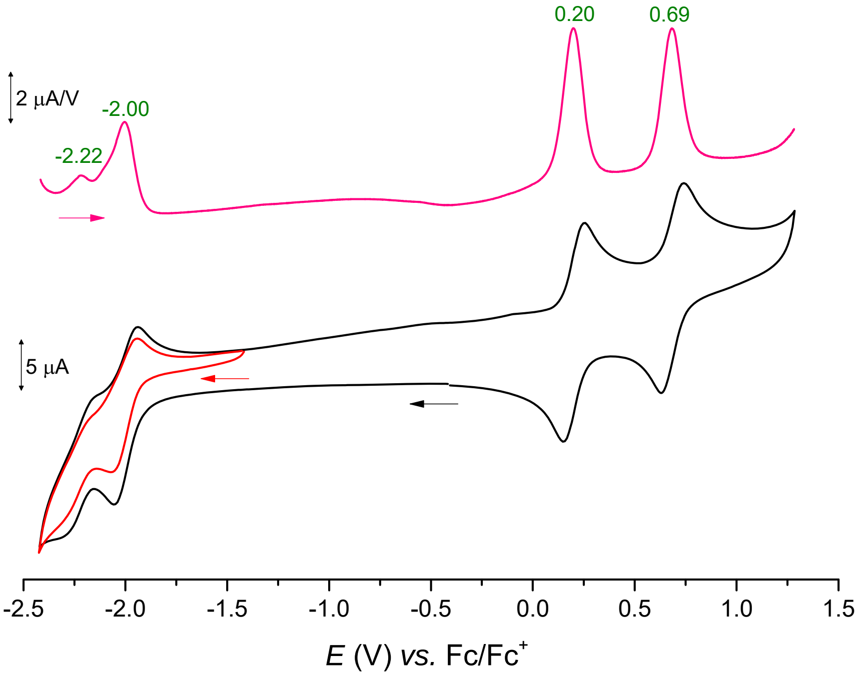

Figure S123. Differential pulse (DP) and cyclic (CV) voltammograms recorded for **3f** in DCM with $[Bu_4N]PF_6$ as supporting electrolyte.

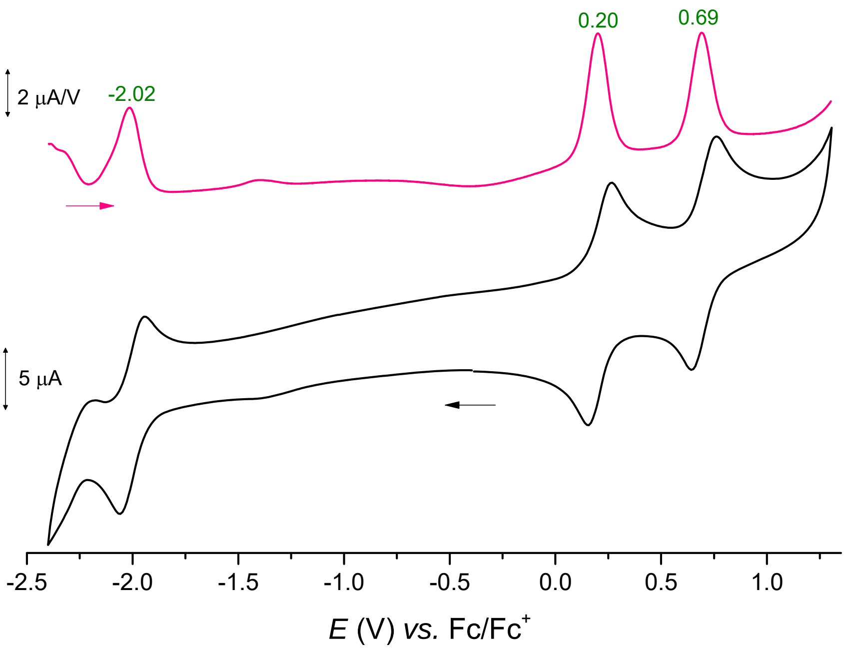

Figure S124. Differential pulse (DP) and cyclic (CV) voltammograms recorded for **3g** in DCM with $[Bu_4N]PF_6$ as supporting electrolyte.

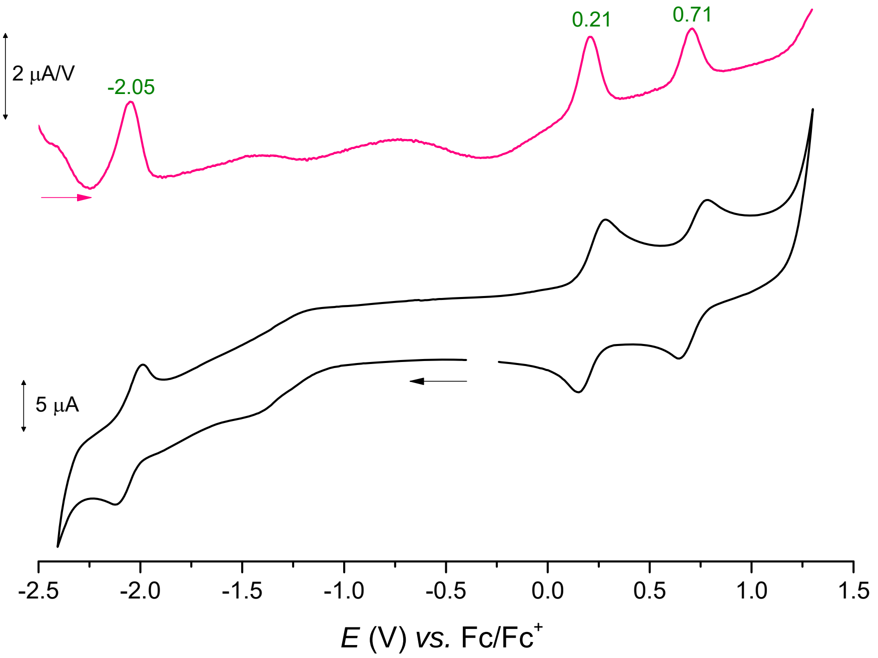

Figure S125. Differential pulse (DP) and cyclic (CV) voltammograms recorded for **3h** in DCM with $[Bu_4N]PF_6$ as supporting electrolyte.

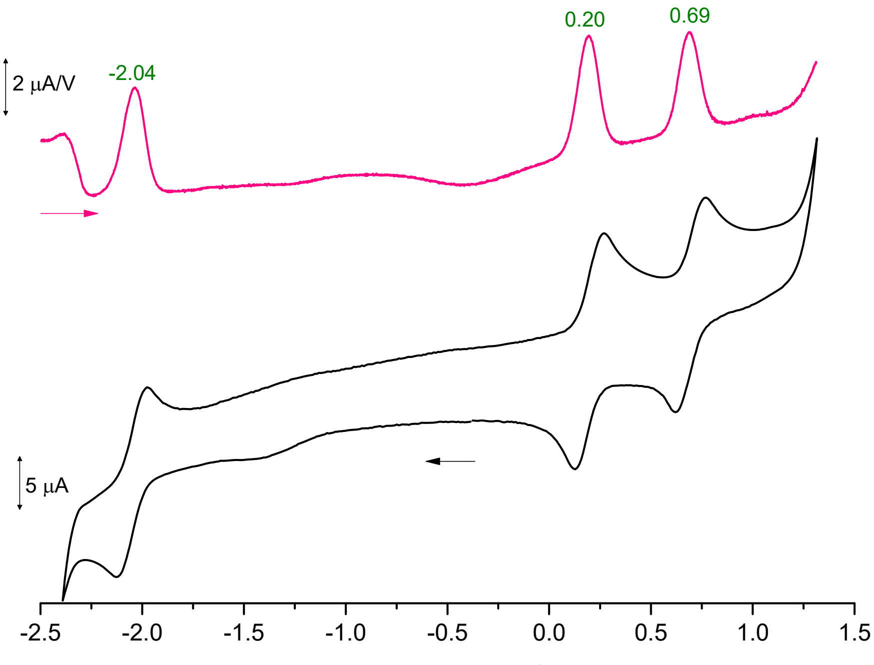

Figure S126. Differential pulse (DP) and cyclic (CV) voltammograms recorded for **3i** in DCM with $[Bu_4N]PF_6$ as supporting electrolyte.

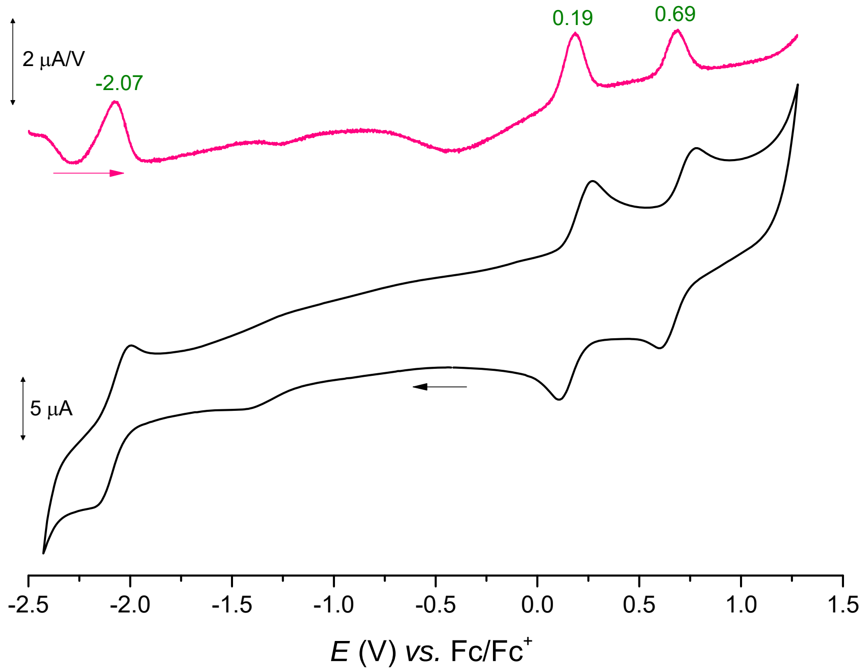

Figure S127. Differential pulse (DP) and cyclic (CV) voltammograms recorded for **3j** in DCM with $[Bu_4N]PF_6$ as supporting electrolyte.

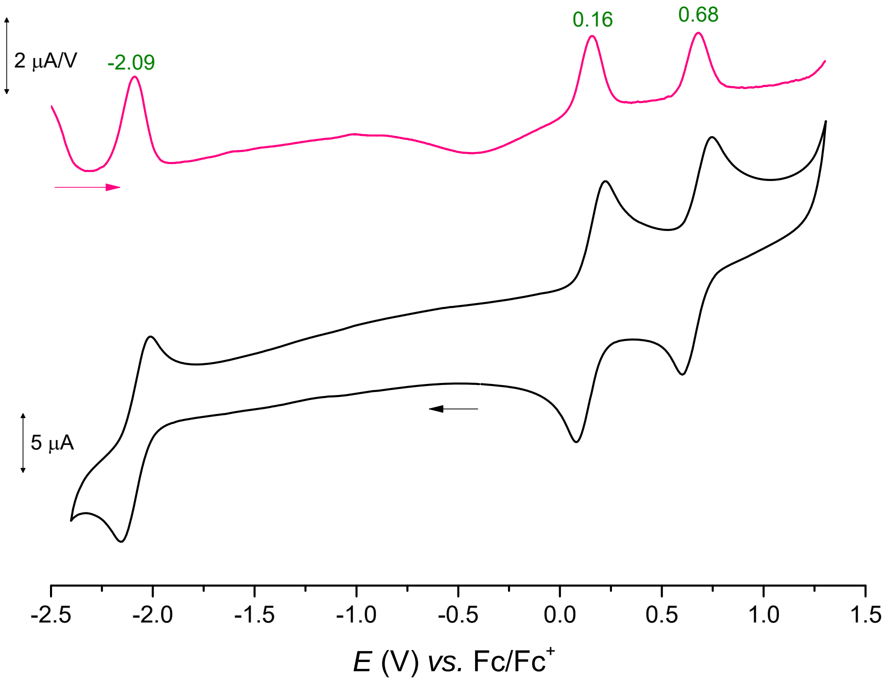

Figure S128. Differential pulse (DP) and cyclic (CV) voltammograms recorded for **3k** in DCM with $[Bu_4N]PF_6$ as supporting electrolyte.

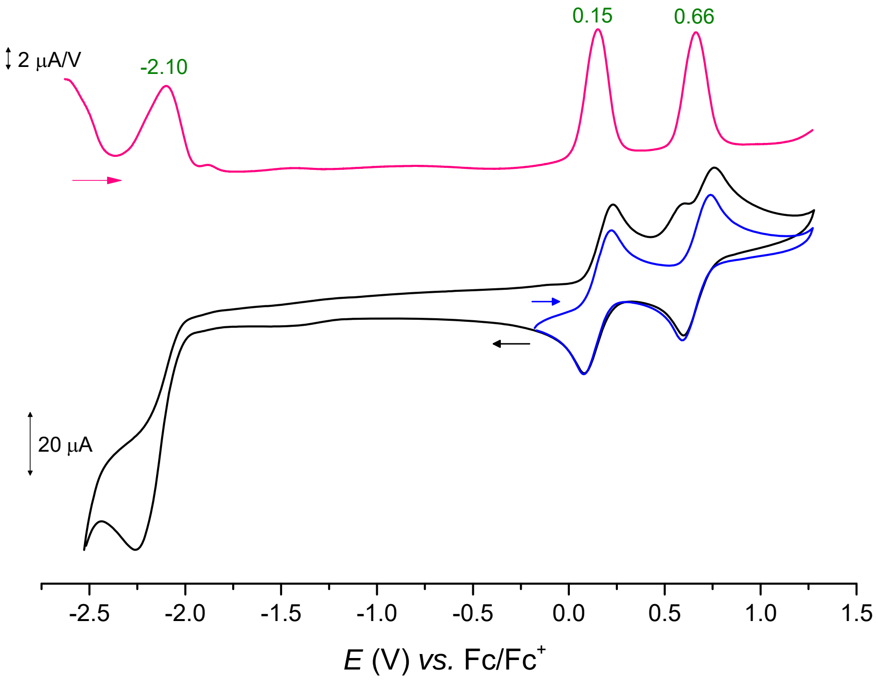

Figure S129. Differential pulse (DP) and cyclic (CV) voltammograms recorded for **3l** in DCM with $[Bu_4N]PF_6$ as supporting electrolyte.

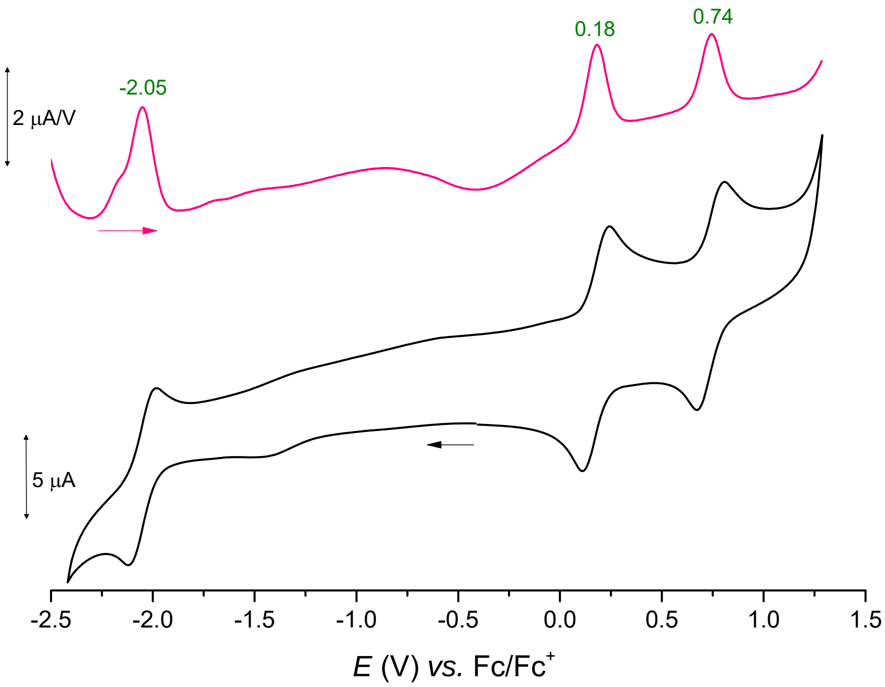

Figure S130. Differential pulse (DP) and cyclic (CV) voltammograms recorded for **3m** in DCM with $[Bu_4N]PF_6$ as supporting electrolyte.

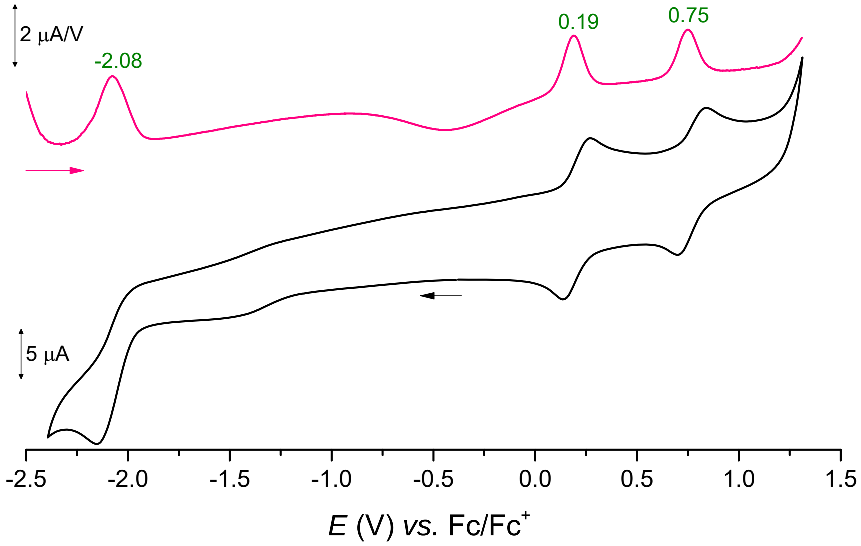

Figure S131. Differential pulse (DP) and cyclic (CV) voltammograms recorded for **3n** in DCM with $[Bu_4N]PF_6$ as supporting electrolyte.

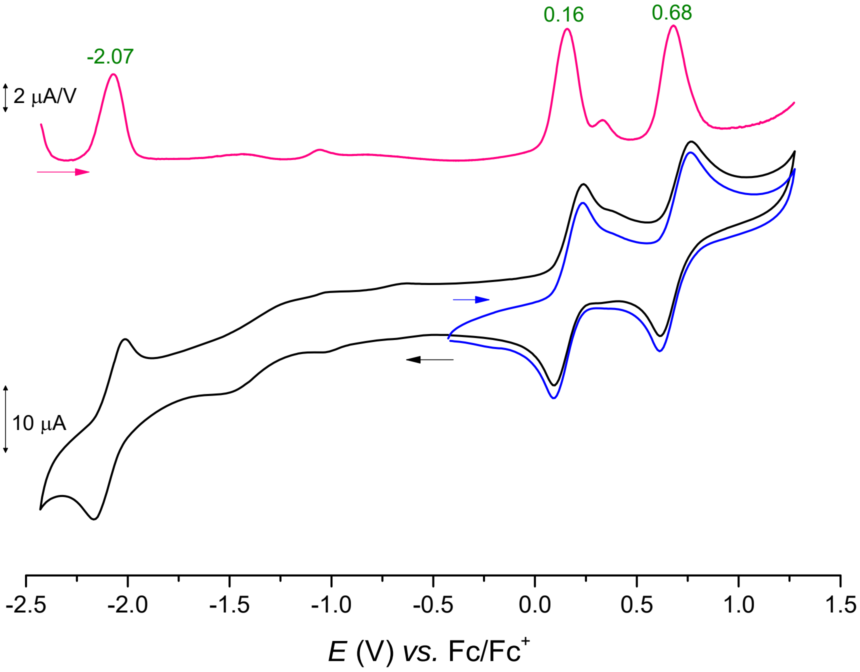

Figure S132. Differential pulse (DP) and cyclic (CV) voltammograms recorded for **3o** in DCM with $[Bu_4N]PF_6$ as supporting electrolyte.

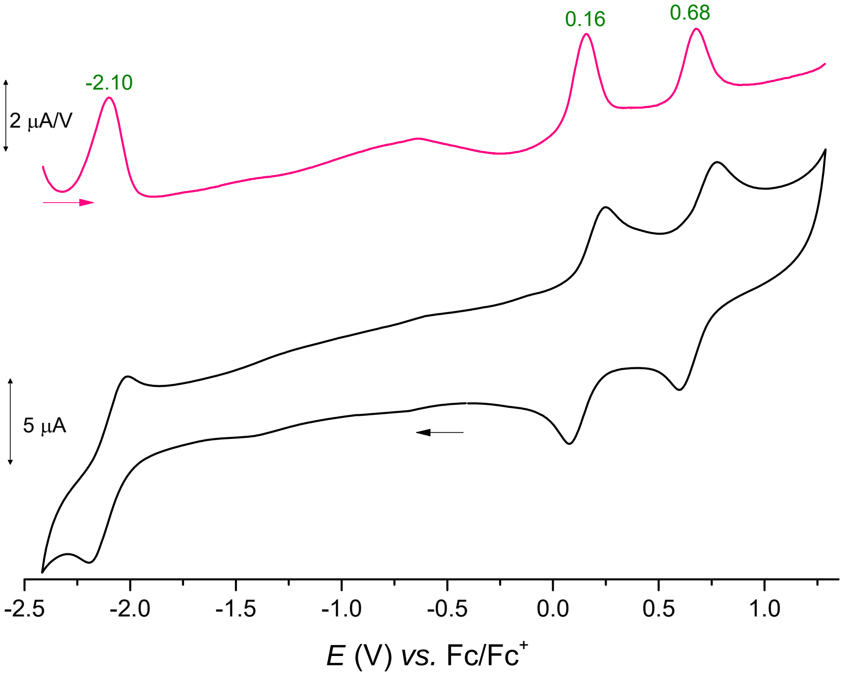

Figure S133. Differential pulse (DP) and cyclic (CV) voltammograms recorded for **3p** in DCM with $[Bu_4N]PF_6$ as supporting electrolyte.

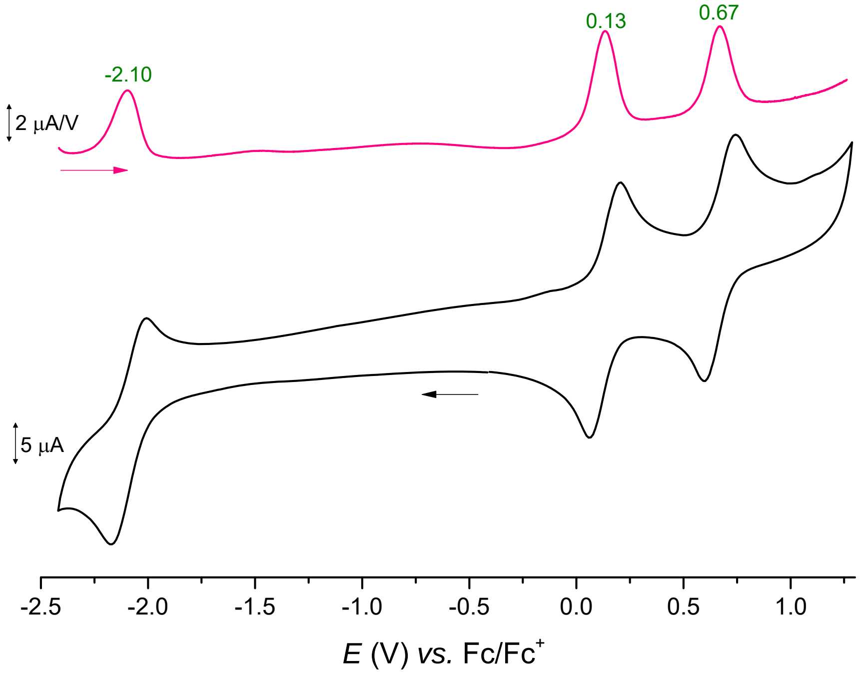

Figure S134. Differential pulse (DP) and cyclic (CV) voltammograms recorded for **3q** in DCM with $[Bu_4N]PF_6$ as supporting electrolyte.

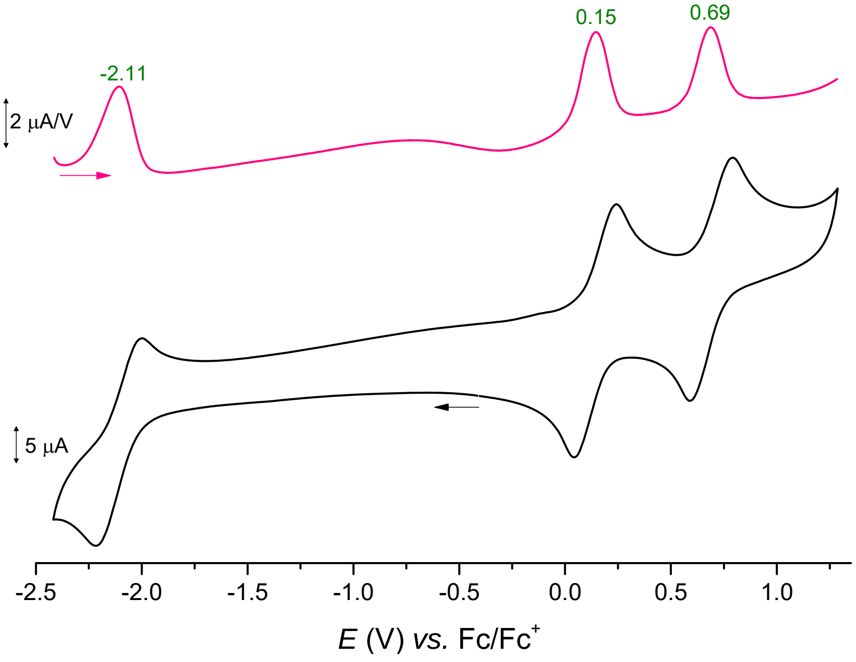

Figure S135. Differential pulse (DP) and cyclic (CV) voltammograms recorded for **3r** in DCM with $[Bu_4N]PF_6$ as supporting electrolyte.

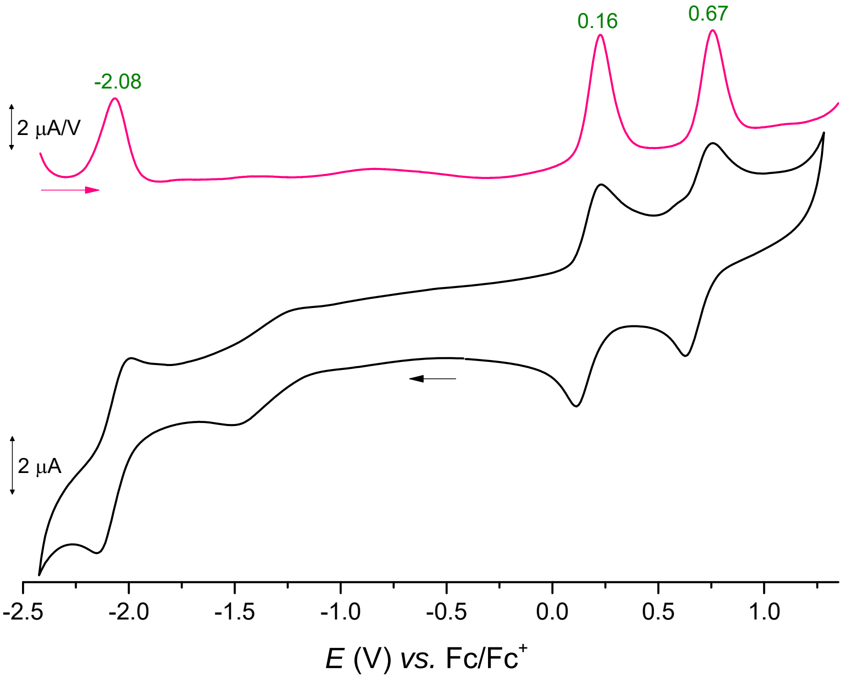

Figure S136. Differential pulse (DP) and cyclic (CV) voltammograms recorded for **3s** in DCM with $[Bu_4N]PF_6$ as supporting electrolyte.

Table S1. Electrochemical data for the compounds **3a**-**3s** (DCM, electrode potentials in V *vs*. Fc/Fc$^+$)

Compd.	E_{Red1}	E_{Ox1}	E_{Ox2}	ΔE
3a	-2.05	0.18	0.68	2.23
3b	-2.08	0.18	0.68	2.26
3c	-2.05	0.17	0.66	2.22
3d	-2.15	0.21	0.68	2.36
3e	-2.00	0.22	0.69	2.22
3f	-2.00	0.20	0.69	2.20
3g	-2.02	0.20	0.69	2.22
3h	-2.05	0.21	0.71	2.26
3i	-2.04	0.20	0.69	2.24
3j	-2.07	0.10	0.69	2.17
3k	-2.09	0.16	0.68	2.25
3l	-2.10	0.15	0.66	2.25
3m	-2.05	0.18	0.74	2.23
3n	-2.08	0.19	0.75	2.27
3o	-2.07	0.16	0.68	2.23
3p	-2.10	0.16	0.68	2.26
3q	-2.10	0.13	0.67	2.23
3r	-2.11	0.15	0.69	2.26
3s	-2.08	0.16	0.67	2.24

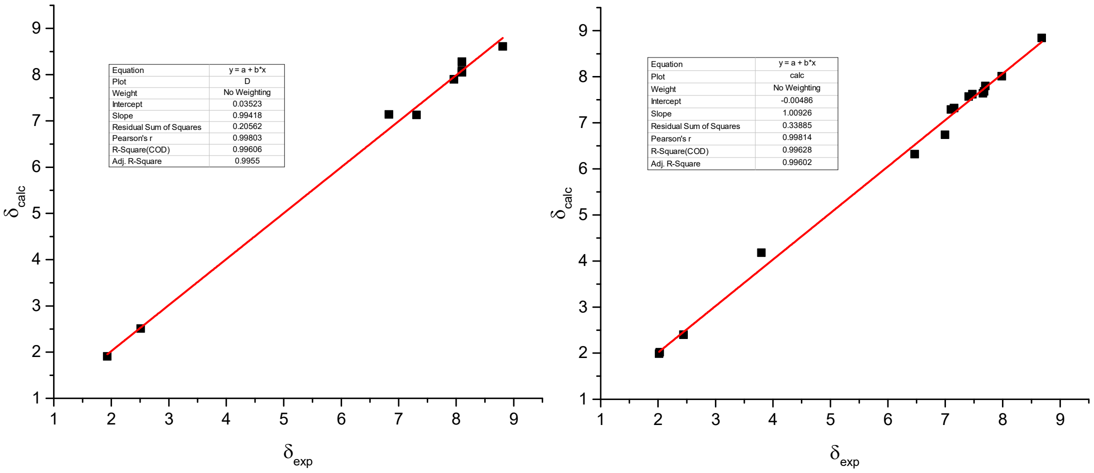

Figure S137. Correlations of the ^{1}H NMR experimental chemical shifts with those calculated by GIAO approach for the DFT-optimized structure of **3d** (left) and [3-*H*-**3d**]$^+$ (right).

Table S2. NICS (1,0,–1) calculated for **3d**.

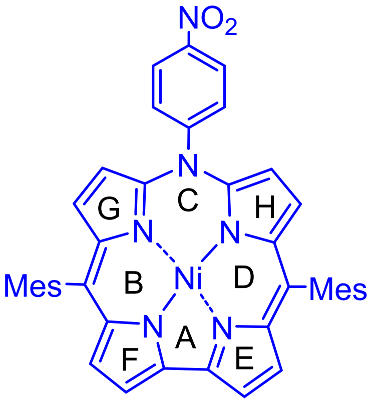

Ring	NICS(1)	NICS(0)	NICS(-1)
A	-9.73	-13.66	-9.73
B	-10.27	-12.73	-10.27
C	-12.19	-16.54	-12.19
D	-10.27	-12.73	-10.27
E	-8.58	-7.55	-8.58
F	-8.59	-7.56	-8.58
G	-8.34	-7.13	-8.34
H	-8.35	-7.14	-8.35

Table S3. NICS (1,0,–1) calculated for [3-*H***3d**]$^+$.

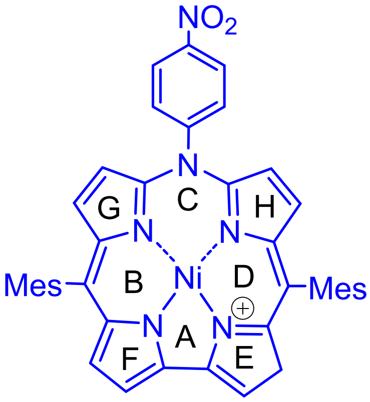

Ring	NICS(1)	NICS(0)	NICS(-1)
A	-3.14	-4.73	-3.14
B	-3.52	-4.35	-3.52
C	-6.49	-9.32	-6.49
D	-5.49	-6,37	-5.49
E	-5.10	-1.52	-5.10
F	-9.84	-9.21	-9.84
G	-8.03	-6.86	-8.03
H	-4.25	-1.04	-4.25

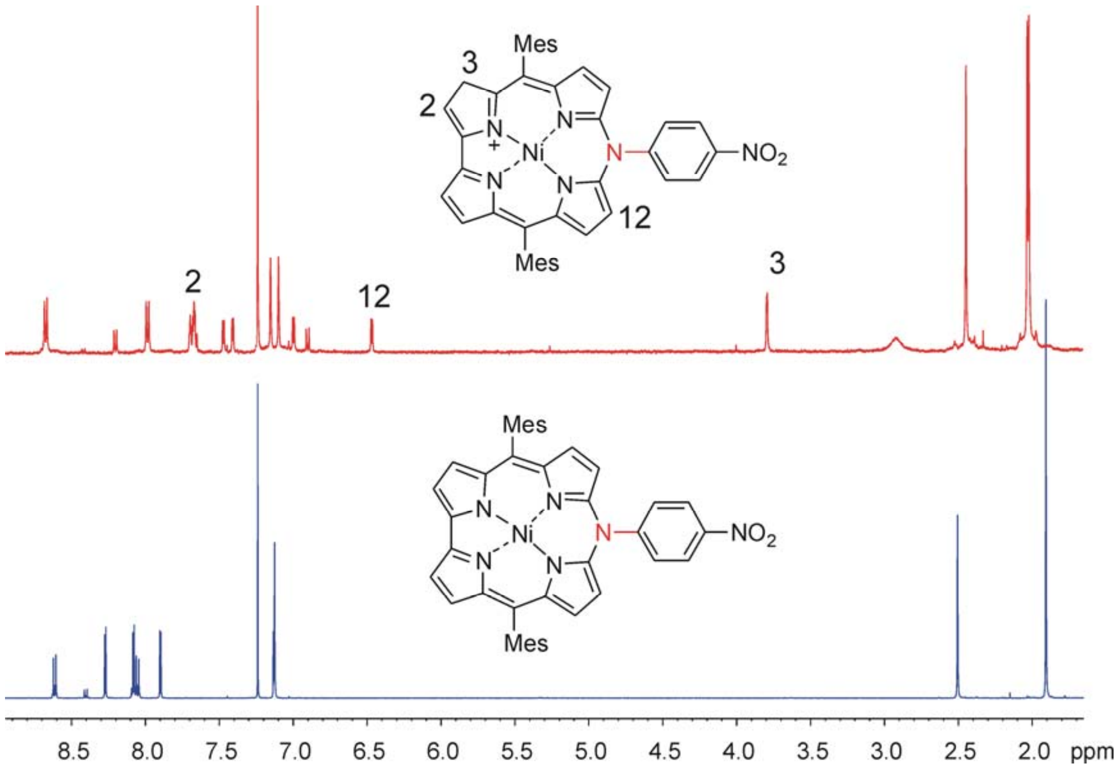

Figure S138. Comparison of the ^{1}H NMR spectrum of **3d** (lower trace) and that [**3d**H]$^+$ (upper trace) obtained by addition of trifluoracetic acid (5 %) to the solution of **3d** in CDCl$_3$ (500 MHz, 300 K).

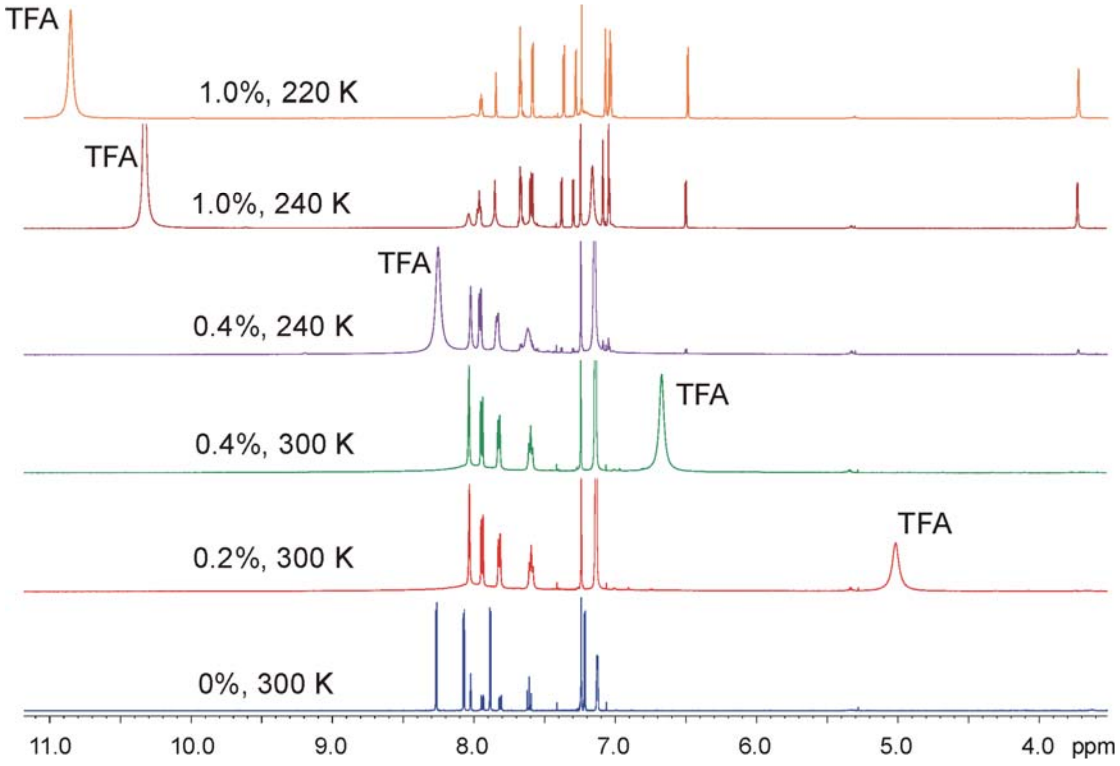

Figure S139. Selected region of the ^{1}H NMR spectra (500 MHz) recorded at specified temperatures upon addition of the specified amount of trifluoracetic acid (v/v) to the CDCl$_3$ solution of **3i**.

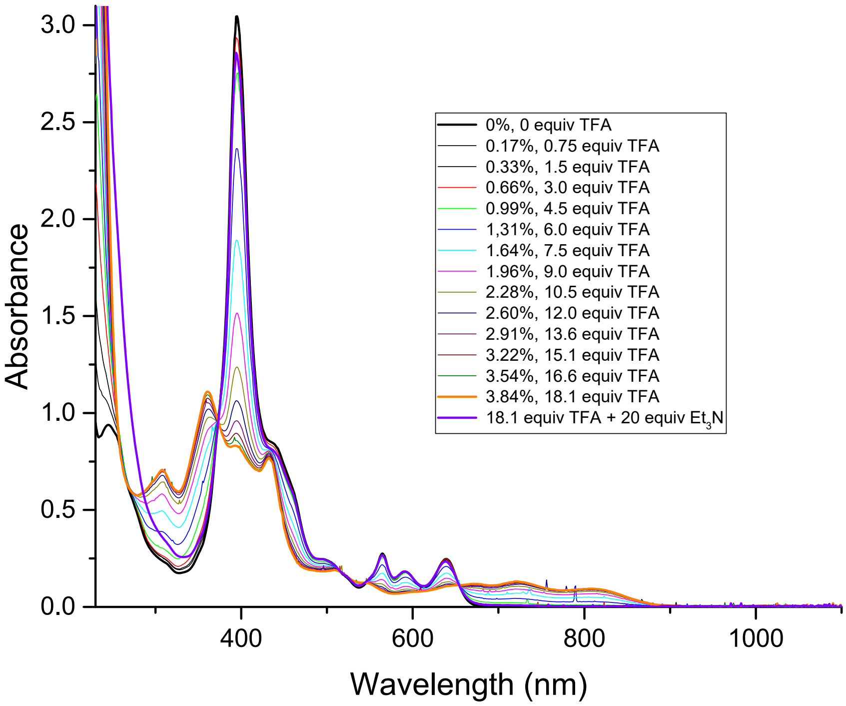

Figure S140. UV-vis-NIR spectra (DCM, 298 K) recorded upon titration of **3d** with trifluoracetic acid (TFA). The amount of the acid added is given in the legend for each spectrum as a volume percentage and as a number of equivalents with respect to **3d** present in solution.

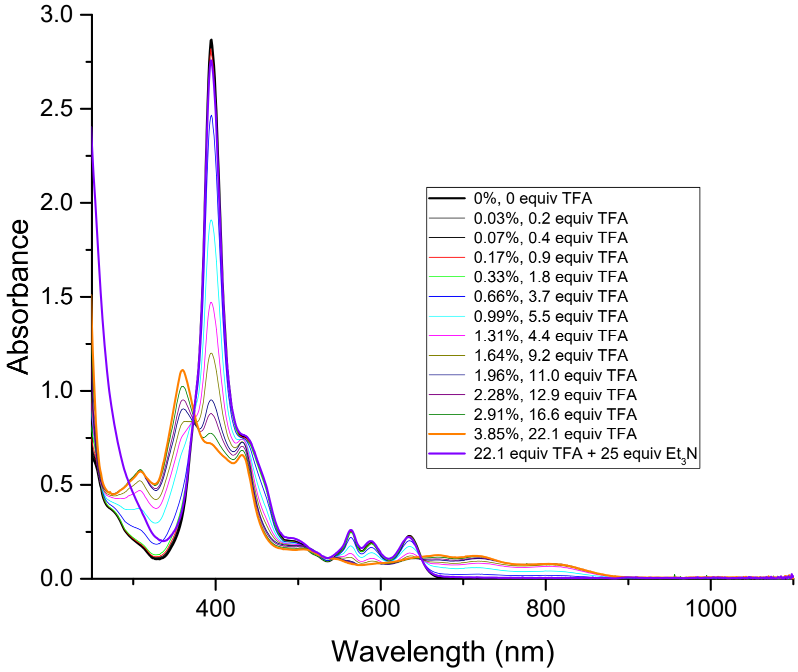

Figure S141. UV-vis-NIR spectra (DCM, 298 K) recorded upon titration of **3i** with trifluoracetic acid (TFA). The amount of the acid added is given in the legend for each spectrum as a volume percentage and as a number of equivalents with respect to **3i** present in solution.

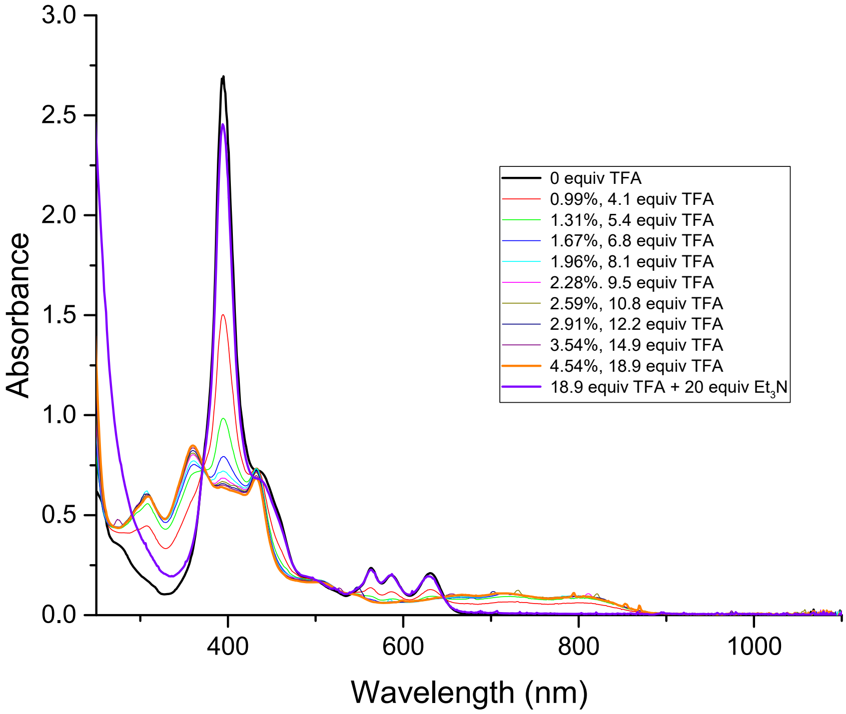

Figure S142. UV-vis-NIR spectra (DCM, 298 K) recorded upon titration of **3p** with trifluoracetic acid (TFA). The amount of the acid added is given in the legend for each spectrum as a volume percentage and as a number of equivalents with respect to **3p** present in solution.

Table S4. TD DFT Calculated Electronic Transitions Calculated for **3d**.

No.	Energy (cm^{-1})	Wavelength (nm)	Osc. Strength	Major contribs	Minor contribs
1	14866.4	672.7	0	HOMO->LUMO (100%)	
2	17328.8	577.1	0	H-1->LUMO (100%)	
3	18720.9	534.2	0.11	HOMO->L+1 (89%)	H-2->L+1 (3%), H-1->L+2 (7%)
4	19982.4	500.4	0.0181	H-1->L+1 (30%), HOMO->L+2 (68%)	
5	20623.6	484.9	0	H-13->L+4 (14%), H-2->L+4 (41%), HOMO->L+4 (37%)	H-15->L+4 (3%), H-9->L+4 (5%)
6	21457.6	466.0	0	H-6->L+4 (93%)	H-2->L+1 (2%)
7	22148.8	451.5	0	H-14->L+4 (22%), H-3->L+4 (76%)	
8	23155.4	431.9	0	H-3->LUMO (99%)	
9	23182.8	431.4	0	H-2->LUMO (99%)	
10	23852.2	419.2	0.3596	H-3->L+1 (32%), H-2->L+2 (10%), H-1->L+1 (44%), HOMO->L+2 (13%)	
11	23913.5	418.2	0.2011	H-2->L+1 (23%), H-1->L+2 (68%)	H-6->L+4 (4%), HOMO->L+1 (3%)
12	25302.4	395.2	0.219	H-3->L+1 (63%), H-2->L+2 (15%), H-1->L+1 (12%)	HOMO->L+2 (9%)
13	25909.8	386.0	0.0001	H-6->LUMO (95%)	H-4->LUMO (5%)
14	26217.1	381.4	0.0026	H-4->LUMO (93%)	H-6->LUMO (5%)
15	26248.5	381.0	0.0009	H-5->LUMO (100%)	
16	26277.5	380.6	0.0007	H-6->L+1 (98%)	
17	26284.0	380.5	0.2055	H-3->L+2 (52%), H-2->L+1 (36%)	H-1->L+2 (5%), HOMO->L+1 (4%)
18	26728.4	374.1	0.4542	H-3->L+2 (42%), H-2->L+1 (34%), H-1->L+2 (16%)	H-6->L+4 (2%), HOMO->L+1 (3%)
19	26883.3	372.0	0	H-7->LUMO (99%)	
20	26885.7	371.9	0	H-8->LUMO (99%)	
21	27651.1	361.6	0.0001	H-9->LUMO (98%)	
22	27753.5	360.3	0	H-5->L+2 (24%), H-4->L+1 (74%)	
23	27772.1	360.1	0	H-5->L+1 (73%), H-4->L+2 (26%)	
24	27860.0	358.9	0.5747	H-2->L+2 (65%), H-1->L+1 (10%), HOMO->L+3 (13%)	HOMO->L+2 (9%)
25	28085.8	356.1	0	H-6->L+2 (98%)	
26	28160.8	355.1	0.0068	H-17->L+4 (88%)	H-26->L+4 (3%), H-24->L+4 (3%), H-22->L+4 (3%)
27	28491.5	351.0	0	H-2->L+4 (28%), HOMO->L+4 (62%)	H-13->L+4 (5%), H-9->L+4 (3%)
28	28810.9	347.1	0.0617	HOMO->L+3 (86%)	H-2->L+2 (8%),

					H-1->L+1 (2%)
29	29070.6	344.0	0.0006	H-7->L+1 (71%), H-7->L+2 (17%)	H-8->L+1 (8%), H-8->L+2 (4%)
30	29074.7	343.9	0.0021	H-8->L+1 (71%), H-8->L+2 (16%)	H-7->L+1 (8%), H-7->L+2 (4%)
31	29336.0	340.9	0	H-1->L+4 (99%)	
32	30315.2	329.9	0.0469	H-9->L+1 (96%)	
33	30441.0	328.5	0	H-18->LUMO (95%)	H-18->L+5 (3%)
34	30848.3	324.2	0.0062	H-1->L+3 (99%)	
35	30983.0	322.8	0	H-5->L+1 (26%), H-4->L+2 (73%)	
36	31009.6	322.5	0	H-5->L+2 (75%), H-4->L+1 (24%)	
37	31829.9	314.2	0.0001	H-7->L+1 (20%), H-7->L+2 (80%)	
38	31833.9	314.1	0.0001	H-8->L+1 (20%), H-8->L+2 (80%)	
39	31937.1	313.1	0	H-10->LUMO (98%)	
40	32363.0	309.0	0.0002	H-9->L+2 (98%)	
41	33401.8	299.4	0.0001	H-11->LUMO (11%), HOMO->L+5 (88%)	
42	33994.7	294.2	0.0055	H-11->LUMO (77%), HOMO->L+5 (10%)	H-15->LUMO (8%), H-13->LUMO (3%)
43	34534.2	289.6	0.0304	H-10->L+1 (97%)	
44	34692.3	288.2	0	H-19->LUMO (97%)	H-19->L+5 (3%)
45	35422.3	282.3	0	H-12->LUMO (15%), H-1->L+5 (28%), HOMO->L+6 (55%)	
46	35464.2	282.0	0	H-12->LUMO (23%), H-1->L+5 (32%), HOMO->L+6 (42%)	
47	35518.2	281.5	0.0002	HOMO->L+7 (94%)	H-15->LUMO (2%), H-1->L+6 (3%)
48	35665.8	280.4	0.0124	H-15->LUMO (57%), H-13->LUMO (23%), H-11->LUMO (11%)	H-16->L+3 (3%), HOMO->L+7 (3%)
49	36212.7	276.1	0	H-12->LUMO (60%), H-1->L+5 (39%)	
50	36456.3	274.3	0.0652	H-10->L+2 (95%)	

Table S5. TD DFT Calculated Electronic Transitions Calculated for [3-*H*3**d**]$^+$.

No.	Energy (cm^{-1})	Wavelength (nm)	Osc. Strength	Major contribs	Minor contribs
1	13447.7	743.6	0.094	HOMO->LUMO (98%)	
2	18569.3	538.5	0	H-3->LUMO (99%)	
3	18889.5	529.4	0.0021	H-6->LUMO (89%)	H-8->L+3 (4%), H-5->LUMO (3%)
4	18991.9	526.5	0	H-1->LUMO (97%)	**H-1->L+2 (2%)**
5	19257.3	519.3	0.0011	H-4->LUMO (98%)	
6	19572.7	510.9	0	H-2->LUMO (98%)	
7	20280.8	493.1	0.0033	H-5->LUMO (47%), HOMO->L+2 (39%)	H-8->L+3 (7%), H-6->LUMO (4%)
8	20666.3	483.9	0	HOMO->L+1 (99%)	

9	20996.2	476.3	0	H-6->L+3 (47%), HOMO->L+3 (19%)	H-18->L+3 (8%), H-17->L+3 (7%), H-15->L+3 (3%), H-9->L+3 (7%), H-7->L+3 (4%)
10	21220.4	471.2	0.0166	H-8->L+3 (69%), H-7->LUMO (16%)	H-6->LUMO (2%), HOMO->L+2 (9%)
11	21505.2	465.0	0.0001	H-8->LUMO (84%)	H-14->L+3 (3%), H-7->L+3 (7%), HOMO->L+3 (2%)
12	22850.5	437.6	0	H-14->L+3 (14%), H-8->LUMO (14%), H-7->L+3 (29%), H-6->L+3 (10%)	H-15->L+3 (5%), H-9->L+3 (5%), H-5->L+3 (9%), HOMO->L+3 (9%)
13	22961.0	435.5	0.0761	H-8->L+3 (19%), H-7->LUMO (61%), H-5->LUMO (11%)	HOMO->L+2 (6%)
14	24457.1	408.9	0	H-1->L+2 (97%)	H-1->LUMO (2%)
15	24995.9	400.1	0.9016	H-7->LUMO (17%), H-5->LUMO (32%), HOMO->L+2 (39%)	H-7->L+2 (3%)
16	25425.0	393.3	0.0143	H-2->L+2 (97%)	
17	25838.8	387.0	0	H-7->L+3 (13%), HOMO->L+3 (70%)	H-15->L+3 (3%), H-14->L+3 (2%), H-6->L+3 (7%)
18	26252.5	380.9	0.009	H-9->LUMO (82%), H-6->L+2 (11%)	H-5->L+2 (2%)
19	26741.3	374.0	0.0005	H-1->L+1 (100%)	
20	27117.2	368.8	0	H-2->L+1 (100%)	
21	27150.2	368.3	0.021	H-9->LUMO (10%), H-6->L+2 (80%)	H-7->L+2 (2%), H-5->L+2 (3%)
22	27843.1	359.2	0	H-5->L+1 (94%)	H-4->L+1 (5%)
23	28223.8	354.3	0.1552	H-5->L+2 (66%)	H-24->L+3 (3%), H-22->L+3 (2%), H-10->LUMO (6%), H-4->L+2 (2%), HOMO->L+4 (7%)
24	28373.0	352.4	0.0169	H-24->L+3 (34%), H-22->L+3 (24%), H-19->L+3 (22%)	H-26->L+3 (8%), H-5->L+2 (5%)
25	28393.1	352.2	0.0011	H-3->L+1 (100%)	
26	28571.4	350.0	0	H-4->L+1 (95%)	H-5->L+1 (5%)
27	28594.8	349.7	0.0001	H-3->L+2 (99%)	
28	28833.5	346.8	0	H-6->L+1 (98%)	
29	28869.8	346.4	0.0015	H-4->L+2 (96%)	H-5->L+2 (3%)
30	29696.5	336.7	0.085	H-10->LUMO (12%), H-7->L+2 (80%)	HOMO->L+2 (2%)
31	30304.7	330.0	0	H-13->L+1 (86%)	H-13->L+6 (3%), H-7->L+1 (8%)
32	30365.2	329.3	0.054	H-10->LUMO (76%), H-7->L+2 (10%)	H-5->L+2 (5%), HOMO->L+4 (3%)

33	30449.8	328.4	0.0006	H-8->L+2 (99%)	
34	30744.2	325.3	0.0001	H-7->L+1 (90%)	H-13->L+1 (8%)
35	31746.0	315.0	0.0047	H-11->LUMO (78%), HOMO->L+4 (14%)	H-14->LUMO (5%)
36	32310.6	309.5	0	H-7->L+3 (14%), H-5->L+3 (80%)	H-4->L+3 (3%)
37	32383.2	308.8	0.0001	H-12->LUMO (97%)	
38	32452.5	308.1	0.5469	HOMO->L+4 (71%)	H-14->LUMO (6%), H-11->LUMO (9%), H-5->L+2 (8%)
39	33351.0	299.8	0.0467	H-14->LUMO (41%), H-1->L+3 (42%)	H-18->LUMO (2%), H-11->LUMO (4%), H-9->L+2 (3%)
40	33408.3	299.3	0.0341	H-14->LUMO (27%), H-1->L+3 (57%)	H-18->LUMO (2%), H-11->LUMO (3%), H-9->L+2 (3%)
41	33580.9	297.8	0	H-8->L+1 (100%)	
42	33897.9	295.0	0.1682	HOMO->L+5 (86%)	H-18->LUMO (4%), H-17->LUMO (3%)
43	34000.3	294.1	0	H-2->L+3 (100%)	
44	34094.7	293.3	0.0847	H-18->LUMO (24%), H-17->LUMO (20%), H-15->LUMO (35%)	H-14->LUMO (4%), H-9->L+2 (5%), HOMO->L+5 (5%)
45	34418.9	290.5	0	H-16->L+1 (97%)	H-16->L+6 (3%)
46	34637.5	288.7	0.0008	H-13->LUMO (95%)	H-15->LUMO (2%)
47	35058.5	285.2	0.0053	H-3->L+3 (99%)	
48	35298.0	283.3	0.0037	H-9->L+2 (80%)	H-15->LUMO (7%), H-14->LUMO (4%), H-10->L+2 (2%)
49	35417.4	282.3	0.01	H-11->L+1 (10%), H-10->L+1 (23%), H-9->L+1 (63%)	
50	35460.2	282.0	0	H-4->L+3 (97%)	H-5->L+3 (3%)

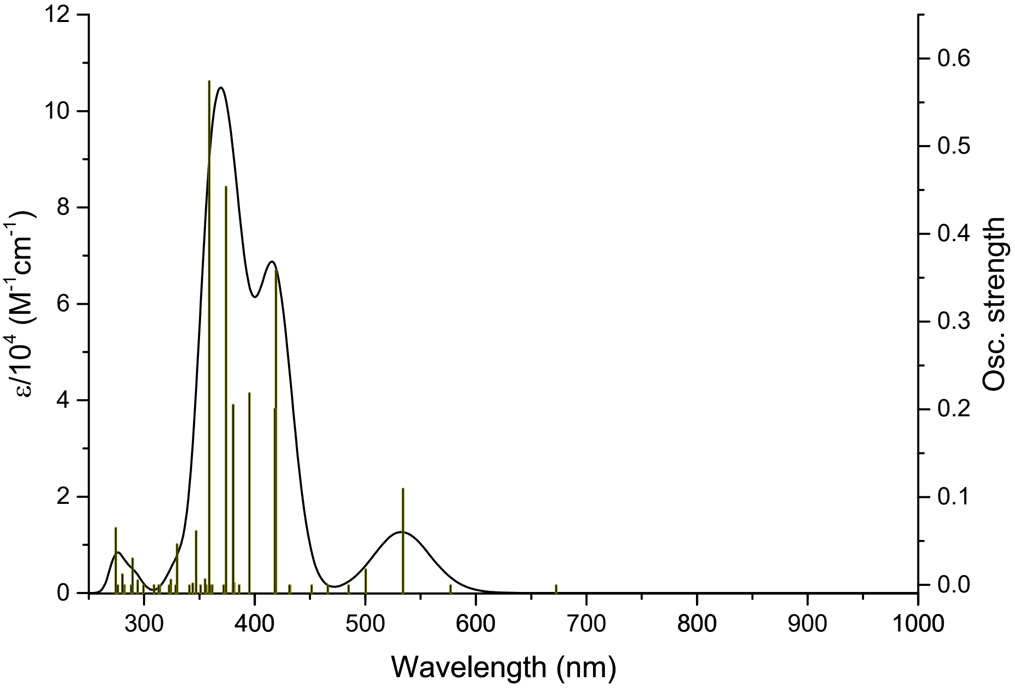

Figure S142. TD DFT-calculated electronic transition (dark yellow sticks) and UV-vis-NIR spectrum (convoluted with 2000 cm^{-1} linewidth) for DFT-optimized model of **3d**.

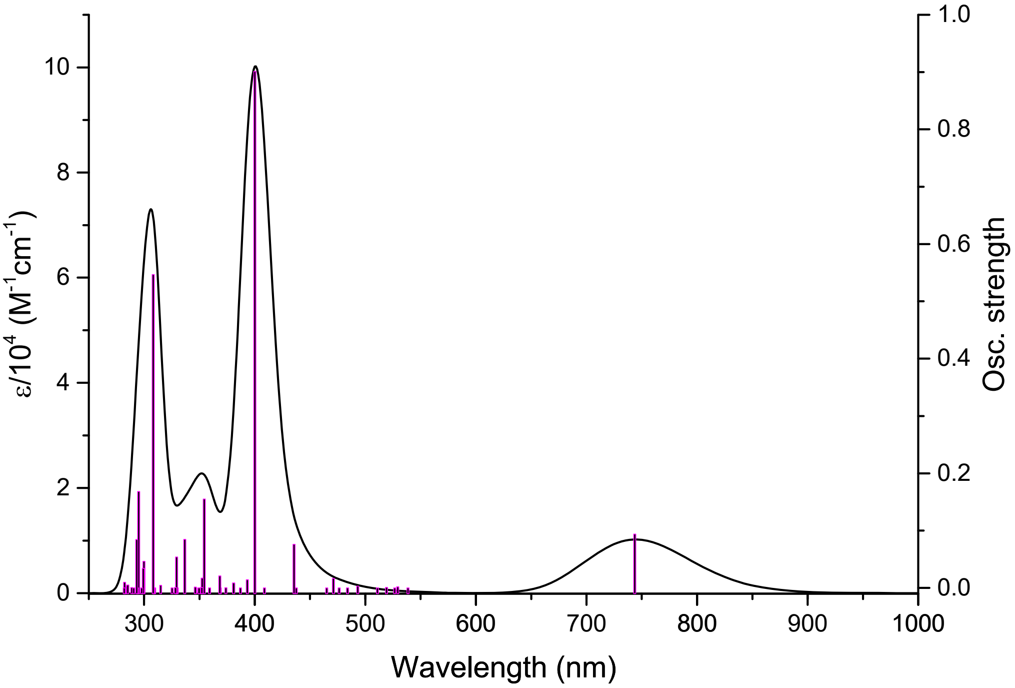

Figure S143. TD DFT-calculated electronic transition (purple sticks) and UV-vis-NIR spectrum (convoluted with 2000 cm^{-1} linewidth) for DFT-optimized model of [3-*H*$\mathbf{3d}$]$^+$.

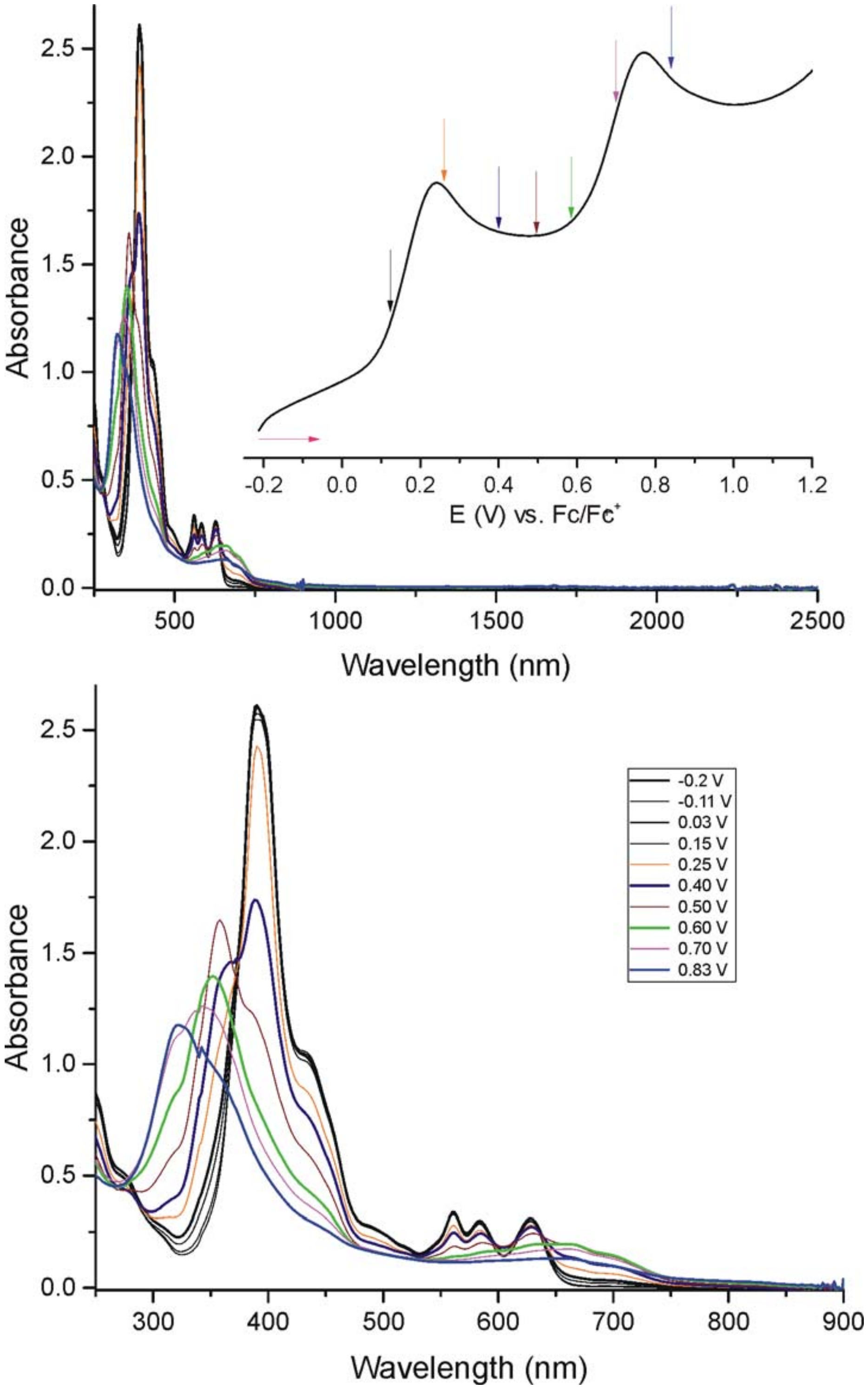

Figure S144. UV-vis-NIR spectra recorded upon electrochemical oxidation of **3p** (0.1 M $[Bu_4N]PF_6$, DCM, Pt gauze as optically transparent working electrode). Upper panel presents spectral changes in the range of 250-2500 nm and anodic scan of linear voltammogram with arrows indicating potentials at which the spectra were recorded; the bottom panel contains expansion of the visible region of these spectra.

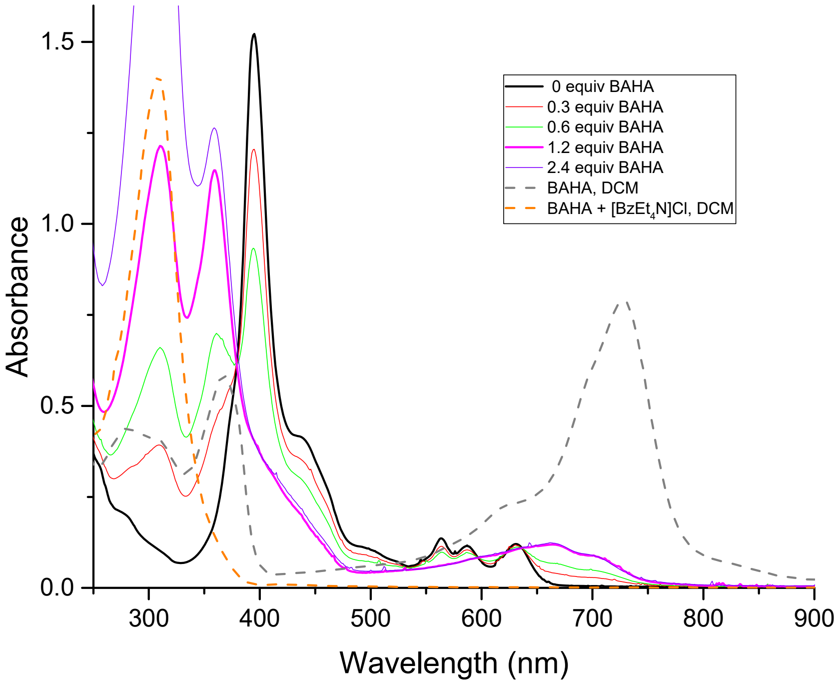

Figure S145. Selected UV-vis-NIR spectra recorded upon addition of tris(4-bromophenyl)ammoniumyl hexachloroantimonate (BAHA) to the DCM solution of **3p** (solid lines) with the amount of the added oxidant specified in the legend. The spectra of oxidized (black dashed line) and reduced (red dashed line) forms of BAHA in DCM are also shown for comparison.

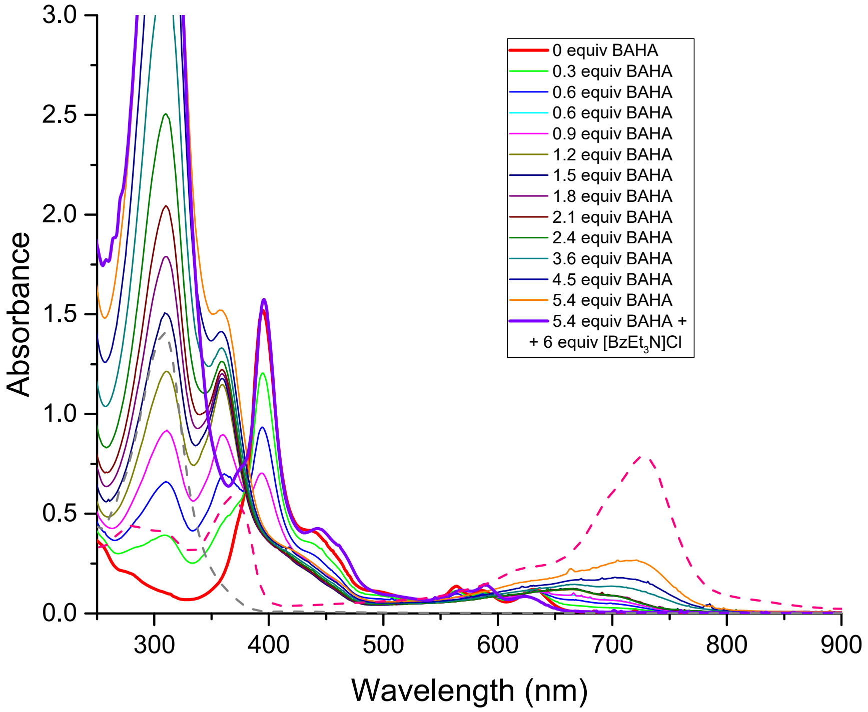

Figure S146. UV-vis-NIR spectra recorded upon addition of tris(4-bromophenyl)ammoniumyl hexachloroantimonate (BAHA) to the DCM solution of **3p** (solid lines) with the amount of the added oxidant specified in the legend. The spectra of oxidized (pink dashed line) and reduced (gray dashed line) forms of BAHA in DCM are also shown for comparison.

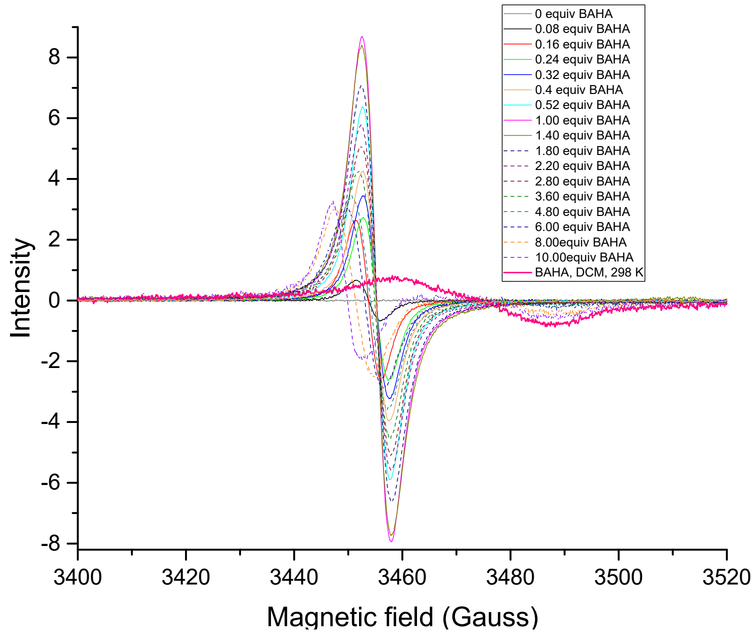

Figure S147. EPR spectra (DCM, 298 K) recorded upon addition of tris(4-bromophenyl)ammoniumyl hexachloroantimonate (BAHA) to the DCM solution of **3p**. Spectra of increasing intensity are drawn with solid lines, and those of decreasing intensity. The intensities were corrected for dilution caused by titration. The amount of the added oxidant is specified in the legend. The spectrum of BAHA in DCM (pink solid line) is also shown for comparison.

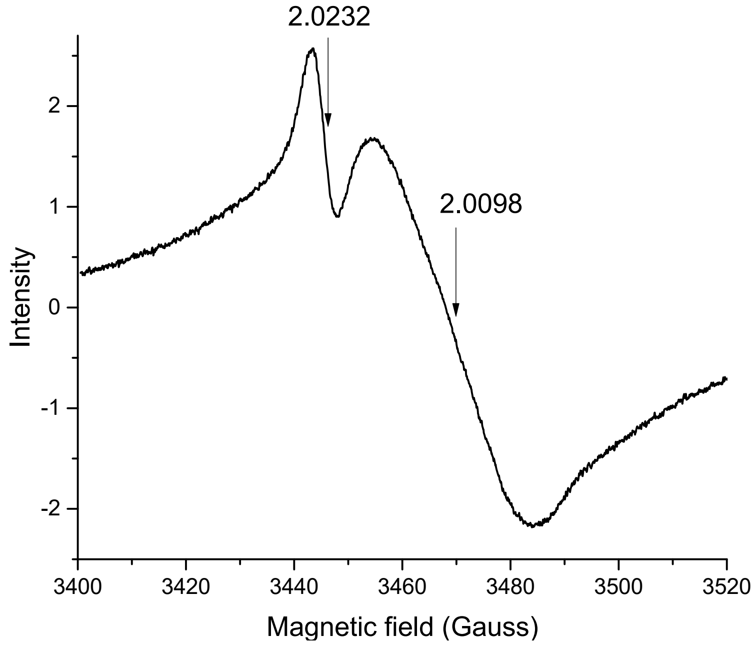

Figure S148. EPR spectrum (DCM, 298 K) of saturated solution of tris(4-bromophenyl)ammoniumyl hexachloroantimonate (BAHA) in DCM solution containing an aliquot of **3p**. The isotropic g_0 values for both signals are given.

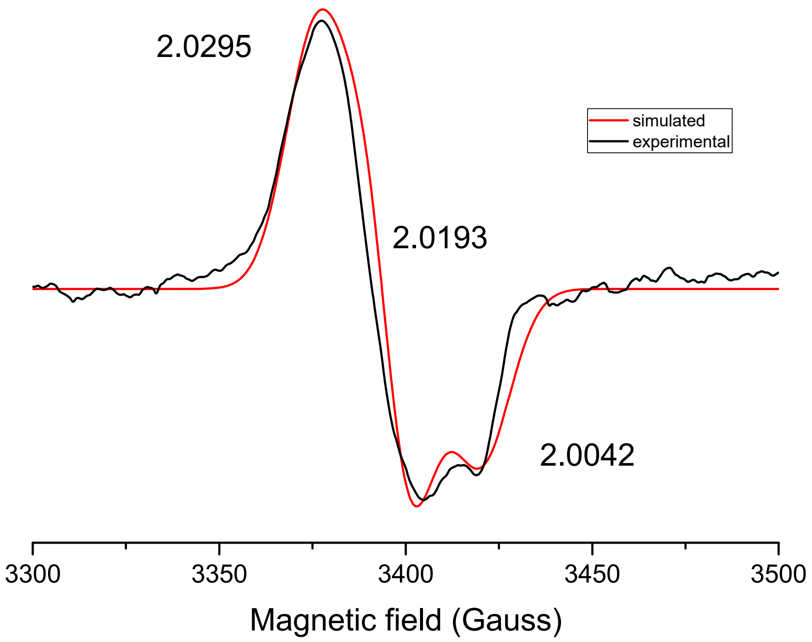

Figure S149. Experimental (frozen DCM, 77 K, black trace) and simulated (red trace) EPR spectra of a radical species formed upon addition of 0.8 equiv of tris(4-bromophenyl)ammoniumyl hexachloroantimonate (BAHA) to the solution of **3p**. Components of the Zeeman tensor determined by simulation are associated with the appropriate regions of the spectrum.

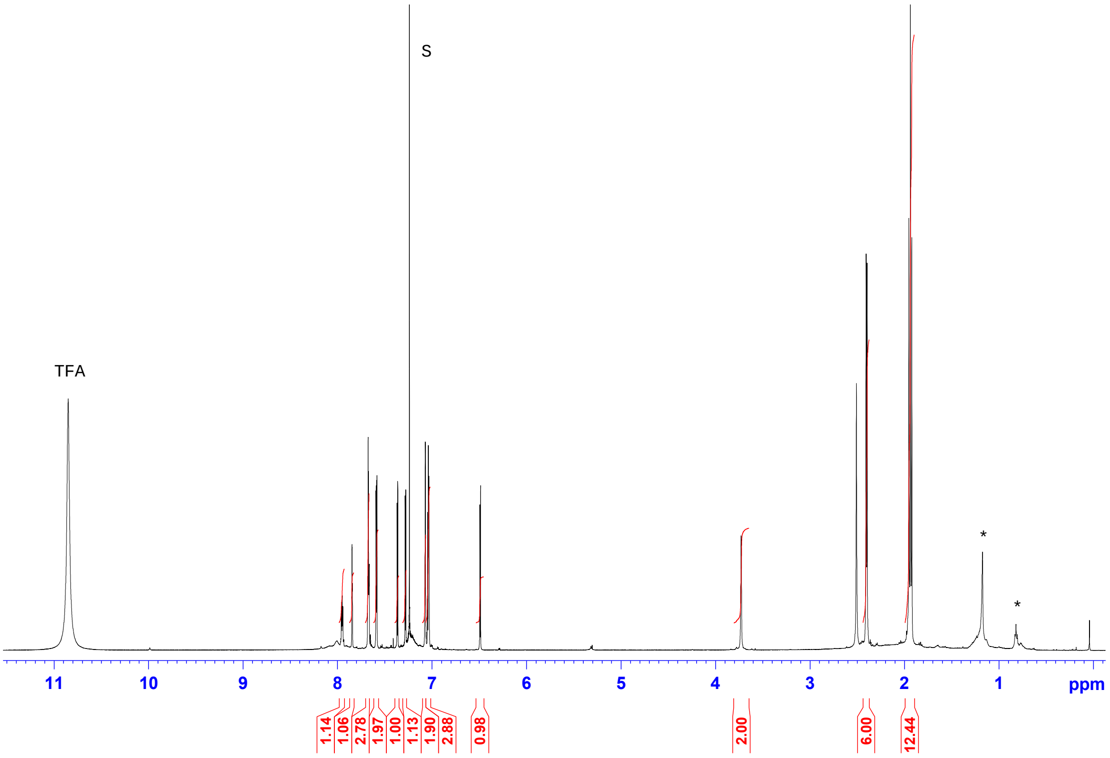

Figure S150. ^{1}H NMR spectrum (600 MHz, $CDCl_{3,}$ 220 K) of **3i** in the solution containing 1% CF_3COOH (TFA).

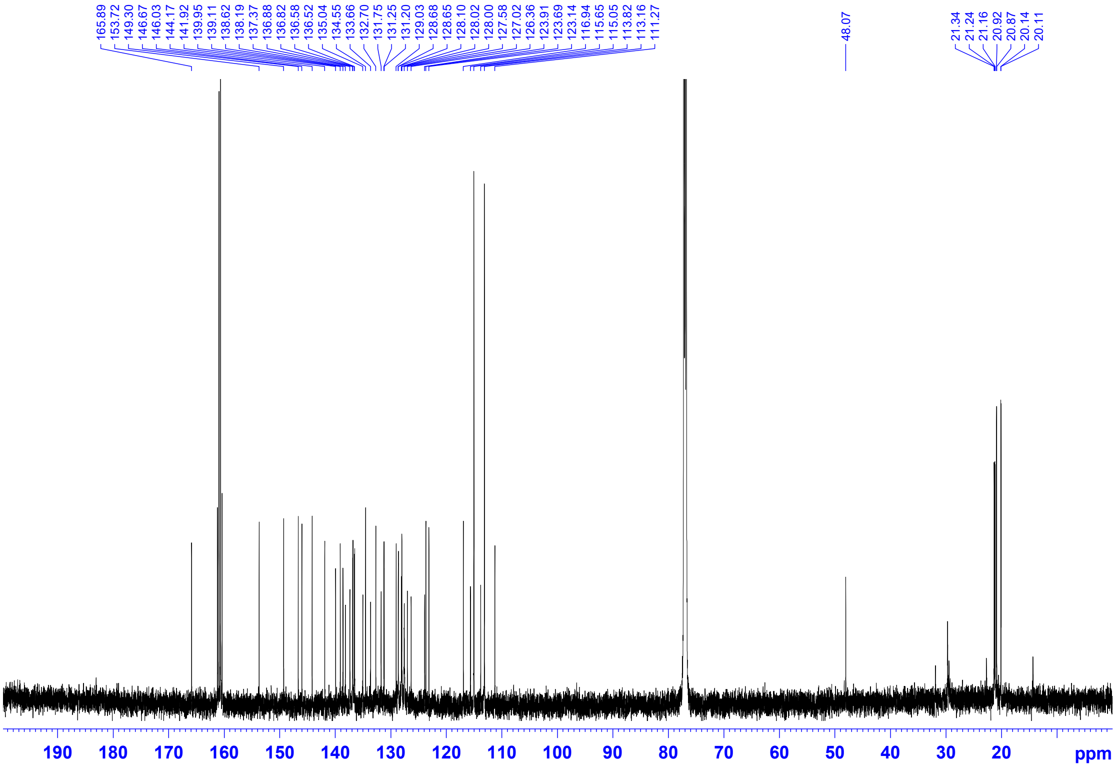

Figure S151. ^{13}C NMR spectrum (150 MHz, $CDCl_{3,}$ 220 K) of **3i** in the solution containing 1% CF_3COOH (TFA).

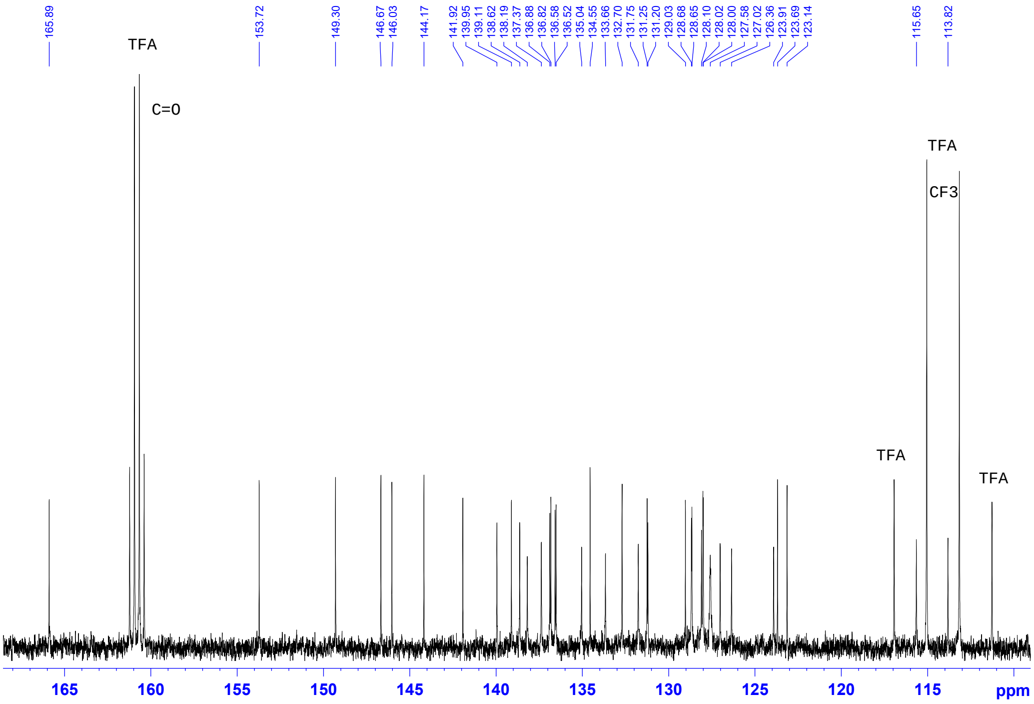

Figure S152. Expansion of a low-field region of the ^{13}C NMR spectrum (150 MHz, CDCl$_3$, 220 K) of **3i** in the solution containing 1% of CF$_3$COOH (TFA).

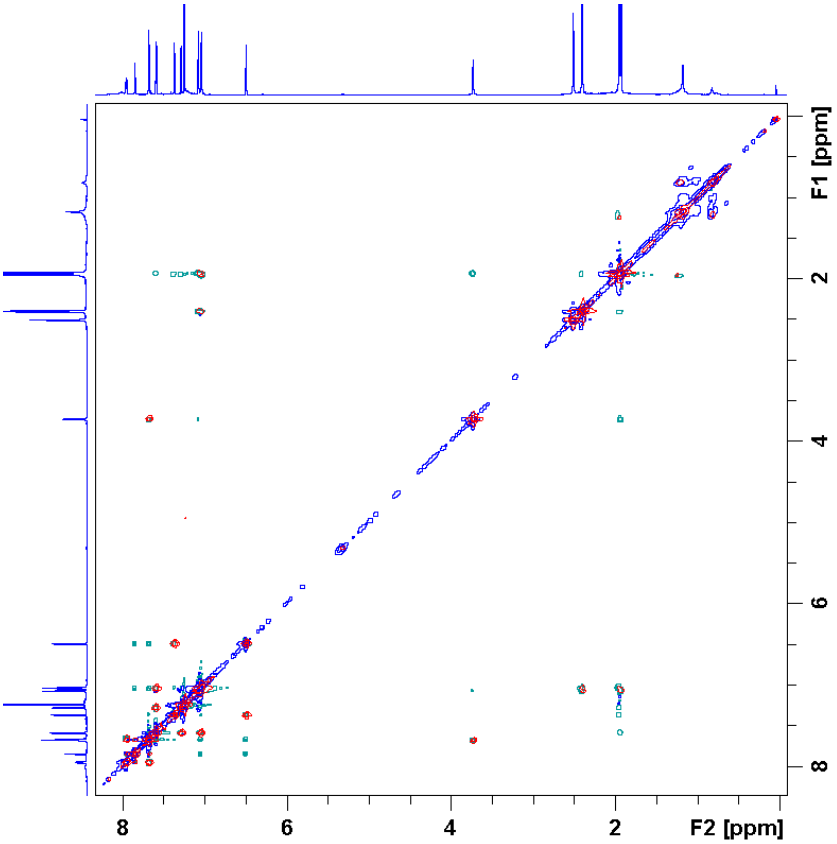

Figure S153. Superimposed ^{1}H,^{1}H COSY (red traces) and ^{1}H,^{1}H ROESY (blue and green traces) of [**3i**H]$^+$ (600 MHz, CDCl$_3$, 220 K).

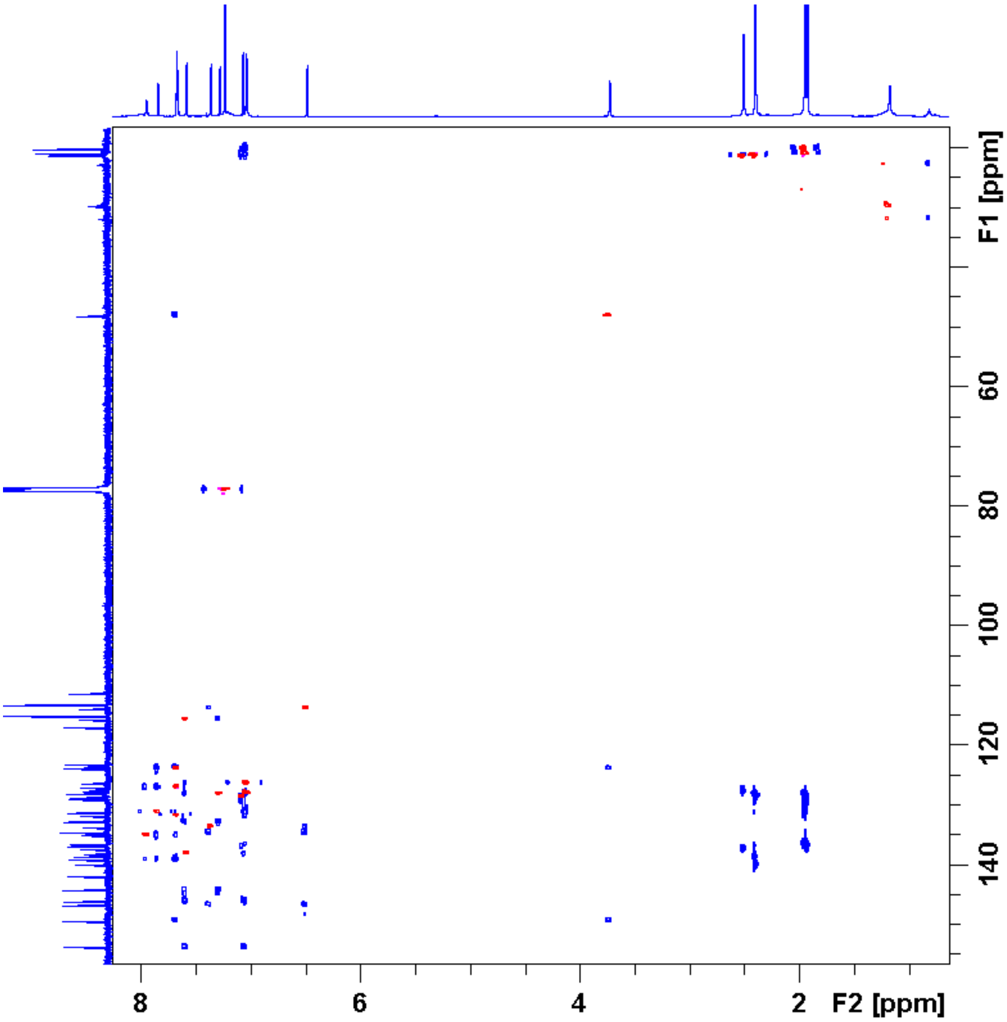

Figure S154. Superimposed ^{1}H,^{13}C HSQC (red traces) and ^{1}H,^{13}C HMBC (blue traces) of [**3i**H]$^+$ (600/150 MHz, $CDCl_3$, 220 K).

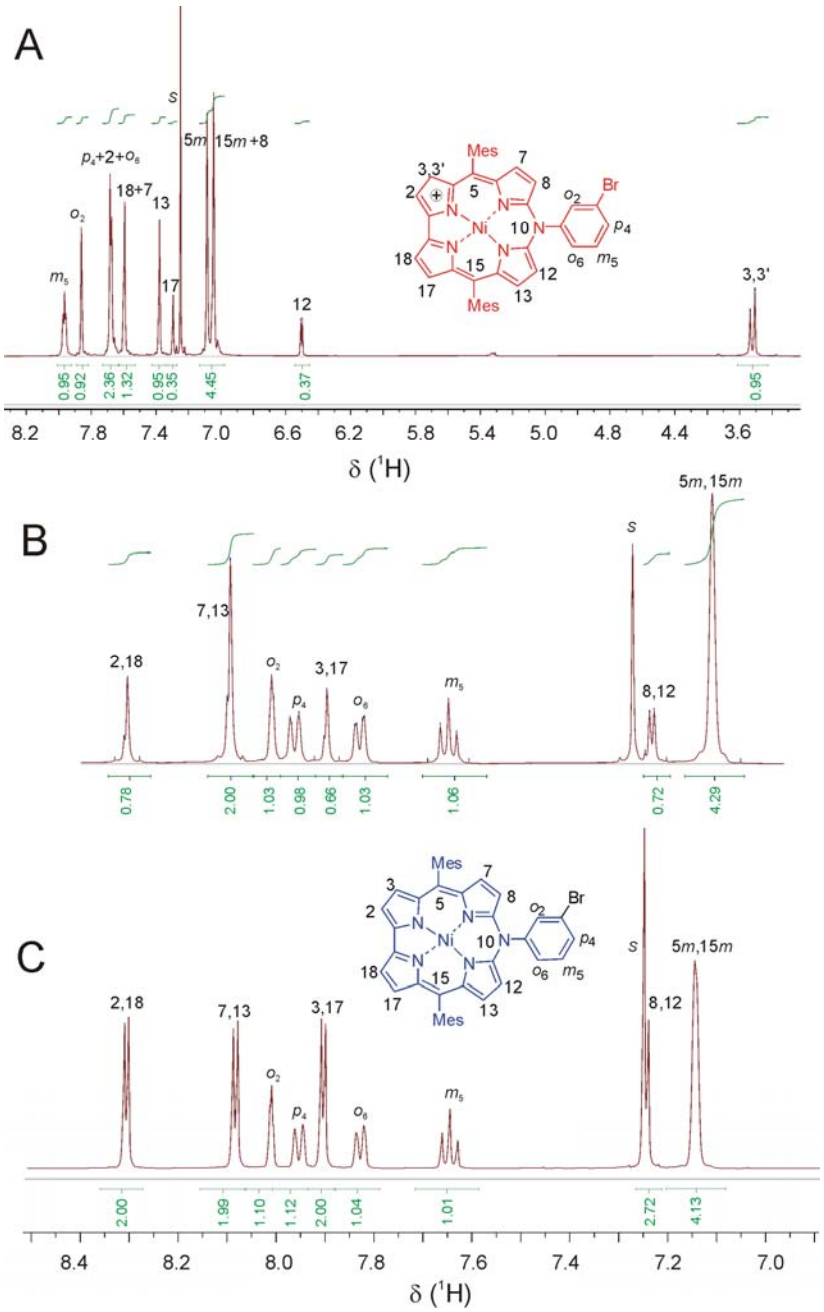

Figure S155. Lower-field region of the ^{1}H NMR spectra (500 MHz, CDCl$_3$, 220 K) of **3i** in the solution containing 1% CF$_3$COOD (TFA-*d*) (A), the same sample after addition of 2% of Et$_3$N (B), and original sample before addition of the deuterated acid. (C). The signal assignments have been made on the basis of 2D experiments. The green numbers under the signals are relative integrals.

Table S6. Crystallographic data for **3d**, **3e**, and **3h**.

Crystal data 1

	3d	**3e**	**3h**
Chemical formula	$2(C_{42}H_{34}N_6NiO_2)$	$C_{43}H_{34}N_6Ni_1,0.9(C_1H_2\ Cl_2)$	$C_{42}H_{34}ClN_5Ni{\cdot}0.93CH_2Cl_2$
M_r	1426.92	769.90	787.83
Crystal system, space group	Orthorhombic, *Pbca*	Monoclinic, $P2_1/n$	Monoclinic, $P2_1/n$
Temperature (K)	100	100	100
a, b, c (Å)	16.1510 (2), 16.0025 (1), 53.1618 (5)	10.7932 (1), 12.0391 (1), 28.0774 (1)	11.5356 (2), 11.7045 (2), 27.2122 (3)
β (°)	-	94.39 (1)	90.987 (1)
V (Å^3)	13740.0 (2)	3637.7 (3)	3673.6 (1)
Z	8	4	4
Radiation type	Cu Kα	Cu Kα	Cu Kα
μ (mm^{-1})	1.19	2.31	3.07
Crystal Size	0.13 × 0.08 × 0.08	0.14 × 0.05 × 0.04	0.16 × 0.07 × 0.07
Data collection			
Diffractometer	XtaLAB Synergy R, DW system, HyPix-Arc 150	XtaLAB Synergy R, HyPix	XtaLAB Synergy R, DW system, HyPix-Arc 150
Absorption correction	Analytical CrysAlis PRO 1.171.41.75a (Rigaku Oxford Diffraction, 2020) Analytical numeric absorption correction using a multifaceted crystal model based on expressions derived by R.C. Clark & J.S. Reid. (Clark, R. C. & Reid, J. S. (1995). Acta Cryst. A51, 887-897) Empirical absorption correction using spherical harmonics, implemented in SCALE3 ABSPACK scaling algorithm.	Analytical CrysAlis PRO 1.171.41.75a (Rigaku Oxford Diffraction, 2020) Analytical numeric absorption correction using a multifaceted crystal model based on expressions derived by R.C. Clark & J.S. Reid. (Clark, R. C. & Reid, J. S. (1995). Acta Cryst. A51, 887-897) Empirical absorption correction using spherical harmonics, implemented in SCALE3 ABSPACK scaling algorithm.	Analytical CrysAlis PRO 1.171.41.75a (Rigaku Oxford Diffraction, 2020) Analytical numeric absorption correction using a multifaceted crystal model based on expressions derived by R.C. Clark & J.S. Reid. (Clark, R. C. & Reid, J. S. (1995). Acta Cryst. A51, 887-897) Empirical absorption correction using spherical harmonics, implemented in SCALE3 ABSPACK scaling algorithm.
Tmin, Tmax	0.887, 0.932	0.821, 0.936	0.719, 0.874
No. of measured, independent and observed [I > 2σ(I)] reflections	77661, 14158, 12986	14455, 14455, 13072	28070, 7161, 6649
Rint	0.029	TWIN	0.018
(sin θ/λ)max (Å^{-1})	0.629	0.588	0.622

Refinement			
$R[F^2>2\sigma(F^2)]$, $wR(F^2)$, S	0.057, 0.124, 1.20	0.043, 0.119, 1.06	0.036, 0.092, 1.05
No. of reflections	14158	14455	7155
No. of parameters	931	486	518
H-atom treatment	H-atom parameters constrained	H-atom parameters constrained	H-atom parameters constrained
$\Delta\rho_{max}$, $\Delta\rho_{min}$ (e Å^{-3})	0.54, −0.56	1.07, −0.45	0.88, −0.49
CCDC number	2217094	2217088	2217087

Table S7. Crystallographic data for **3s**.

	3s
Chemical formula	2($C_{43}H_{37}N_5NiO$)
M$_r$	1396.97
Crystal system, space group	Orthorhombic, *Pbcn*
Temperature (K)	100
a, b, c (Å)	24.4075 (2), 19.0859 (2), 9.0939 (1)
β (°)	-
V (Å^3)	4236.29 (7)
Z	2
Radiation type	Cu Kα
μ (mm^{-1})	0.93
Crystal Size	0.19 × 0.12 × 0.09
Diffractometer	XtaLAB Synergy R, HyPix
Absorption correction	Analytical CrysAlis PRO 1.171.41.75a (Rigaku Oxford Diffraction, 2020) Analytical numeric absorption correction using a multifaceted crystal model based on expressions derived by R.C. Clark & J.S. Reid. (Clark, R. C. & Reid, J. S. (1995). Acta Cryst. A51, 887-897) Empirical absorption correction using spherical harmonics, implemented in SCALE3 ABSPACK scaling algorithm.
Tmin, Tmax	0.874, 0.935

No. of measured, independent and observed [I > 2σ(I)] reflections	24044, 4350, 3949
Rint	0.023
(sin θ/λ)max (Å^{-1})	0.628
$R[F^2 > 2\sigma(F^2)]$, $wR(F^2)$, S	0.048, 0.137, 1.04
No. of reflections	4350
No. of parameters	237
H-atom treatment	H-atom parameters constrained
$\Delta\rho_{max}$, $\Delta\rho_{min}$ (e Å^{-3})	0.87, −0.44
CCDC number	2217098

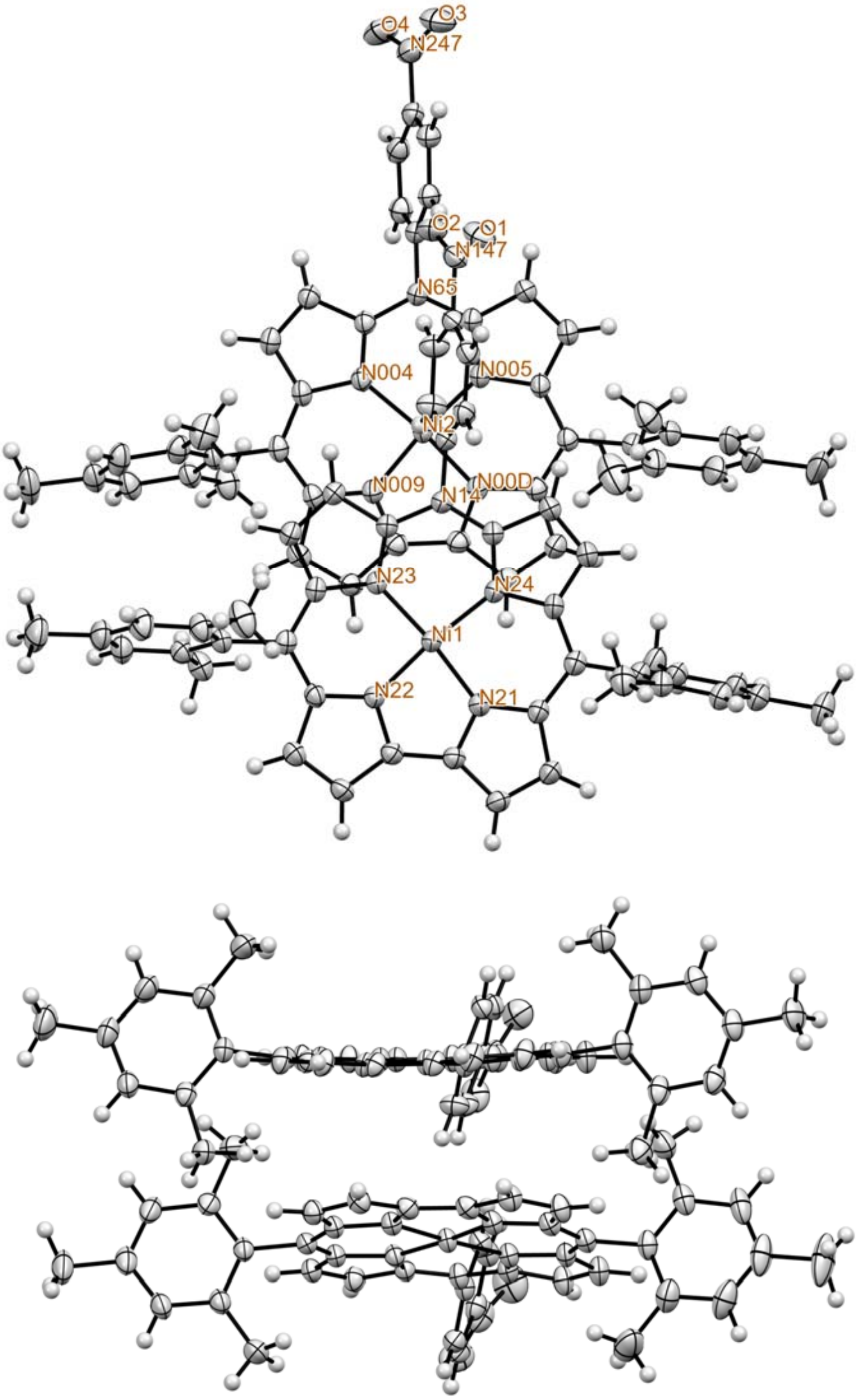

Figure S156. Two views of the ORTEP representations (ellipsoids set on the 50% probability level) of the asymmetric unit of the crystal structure o **3d**.

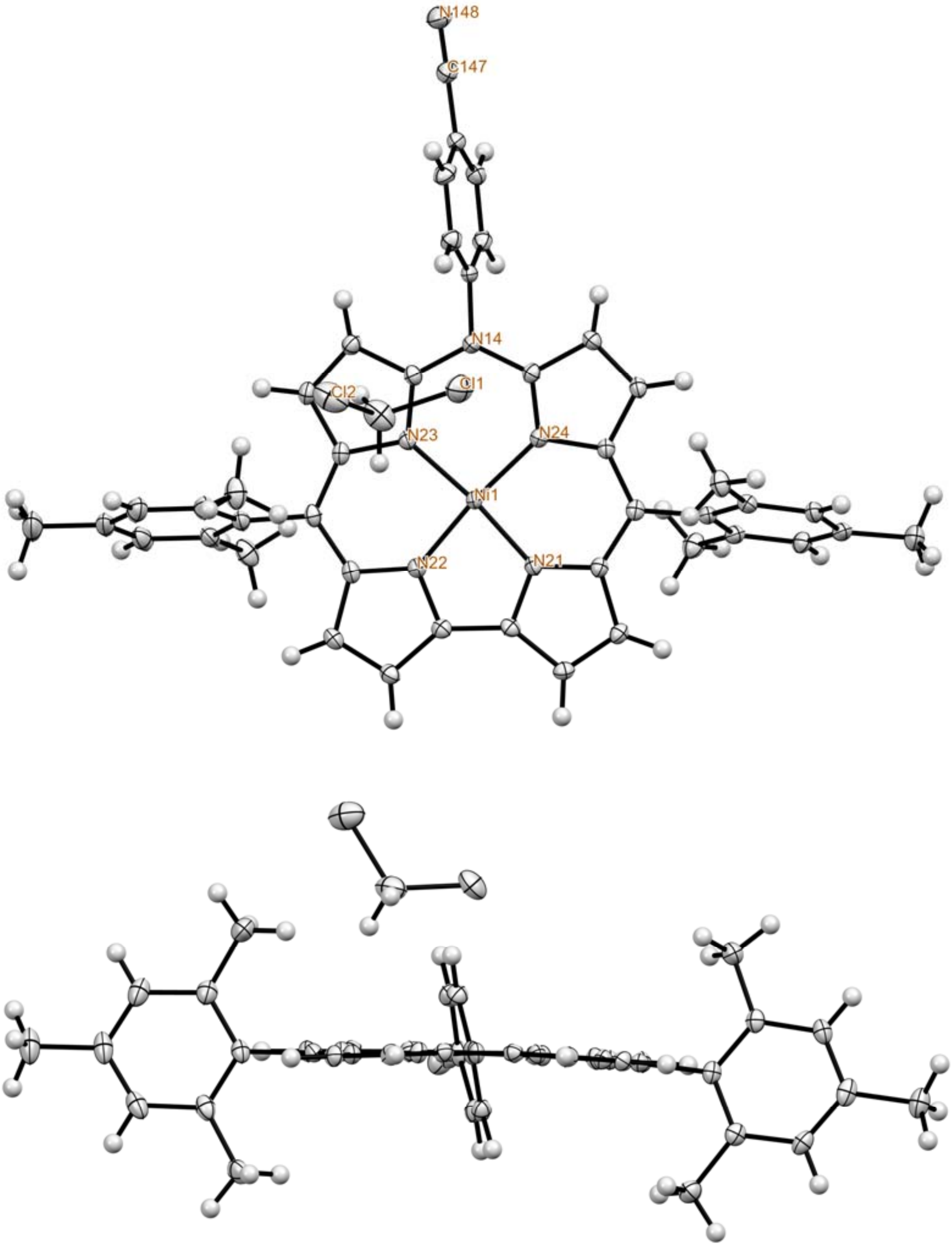

Figure S157. Two views of the ORTEP representations (ellipsoids set on the 50% probability level) of the asymmetric unit of the crystal structure o **3e**.

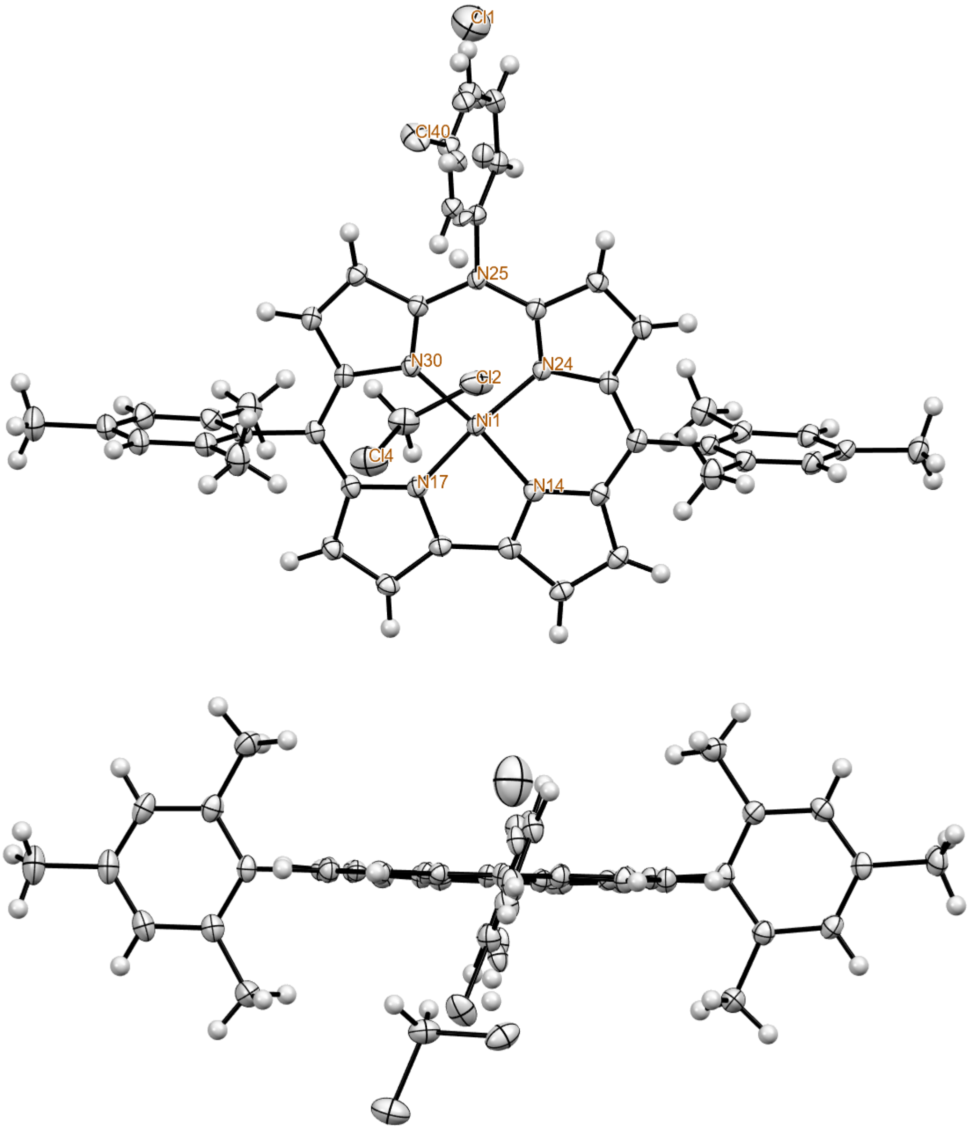

Figure S158. Two views of the ORTEP representations (ellipsoids set on the 50% probability level) of the asymmetric unit of the crystal structure o **3h**.

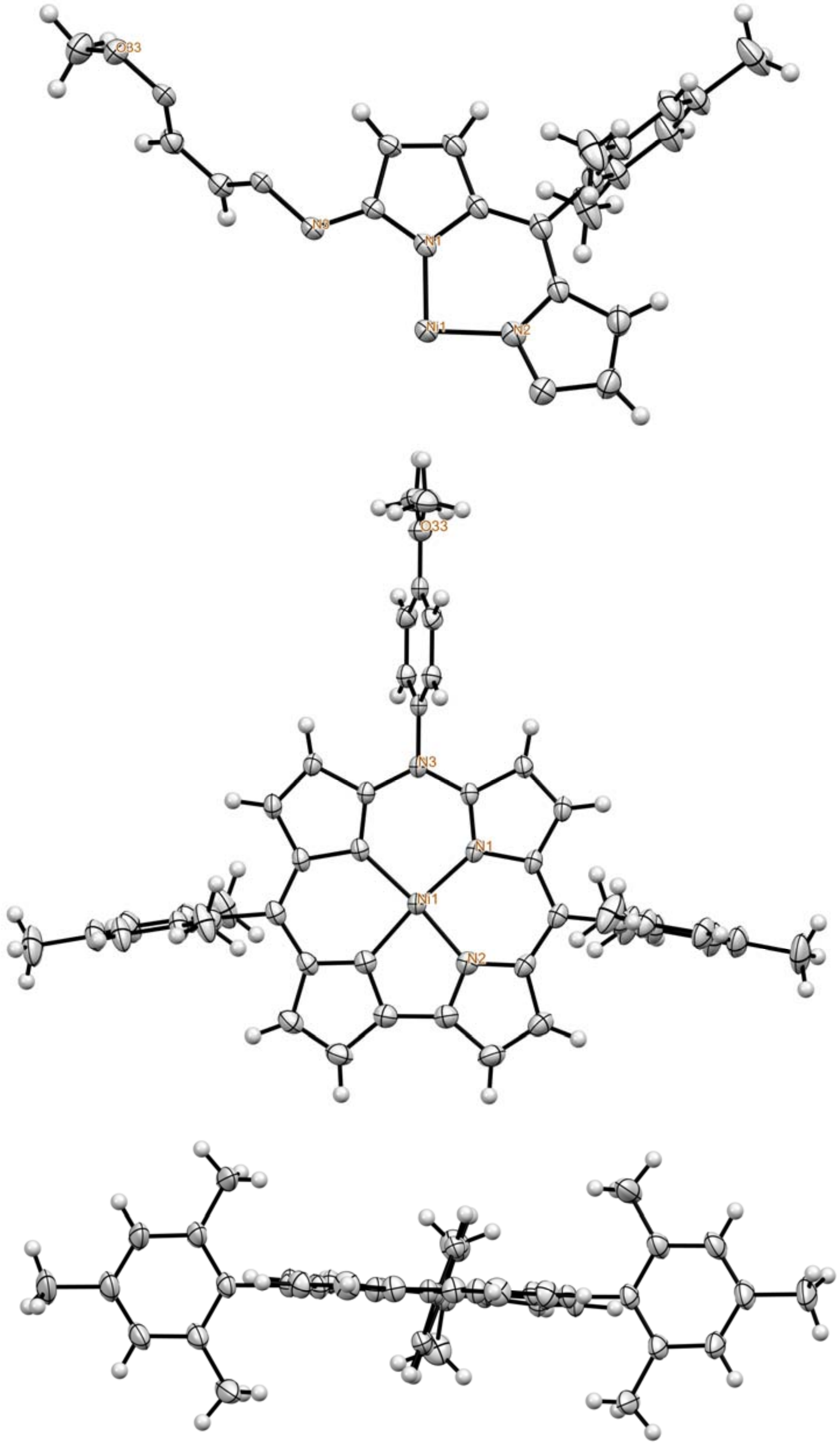

Figure S159. ORTEP representations (ellipsoids set on the 50% probability level) of the asymmetric unit of the crystal structure of **3s** and two views of its molecular structure.

Table S8. Computational details for the optimized structures of compounds

Structure / Name[a]	SCF E	ZPV[b]	lowest freq.	E	ΔH	ΔG[c]	ΔG_{rel}	HOMO	LUMO	HLG
	a.u.	a.u.	cm^{-1}	a.u.	a.u.	a.u.	kcal/mol	eV	eV	eV
3d /PJC_5_008	-2269.277584	-2268.610306	12.91	-2268.565929	-2268.564985	-2268.693210	-	−5.03	−2.82	2.21
[2-*H***3d**]$^+$/ PJC_5_012_NMR	-2269.700601	-2269.022220	8.75	-2268.978222	-2268.977278	-2269.103965	2.5	−6.33	−3.88	2.45
[3-*H***3d**]$^+$ / PJC_5_013_NMR	-2269.703847	-2269.025062	10.06	-2268.980442	-2268.979498	-2269.107943	0	−6.22	−4.10	2.12
[7-*H***3d**]$^+$ / PJC_5_010_NMR	-2269.689381	-2269.011494	3.08	-2268.966697	-2268.965753	-2269.095254	8.0	−6.33	−4.37	1.96
[8-*H***3d**]$^+$ / PJC_5_011_NMR	-2269.700783	-2269.021601	14.03	-2268.977050	-2268.976106	-2269.103934	2.5	−6.24	−3.96	2.28
[10-*H***3d**]$^+$/ PJC_5_009_NMR	-2269.651527	-2268.970837	13.72	-2268.926342	-2268.925398	-2269.052816	34.6	−6.21	−3.93	2.28

[a] Data set name (Cartesian coordinated available as *.pdb files). [b] Zero-point vibrational energy. [c] Gibbs free energy.

References

[1] G. M. Sheldrick, *Acta Cryst.* **2008,** *A64* 112-122.

[2] C. B. Hübschle, G. M. Sheldrick, B. Dittrich, *J.Appl.Cryst.* **2011,** *44* 1281-1284.

[3] Frisch, M. J., Trucks, G. W., Schlegel, H. B., Scuseria, G. E., Robb, M. A., Cheeseman, J. R., Montgomery, J. A., Vreven, T, Kudin, K. N., Burant, J. C., Millam, J. M., Iyengar, S. S., Tomasi, J., Barone, V., Mennucci, B., Cossi, M., Scalmani, G., Rega, N., Petersson, G. A., Nakatsuji, H., Hada, M., Ehara, M., Toyota, K., Fukuda, R., Hasegawa, J., Ishida, M., Nakajima, T., Honda, Y., Kitao, O., Nakai, H., Klene, M., Li, X., Knox, J. E., Hratchian, H. P., Cross, J. B., Adamo, C., Jarmillo, J., Gomperts, R., Stratmann, R. E., Yazyev, O., Austin, A. J., Cammi, R., Pomelli, C., Ochterski, J., Ayala, P. Y., Morokuma, K., Voth, G. A., Salvador, P., Dannenberg, J. J., Zakrzewski, V. G., Dapprich, S., Daniels, A. D., Strain, M. C., Farkas, O., Malick, D. K., Rabuck, A. D., Raghavachari, K., Foresman, J. B., Ortiz, J. V., Cui, Q., Baboul, A. G., Clifford, S., Cioslowski, J., Stefanov, B. B., Liu, G., Liashenko, A., Piskorz, P., Komaromi, I., Martin, R. L., Fox, D. J., Keith, T., Al-Laham, M. A., Peng, C. Y., Nanayakkara, A., Challacombe, M., Gill, P. M. W., Johnson, B. G., Chen, W., Wong, M. W., Gonzales, C., and Pople, J. A. Gaussian 03. [Revision C.01]. 2004. Pittsburgh, PA.

[4] A. D. Becke, *Phys.Rev.A* **1988,** *38* 3098-3100.

[5] A. D. Becke, *J.Chem.Phys.* **1993,** *98* 5648.

[6] C. Lee, W. Yang, R. G. Parr, *Phys.Rev.B* **1988,** *37* 785-789.

[7] N. M. O'Boyle, A. L. Tenderholt, K. M. Langner, *J.Comp.Chem.* **2008,** *29* 839-845.

[8] T. Ito, Y. Hayashi, S. Shimizu, J.-Y. Shin, N. Kobayashi, H. Shinokubo, *Angew.Chem.Int.Ed.* **2012,** *51* 8542-8545.

[9] Z. Deng, X. Li, M. Stępień, P. J. Chmielewski, *Chem.Eur.J.* **2016,** *22* 4231-4246.

[10] S. Ito, Y. Tokimaru, K. Nozaki, *Chem.Commun.* **2015,** *51* 221-224.

[11] J. Krumsieck, M. Bröring, *Chem.Eur.J.* **2021,** *27* 11580-11588.

[12] W. Jentzen, X.-Z. Song, J. A. Shelnutt, *J.Phys.Chem.B* **1997,** *101* 1684-1699.

[13] W. Jentzen, J.-G. Ma, J. A. Shelnutt, *Biophys.J.* **1998,** *74* 753-763.

[14] T. Yonezawa, S. A. Shafie, S. Hiroto, H. Shinokubo, *Angew.Chem.Int.Ed.* **2017,** *56* 11822-11825.